CYCLIZATION OF POLYPHENOLS FROM NATURAL PRODUCTS: POTENTIAL PHARMACOLOGICAL AND TOXICOLOGICAL IMPLICATIONS

A Thesis Submitted to the

College of Graduate and Postdoctoral Studies

In Partial Fulfillment of the Requirements

For the Degree of Doctor of Philosophy

In the College of Pharmacy and Nutrition

University of Saskatchewan

Saskatoon

By

GABRIEL DALIO BERNARDES DA SILVA

PERMISSION TO USE

In presenting this thesis/dissertation in partial fulfillment of the requirements for a Postgraduate degree from the University of Saskatchewan, I agree that the Libraries of this University may make it freely available for inspection. I further agree that permission for copying of this thesis/dissertation in any manner, in whole or in part, for scholarly purposes may be granted by the professor Dr Ed Krol who supervised my thesis work or, in their absence, by the Head of the Department or the Dean of the College in which my thesis work was done. It is understood that any copying or publication or use of this thesis/dissertation or parts thereof for financial gain shall not be allowed without my written permission. It is also understood that due recognition shall be given to me and to the University of Saskatchewan in any scholarly use which may be made of any material in my thesis/dissertation.

Requests for permission to copy or to make other uses of materials in this thesis/dissertation in whole or part should be addressed to:

Dean of the College of Pharmacy and Nutrition
University of Saskatchewan
107 Wiggins Rd
Saskatoon, Saskatchewan S7N 5E5 Canada

OR

Dean
College of Graduate and Postdoctoral Studies
University of Saskatchewan
116 Thorvaldson Building, 110 Science Place
Saskatoon, Saskatchewan S7N 5C9 Canada

ABSTRACT

Previously our group identified that the dicatechol lignan nordihydroguaiaretic acid (NDGA) can undergo spontaneous autoxidation and intramolecular cyclization at pH 7.4 to form a dibenzocyclooctadiene (cNDGA). We also observed that autoxidation of NDGA or cNDGA was required for inhibition of α-synuclein aggregation in vitro, a protein associated with Parkinson's disease.

A number of dicatechol ethanes have been shown to inhibit α-synuclein aggregation in vitro and we propose that the anti-aggregation effects are the result of autoxidation/ intramolecular cyclization. My first goal was to determine if dicatechol ethanes could spontaneously autoxidize/ cyclize and inhibit α-synuclein aggregation in vitro.

In order to assess the formation of 6-membered ring dicatechols, I synthesized and characterized three diphenylethane analogs with 0, 2 or 4 methyl groups on the 2-carbon linker. I determined that all of the analogs spontaneously cyclize at pH 7.4 into the corresponding dibenzocyclohexadienes which were also oxidatively labile and formed additional oxidation products. The rate of cyclization to form dibenzocyclohexadienes is 10-30 times faster than for dibenzocyclooctadienes and both the diphenylethanes and dibenzocyclohexadienes inhibit α-synuclein aggregation in vitro.

A second goal of my project was to study the metabolism of quebecol, a triphenylethane natural product isolated from maple syrup production which is under investigation as a chemopreventive and chemotherapeutic, although there are no reports on the hepatic metabolism of quebecol. In order to assess hepatic metabolism, I synthesized and isolated quebecol and investigated its in vitro metabolism in rat liver microsomes (RLM) and human liver microsomes

(HLM). I anticipated that phase II metabolism would predominate, and I observed formation of three glucuronide metabolites in both RLM and HLM. To determine the hepatic contribution to first-pass glucuronidation, I validated an HPLC-UV method following FDA and EMA guidelines (selectivity, linearity, accuracy and precision) to quantify quebecol metabolism in microsomes. In vitro enzyme kinetics were performed for quebecol glucuronidation in HLM including 8 concentrations from 5-30 μM. I determined a Michaelis-Menten constant (K_M) of 5.1 μM, intrinsic clearance (Cl_{int}) of 0.04 mL/min/mg and maximum velocity (V_{max}) of 0.22 μmol/min/mg.

In contrast I was unable to detect any P450 metabolites of quebecol in either RLM or HLM. In spite of the presence of three phenols that could form *para*-quinone methides, glutathione (GSH) trapping experiments provided no evidence for reactive intermediate formation. To confirm the absence of *para*-quinone methides I attempted to prepare standards using MnO_2 as oxidant and trapping with GSH. Rather than observe the expected *para*-quinone methides, instead I observed *ortho*-quinone formation resulting from MnO_2-mediated dealkylation. Together with extensive phase II glucuronidation, this suggests that the risk of reactive intermediate formation from quebecol is negligible.

ACKNOWLEDGEMENTS

I would like to thank my supervisor Dr Ed Krol for all support, guidance, and wisdom during my academic program. I am fortunate to have had you as my supervisor. I will miss your daily check-ins in the lab. I also extend my gratitude to my committee members Dr Ekaterina Dadachova (chair), Dr David Palmer, Dr Brian Bandy, Dr Jian Yang, Dr Chris Phenix, Dr Richard Manderville (external) for all the valuable suggestions towards my academic program and/or to my thesis.

I would like to thank my past and current lab members, and fellow colleagues from the College of Pharmacy and Nutrition, particularly Omozojie Paul Aigbogun, Brigitte Moser, Deborah Michel, Ayat Zagzoog, and Stephanie Voung, for all help, patience, and support both scientifically and socially.

I would like to thank the following organizations to provide awards to me: College of Pharmacy and Nutrition (U of S), International Student and Study Abroad Centre (U of S), Drug Metabolism Discussion Group (DMDG), and International Society for the Study of Xenobiotics (ISSX). I would like to thank the College of Pharmacy and Nutrition, the College of Graduate and Postdoctoral Studies, and the Natural Science and Engineering Research Council of Canada (NSERC) for providing me funding for this work.

Lastly and most important, I want to specially thank my wife Camila, my daughters Bella and Linda for their support, love, and patience throughout my academic studies. You have given me so much encouragement, motivation, and support towards my journey. I also extend my gratitude to my parents Celso and Ana for all support, love, and prayers.

DEDICATION

I dedicate this thesis to my wife Camila, my daughters Bella and Linda, and my parents Celso and Ana.

TABLE OF CONTENTS

LIST OF ABBREVIATIONS

(MeO)2-DPE	4,4'-(ethane-1,2-diyl)bis(2-methoxyphenol)
AS	Alpha-synuclein
BnBr	Benzyl bromide
CI	Confidence interval
Cl_{int}	Intrinsic Clearance
cNDGA	Cyclized NDGA
COSY	Homonuclear correlation spectroscopy
CV	Coefficient of variation
DCM	Dichloromethane
DFT	Density-functional theory
DMAP	4-Dimethylaminopyridine
DMSO	Dimethyl sulfoxide
DNA	Deoxyribonucleic acid
DPE	4, 4'-(ethane-1,2-diyl)bis(benzene-1,2-diol)
EMA	European Medicines Agency
EPI	Enhanced product ion
ESI	Electrospray ionization
EtOAc	Ethyl acetate
FDA	Food and Drug Administration
Glu	Glucuronide
GSH	Glutathione

HIV	Human immunodeficiency virus
HLM	Human liver microsomes
HOAc	Acetic acid
HPLC	High-performance liquid chromatography
HQC	High quality control
HSQC	Heteronuclear Single Quantum Coherence
IL	Interleukins
K_M	Michaelis–Menten constant
k_{obs}	Observed rate constant
LC	Liquid chromatography
LC-MS	Liquid chromatography–mass spectrometry
LDA	Lithium diisopropylamide
LDL	Low-density lipoprotein
LLOQ	Lower limit of quantification
LOD	Limit of detection
LQC	Lower quality control
M2-DPE	2,3-bis(3,4-dihydroxyphenyl)butane
M4-DPE	2-(3,4-dimethoxyphenyl)propan-2-ol
MeOH	Methanol
MLM	Mouse liver microsomes
mM	Millimolar
MMPPD	2,2-di-(3-methoxymethylphenyl)-1,3-propanediol

MQC	Medium quality control
MS	Mass spectrometry
MsCl	Mesyl chloride
MW	Molecular weight
NADPH	Reduced nicotinamide adenine dinucleotide phosphate
NBS	N-Bromosuccinimide
n-BuLi	n-Butyllithium
NDGA	Nordihydroguaiaretic Acid
NL	Neutral loss
NMR	Nuclear Magnetic Resonance
NMS	Non-motor symptoms
o-Q	*ortho*-Quinone
P450	Cytochrome P450
PBS	Phosphate-buffered saline
PD	Parkinson's disease
Pd/C	Palladium on carbon
PI	Precursor ion
p-QM	*para*-Quinone methide
r^2	Coefficient of determination
RLM	Rat liver microsomes
rt	Room temperature
SD	Standard deviation

SECO	Secoisolariciresinol
SPP	Sodium pyrophosphate decahydrate
$t_{1/2}$	Half-life
TEA	Triethylamine
THF	Tetrahydrofuran
ThT	Thioflavin T
TLC	Thin-layer chromatography
TNF-α	Tumor necrosis factor alpha
UDP	Uridine 5’-diphosphoglucuronic acid trisodium salt
UGT	Uridine diphosphate glucuronosyl transferase
V_{MAX}	Maximum Velocity
XIC	Extracted ion chromatogram

LIST OF FIGURES

LIST OF TABLES

LIST OF SCHEMES

Chapter 1: Literature Review

1.1 Introduction

Polyphenols are a widely distributed class of bioactive molecules with a number of biological activities reported in the literature [1]. One of the major groups of polyphenols are lignans, which represent a large class of secondary metabolites in plants. Nordihydroguaiaretic acid (NDGA) is a lignan from the creosote bush and has been used in traditional medicine for a wide range of ailments due to its suggested medicinal properties [2]. This natural polyphenol has been also associated with kidney and liver toxicity, when ingested at higher doses [3]. Studies have reported that NDGA can undergo *in vitro* biotransformation to form reactive *ortho*-quinones, which are likely responsible for toxicity *in vivo*, such as severe hepatic and renal injuries [4].

In the absence of a trapping agent, NDGA can spontaneously cyclize at pH 7.4 to form a dibenzocyclooctadiene that may be responsible for the pharmacological properties [5] However, the mechanism of the intramolecular cyclization remains unknown. A series of NDGA analogs were synthesized by our group to investigate the structural features necessary for the intramolecular cyclization process and we determined that only compounds possessing a dicatechol could form dibenzocyclooctadienes [6]. In addition, the analogue having no methyl functional groups on the alkyl linker chain was observed to cyclize more rapidly than NDGA, in opposition to the anticipated Thorpe-Ingold effect. This would imply that additional methyl groups on the alkyl chain would slow intramolecular cyclization.

The oxidative metabolism of NDGA suggests that an *ortho*-quinone (*o*-Q) is the only quinone intermediate formed which is responsible for the toxicities associated with NDGA use [4]. Interestingly, the lignan secoisolariciresinol (SECO) undergoes oxidative metabolism to a

para-quinone methide (*p*-QM) followed by an intramolecular cyclization to form lariciresinol [7]. There is no evidence that oral consumption of SECO causes serious toxic effects, suggesting the intramolecular cyclization minimizes any toxicity related to formation of the *p*-QM [8].

While dicatechol cyclization of lignans to dibenzocyclooctadienes is facile at pH 7.4, it is unknown if 6 or 7 membered rings would also form easily. A series of substituted diphenylethane dicatechols (Figure 1.1) have been shown to inhibit α-synuclein aggregation *in vitro* [9]. This led us to speculate that these compounds may also undergo autoxidative intramolecular cyclization to dibenzocyclohexadienes. We hypothesized that diphenyl *in vitro* autoxidation/ intramolecular cyclization of these dicatechols may be associated with their α-synuclein anti-aggregation properties.

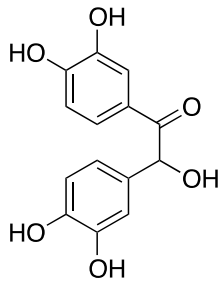

1,2-bis(3,4-dihydroxyphenyl)-2-hydroxyethanone

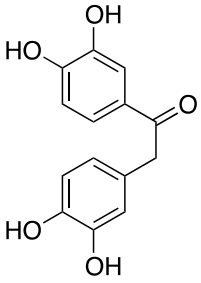

1,2-bis(3,4-dihydroxyphenyl)ethanone

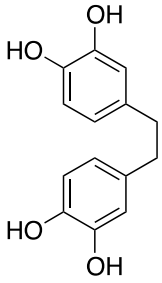

4,4'-(ethane-1,2-diyl)bis(benzene-1,2-diol)

Figure 1.1 Diphenylethane dicatechol compounds from patent literature that could potentially form dibenzohexadienes.

Recently, a new polyphenolic compound, quebecol, was isolated from maple syrup and is under investigation for potential applications as a chemopreventive or chemotherapeutic agent [10]. Currently, the hepatic metabolism of quebecol has not been studied. Considering the lack of

information about phase I and phase II metabolism of quebecol, our group has an interest to investigate its metabolism in general. Quebecol could potentially undergo oxidative metabolism leading to 6-membered ring formation, and the cyclized form could be responsible for the biological activity.

The primary interest for studying the intramolecular cyclization is that the NDGA-dibenzocyclooctadiene has been reported to inhibit *in vitro* aggregation of α-synuclein, a protein associated with Parkinson's disease [11]. This recent study also showed that cyclized NDGA reduced α-synuclein-driven neurodegeneration in a relevant animal model. Therefore, an investigation of the ability of other cyclized analogs to inhibit α-synuclein aggregation will allow the development of structure-activity relationships for this process and insight into α-synuclein misfolding.

Therefore, the overall goals of this project are to synthesize and investigate the ability of diphenylethane dicatechols to undergo oxidative metabolism to form cyclized metabolites, and the ability of these forms to inhibit α-synuclein aggregation.

1.2 Lignans

Lignans are polyphenolic compounds found in plants as active secondary metabolites derived from the oxidative coupling of two phenylpropanoid units [12]. Similarly to other secondary metabolites, lignans serve as protection against microorganisms and herbivores for the plants that synthesize them [13]. Even though their molecular backbones are formed by two phenylpropane (C_6–C_3) units, lignans have a vast structural diversity consisting of different linkage patterns. Considering this, the classification of lignans is based on their general chemical structure.

The extensive analysis of the biological properties of lignans continues to attract investigation due to the wide pharmacological properties such as anti-cancerous, antiasthma anti-inflammation, antioxidant, antimicrobial, antihypertensive and hypocholesterolemic activities [14,15].

1.3 Nordihydroguaiaretic Acid (NDGA)

1.3.1 Definition

NDGA (Figure 1.2) is a secondary metabolite found in the leaves of Creosote bush (*Larrea tridentate*), an evergreen shrub found in southwestern deserts of the United States and Southern Mexico [16]. Creosote bush extracts have been used by Native Americans to treat a variety of ailments including pain, inflammation, kidney stones and diabetes [17].

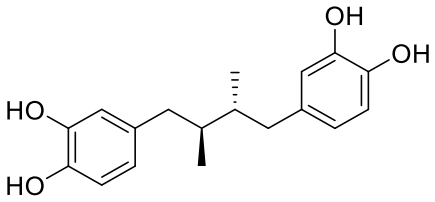

Figure 1.2. Structure of nordihydroguaiaretic acid (NDGA)

In terms of distribution of secondary phenolic compounds in Creosote bush, NDGA is found in flowers, leaves, green stems and small woody stems, with the highest concentrations found in leaves (38.3 mg/g) and green stems (32.5 mg/g) [18]. It has been reported that 5-10% of the leave's dry weight consist of NDGA, being 80% of all phenolics in the resin.

1.3.2 Metabolism and Autoxidation

NDGA is extensively metabolized by hepatic phase II enzymes, glucuronide conjugation being the major metabolic elimination pathway of this compound *in vivo* [19]. Mono- and di-glucuronide conjugates of NDGA were reported in the plasma of mice after intravenous administration [3].

In aqueous solution at physiological pH (pH 7.4), NDGA can undergo an autoxidation reaction forming an *o*-Q which can be trapped as a glutathione (GSH) conjugate [4]. In the absence of a trapping agent, an oxidative cyclization leads to a schisandrin-like dibenzocyclooctadiene lignan that could be involved with the biological effects of NDGA (Figure 1.3). Naturally-occurring schisandrins have been studied for various biological properties including anti-inflammatory, anti-tumor activity and neuroprotective effect [20,21].

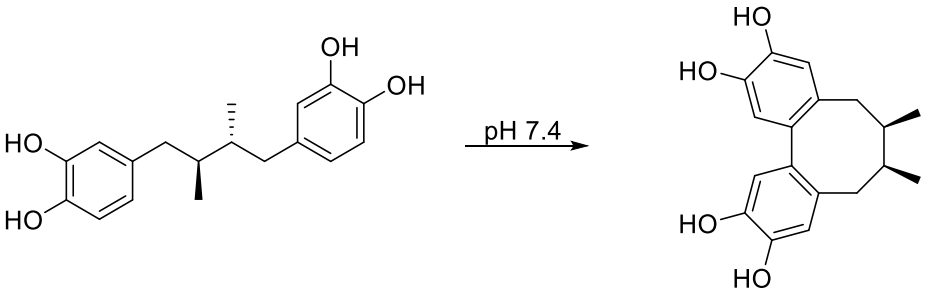

Figure 1.3. Intramolecular cyclization of NDGA

Our group has determined how functional groups on the aromatic rings of NDGA lignan analogs can influence the formation of dibenzocyclooctadienes under physiologically relevant conditions [6]. Only compounds with a dicatechol-substituted ring could form dibenzocyclooctadienes, whereas a single catechol is not sufficient for dibenzocyclooctadiene formation. These studies suggest that intramolecular cyclization likely occurs via a radical-mediated mechanism instead of an electrophilic substitution process (Figure 1.4).

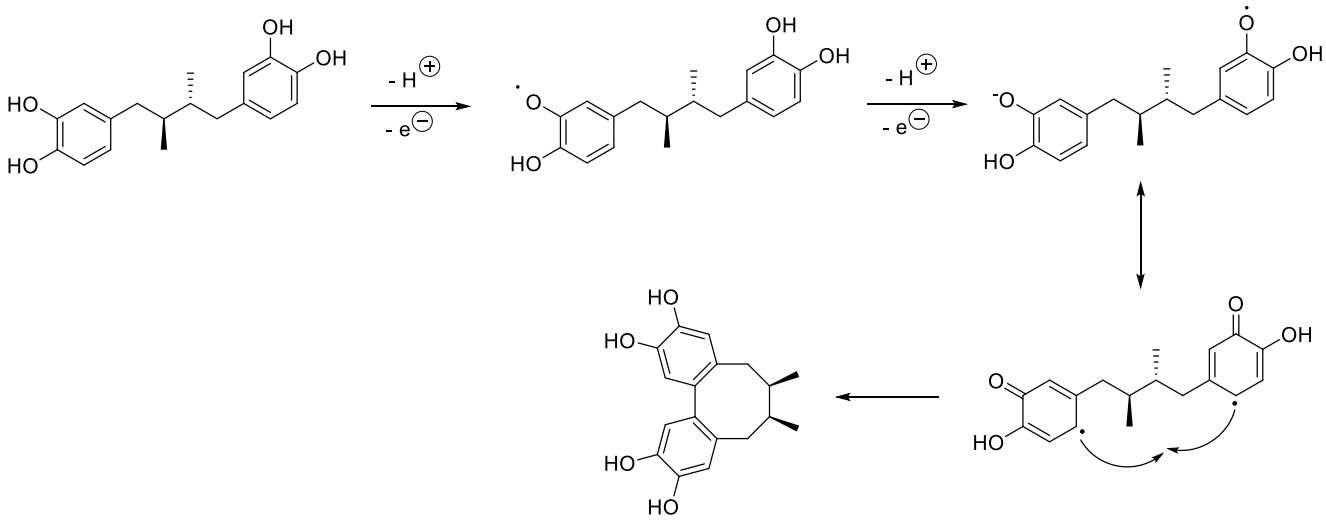

Figure 1.4 - Intramolecular cyclization of NDGA via radical-mediated process (adapted from [6])

As part of these studies, it was shown that the methyl functional groups on the alkyl linker chain would have an influence on the rate of intramolecular cyclization [6]. The desmethyl analogue de-Me-NDGA was synthesized and determined to cyclize more rapidly (pseudo 1st order rate 13.1 × 10^{-5} s^{-1}) than NDGA (4.88 × 10^{-5} s^{-1}). The Thorpe-Ingold effect would have predicted the removal of methyl groups of NDGA should have resulted in a slower rate of cyclization for de-Me-NDGA [22]. It is likely that the more rapid cyclization for de-Me-NDGA is a result of decreased steric interactions between the methyl groups during cyclization. Conformation II/III (NDGA) or V/VI (de-Me-NDGA) (Figure 1.5) are necessary in order for intramolecular cyclization to occur. The presence of additional steric interactions CH_3-CH_3 and CH_3-CH_2-Ar for NDGA indicates that conformations II/III are energetically less favourable as compared to V or VI, for de-Me-NDGA as shown in Figure 1.5.

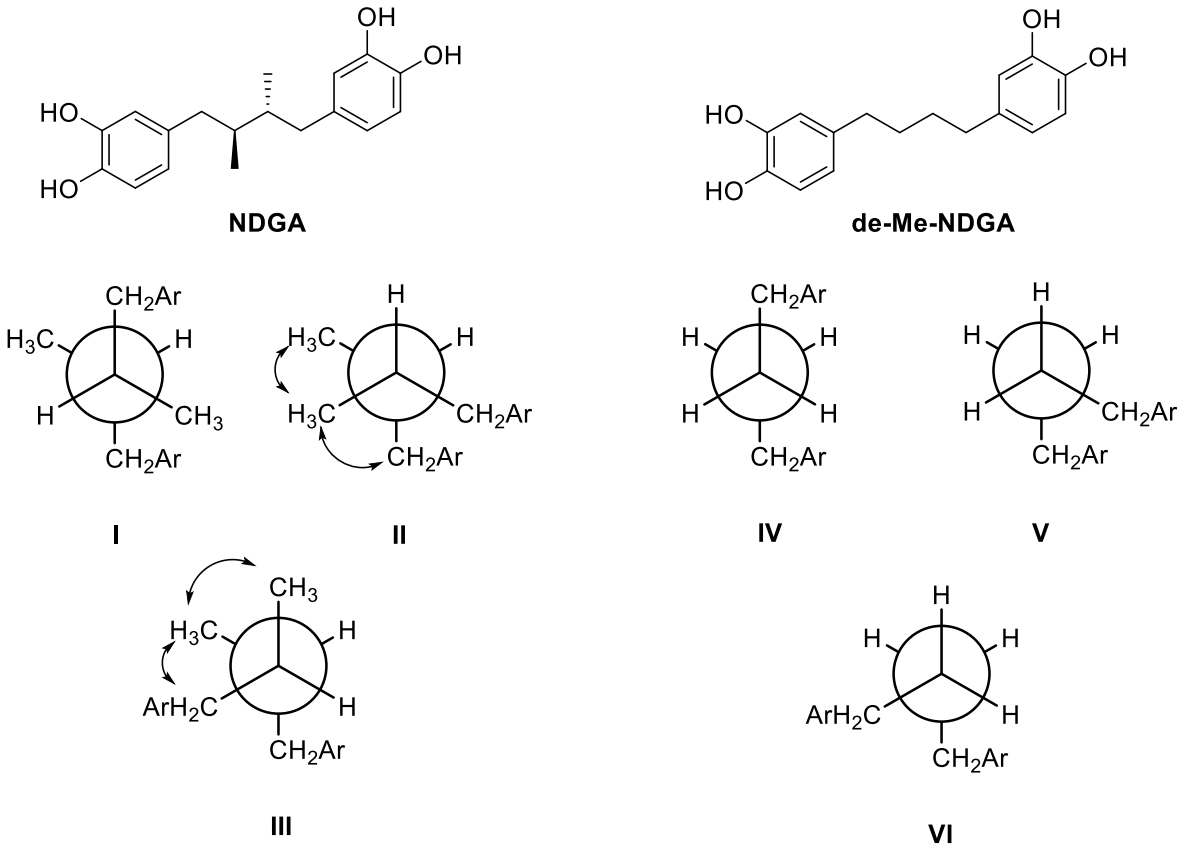

Figure 1.5 – Newman projection for NDGA (I, II, III) and de-Me-NDGA (IV, V, VI). Most stable conformations are represented in I and IV. Conformers II or III, and V or VI are the required conformations for the intramolecular cyclization.

This would imply that additional methyl groups on the alkyl chain would slow intramolecular cyclization. Preparation of the tetra-methyl NDGA would be necessary to confirm that the additional methyl groups will further slow cyclization and whether that may be sufficient to prevent cyclization.

1.3.3 Toxicological properties

In 1968, NDGA was reported to induce cystic nephrotoxicity by the Canadian Food and Drug Directorate, and since then its use as a food preservative has been banned in Canada [3]. A few years later, the Food and Drug Administration in the United States removed the "Generally Recognized As Safe" (GRAS) designation for NDGA. The use of extracts or decoctions of creosote bush have been used in traditional medicine for a wide variety of human ailments [23]. Marketed tablets and capsules of powdered leaves have been used as dietary supplements largely based on their antioxidant properties [24]. However, chronic consumption of tablets or capsules have been associated with drug-induced hepatitis and cystic renal disease [25]. In most of the cases, the discontinuation of these products led to a decrease of symptoms [18].

NDGA was found to act as a pro-oxidant in clone-9 rat hepatocyte cultures at higher concentrations triggering oxidative stress, oxidative cell injury and cytotoxicity [25]. At lower concentrations, however, NDGA has shown beneficial antioxidant effects.

1.3.4 Biological properties of dibenzocyclooctadienes

Naturally occurring and synthetic dibenzocyclooctadienes lignans have been reported to display biological properties including anticancer [26], antihepatocarcinogenesis [27], antihepatotoxic [28], anti-HIV [29], antioxidant [30] and anti-inflammatory activities [31].

Recently, NDGA dibenzocyclooctadiene was shown to interact with α-synuclein, a major constituent of Lewy bodies, a pathological hallmark in Parkinson's disease [11]. This interaction led to a decrease in α-synuclein-driven neurodegeneration in *Caenorhabditis elegans.* However, it remains unknown how the NDGA dibenzocyclooctadiene prevents α-synuclein aggregation.

Considering these findings, NDGA-derived dibenzocyclooctadienes could contribute as potential therapies for Parkinson's disease.

1.4 Parkinson's Disease

1.4.1 Definition

Parkinson's disease (PD) is a chronic, degenerative and progressive disease of the central nervous system (CNS) characterized by the loss or degeneration of dopaminergic neurons in the substantia nigra [32]. These cells are responsible for dopamine production and its loss in the brain leads to postural, gait and cognitive dysfunction [33].

Parkinsonism is the umbrella term given to describe a group of clinical conditions that feature PD symptoms. While most Parkinsonism cases are due to PD, cases also result because of other neurological disorders, antidopaminergic drugs side effects, or exposure to toxins [34]. However, PD is different from Parkinsonism etiologically [35]. The presence of Lewy bodies (abnormal aggregates of α-synuclein protein) in the substantia nigra is necessary for idiopathic PD diagnosis.

In the early stages of PD, non-motor symptoms (NMS) are more prevalent such as olfactory dysfunction, cognitive impairment, psychiatric symptoms, sleep disorders and autonomic dysfunction [36]. On the other hand, the motor symptoms are present at the later stages of PD, which considerable impact on quality of life and patient disability [37]. In addition, NMS tend to progress together with motor symptoms and can occur with more frequency and more intensity in later disease stages.

1.4.2 Epidemiology

PD is the second most prevalent neurodegenerative disease worldwide after Alzheimer's disease [38]. The worldwide incidence of PD ranges from 5 to 35 new cases per 100,000 individuals every year [39]. Considering the growing and ageing population in Canada, it is estimated the number of Parkinsonism cases among Canadians will double between 2011 and 2031, increasing the incidence by 50% [40].

Studies suggested that mortality is not increased on the first 10 years of the disease, but after 20 years these numbers double compared with the general population [41]. It was also shown that there was an increased risk of PD patients dying from pneumonia and cardiovascular or cerebrovascular diseases, highlighting the importance of mobilization of these patients [42].

Age is the greatest risk factor for PD, being 50-60 years the average age of onset [32]. The incidence of PD is rare before 50 years-old, however the incidence increases 5-10 fold from 60 to 90 years of age [43]. Even though PD is rare before this age, 5-10% of people are diagnosed with young onset PD before 40 years of age, and 20% are under the age of 50 [44]. Nevertheless, PD progresses in a slow rate in younger people resulting in longer survival.

In terms of gender, more men are diagnosed with PD compared to women by a ratio of approximately 2:1 [45]. Interestingly, some clinical characteristics are reported more often in men, such as rigidity and rapid eye movement; while in women, dyskinesias and depression are more common [46,47]. The sex-based difference in PD may be related with estrogen’s protective effect, but more studies need to be done to correlate the hormonal influence on PD [48].

1.4.3 Pathology and Pathogenesis

The neuropathological feature of PD is the association between the dopaminergic cell loss within the *substantia nigra* and the development of Lewy bodies, which are round protein-rich inclusions [49]. As the main component of Lewy bodies, α-synuclein is a 140 amino acid, natively unfolded protein located in the presynaptic terminals of neurons [50]. Studies observed that the misfolding of α-synuclein might lead to its aggregation and dissemination in certain sites, which triggers an inflammatory process involved in the pathogenic dysfunction of PD [51–53]. These findings indicate that α-synuclein is involved in the pathogenesis of PD.

1.5 Secoisolariciresinol (SECO)

Another lignan of interest due to its numerous pharmacological properties is the flaxseed lignan SECO (Figure 1.6). SECO is classified as a dibenzylbutane lignan and has a similar structure to NDGA [54].

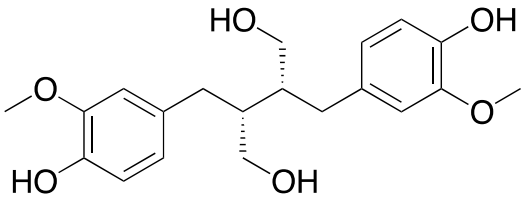

Figure 1.6. Structure of secoisolariciresinol

SECO is biotransformed into the mammalian lignan, enterodiol (ED) via demethylation and dehydroxylation, followed by further oxidation to enterolactone (ENL) by the gut microbiota of humans (Figure 1.7) [55]. Enterodiol and enterolactone were observed to undergo extensive

first-pass metabolism, mainly by phase II processes to the glucuronide and sulfonate conjugates [56,57].

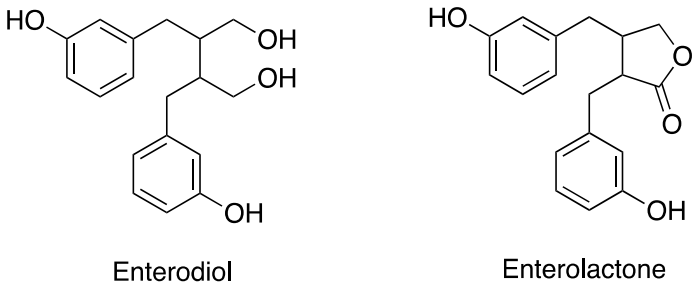

Figure 1.7. Structures of enterolignans enterodiol and enterolactone

In vitro, phase I metabolism of SECO in both rat and human hepatic microsomes leads to the oxidation to a *p*-QM [7]. Lariciresinol is the major metabolite of this process, which is believed to be formed as a product after intramolecular cyclization of SECO *p*-QM (Figure 1.8).

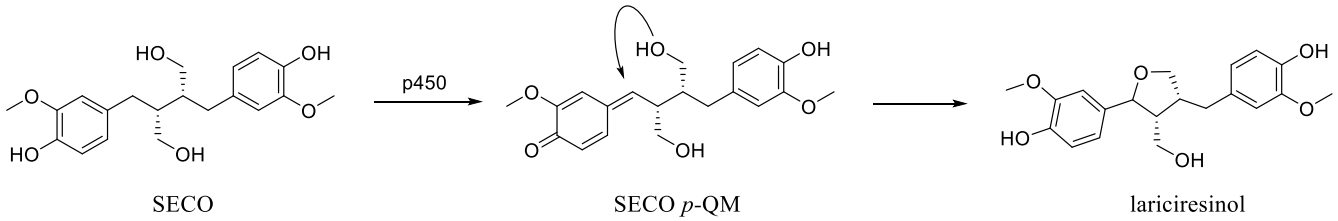

Figure 1.8. Intramolecular cyclization of SECO to lariciresinol

The consumption of SECO among adult populations is well tolerated and there is no report of significant toxicity in humans, which might be related to the intramolecular cyclization after *p*-QM formation that minimizes any toxicity by removing the reactive portion and the small contribution to overall metabolism [58]. In terms of pharmacological properties, SECO has been

observed to reduce serum LDL and total cholesterol levels, cardiovascular diseases, and breast and prostate cancers [7].

1.6 Quebecol

Quebecol, 2,3,3-tri-(3-methoxy-4-hydroxyphenyl)-1-propanol (Figure 1.9) is a polyphenolic compound, which is formed during maple syrup production from *Acer saccharum* spp [59]. The name of quebecol was assigned because of the world's premier producer of maple syrup, the Canadian province of Quebec. Structurally quebecol has some similarities with the chemotherapy drug tamoxifen, a cancer chemopreventive widely used for breast cancer, as both possesses three aromatic rings linked via a two-carbon chain although the compounds differ in the nature of the linker (saturated vs. unsaturated)[60].

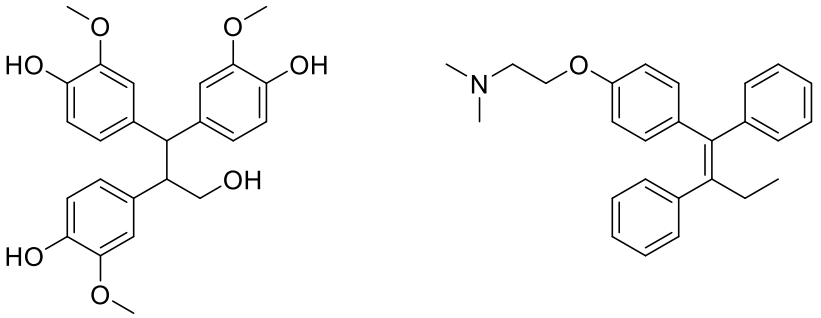

Quebecol Tamoxifen

Figure 1.9. Structure of quebecol and tamoxifen

The antiproliferative activity of quebecol was evaluated against a panel of cancer lines, and a cytotoxic effect was observed suggesting its potential as a cancer chemopreventive agent [61]. Quebecol also showed anti-inflammatory activity in bioassays by inhibiting the secretion of two

pro-inflammatory cytokines: IL-6 and TNF-α [62]. There are no studies about quebecol metabolism or toxicity. Even though the concentration of quebecol present in maple syrup is not reported in literature, it is important to note that maple syrup has been consumed for a long time without showing toxicity. Since analogs of quebecol are being synthesized as potential drug leads, it will be important to identify the metabolites of quebecol [61].

Based on other lignans metabolism, such as SECO, it is most likely that the main metabolism of quebecol is phase II by glucuronidation or sulfonation (Figure 1.10). However, because of the phenol groups, it is possible that quebecol may undergo P450 oxidation to a *p*-QM. Alternative pathways could be dealkylation of the methoxy groups to give a catechol which could undergo further oxidation to an *o*-Q [63].

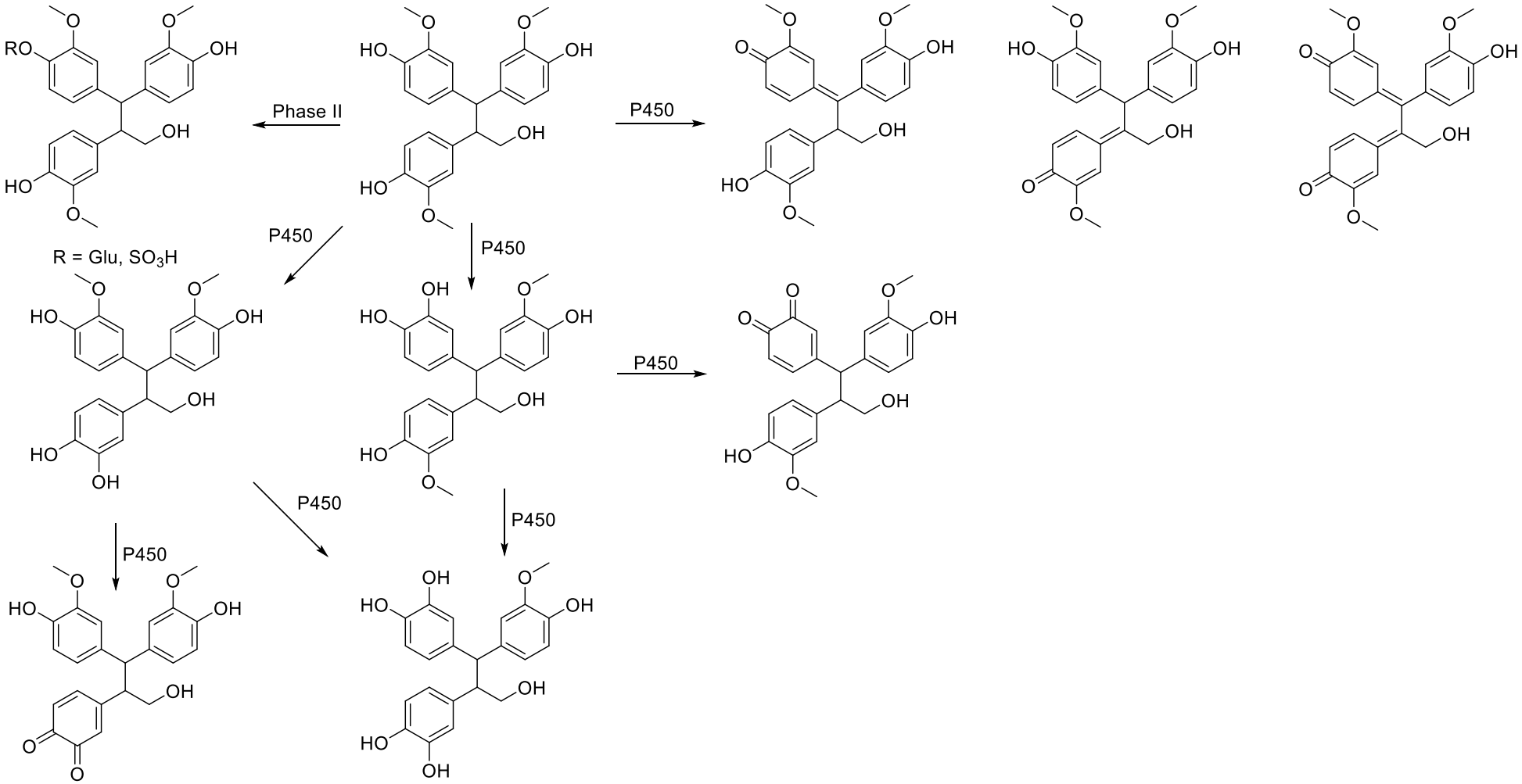

Figure 1.10. Proposed metabolism of quebecol

Although it is unlikely that two dealkylation reactions would occur without having phase II metabolism (glucuronidation, sulfonation), it is important to verify whether a dicatechol metabolite of quebecol and its analogs could spontaneously cyclize to form a six membered ring (Figure 1.11).

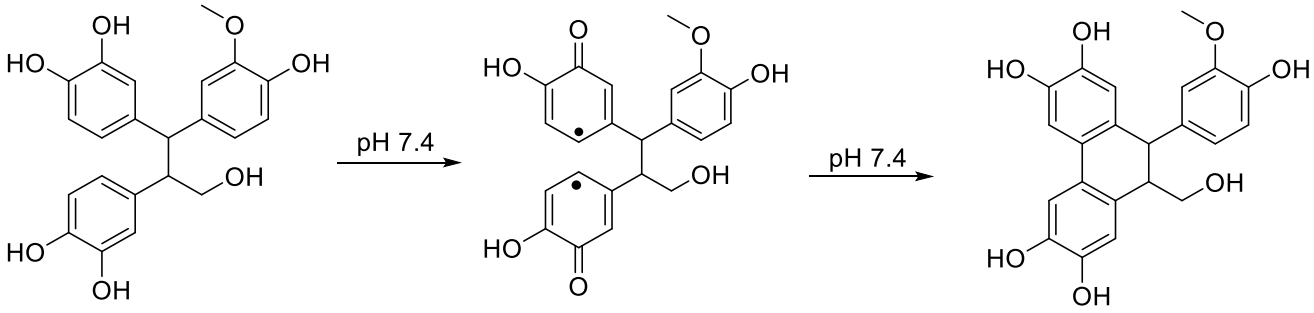

Figure 1.11 Potential dibenzocyclohexadiene formation from quebecol metabolite

There are a variety of natural products reported in the literature, however in many cases their metabolism and stability are not well understood. Considering that there are numerous proposed biological applications for these compounds, we are inspired to better understand the metabolism of these naturally occurring phenolic compounds and wish to prepare analogs to better understand aspects of their metabolism and stability.

Chapter 2: Hypotheses and Objectives

2.1 Hypotheses

2.1.1 Diphenylethane dicatechols undergo oxidative metabolism to form dibenzocyclohexadienes.

2.1.2 Quebecol will form glucuronide conjugates in vitro.

2.1.3 Quebecol can be oxidized to form quinones and dibenzocyclohexadienes.

2.1.4 Presence of additional functional groups on the side chain of NDGA slow the rate of oxidative dibenzocyclooctadiene formation.

2.1.5 Dibenzocyclohexadienes can inhibit α-synuclein aggregation in vitro.

2.2 Objectives

Hypothesis 2.1.1

2.2.1 Synthesize and characterize diphenylethane dicatechols with different numbers of methyl groups on the side chain.

2.2.2 Evaluate the synthesized diphenylethane dicatechols for their potential to undergo autoxidative cyclization.

Hypothesis 2.1.2

2.2.3 Synthesize and characterize quebecol.

2.2.4 Assess contribution of glucuronidation to the phase II metabolism of quebecol

Hypothesis 2.1.3

2.2.5 Determine if quebecol can form quinones and dibenzocyclohexadienes in hepatic microsomes.

Hypothesis 2.1.4

2.2.6 Synthesize and characterize a tetramethyl-substitued NDGA with the intent of understanding the influence on rate of intramolecular cyclization of two quaternary carbons on the side chain.

Hypothesis 2.1.5

2.2.7 Evaluate the ability of different dibenzocyclohexadienes to inhibit α-synuclein aggregation using the Thioflavin-T assay.

Chapter 3: The Effect of Diphenylethane Side-chain Substituents on Dibenzocyclohexadiene Formation

Gabriel Bernardes, Omer Munir, Ed S. Krol*

Drug Discovery and Development Research Group, College of Pharmacy and Nutrition, University of Saskatchewan, Saskatoon, SK

Contribution statement: Gabriel Bernardes contributed to the experimental design, conducted the experimental work and data analysis, and drafted the manuscript. Omer Munir contributed to scale up chemical synthesis and purification. Dr Ed Krol supervised the work and revised the manuscript.

3.1 Abstract

The naturally-occurring dicatechol lignan nordihydroguaiaretic acid and an analog without methyl groups on the butyl linker both undergo intramolecular cyclization at pH 7.4 to form dibenzocyclooctadienes. These dibenzocyclooctadienes have been shown to prevent *in vitro* aggregation of α-synuclein, an intrinsically disordered protein associated with Parkinson's disease. Nordihydroguaiaretic acid possesses two vicinal methyl groups on the butyl linker and the presence of these methyl groups attenuates the rate of intramolecular cyclization versus the unsubstituted analog, in opposition to the anticipated Thorpe-Ingold effect, likely due to steric repulsions during cyclization.

We are interested in developing a better understanding of the influence of methyl substituents on intramolecular cyclization of dicatechols. To further probe the generality of this reaction we prepared a series of 1,2-bis-ethane dicatechols with 0, 2 and 4 methyl substituents on the linker. We have confirmed that these compounds undergo intramolecular cyclization to form dibenzocyclohexadienes and that steric interactions between the methyl substituents leads to an increase in the rate of intramolecular cyclization, which is in contrast to what was observed for lignan dicatechols. The rate of cyclization to form six-membered rings is 10-30 times more rapid than formation of eight membered rings and the dibenzocyclohexadienes also prevent *in vitro* aggregation of α-synuclein.

3.2 Introduction

Many natural products with reported pharmacological activity *in vivo* have been studied in *in vitro* systems in an effort to better understand their mechanisms of action at the biochemical level and provide screening methods for carrying out structure-activity studies. A concern over this approach is the instability of many natural products when exposed to *in vitro* systems. Curcumin has been suggested to possess a range of pharmacological properties [64–69], yet it's *in vivo* metabolic fate of reduction and phase 2 metabolism [70,71] is divergent from its known instability *in vitro* [72,73] which results in an oxidative rearrangement to produce a dioxygenated bicyclopentadione. Other natural products including flavonols and catechins have reported similar *in vitro* instabilities which differ from their *in vivo* metabolism [74,75]. We previously reported that the lignan nordihydroguaiaretic acid (NDGA, Figure 1.2) undergoes oxidative intramolecular cyclization to a dibenzocyclooctadiene in phosphate buffer [5], as does an analog which does not possess methyl groups on the alkyl linker (de-Me-NDGA), and that the presence of catechols on both aromatic rings is a requirement for intramolecular cyclization [6]. We recently showed that NDGA, de-Me-NDGA and their cyclized forms are able to prevent the *in vitro* aggregation of α-synuclein [11], an intrinsically misfolded protein whose aggregation has been associated with the pathophysiology of Parkinson's disease [50,52]. Interestingly, the presence of reducing agents which prevent oxidation/ cyclization attenuate the anti-aggregation effect. There have been previous reports of the potential for NDGA to treat neurological conditions *in vitro* [76,77] and we hypothesize that this may be due to formation of the dibenzocyclooctadiene during *in vitro* incubation.

A report on a series of substituted 1,2-bis-ethane dicatechols that were demonstrated to

inhibit α-synuclein aggregation *in vitro* [9] led us to speculate that these compounds may undergo autoxidative intramolecular cyclization to dibenzocyclohexadienes. To address the question of the generality of this oxidative process led us to investigate whether dicatechols with shorter linker chains than NDGA would also undergo similar intramolecular cyclizations, specifically focusing on the formation of six-membered ring dibenzocyclohexadienes. We hypothesized that diphenyl *in vitro* autoxidation/ intramolecular cyclization of the 1,2-bis-ethane dicatechols may be associated with their α-synuclein anti-aggregation properties. Although we found evidence in the literature of dibenzocyclohexadienes, they were formed through processes other than oxidative cyclization of a dicatechol [78]. In addition, we had previously noted that the rate of cyclization for de-Me-NDGA (Figure 3.1), which does not possess methyl groups on the linker is more rapid than for NDGA. We had originally anticipated that the presence of methyl groups on the linker would enhance cyclization as a result of a Thorpe-Ingold effect [22], however our results suggested that steric interactions between the vicinal methyl groups during cyclization may rather impede this process [6]. Our goals are to prepare a series of 1,2-bisethane dicatechols with 0, 2 or 4 methyl groups on the alkyl linker in order to probe intramolecular cyclization products, rate of cyclization and ability to inhibit *in vitro* α-synuclein aggregation.

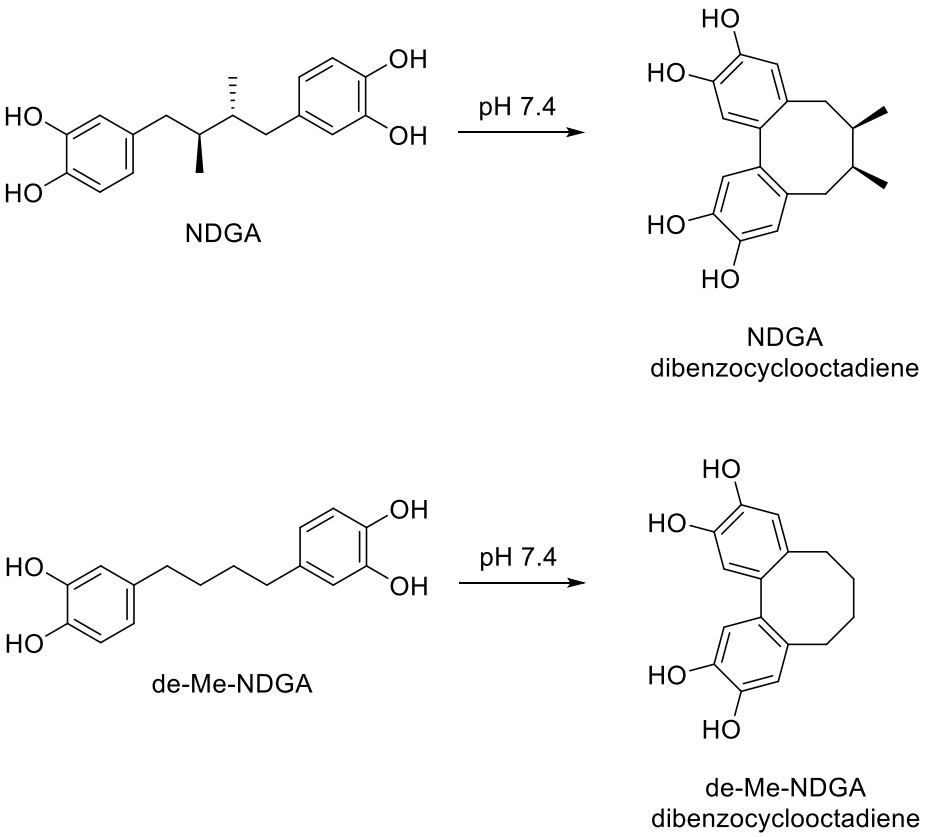

Figure 3.1. Structures of NDGA (2 methyl groups on the alkyl linker) and de-Me-NDGA (0 methyl groups on the alkyl linker) and their respective dibenzocyclooctadienes formed via intramolecular cyclization.

3.3 Materials and Methods

3.3.1 **Materials**

Reduced glutathione (GSH), Thioflavin T, phosphate buffered saline (PBS), and K_2HPO_4 were purchased from Sigma-Aldrich while 2,2-di-(3-methoxymethylphenyl)-1,3-propanediol (MMPPD) and cyclized NDGA (cNDGA) were prepared following literature procedures [6,79].

Citric acid, HCl and $MgSO_4$ were purchased from Fisher Scientific. All solvents, including formic acid were LC-MS grade. α-Synuclein (> 95% purity) was purchased from rPeptide (Watkinsville, GA, USA). Water was purified via a Millipore (Mississauga, ON) Milli-Q system with a Quantum EX Cartridge**.** Diphenyl ethanes were prepared by modifications of literature procedures.

3.3.2 **Instrumentation**

3.3.2.1 HPLC-UV Diode Array Analysis

The autoxidation studies and reaction kinetics was performed on an Agilent 1200 high-performance liquid chromatography (HPLC) system (Agilent Technologies; Mississauga, ON) equipped with a degasser (G1379A), quaternary pump (G1311A), autosampler (G1329A), and diode array detector (G1315D). The HPLC column was a ThermoFisher Hypersil GOLD™ C_{18} (2.1 x 150 mm, 3µm), and the solvent system consisted of 0.1% LC-MS grade formic acid in water (solvent A) and 0.1% LC-MS grade formic acid in acetonitrile (solvent B) operating at a flow rate of 0.2 mL/min. Different methods were developed to ensure separation between the parent compounds and the oxidative metabolites. Method I: an initial isocratic condition at 90% solvent A for 5 minutes, decreased gradually to 60% solvent A over 5 minutes, then decreased to 10% over 15 minutes then returning to the initial conditions, with a 10 minute equilibration period prior to the next sample injection. Method II: an initial isocratic condition at 90% solvent A for 5 minutes, decreased gradually to 50% solvent A over 25 minutes, then 10% over 4 minutes then returning to the initial conditions, with a 7 minute equilibration period prior to the next sample injection. Method III: an initial isocratic condition at 90% solvent A for 2.5 minutes, decreased

gradually to 10% solvent A over 22.5 minutes, then returning to the initial conditions, with a 10 minute equilibration period prior to the next sample injection. HPLC data was exported from OpenLab CDS ChemStation Edition C.01.09 (Santa Clara, California, USA) to GraphPad Prism version 8.0 for data analysis (San Diego, California, USA).

3.3.2.2 ESI-MS Analysis

Mass spectroscopy analysis of intermediates was conducted using an AB SCIEX 4000 QTRAP (Redwood City, CA, USA) quadrupole linear ion trap mass spectrometer. Final compounds were analyzed on an AB SCIEX QSTAR XL quadrupole orthogonal time-of-flight hybrid mass spectrometer (Q-TOF MS) equipped with an electrospray ionization (ESI) source (AB SCIEX, Redwood City, CA, USA). Samples were infused directly using a flow of 10 μL/min. Data acquisition and analyses were performed using Analyst 1.7 software from AB SCIEX.

3.3.2.3 NMR Analysis

All NMR experiments were performed on a Bruker AVANCE DPX-500 spectrometer (Karlsruhe, Germany) and data processed using MestRreNova 14.1. All compounds were drawn and named using ChemDraw 20.0.

3.3.3 **Methods**

3.3.3.1 Synthesis and Characterization of Diphenyl Ethane Analogs

3.3.3.1.1 Synthesis of 4,4'-(ethane-1,2-diyl)bis(benzene-1,2-diol) (**DPE**)

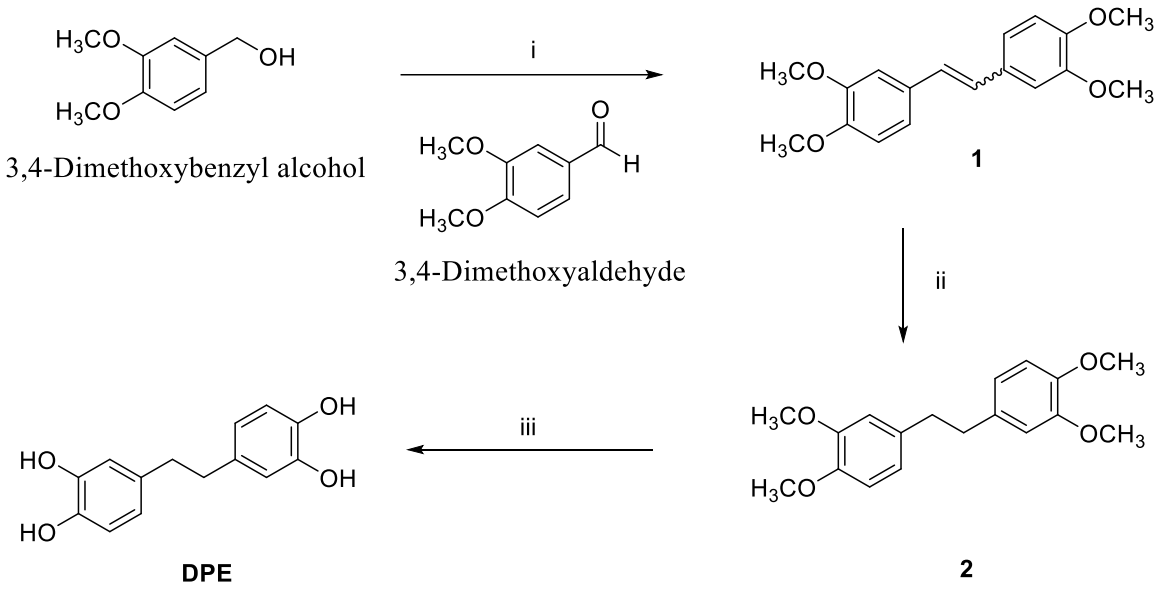

Scheme 3.1. Synthesis of DPE. Reagents and Conditions: i) NBS, PPh_3, K_2CO_3, toluene, reflux, 37%; ii) H_2, Pd/C, THF, rt, >99%; iii) BBr_3/CH_2Cl_2, -78 °C, 88%.

Synthesis of 1,2-bis(3,4-dimethoxyphenyl)ethene (1): To a stirred solution of 3,4-Dimethoxybenzyl alcohol (0.5 g, 2.97 mmol) and triphenylphosphine (1.87 g, 7.13 mmol) in toluene (15 mL), N-bromosuccinimide (0.29 g, 1.63 mmol) was added. The reaction mixture was refluxed under N_2 for 4 hours. After completion, the mixture was cooled to room temperature. At room temperature, 3,4-Dimethoxyaldehyde (0.49 g, 2.97 mmol) was added followed by K_2CO_3 (4.1 g, 29.7 mmol) and then refluxed overnight. After cooling to room temperature, toluene was removed under reduced pressure. The residue was dissolved in ethyl acetate, and washed with

brine and dried over $MgSO_4$. After evaporation of solvents, the residue was recrystallized using isopropanol to give yield alkene (*Z*)-**1** as a white solid (0.4 g, 37%). ^{1}H NMR (500 MHz, $CDCl_3$) δ 7.06 (d, *J* = 2.0 Hz, 2H), 7.04 (dd, *J* = 8.2, 2.0 Hz, 2H), 6.93 (s, 2H), 6.86 (d, *J* = 8.2 Hz, 2H), 3.95 (s, 6H), 3.91 (s, 6H). ^{13}C NMR (126 MHz, $CDCl_3$) δ 149.25, 148.82, 130.80, 126.77, 119.70, 111.36, 108.68, 56.10, 56.00. ESI-MS (*m/z*) 323.1 $[M + Na]^+$.

Synthesis of 1,2-bis(3,4-dimethoxyphenyl)ethane (2): Pd/C (10% w/w, 40 mg) was added to a reaction flask under N_2. The flask was sealed, and dry THF (10 mL) was added. The alkene **1** (400 mg, 1.33 mmol) in dry THF (2 mL) was added to the reaction dropwise. The flask was evacuated, then flushed with H_2 gas. The reaction was left to stir under H_2 overnight. The reaction mixture was filtered through a Celite pad and washed with MeOH. The solvent was removed under reduced pressure to give compound **2** as a white solid (0.4 g, 99%). ^{1}H NMR (500 MHz, $CDCl_3$) δ 6.79 (d, *J* = 8.1 Hz, 2H), 6.71 (dd, *J* = 8.0, 2.0 Hz, 2H), 6.66 (d, *J* = 2.0 Hz, 2H), 3.86 (s, 6H), 3.84 (s, 6H), 2.85 (s, 4H). ^{13}C NMR (126 MHz, $CDCl_3$) δ 148.66, 147.24, 134.55, 120.47, 112.02, 111.27, 56.07, 55.94, 37.88.

Synthesis of 4,4'-(ethane-1,2-diyl)bis(benzene-1,2-diol) (DPE): To a solution of **2** (0.4 g, 1.32 mmol) in dry CH_2Cl_2 (15 mL) at –78 °C under N_2, BBr_3 (5.3 mL, 5.28 mmol) was added dropwise. The reaction mixture was stirred and allowed to warm to room temperature overnight. After completion, the reaction mixture was poured onto crushed ice and extracted with ethyl acetate (3 × 15 mL). The organic layer was washed with water and brine and dried over Na_2SO_4 to give **DPE** as a purple solid (0.28 g, 88%). ^{1}H NMR (500 MHz, CD_3CN) δ 6.69 (d, *J* = 8.0 Hz, 2H), 6.64 (d,

J = 2.0 Hz, 2H), 6.54 (dd, *J* = 8.0, 2.0 Hz, 2H), 6.50 (s, 2H), 6.44 (s, 2H), 2.70 (s, 4H). ^{13}C NMR (126 MHz, CD_3CN) δ 145.10, 143.28, 135.18, 120.96, 116.32, 115.88, 37.85. HRMS (TOF ESI-MS) calcd for $C_{14}H_{14}O_4$ $(M+CH_3OH)^+$ 279.0892, found 279.0953.

3.3.3.1.2 Synthesis of 2,3-Bis(3,4-dihydroxyphenyl)butane (**M2-DPE**)

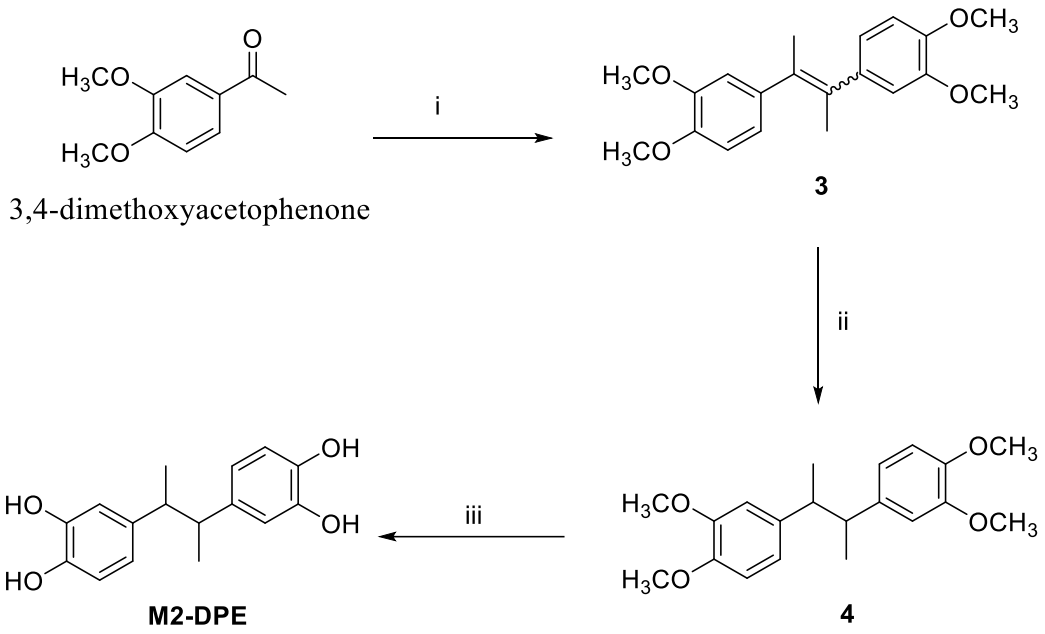

3,4-dimethoxyacetophenone

Scheme 3.2. Synthesis of M2-DPE. *Reagents and Conditions:* i) $TiCl_4$, Zinc, THF, -78 °C, 43%; ii) H_2, Pd/C, THF, rt, >99%; iii) BBr_3/CH_2Cl_2, -78 °C, 88%.

Synthesis of 4,4'-(but-2-ene-2,3-diyl)bis(1,2-dimethoxybenzene) (3): To a suspension of zinc powder (233.5 mg, 3.57 mmol) in dry THF (10 mL) at –78 °C under N_2, $TiCl_4$ (1.8 mL, 1.83 mmol) was added dropwise. Reaction was stirred at room temperature for 30 minutes and then refluxed.

To this refluxing mixture, a solution of 3,4-dimethoxyacetophenone (100 mg, 0.55 mmol) in dry THF (2 mL) was added, and the reaction mixture was refluxed overnight under N_2. After cooling to room temperature, the mixture was cooled to 0 °C. HCl 1M (30 mL) was added and then ethyl acetate (30 mL). After stirring at room temperature for 30 minutes, the mixture was filtered through a Celite pad. The aqueous layer was extracted with ethyl acetate (3 × 15 mL) and the organic layer was dried over Na_2SO_4. Solvent was evaporated, and the residue was purified by flash column chromatography (1:1 CH_2Cl_2/EtOAc) to afford **3** as a yellow oil (70 mg, 43%). ^{1}H NMR (500 MHz, $CDCl_3$) δ 6.65 (d, *J* = 8.3 Hz, 2H), 6.59 (dd, *J* = 8.2, 2.0 Hz, 2H), 6.46 (d, *J* = 2.0 Hz, 2H), 3.80 (s, 6H), 3.58 (s, 6H), 2.15 (s, 6H). ^{13}C NMR (126 MHz, $CDCl_3$) δ 148.77, 147.37, 121.13, 119.67, 111.08, 110.96, 56.03, 55.74, 47.06, 20.88. ESI-MS (*m/z*) 351.0 $[M + Na]^+$.

Synthesis of 4,4'-(butane-2,3-diyl)bis(1,2-dimethoxybenzene) (4): Pd/C (10% w/w, 7 mg) was added to a reaction flask under N_2. The flask was sealed, and dry THF (10 mL) was added. The alkene **3** (70 mg, 0.21 mmol) in dry THF (1 mL) was added to the reaction dropwise. The flask was evacuated, then flushed with H_2 gas. Reaction was left to stir under H_2 overnight. The reaction mixture was filtered through Celite pad and washed with MeOH (50 mL). The solvent was removed under pressure to give compound **4** as a white solid (66 mg, 60%). ^{1}H NMR (500 MHz, $CDCl_3$) δ 6.82 (d, *J* = 8.2 Hz, 2H), 6.74 (dd, *J* = 8.1, 2.0 Hz, 2H), 6.68 (d, *J* = 2.0 Hz, 2H), 3.88 (s, 6H), 3.87 (s, 6H), 2.75 – 2.70 (m, 2H), 1.04 (d, *J* = 6.6 Hz, 6H). ^{13}C NMR (126 MHz, $CDCl_3$) δ 148.79, 147.37, 139.14, 119.67, 111.08, 110.96, 56.03, 55.99, 47.07, 20.89. ESI-MS (*m/z*) 353.2 $[M + Na]^+$.

Synthesis of 4,4'-(butane-2,3-diyl)bis(benzene-1,2-diol) (M2-DPE): To a solution of **4** (66 mg, 0.19 mmol) in dry CH_2Cl_2 (5 mL) at –78 °C under N_2, BBr_3 (0.8 mL, 0.79 mmol) was added dropwise. The reaction mixture was stirred and allowed to warm to room temperature overnight. After completion, reaction mixture was poured onto crushed ice and extracted with ethyl acetate (3 × 15 mL). The organic layer was washed with water (15 mL) and brine (15 mL) and dried over $MgSO_4$ to give **M2-DPE** as a purple solid (11 mg, 20%). ^{1}H NMR (500 MHz, CD_3CN) δ 6.74 (d, *J* = 8.1 Hz, 2H), 6.70 (d, *J* = 2.0 Hz, 2H), 6.60 (dd, *J* = 8.1, 2.1 Hz, 2H), 6.49 (s, 2H), 6.47 (s, 2H), 2.62 – 2.57 (m, 2H), 0.91 (d, *J* = 6.5 Hz, 6H).^{13}C NMR (126 MHz, CD_3CN) δ 145.18, 143.31, 140.11, 120.09, 115.86, 115.23, 47.20, 21.51. HRMS (TOF ESI-MS) calcd for $C_{16}H_{18}O_4$ $(M-H)^-$ 273.1205, found 273.1130.

3.3.3.1.3 Synthesis of 4,4'-(2,3-dimethylbutane-2,3-diyl)bis(benzene-1,2-diol) (**M4-DPE**)

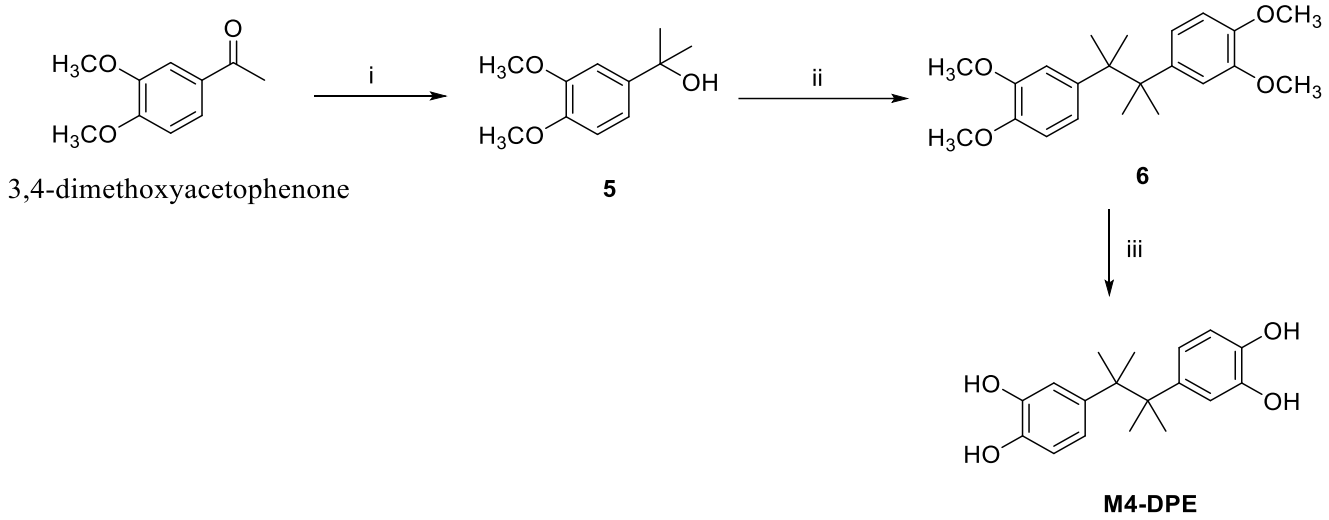

3,4-dimethoxyacetophenone **5** **6** **M4-DPE**

Scheme 3.3. Synthesis of M4-DPE. *Reagents and Conditions:* i) $MgCH_3I$, Et_2O, rt, 41%; ii) $TiCl_4$, Zinc, THF, -78 °C, 20%; iii) BBr_3/CH_2Cl_2, -78 °C, 91%.

Synthesis of 2-(3,4-dimethoxyphenyl)propan-2-ol (5): Magnesium turnings (31 mg, 1.27 mmol) were added to an oven-dried flask with 5 mL of ether. Iodomethane (181 mg, 1.27 mmol) was dissolved in ether (3 mL) and added dropwise to the reaction. Magnesium turnings were crushed with a glass rod, and the reaction initiated. After completion, the reaction mixture was cooled to 0 °C and 3,4-dimethoxyacetophenone (91 mg, 0.5 mmol) were added dropwise under N_2. After stirring overnight, the reaction mixture was cooled 0 °C and 2 M HCl (2 mL) was added dropwise, and the mixture extracted with ethyl acetate (3 × 15 mL). The organic layer was dried over $MgSO_4$, and solvent evaporated. The residue was purified by flash column chromatography (2:1 hexane/EtOAc) to afford **5** as a yellow oil (40 mg, 41%). ^{1}H NMR (500 MHz, $CDCl_3$) δ 7.09 (d,

J = 2.2 Hz, 1H), 6.98 (dd, *J* = 8.3, 2.2 Hz, 1H), 6.83 (d, *J* = 8.4 Hz, 1H), 3.91 (s, 4H), 3.88 (s, 3H), 1.58 (s, 6H). ^{13}C NMR (126 MHz, $CDCl_3$) δ 148.77, 147.85, 142.06, 116.46, 110.75, 108.34, 72.51, 56.05, 56.01, 31.94. ESI-MS (*m/z*) 219.1 $[M + Na]^+$.

Synthesis of 4,4'-(2,3-dimethylbutane-2,3-diyl)bis(1,2-dimethoxybenzene) (6): To a suspension of zinc powder (87.6 mg, 1.34 mmol) in dry THF (10 mL) at –78 °C under N_2, $TiCl_4$ (0.7 mL, 0.68 mmol) was added dropwise. The reaction was stirred at room temperature for 30 minutes and then refluxed. To this refluxing mixture, a solution of the tertiary alcohol **5** (40 mg, 0.2 mmol) in dry THF (1 mL) was added, and the reaction mixture was refluxed overnight under N_2. After cooling to room temperature, the mixture was cooled to 0 °C. HCl 1 M (10 mL) was added and then ethyl acetate (15 mL). After stirring at room temperature for 30 minutes, the mixture was filtered through a Celite pad. The aqueous layer was extracted with ethyl acetate (3 × 15 mL) and the organic layer was dried over $MgSO_4$. The solvent was evaporated, and the residue was purified by flash column chromatography (4:1 hexane/EtOAc) to afford **6** as a yellow oil (17 mg, 20 %). ^{1}H NMR (500 MHz, $CDCl_3$) δ 6.71 (d, *J* = 8.5 Hz, 1H), 6.64 (dd, *J* = 8.4, 2.2 Hz, 1H), 6.39 (d, *J* = 2.2 Hz, 1H), 3.85 (s, 3H), 3.66 (s, 3H), 1.32 (s, 6H). ^{13}C NMR (126 MHz, $CDCl_3$) δ 146.97, 146.96, 139.73, 121.04, 113.04, 109.42, 55.93, 55.75, 43.71, 25.42. ESI-MS (*m/z*) 381.2 $[M + Na]^+$.

Synthesis of 4,4'-(2,3-dimethylbutane-2,3-diyl)bis(benzene-1,2-diol) (M4-DPE): To a solution of **6** (17 mg, 0.04 mmol) in dry CH_2Cl_2 (5 mL) at –78 °C under N_2, BBr_3 (0.2 mL, 0.19 mmol) was added dropwise. The reaction mixture was stirred and allowed to warm to room temperature

overnight. After completion, the reaction mixture was poured onto crushed ice and extracted with ethyl acetate (3 × 15 mL). The organic layer was washed with water (15 mL) and brine (15 mL) and dried over $MgSO_4$ to give **M4-DPE** as a purple solid (13 mg, 91 %). ^{1}H NMR (500 MHz, CD_3CN) δ 6.62 (d, *J* = 8.3 Hz, 2H), 6.53 (d, *J* = 2.3 Hz, 2H), 6.49 (dd, *J* = 8.4, 2.4 Hz, 2H), 1.20 (s, 12H). ^{13}C NMR (126 MHz, CD_3CN) δ 143.46, 142.93, 140.26, 121.37, 117.14, 114.13, 43.74, 25.88. HRMS (TOF ESI-MS) calcd for $C_{18}H_{22}O_4$ $(M-H)^-$ 301.1518, found 301.1438.

3.3.3.1.4 Synthesis of 2,3,6,7-tetrahydroxy-9,10-dihydrophenanthrene (**o-DPE B**)

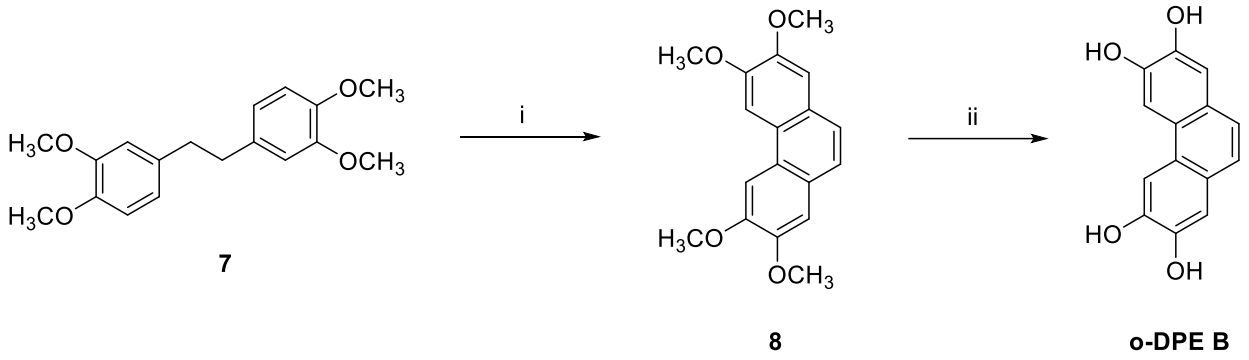

Scheme 3.4. Synthesis of o-DPE-B. *Reagents and Conditions:* i) $BF_3{\cdot}OEt_2$, PIFA, CH_2Cl_2, -20 °C, 11%; ii) BBr_3/ CH_2Cl_2, -78 °C, 92%

Synthesis of 2,3,6,7-tetramethoxyphenanthrene (8): First, a solution of PIFA (365.5 mg, 0.85 mmol) and $BF_3{\cdot}OEt_2$ (0.16 mL, 1.3 mmol) in CH_2Cl_2 (2 mL) was prepared and cooled at -20 °C. This solution was added dropwise over 15 minutes to another solution in CH_2Cl_2 (5 mL) containing **7** (172.3 mg, 0.57 mmol) at -20 °C under nitrogen. The solution was stirred at -20 °C for 40

minutes. After completion, the solvent was removed under pressure, and the residue purified by flash column chromatography (1:2 EtOAc/hexane) to afford **8** as a yellow solid (86 mg, 51 %). ^{1}H NMR (500 MHz, CDCl3) δ 7.81 (s, 1H), 7.56 (s, 1H), 7.23 (s, 1H), 4.13 (s, 3H), 4.04 (s, 3H).

Synthesis of phenanthrene-2,3,6,7-tetraol (o-DPE B): To a solution of **8** (20 mg, 0.067 mmol) in dry CH_2Cl_2 (2 mL) at –78 °C under N_2, BBr_3 (0.26 mL, 0.268 mmol) was added dropwise. The reaction mixture was stirred and allowed to warm to room temperature overnight. After completion, reaction mixture was poured onto crushed ice and extracted with ethyl acetate (3 × 15 mL). The organic layer was washed with water (15 mL) and brine (15 mL) and dried over $MgSO_4$ to give **o-DPE B** as a brown solid (15 mg, 92%). ^{1}H NMR (500 MHz, MeOD) δ 7.77 (s, 1H), 7.29 (s, 1H), 7.11 (s, 1H). ^{13}C NMR (126 MHz, MeOD) δ 147.06, 146.26, 127.41, 125.75, 124.29, 112.73, 107.40. ESI-MS (*m/z*) 241.02 $[M - H]^-$.

3.3.3.2 Chemical Stability and Reaction Kinetics

Test compounds in CH_3CN (20 mM) were incubated in phosphate-citric acid buffer (0.5 M, pH 7.4) at 37 °C to yield a final concentrations of 0.5 mM each [4]. Before adding the compound, buffer was treated under three conditions: nitrogen purged, oxygen purged or ambient conditions (no purging). The mixture was then incubated at 37 ºC using an orbital shaker (VWR). Aliquots (90 µL) were taken at different times and quenched by adding 2M HCl (30 µL) spiked with internal standard 2,2-di-(3-methoxymethylphenyl)-1,3-propanediol (MMPPD). The samples were analyzed directly by HPLC-UV. The kinetics of the loss of the diphenylethanes were established from the concentration that remained in the buffer solution over time [4]. The loss of diphenylethanes in buffer at pH 7.4 follows apparent first-order kinetics. Therefore, the rate of loss can be described by:

$$ln\frac{C}{C_o} = -k_{dep} \quad (3.1)$$

where C_0 and C are initial concentration and concentration at time t respectively; k_{dep} is the reaction rate for loss of starting material and t is time. k_{dep} was obtained as the gradient from a plot of ln $(\frac{C}{C_o})$ as a function of time t.

3.3.3.3 Quantification of DPEs and autoxidation products

Standard curves were prepared in triplicates for the DPEs (DPE, M2-DPE, and M4-DPE) ranging from 10 to 500 µM at a wavelength of 280 nm, and for o-DPE B ranging from 10 to 100 µM at a wavelength of 254 nm. Calibration curves were calculated by using linear regression analysis using GraphPad Prism version 8.0 (San Diego, California, USA).

3.3.3.4 Thioflavin T Assay

The protein α-synuclein (AS) was diluted in phosphate buffered saline (PBS) at a concentration of 2 mg/mL. Experiments were performed in triplicate with or without test compounds at final concentrations of 100 and 500 μM in PBS at pH 7.4. Both drug and protein were added to a microcentrifuge tube producing 1.5 mg/mL of AS. The mixture was incubated for 5 days at 37 °C shaking at 1400 rpm using a Thermomixer R (Eppendorf, Hamburg, Germany). Upon completion, 10 μL of each mixture was pipetted in triplicate onto a 96-well plate containing 144 μL of Thioflavin-T (ThT) solution (26 μM). The fluorescence was measured with a plate reader at excitation of 444 nm and emission of 484 nm. Data analysis was performed by averaging the readings per tube and comparing with control and/or different concentrations using one-way ANOVA followed by Dunnett's test.

3.4 Results

3.4.1 Synthesis and characterization of diphenylethane analogs

We prepared three diphenylethane analogs (DPE, M2-DPE, M4-DPE, Figure 3.2), all three were prepared through coupling reactions involving 3,4-dimethoxyphenyl derivatives.

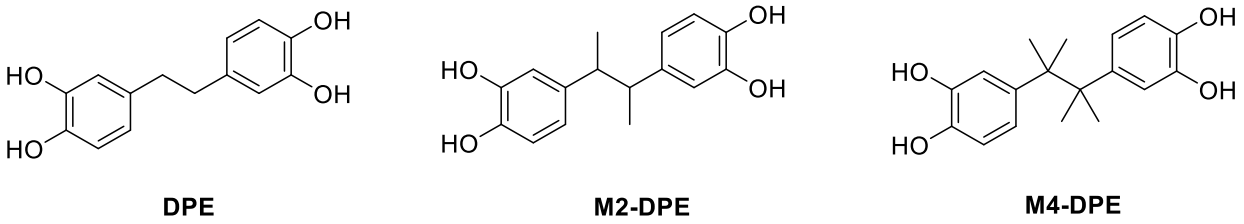

Figure 3.2. Proposed diphenylethanes with 0 (DPE), 2 (M2-DPE), and 4 (M4-DPE) methyl groups on the side chain.

The diphenylethane derivative with no substituents on the alkyl linker chain(DPE) was prepared using a literature procedure for the preparation of the tetramethoxy precursor (Scheme 3.1) [78]. We employed a Wittig reaction between 3,4-dimethoxybenzyl alcohol and 3,4-dimethoxybenzaldehyde in the first step to yield the tetramethoxyalkene intermediate as a white solid in 37% yield. The alkene was hydrogenated over Pd/C under H_2 atmosphere to give the corresponding saturated compound in 99% yield. We obtained the final compound, DPE, through boron tribromide demethylation of the tetramethoxyalkane intermediate in DCM at -78 °C in 88% yield for a 32% overall yield. We confirmed that we had DPE through high-resolution time-of-flight electrospray mass spectrometry (negative mode) which yielded an *m/z* of 279.0953. In our ^{1}H NMR we observed aromatic C-H signals at δ6.69, 6.64 and 6.54, aromatic OH signals at δ6.50 and 6.44 and a benzyl H signal at δ2.70. Due to the symmetry of DPE, the benzyl protons appear as a singlet corresponding to 4H.

We prepared 2,3-bis(3,4-dihydroxyphenyl)butane (M2-DPE) by first carrying out a McMurray coupling using Zn and $TiCl_4$ to combine 2 molecules of 3,4-dimethoxyacetophenone to produce the alkene intermediate in 43 % yield (Scheme 3.2) [80]. We isolated the *Z*-isomer based on comparison with the literature coupling constants, but we observed a negligible amount of *E*-isomer and therefore did not collect it. We subsequently reduced the alkene to a mixture of alkane isomers (meso and racemic) via hydrogenation over Pd/C in 60% yield and the methoxy groups were removed with boron tribromide to give M2-DPE (20% yield) to give 23% overall yield. We confirmed the structure of M2-DPE through high-resolution time-of-flight electrospray mass spectrometry (negative mode) which gave an *m/z* of 273.1130. We further confirmed the structure from observed NMR signals at δ6.74, 6.70, 6.60 (aromatic C-H), δ6.49, 6.47 (aromatic OH), δ2.57-2.62 (benzyl H) and δ0.91 (CH_3). Unlike DPE, the benzyl protons of M2-DPE appear as a multiplet from δ2.57-2.62 due to coupling with the adjacent methyl protons (δ0.91) and the mixture of meso and racemic isomers.

The starting material needed for M4-DPE, 2-(3,4-dimethoxyphenyl)propan-2-ol, was prepared via methylmagnesium iodide methylation of 3,4-dimethoxyacetophenone in 41% yield (Scheme 3.5) [81]. We then coupled two 2-(3,4-dimethoxyphenyl)propan-2-ol units by treatment with Zn and $TiCl_4$ at -78 °C in dry THF to produce the tetramethoxyalkane-linked product (20% yield). The dicatechol was realized via boron tribromide deprotection of the methoxy groups (91% yield) for an overall yield of 7%. We confirmed the structure of M4-DPE through high-resolution time-of-flight electrospray mass spectrometry (negative mode) which gave an *m/z* of 301.1438. Similar to DPE, M4-DPE is symmetrical so that the methyl groups appear as a singlet of 12H at δ1.20.

DPE and M4-DPE exist as single entities however M2-DPE is likely present as a mixture of the meso compound and a racemic mixture; we could not separate the isomers so the isomeric mixture was used for the autoxidation experiments.

3.4.2 Autoxidation of diphenylethane analogs

3.4.2.1 Rates of autoxidation of diphenylethanes at pH 7.4

The three dicatechol diphenylethanes, DPE, M2-DPE, and M4-DPE, were investigated for their ability to autoxidize to their corresponding dibenzocyclohexadienes. The spontaneous cyclization in buffer was carried out using a protocol already established in our group [4]. DPE, M2-DPE, or M4-DPE and internal standard (MMPPD) were incubated in phosphate-citric acid buffer (0.5 M, pH 7.4) at 37 °C to a final concentration of 0.5 mM each. Aliquots were taken at different times for DPE, M2-DPE, and M4-DPE (Table S1). The reaction was stopped by acidifying to pH 1.5 with HCl. Samples were analyzed by HPLC using Method I (DPE and M4-DPE) or Method II (M2-DPE) (Table S2). Each compound was investigated under three conditions: (i) N_2 purged, (ii) O_2 purged and (iii) ambient conditions to confirm that loss of starting material was an autoxidative process.

The autoxidation kinetics were determined by following the loss of starting compound in phosphate-citric acid buffer over time, which was calculated using peak area ratio of starting compound and internal standard. The rate of loss (k_{dep}) of DPE, M2-DPE and M4-DPE followed pseudo first-order kinetics. Figure 3.3 shows the results for the loss of starting dicatechol diphenylethane against time.

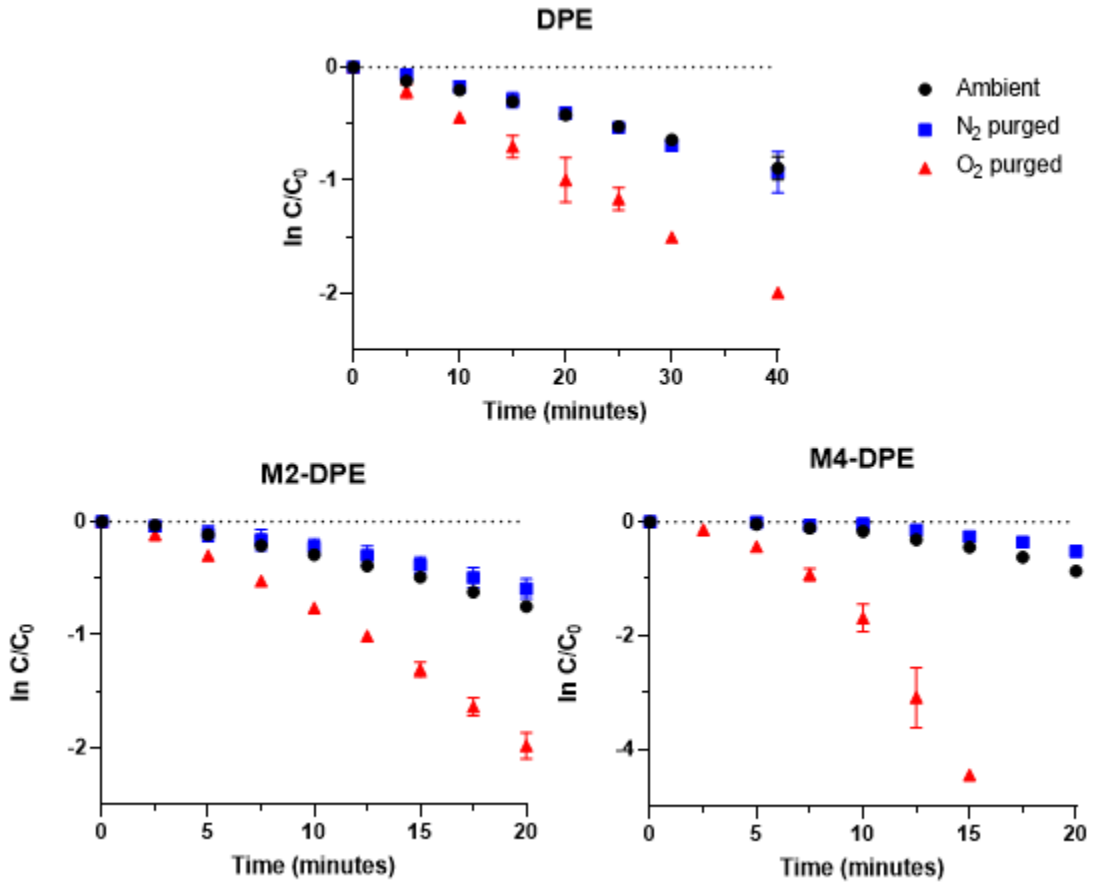

Figure 3.3. Plot of ln C/C_0 *vs* time of DPE (n=3), M2-DPE (n=3), and M4-DPE (n=3) in phosphate-citric buffer (pH 7.4) at 37 ºC using different experimental conditions.

For all three compounds, the loss of diphenylethane starting material occurs most rapidly for the O_2 purged sample; the rate of loss for the N_2 purged samples was the slowest although the difference compared to the ambient conditions is small (Table 3.1). The ratio of the O_2 purged versus the N_2 purged rates ($k_{dep}(O_2)/k_{dep}$ (N_2)) is: 1.55 (DPE); 2.33 (M2-DPE); 4.48 (M4-DPE). Our data show that the rate of loss is dependent on the number of methyl groups on the alkyl linker as the rate of decomposition increases with the number of methyl groups for all three experimental conditions.

Table 3.1. Autoxidation rate of DPE (n=3), M2-DPE (n=3), and M4-DPE (n=3) in phosphate-citric acid buffer (pH 7.4) at 37 ºC using different experimental conditions.

Compound	**Ambient**		**Nitrogen**		**Oxygen**	
	k_{dep} (min^{-1})	$t_{1/2}$ (min)	k_{dep} (min^{-1})	$t_{1/2}$ (min)	k_{dep} (min^{-1})	$t_{1/2}$ (min)
DPE	$2.87 \times 10^{-2} \pm 0.0006$	24.14	$2.84 \times 10^{-2} \pm 0.0012$	24.4	$4.4 \times 10^{-2} \pm 0.0011$	15.75
M2-DPE	$6.16 \times 10^{-2} \pm 0.0016$	11.25	$4.93 \times 10^{-2} \pm 0.0033$	14.05	$1.15 \times 10^{-1} \pm 0.0057$	6.02
M4-DPE	$9.0 \times 10^{-2} \pm 0.012$	7.7	$6.53 \times 10^{-2} \pm 0.0061$	10.61	$2.93 \times 10^{-1} \pm 0.0173$	2.36

3.4.2.2 Products of diphenylethane autoxidation at pH 7.4

We hypothesized that the dicatechol diphenylethane derivatives would undergo intramolecular cyclization to dibenzocyclohexadienes at pH 7.4. We determined that for DPE three distinct products resulted from autoxidation (Figure 3.4), whereas two distinct products were formed for each of M2-DPE (Figure 3.5) and M4-DPE (Figure 3.6).

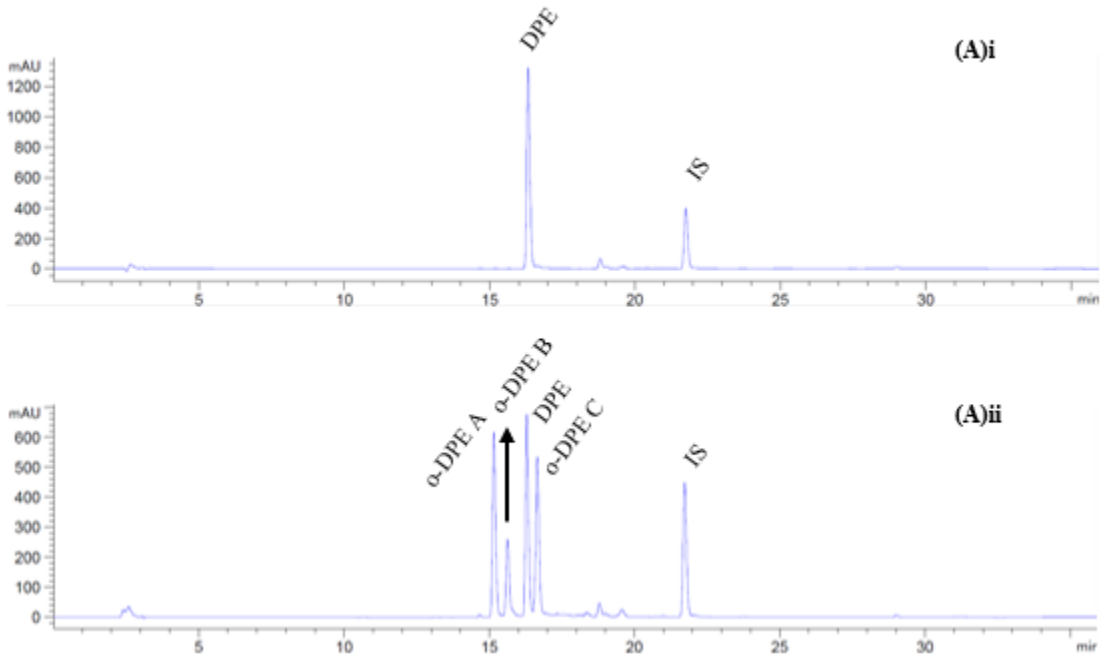

Figure 3.4. HPLC chromatogram for DPE incubation (pH 7.4) at 37 ºC at time 0 (i) and 20 minutes (ii). DPE retention time was observed at 16.3 minutes, while for its oxidized products were 15.1 minutes (o-DPE A), 15.6 minutes (o-DPE B), and 16.6 minutes (o-DPE C). IS is the internal standard (MMPPD) at 21.7 minutes.

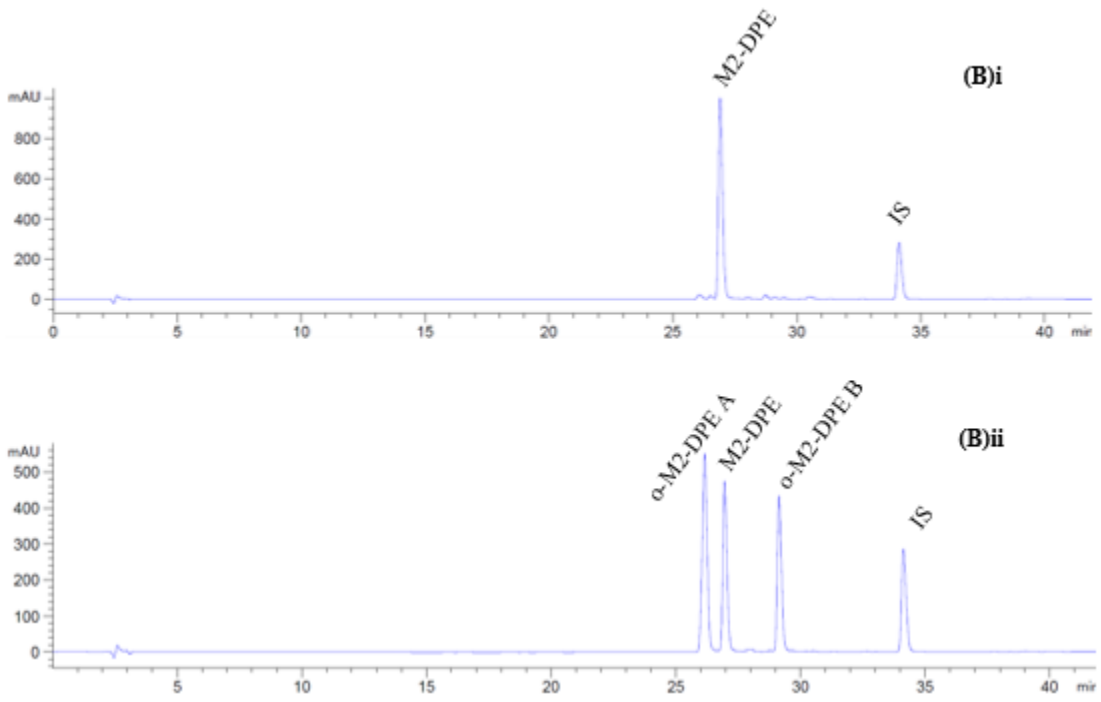

Figure 3.5. HPLC chromatogram for M2-DPE incubation (pH 7.4) at 37 ºC at time 0 (i) and 10 minutes (ii). M2-DPE retention time was observed at 26.9 minutes, while for its oxidized products were 26.1 minutes (o-M2-DPE A) and 29.1 minutes (o-M2-DPE B). IS is the internal standard (MMPPD) at 34.1 minutes.

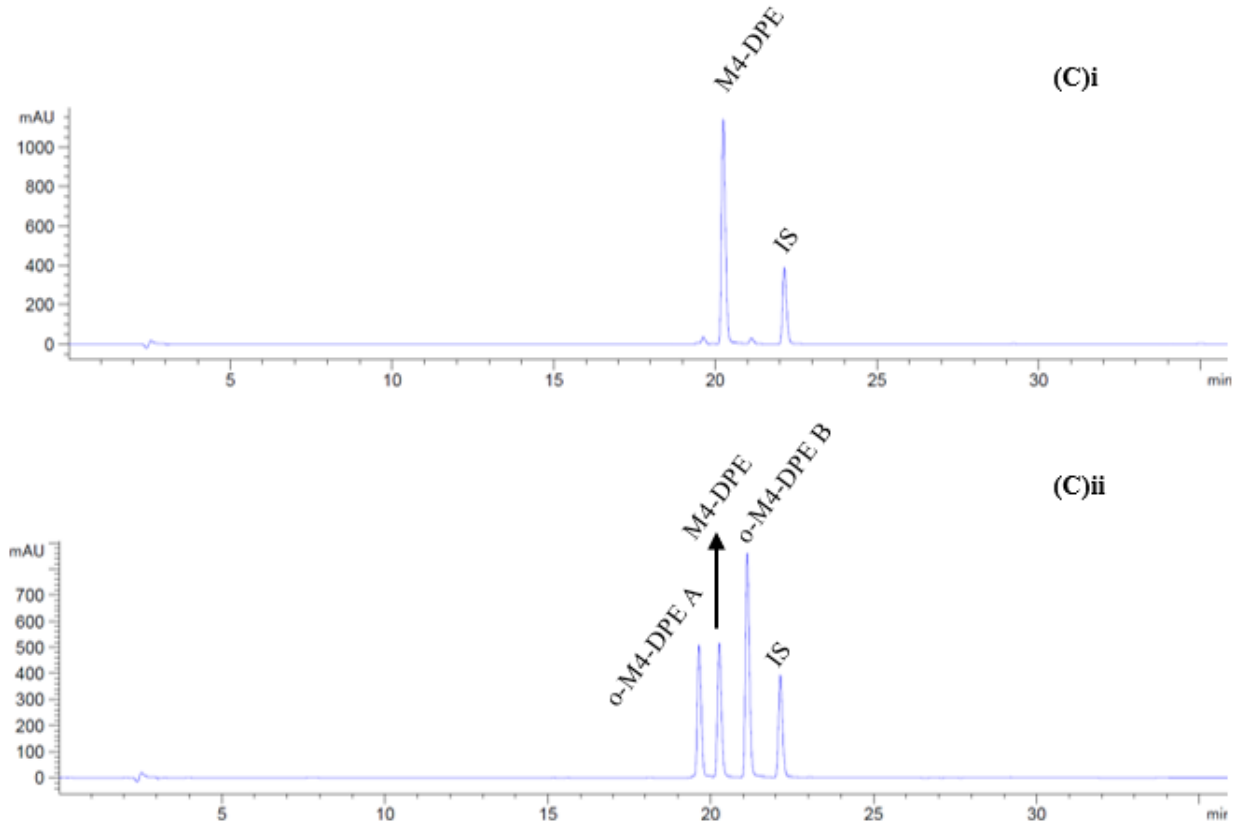

Figure 3.6. HPLC chromatogram for M4-DPE incubation (pH 7.4) at 37 ºC at time 0 (i) and 7.5 minutes (ii). M4-DPE retention time was observed at 20.2 minutes, while for its oxidized products were 19.6 minutes (o-M4-DPE A) and 21.1 minutes (o-M4-DPE B). IS is the internal standard (MMPPD) at 22.1 minutes.

For our dicatechol diphenylethanes, we isolated the product peaks through reverse-phase preparative chromatography and analyzed the isolated products via HPLC, NMR and mass spectrometry. Several of the decomposition products displayed poor solubility in typical NMR solvents (chloroform, acetonitrile, methanol, DMSO) so we used a mixed solvent system consisting of D_2O, CD_3CN and DCl. All of our compounds were soluble in this mixed system allowing us to compare NMR spectra across the DPE derivatives and their autoxidation products. Since the compounds were stable in an acidic

environment (HCl was used to quench the autoxidation reaction) we observed no stability issues with the D_2O/ CD_3CN/ DCl solvent system. However, products o-M2-DPE A and o-M4-DPE A still displayed limited solubility in the solvent system, and due to the low concentration we were unable to generate satisfactory ^{13}C NMR.

3.4.2.2.1 Autoxidation products of **DPE**

DPE formed three autoxidation products (Figure 3.7), two were formed directly from DPE (o-DPE-A and o-DPE-C). When we subsequently exposed isolated o-DPE-A and o-DPE-C to our autoxidation conditions we observed that o-DPE-A formed o-DPE-B, whereas o-DPE-C formed an additional product which was trapped as a GSH adduct (see section 3.4.2.4). o-DPE-A had an ESI (-) *m/z* 242.9 corresponding to a MW of 244, and the ^1H NMR showed aromatic singlets at δ6.60 and δ7.02 each representing one proton and a singlet at δ2.61 of four protons. This was consistent with intramolecular cyclization to form the dibenzocyclohexadiene 2,3,6,7-tetrahydroxy-9,10-dihydrophenanthrene. o-DPE-B had an ESI (-) *m/z* of 241.02 corresponding to a MW of 242 and a ^1H NMR showing three aromatic singlets at δ7.11, δ7.29 and δ7.77 consistent with aromatization of the cyclohexadiene ring to form 2,3,6,7-tetrahydroxy-phenanthrene. This was confirmed through formation of the phenanthrene using the method of Zeng & Chemler (2008) [82] which was identical to o-DPE-B (Scheme 3.4).

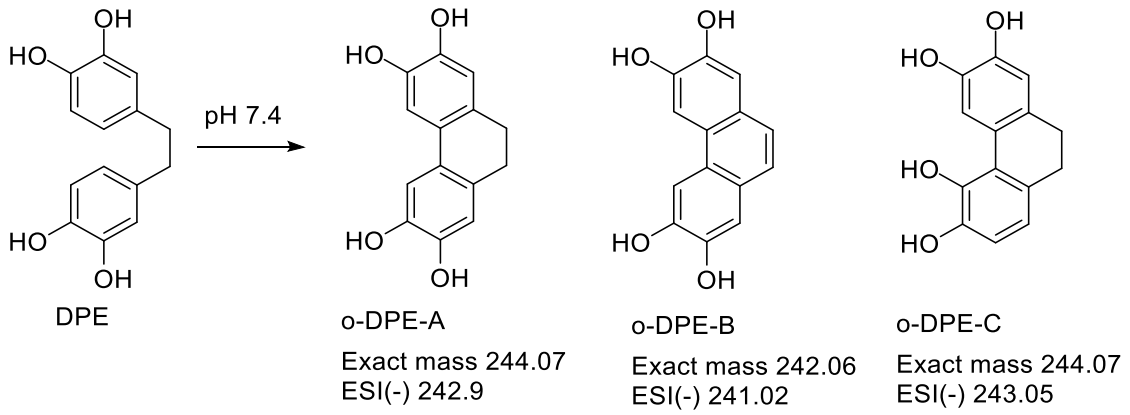

Figure 3.7. DPE and its oxidized products formed in phosphate buffer (pH 7.4) at 37 ºC. Exact mass and *m/z* (ESI negative ion mode) are shown for each product.

Finally, we investigated o-DPE-C which was formed directly from DPE. We determined that o-DPE-C had an ESI (-) *m/z* of 243.05 corresponding to a MW of 244 and ^{1}H NMR that in the aromatic region showed a pair of doublets at δ7.15 and δ7.21 of one proton each and singlets at δ7.25 and δ8.44 of one proton each and a multiplet at δ3.13 of four protons corresponding to the CH_2 protons. This suggested to us that intramolecular cyclization had occurred, but that substitution had occurred at different positions on the aromatic rings. Our HSQC and COSY results supported this observation leading us to conclude that o-DPE-C is 2,3,5,6-tetrahydroxy-9,10-dihydrophenanthrene. Unlike o-DPE-A, we did not observe formation of a corresponding aromatized product derived from o-DPE-C.

3.4.2.2.2 Autoxidation products of M2-DPE

The two HPLC peaks observed for the M2-DPE autoxidation elute at 26.1 min (o-M2-DPE-A) and 29.1 min (o-M2-DPE-B), whereas M2-DPE elutes at 26.9 min. For o-M2-DPE-A we observed an ESI (-) *m/z* 269.0 corresponding to a MW of 270 and for o-M2-DPE-B we observed an ESI (-) *m/z* 271.07,

corresponding to a MW of 272. For o-M2-DPE-A we observed that the ^{1}H NMR was similar to o-DPE-B as there were two aromatic singlets (δ7.38 and 7.79) each integrating to one proton, a singlet at δ2.49 integrating to three protons and a singlet at δ8.12 (1H). Together these results in addition to the lack of aliphatic C-H signals suggested to us the o-M2-DPE-A is 2,3,6,7-tetrahydroxy-9,10-dimethylphenanthrene. In contrast, we observed that o-M2-DPE-B displayed ^{1}H NMR characteristics similar to o-DPE-C with doublets at δ6.57 and δ6.67 integrating to one proton each and singlets at δ6.68 and δ7.85 or 8.25 integrating to one proton each. In addition, multiplets at δ1.2-1.29 (3H), δ2.61-2.65 (1H) and δ2.7-2.73 (3H) correspond to CH_3 and CH. From this data we concluded that o-M2-DPE-B is 2,3,5,6-tetrahydroxy-9,10-dimethylphenanthrene (Figure 3.8).

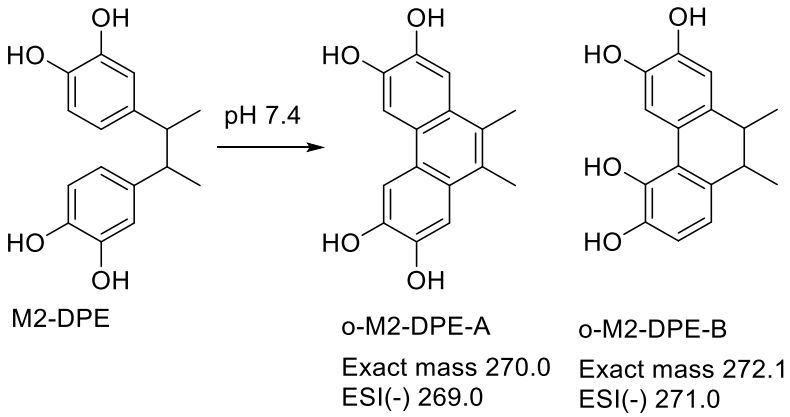

Figure 3.8. M2-DPE and its oxidized products formed in phosphate buffer (pH 7.4) at 37 ºC. Exact mass and *m/z* (ESI negative ion mode) are shown for each product.

These results are consistent with intramolecular cyclization and formation of a new C-C bond between the aromatic rings. Our ^{1}H NMR analysis was complicated by the potential presence of both meso and racemic M2-DPE starting material. In the cyclized products loss of free rotation of the alkyl linker may be anticipated to result in different chemical shifts and coupling constants for meso and

racemic o-M2-DPEs. The methyl groups of the *meso* o-M2-DPE-B would be in axial/equatorial positions leading to the benzyl protons adopting dihedral torsion angles of approximately 45°; the racemic o-M2-DPE-B would likely place the methyl groups in a di-axial position with the dihedral torsion angles of the benzyl protons closer to 60°. From the Karplus equation we would anticipate a coupling constant for the benzyl protons of approximately 6-10 Hz for the potential products. In the chemical shift range 2.6-2.7 we can observe overlapping doublets of quartets, but we were unable to calculate the coupling constant due to the presence of the mixture of diastereomers.

3.4.2.2.3 Autoxidation products of M4-DPE

Since the alkyl linker of M4-DPE already possesses adjacent dimethyl substituted carbons we anticipate that a fully aromatized cyclic product analogous to o-DPE-B and o-M2-DPE A could not be formed. We observed two HPLC peaks for M4-DPE autoxidation that elute at 19.6 min (o-M4-DPE-A) and 21.1 min (o-M4-DPE-B), whereas M4-DPE elutes at 20.2 min. For o-M4-DPE-A we observed an ESI (-) *m/z* 299.08 (MW 300) and for o-M4-DPE-B we observed an ESI (-) *m/z* 299.1 (MW 300). This suggested that both autoxidation products are consistent with intramolecular cyclization and formation of a new C-C bond between the aromatic rings. Our ^{1}H NMR for o-M4-DPE-A displayed aromatic singlets at δ6.82 (1H) and δ7.03 (1H) and singlets at δ3.23 (3H) and δ8.12 (1H). For o-M4-DPE-B the ^{1}H NMR displayed doublets at δ6.67 (1H) and δ6.73 (1H) and a singlet at δ6.83 (1H) in the aromatic region, and singlets at δ7.87 (1H) and δ8.12 (1H). We observed singlets at δ0.72, δ0.76, δ1.29 and δ1.30 each integrating to three protons that correspond to the four CH_3 groups. Together these results suggested to us that o-M4-DPE-A is 2,3,6,7-tetrahydroxy-9,9,10,10-tetramethylphenanthrene and o-M4-DPE-B is 2,3,5,6-tetrahydroxy-9,9,10,10-tetramethylphenanthrene (Figure 3.9).

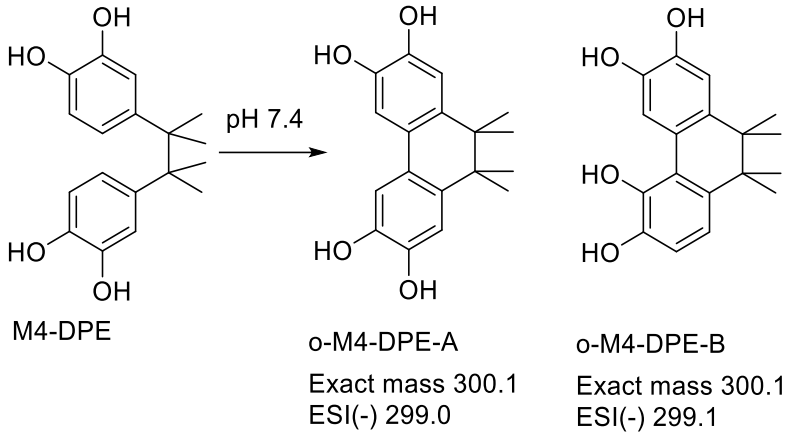

Figure 3.9. M4-DPE and its oxidized products formed in phosphate buffer (pH 7.4) at 37 ºC. Exact mass and *m/z* (ESI negative ion mode) are shown for each product.

We compared the HPLC-UV absorption spectra of our diphenylethane autoxidation products and observed that the spectra for o-DPE-A and o-M4-DPE-A are similar in appearance (λ 276, 328 nm and λ 280, 325 nm respectively) corresponding to the 2,3,6,7-tetrahydroxy phenanthrene structure, whereas the spectra for o-DPE-C, o-M2-DPE-B, and o-M4-DPE-B are also similar in appearance (λ 279, 304 nm, λ 280, 304 nm and λ 280, 306 nm respectively) corresponding to the 2,3,5,6-tetrahydroxy phenanthrene structure. Finally, the UV spectra for o-DPE-B and o-M2-DPE-A are similar in appearance (λ 254, 289, 305 nm and λ 256, 291, 308 nm respectively) corresponding to the aromatized 2,3,6,7-tetrahydroxy phenanthrene structure (Figure 3.10).

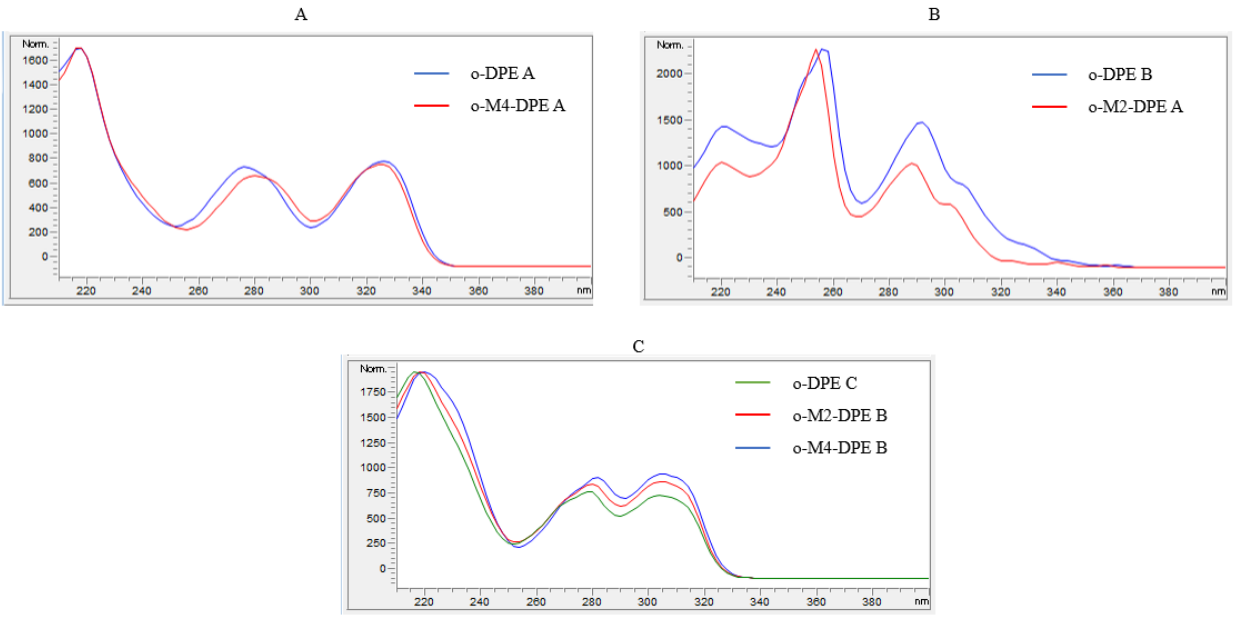

Figure 3.10. UV absorption extracted from HPLC chromatogram for all the oxidized products grouped in three panels (A, B, C) according to their structure similarity. Panel A contains cyclized symmetrical o-DPE A and o-M4-DPE A; Panel B contains cyclized fully aromatized o-DPE B and o-M2-DPE A; Panel C contains asymmetrical cyclized o-DPE C, o-M2-DPE B, and o-M4-DPE B.

3.4.2.3 Quantification of DPEs and autoxidation products in the incubation mixture

The concentration of each DPE and their autoxidation products were determined from the standard curves prepared (Figure S13). We extrapolated the standard curves from each DPE to their respective autoxidative metabolite with the exception of o-DPE B and o-M2-DPE A. We prepared a standard curve for o-DPE B at 254 nm, and extrapolated to o-M2-DPE A given the same UV absorption profile. We observed that for both DPE and M2-DPE symmetric cyclization predominated, whereas for M4-DPE asymmetric cyclization was greater.

Table 3.2. Concentration of DPEs and their autoxidative products at 10 minutes of incubation

Compound	Concentration (μM)	%
DPE	220.8	44
o-DPE A	120.3	24
o-DPE B	45.5	9
o-DPE C	110.7	22
M2-DPE	148.9	30
M2-DPE A	200.5	40
M2-DPE B	140.5	28
M4-DPE	41.3	8
o-M4-DPE A	170.5	34
o-M4-DPE B	285.1	57

3.4.2.4 Stability of diphenylethane autoxidation products and reactivity with glutathione

After isolation of the autoxidation products for DPE, M2-DPE and M4-DPE we investigated the ability of the compounds to react with reduced glutathione (GSH). GSH is commonly used for trapping of quinones and this experiment was designed to confirm which of the autoxidation products could form reactive quinones via autoxidation. GSH formed adducts with o-DPE-A, o-DPE-C, o-M2-DPE-B, o-M4-DPE-A and o-M4-DPE-B, but not with the fully aromatized compounds o-DPE B and o-M2-DPE-A (Figure S14).

ESI (+) MS fragmentation of GSH adducts shows a neutral loss of 129 corresponding to

pyroglutamic acid, which was observed for all of the GSH adducts. Since there is no exocyclic position for the GSH to react with the quinones, the GSH adducts should form on the ring which subsequently re-aromatizes [83]. ESI (-) MS fragmentation of ring-adducted GSH produces a diagnostic fragment ion at *m/z* 272 indicating scission of the S-CH_2 bond of GSH; this diagnostic fragment ion was present for all of the adducts.

Additionally, we also determined that the cyclized diphenylethanes were unstable in the phosphate buffer over time (Table 3.3), except for the fully aromatized compounds o-DPE B and o-M2-DPE-A. Both fully aromatized compounds were stable in phosphate buffer up to 24 hours. It was also observed that o-DPE A oxidizes to o-DPE B.

Table 3.3. Oxidation rates of cyclized diphenylethanes (n=3) in phosphate-citric acid buffer (pH 7.4) at 37 ºC

Compound	k_{dep} **(min^{-1})**	$t_{1/2}$ **(min)**
o-DPE A	$1.3 \times 10^{-2} \pm 0.0010$	50
o-DPE C	$3.2 \times 10^{-2} \pm 0.0038$	21
o-M2-DPE B	$8.9 \times 10^{-3} \pm 0.0004$	77
o-M4-DPE A	$5.4 \times 10^{-3} \pm 0.0003$	128
o-M4-DPE B	$4.9 \times 10^{-3} \pm 0.0004$	141

3.4.2.5 Inhibition of *in vitro* α-synuclein aggregation

The Thioflavin T (ThT) assay was used to determine the effect of the diphenylethanes and their oxidized products on the aggregation of α-synuclein. We measured the fluorescence at a single time point by incubating the test compounds with the protein for 5 days. Negative controls containing no drug were used to obtain an aggregated fluorescent response and were normalized to 100% of ThT fluorescence. We used cyclized nordihydroguaiaretic acid (cNDGA) as our positive control as it has been shown to inhibit the aggregation of α-synuclein in ThT assays [11]. Graphs containing ThT fluorescence results of different diphenylethanes and oxidized products are presented in Figure 3.11, and we normalized the readings averages and compared to controls/concentrations in Table 3.4.

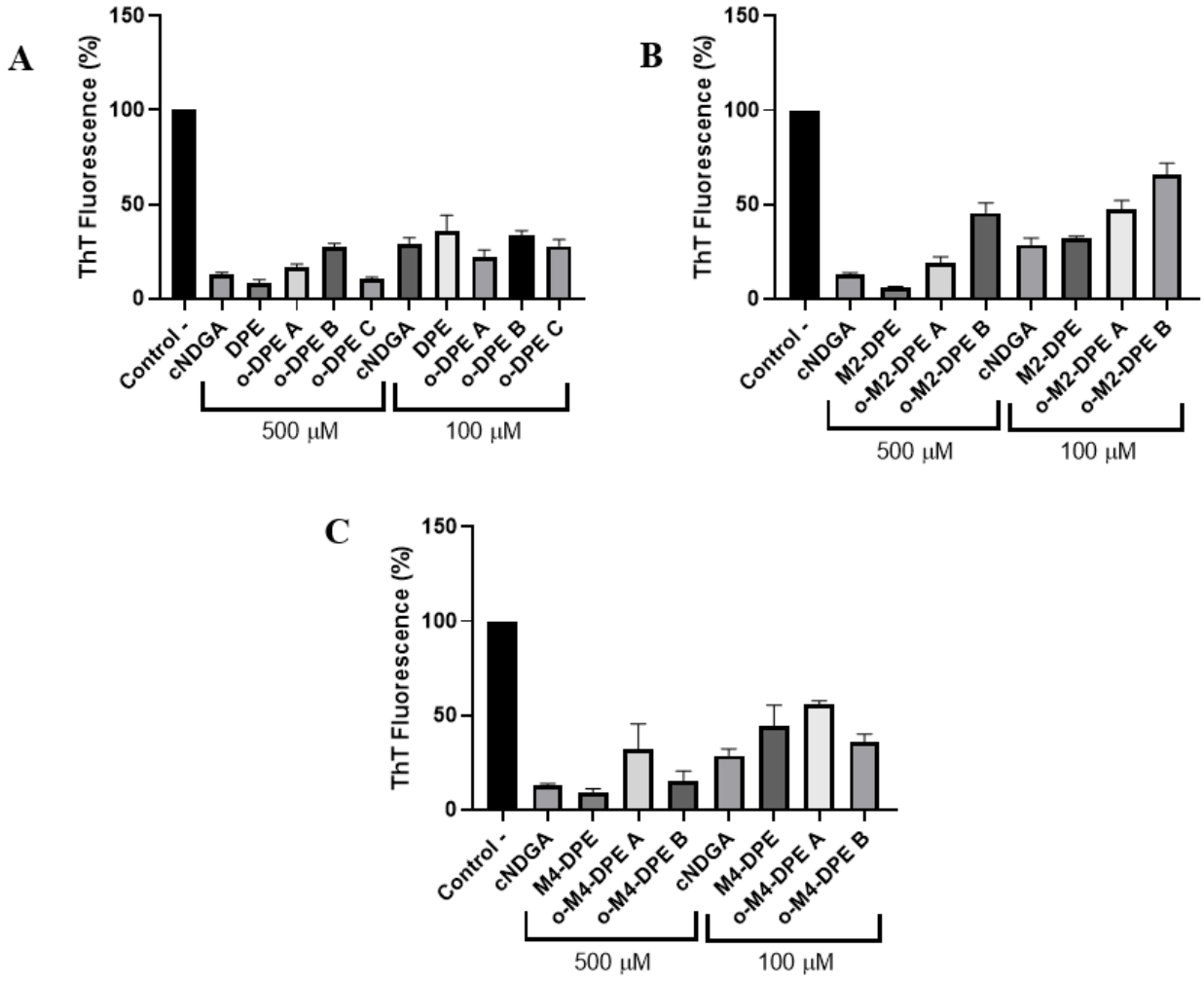

Figure 3.11. α-Synuclein aggregation represented as thioflavin T fluorescence percentage of positive control. Compounds are grouped in three panels according to their structures: DPE and o-DPEs (panel A), M2-DPE and o-M2-DPEs (panel B), and M4-DPE and o-M4-DPEs (panel C). All compounds were run in triplicate.

Table 3.4. *In vitro* activity of diphenylethanes (n=3) and their oxidized products (n=3) on α-synuclein aggregation.

	α-Synuclein aggregation (%)	
Compound	**100 μM**	**500 μM**
Control - (no drug)	100 [b]	100 [b]
Control + (cNDGA)	28.6 ± 3.6 [a]	13.6 ± 2.3 [a]
DPE	35.6 ± 8.5 [a]	8.1 ± 1.8 [a]
o-DPE A	22.2 ± 3.4 [a]	16.8 ± 1.4 [a]
o-DPE B	33.6 ± 2.3 [a]	25.9 ± 1.3 [a]
o-DPE C	27.8 ± 3.5 [a]	10.7 ± 0.5 [a]
M2-DPE	31.8 ± 1.3 [a]	6.1 ± 0.3 [a,c]
o-M2-DPE A	47.3 ± 4.8 [a,b]	19.3 ± 3 [a]
o-M2-DPE B	66.1 ± 5.8 [a,b]	45.6 ± 5.3 [a,b,c]
M4-DPE	44.4 ± 11 [a]	9.2 ± 1.9 [a]
o-M4-DPE A	56.1 ± 1.5 [a,b]	39.8 ± 1.6 [a]
o-M4-DPE B	36.1 ± 3.9 [a]	15.5 ± 4.9 [a]

[a] indicates a compound is statistically significant ($p<0.05$) compared to the control –
[b] indicates a compound is statistically significant ($p<0.05$) compared to the positive control at the same concentration
[c] indicates a compound is statistically significant ($p<0.05$) compared both concentrations 100 μM and 500 μM
Data analyzed using a one-way ANOVA with Dunnett's t-test.

3.5 Discussion

The formation of intramolecular cyclized lignans such as cNDGA forming as a result of autoxidation in aqueous solution was previously discovered by our group [5] although many examples of similar cyclized lignans, for example the schisandrins [84], are known to occur in plants. In the case of NDGA, many *in vitro* studies have been carried out under conditions that would be expected to result in autoxidation occurring on a time scale shorter than the *in vitro* experiment, potentially confounding the results. Indeed, we have demonstrated that oxidation of NDGA or cNDGA is responsible for the inhibition of α-synuclein aggregation *in vitro* [11]. The intriguing observation that methyl substitution on the alkyl linker of NDGA decreased the rate of intramolecular cyclization [6], which is opposite to that predicted for a vicinal dimethyl effect [85], led us to speculate whether dicatechol intramolecular autoxidative cyclizations occurred for other alkyl linker lengths and if this reversed vicinal dimethyl effect also occurred in diphenyl ethane-type dicatechols.

In our study we determined that our dicatechol substituted diphenylethane analogs underwent autoxidation to form dibenzocyclohexadienes 10-30 times more rapidly than dibenzocyclooctadienes formed from NDGA and contrary to NDGA cyclization, the diphenylethanes autoxidized to intramolecular cyclization products at a rate that was proportional to the number of methyl substituents on the alkyl linker. The increase in rate of cyclization from DPE to M2-DPE (rate increase of 2.6 fold for O_2 purged) and from M2-DPE to M4-DPE (rate increase of 2.6 fold for O_2 purged) follows the same trend as observations of a vicinal dimethyl effect reported for lactone cyclization [85]. The authors observed that addition of vicinal methyl groups at the 3,4 positions to ethyl 4-hydroxybutanoate resulted in an increase in cyclization rate of at least 5.3 and addition of gem dimethyl groups at the 3,3' position resulted in an increase in cyclization rate of 4.4. Our results indicate that both vicinal and gem dimethyl

effects may contribute to enhanced cyclization for the diphenylethanes.

We had previously proposed that the NDGA autoxidative cyclization was likely the result of a radical-mediated process [5] which was supported through subsequent *in silico* studies by Galano [86]. The dependence of cyclization in this study on oxygen in the buffer solution would indicate a similar radical mechanism. In our autoxidation study of NDGA, C-C bond formation occurred exclusively *para* to the 3-hydroxy group of the catechol. We observed however that for all of our diphenylethane analogs a mixture of regioisomers was formed. In addition to C-C bond formation occurring *para* to the 3-hydroxy group (o-DPE-A, o-DPE-B, o-M2-DPE-A, o-M4-DPE-A), we also observed C-C bond formation between the position *para* to the 3-hydroxy group of one ring with the position *ortho* to the 3-hydroxy group of the second ring (o-DPE-C, o-M2-DPE-B, o-M4-DPE-B), presumably occurring through a process as outlined in Figure 3.12 for o-DPE-C. It is possible that a small amount of the *ortho* 3-hydroxy regioisomer was formed however we were unable to detect this product. Additionally, we have determined that the relative amount of symmetrical cyclization was higher for DPE and M2-DPE, whereas relative amounts of asymmetrical cyclization was higher for M4-DPE (Table 3.2) although these differences are not large.

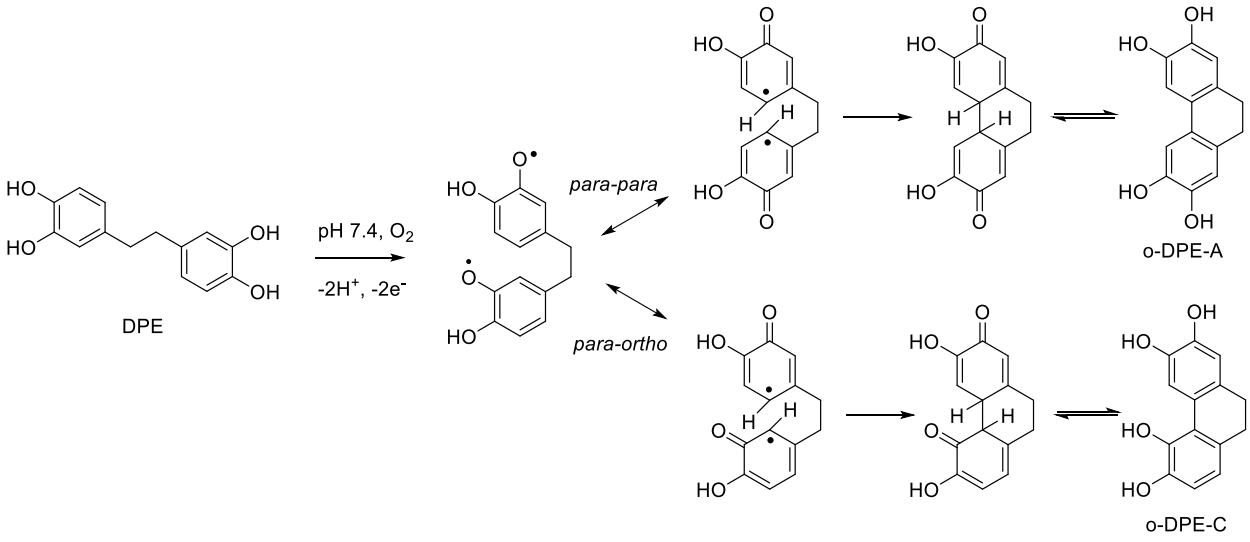

Figure 3.12. Proposed autoxidation mechanism of DPE to yield symmetrical (o-DPE A) and asymmetrical (o-DPE C) products

Our results led us to wonder why do we not observe an additional regioisomer for C-C bond formation between the positions *ortho* to the 3-hydroxy groups and why is the mixed product not observed for NDGA cyclization. The aromatic rings are free to rotate in both NDGA and the diphenyethanes although the closer proximity of the rings in the diphenylethanes may result in H-bonding interactions although that may be anticipated to favour the *ortho-ortho* product which we did not observe. Alsoufi *et al* [87] carried out a DFT study which determined that biphenyl compounds resulting from phenoxyl radical coupling of catechols occurred preferentially in the order *para-para* followed by the mixed *para-ortho* and finally the *ortho-ortho* product, which is in agreement with our observations for the DPE and M2-DPE autoxidation products. The results reported by Alsoufi *et al* depicted the biphenyls in the lowest energy conformation with OH or C=O groups on opposite sides of the rings as shown for the keto-enol forms of the biphenyls (Figure 3.13). It should be noted that for our cyclized compounds the lowest energy conformations described by Alsoufi *et al* (Figure 3.13) cannot be attained as the

biphenyl bond cannot rotate the OH and C=O groups in the same manner due to the alkyl linker. The 10-30 fold slower rate of NDGA oxidation compared to DPE leading to greater selectivity for the more stable *para-para* cyclization product observed exclusively with NDGA is in line with the observations of Alsoufi *et al*. Curiously, we were unable to observe an aromatic autoxidation product for the asymmetric cyclization products o-DPE C and o-M2-DPE B however, we were also unable to find evidence of this structure in the literature.

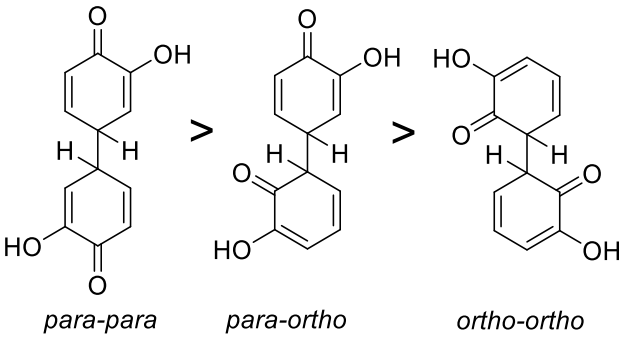

Figure 3.13. From the lowest to the highest energy conformation of biphenols resulting from phenoxyl radical coupling of catechols

We had previously observed that the rate of autoxidation of the cyclized NDGA compounds was more rapid than the initial autoxidation to the cyclized species [6]. For the DPE's however we observed that the cyclized products underwent further autoxidation at a slower rate than formation of the initial cyclized product and the *para-ortho* compounds o-M2-DPE-B and o-M4-DPE-B autoxidized slower than the corresponding *para-para* compounds. The only exception was the precursor of o-M2-DPE-A, which we assume to be the cyclized, non-aromatized compound that we were unable to observe or isolate as it autoxidized to the aromatic species nearly instantaneously. The influence of methyl substituents on autoxidation rate of the cyclized compounds is variable, suggesting an electron-donating effect is

unlikely.

While we were able to detect and isolate both the cyclized *para-para* non-aromatized product arising from DPE (o-DPE-A) and the cyclized *para-para* aromatized product (o-DPE-B), we were unable to detect or isolate the cyclized *para-para*, non-aromatized product arising from M2-DPE, instead only observing the cyclized *para-para* aromatized product (o-M2-DPE-A). Evidently the cyclized *para-para*, non-aromatized M2-DPE product is highly unstable under these autoxidative conditions although it is not abundantly clear why. For the *meso* isomer of M2-DPE the gain in stabilization going from the twisted 6-membered ring with eclipsed vicinal methyl groups to the planar aromatic species may drive the reaction. For the racemic isomers the methyl groups could be in either a di-axial or di-equatorial conformation, but only the higher energy di-equatorial conformation may be expected to benefit from stabilization derived from aromatization. This suggests to us that M2-DPE may be the *meso* isomer which agrees with our observation that the alkene precursor was the E-isomer and hydrogenation could yield the *meso* isomer exclusively.

Previously we have reported that NDGA and two cyclized analogs of NDGA inhibited α-synuclein aggregation [11] and others have reported that ethane dicatechol analogs inhibited α-synuclein aggregation *in vitro*. Based on these observations, we expected that our DPEs and their cyclized products would also show the same effect. Indeed, we observed a significant reduction ($p<0.05$) in α-synuclein aggregation at both 100 and 500 μM. Even though only M2-DPE and o-M2-DPE B are statistically significant ($p<0.05$) between the two concentrations tested, we observed a trend of concentration-dependent inhibition of α-synuclein for all compounds tested. Interestingly, both cyclized products of M2-DPE and one cyclized product of M4-DPE (o-M4-DPE A) significantly reduced ($p<0.05$) the aggregation as compared to cNDGA at the same concentration. Our NDGA study indicated that the

autoxidation process is required for the anti-aggregation effect and our DPE experiments agree with the earlier study.

In this study, we have prepared a series of 1,2-bis-ethane dicatechols to probe the influence of methyl substituents on intramolecular cyclization of dicatechols. We have determined that these compounds undergo intramolecular cyclization to form dibenzocyclohexadienes and that steric interactions between the methyl substituents increased the rate of intramolecular cyclization. The cyclization of six-membered rings occurred 10-30 times more rapid than formation of eight membered rings and both the DPEs and the dibenzocyclohexadienes prevent *in vitro* aggregation of α-synuclein. Our results strongly suggest that previously reported DPE analogs developed for the treatment of Parkinson's Disease likely owe their *in vitro* α-synuclein anti-aggregation activity to autoxidative processes.

Chapter 4: *In Vitro* Hepatic Metabolism of the Natural Product Quebecol

Gabriel Bernardes & Ed S. Krol

Drug Discovery and Development Research Group, College of Pharmacy and Nutrition, University of Saskatchewan, Saskatoon, SK

Transitioning rationale: In the last chapter, we reported that diphenylethane dicatechol compounds can spontaneously cyclize at pH 7.4 to form dibenzocyclohexadienes. We became curious if the same process would occur in quebecol, a new polyphenolic compound isolated from maple syrup. Since a dicatechol is required for the cyclization process, phase I metabolism of quebecol could lead to dealkylation of the methoxy groups, and form dicatechols. In this chapter, we assess the metabolic fate of the natural product quebecol using liver microsomes.

Contribution statement: Gabriel Bernardes contributed to the experimental design, conducted the experimental work and data analysis, and drafted the manuscript. Dr Ed Krol supervised the work and revised the manuscript.

4.1 Abstract

Quebecol (2,3,3-tri-(3-methoxy-4-hydroxyphenyl)-1-propanol) is a polyphenolic compound, which is formed during maple syrup production from *Acer saccharum spp*. Quebecol is similar in structure to the chemotherapy drug tamoxifen, which has led to synthesis of structural analogs and investigations into their pharmacological properties. However, there are no reports on the hepatic metabolism of quebecol. This interest in therapeutic properties spurred us to investigate the *in vitro* Phase I and II metabolism of quebecol. We were unable to detect any P450 metabolites for quebecol in either human liver microsomes (HLM) or rat liver microsomes (RLM). In contrast we observed marked formation of three glucuronide metabolites in both RLM and HLM, suggesting that clearance via Phase II pathways is likely to predominate. To further understand the hepatic contribution to first-pass glucuronidation we have validated an HPLC method following FDA and EMA guidelines (selectivity, linearity, accuracy, and precision) to quantify quebecol in microsomes. *In vitro* enzyme kinetics were performed for quebecol glucuronidation by HLM including 8 concentrations from 5-30 µM. We determined a Michaelis-Menten constant (K_M) of 5.1 µM, intrinsic clearance (Cl_{int}) of 0.04 mL/min/mg, and maximum velocity (V_{max}) of 0.22 µmol/min/mg.

4.2 Introduction

Maple syrup is produced by concentrating the sap from *Acer* maple tree species via thermal evaporation [88]. During this process, the intensive heating facilitates the formation of distinct bioactive compounds that are not naturally present in the xylem sap [89]. Maple syrup has shown a wide range of biological effects including antiproliferative [90–92], anti-inflammatory [93–95], and antioxidant [96–98]. Recently there has been an interest in the isolation, identification, and biological investigation of phenolic compounds from maple syrup products [98–100]. As part of these investigations, a novel phenolic compound quebecol was isolated and characterized [59].

Quebecol (Figure 4.1) is a triphenyl propanol and shares the triphenyl feature of therapeutics such as tamoxifen [60]. The potential therapeutic properties of maple syrup has led others to the synthesis of quebecol analogs in an effort to probe it's pharmacological activity [101–103].

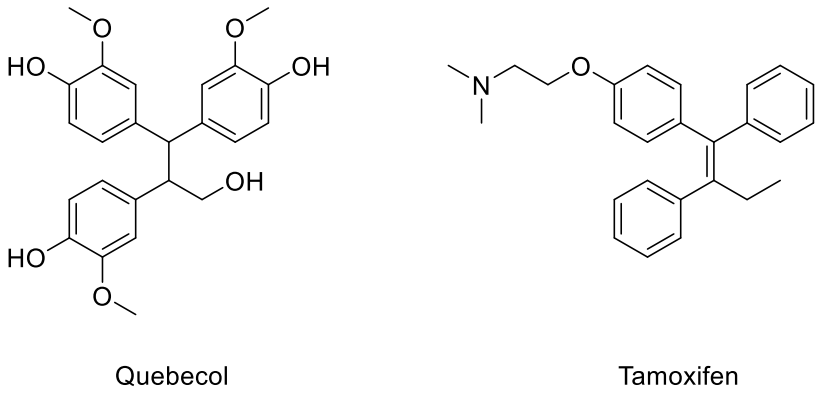

Figure 4.1. Structure of quebecol and tamoxifen

Despite the great interest in the biological effects of quebecol and the development of analogs of quebecol as potential drug leads, there are no studies regarding quebecol's hepatic metabolism. The presence of three phenolic OH groups and an alcohol suggest that phase 2 processes likely predominate

the hepatic metabolism of quebecol. Our goal in this study is to investigate the *in vitro* hepatic metabolism of quebecol in both human and rat liver microsomes, and to measure UGT-mediated microsomal metabolism kinetics parameters in human liver microsomes.

4.3 Materials and Methods

4.3.1 Materials

Dipotassium orthophosphate (K_2HPO_4), potassium dihydrogen orthophosphate (KH_2PO_4), magnesium sulfate ($MgSO_4$), chlorzoxazone, enterolactone, acetonitrile (LC-MS grade), methanol (HPLC grade), formic acid (LC-MS grade) were purchased from Sigma-Aldrich (St. Louis, MO). Magnesium chloride ($MgCl_2$), sodium pyrophosphate decahydrate (SPP), D-saccharic acid 1,4-lactone monohydrate, uridine 5'-diphosphoglucuronic acid trisodium salt (UDP) were purchased from Fisher Scientific (Ottawa, ON). Reduced nicotinamide adenine dinucleotide (NADPH) were obtained from Roche Diagnostics (Indianapolis, IN). Water was purified via a Millipore (Mississauga, ON) Milli-Q system with a Quantum EX Cartridge. Pooled human liver microsomes and rat liver microsomes were purchased from Gibco (Waltham, MA). 2,2-di-(3-methoxymethylphenyl)-1,3-propanediol (MMPPD) was prepared following literature procedures [104].

4.3.2 Instrumentation

4.3.2.1 HPLC-UV Diode Array Analysis

The autoxidation studies and reaction kinetics were performed on an Agilent 1200 high-performance liquid chromatograph (HPLC) (Agilent Technologies; Mississauga, ON) equipped with a degasser (G1379A), quaternary pump (G1311A), autosampler (G1329A), and diode array detector (G1315D). The HPLC column was a Waters Symmetry C_{18} (2.1 x 150 mm, 3.5 μm) and the solvent system consisted of 0.1% LC-MS grade formic acid in water (solvent A) and 0.1% LC-MS grade formic acid in acetonitrile (solvent B) operating at a flow rate of 0.2 mL/min. The gradient method consisted of

an initial isocratic phase at 90% solvent A for 2.5 minutes, decreased gradually to 10% solvent A over 12.5 minutes, and holding for 5 minutes before returning to the initial conditions and equilibrating for 10 minutes.

4.3.2.2 ESI-MS Analysis

Mass spectroscopy analysis of quebecol and its intermediates was conducted using an AB SCIEX 4000 QTRAP (Redwood City, CA, USA) quadrupole linear ion trap mass spectrometer. Samples were infused directly using a flow of 10 μL/min. Phase I and Phase II metabolism investigations were conducted using LC-MS which consisted of an Agilent 1100 high-performance liquid chromatography (HPLC) (Agilent technologies; Mississauga, ON) coupled with the AB SCIEX 4000 QTRAP (Redwood City, CA, USA) quadrupole linear ion trap mass spectrometer. The reverse phase column and gradient method was the same as for the HPLC-UV analysis. The mass spectroscopy analysis was performed in negative ion mode, and fragmentation patterns were studied by tandem ESI-MS/MS operated in negative ion mode. Data acquisition and analyses were performed using Analyst 1.7 software from AB SCIEX.

4.3.2.3 NMR Analysis

All NMR experiments were performed on a Bruker AVANCE DPX-500 spectrometer (Karlsruhe, Germany) and data processed by MestreNova 14.1. All compounds were drawn and named using ChemDraw 20.0.

4.3.3 Methods

4.3.3.1 Synthesis and Characterization of Quebecol

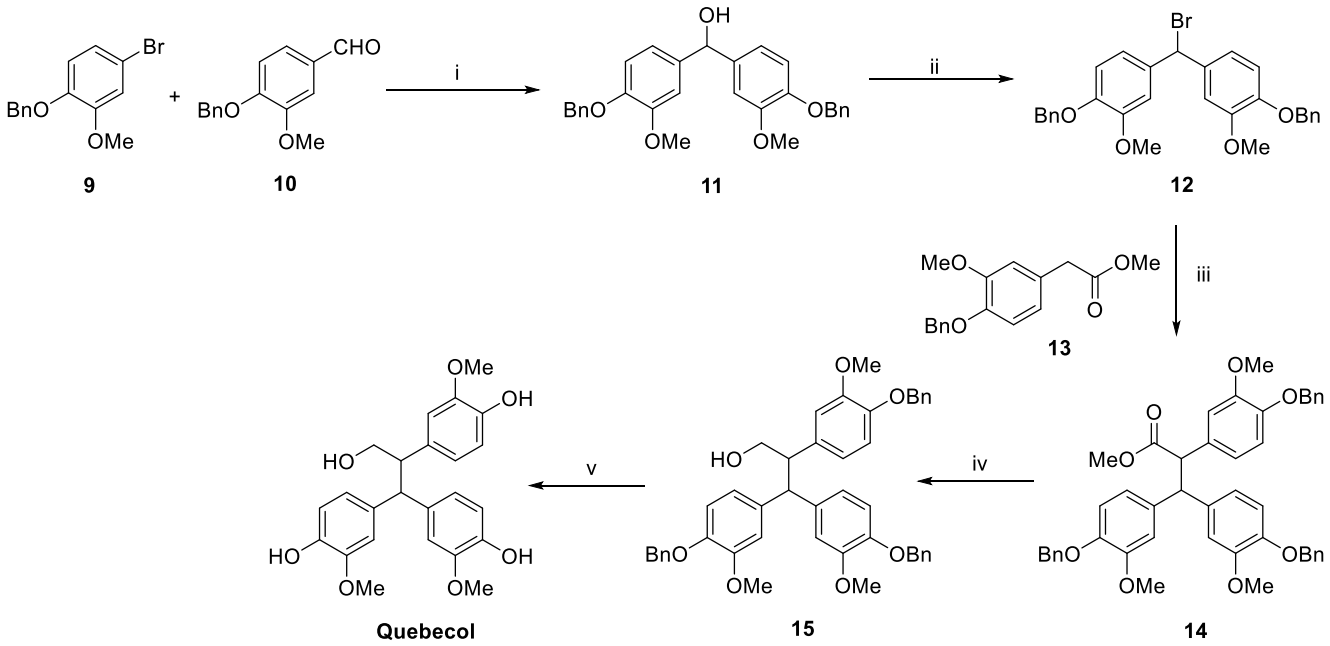

Scheme 4.1. Synthesis of Quebecol. *Reagents and Conditions:* i) *n*-BuLi, THF, -78 °C, 35%; ii) CH_3COBr, THF, r.t., 91%; iii) LDA, THF, -78 °C, 30%; iv) $LiAlH_4$, THF, 0 °C, 49%; v) Pd/C, H_2, THF, r.t., 94% (adapted from [61])

Synthesis of 1-(benzyloxy)-4-bromo-2-methoxybenzene (9)

K_2CO_3 (1.3 g, 9.85 mmol) and MeOH (20 mL) were added to a reaction flask, and the mixture was stirred at 0 °C under N_2. 4-Bromo-2-methoxyphenol (1 g, 4.92 mmol) was dissolved in MeOH (3 mL) and added dropwise to the reaction. After 5 minutes, benzyl bromide (1.6 g, 9.85 mmol) was added dropwise to the mixture. The reaction was refluxed at 85 °C, and the loss of starting material was monitored by TLC. After 4 hours, the reaction was cooled to room temperature, and solvent evaporated.

The residue was dissolved in chloroform (80 mL) and washed with water (3 × 15 mL). The organic layer was dried over $MgSO_4$, and evaporated to afford **9** as a yellow solid (1.3 g, 91 %). ^{1}H NMR (500 MHz, $CDCl_3$) δ 7.45 – 7.40 (m, 2H), 7.38 – 7.34 (m, 2H), 7.32 – 7.29 (m, 1H), 7.00 (d, J = 2.3 Hz, 1H), 6.95 (dd, J = 8.5, 2.3 Hz, 1H), 6.74 (d, J = 8.5 Hz, 1H), 5.12 (s, 2H), 3.87 (s, 3H).

Synthesis of 4-(benzyloxy)-3-methoxybenzaldehyde (10)

K_2CO_3 (0.9 g, 6.56 mmol) and MeOH (20 mL) were added to a reaction flask, and the mixture was stirred at 0 °C under N_2. Vanillin (0.5 g, 3.28 mmol) was dissolved in MeOH (3 mL) and added dropwise to the reaction. After 5 minutes, benzyl bromide (1.1 g, 6.56 mmol) was added dropwise to the mixture, and the reaction was refluxed at 85 °C for 4 hours. On completion, the reaction was cooled to room temperature, and solvent evaporated. The residue was dissolved in chloroform (80 mL) and washed with water (3 × 15 mL). The organic layer was dried over $MgSO_4$, and evaporated to afford **10** as a yellow oil (0.53 g, 70%). ^{1}H NMR (500 MHz, $CDCl_3$) δ 9.84 (s, 1H), 7.46 – 7.42 (m, 3H), 7.41 – 7.37 (m, 3H), 7.35 – 7.31 (m, 1H), 6.99 (d, *J* = 8.2 Hz, 1H), 5.25 (s, 2H), 3.95 (s, 3H).

Synthesis of bis(4-(benzyloxy)-3-methoxyphenyl)methanol (11)

Bromobenzene **9** (0.87 g, 2.98 mmol) and THF (10 mL) were added to a reaction flask at –78 °C under N_2. After 10 minutes, *n*-BuLi (1.25 mL, 3.13 mmol) was slowly added to the reaction, and stirred for 30 minutes at the same temperature. Aldehyde **10** (0.84 g, 3.27 mmol) in THF (2 mL) was added dropwise slowly to the reaction. Reaction was stirred for 30 minutes at –78 °C, and the loss of starting material was monitored by TLC. After completion, the reaction was allowed to warm to 0 °C, and

quenched with saturated NH_4Cl solution, followed by an extraction with ethyl acetate (3 × 15 mL). The organic layer was dried over $MgSO_4$, and the solvent evaporated. The residue was purified by flash column chromatography (2:1 hexane/EtOAc) to afford alcohol **11** as an off-white solid (0.46 g, 35%). ^{1}H NMR (500 MHz, $CDCl_3$) δ 7.44 – 7.40 (m, 4H), 7.38 – 7.33 (m, 4H), 7.32 – 7.27 (m, 2H), 6.94 (d, J = 1.9 Hz, 2H), 6.83 (d, J = 8.3 Hz, 2H), 6.79 (dd, J = 8.3, 1.9 Hz, 2H), 5.73 (d, J = 3.1 Hz, 1H), 5.14 (s, 4H), 3.86 (s, 6H), 2.11 (d, J = 3.5 Hz, 1H). ^{13}C NMR (126 MHz, $CDCl_3$) δ 149.64, 147.65, 137.34, 135.47, 128.68, 127.97, 127.38, 119.80, 118.98, 113.60, 111.09, 110.36, 71.13, 56.11.

Synthesis of 4,4'-(bromomethylene)bis(1-(benzyloxy)-2 methoxybenzene) (12)

Acetyl bromide (64 mg, 0.52 mmol) was added to a stirred solution of alcohol **11** (80 mg, 0.17 mmol) in THF (5 mL) at room temperature under N_2. The mixture was stirred for 5 h. The solvent was evaporated, and the residue was washed multiple times with hexane to remove traces of acetic acid. Then, the residue was dried under *vacuo* to afford **12** as a pink solid (0.1 g, 91%). Compound **12** was carried to the next step without further purification due to it's instability as reported by Pericherla *et al.* [61].

Synthesis of methyl 2-(4-(benzyloxy)-3-methoxyphenyl)acetate (13)

K_2CO_3 (0.65 g, 4.75 mmol) and MeOH (20 mL) were added to a reaction flask, and the mixture was stirred at 0 °C under N_2. Ethyl homovanillate (0.5 g, 2.37 mmol) was dissolved in MeOH (3 mL) and added dropwise to the reaction. After 5 minutes, benzyl bromide (0.8 g, 4.75 mmol) was added dropwise to the mixture, and the reaction was refluxed at 85 °C overnight. After completion, the reaction was cooled to room temperature and solvents evaporated. The residue was dissolved in chloroform (80 mL) and washed with water (3 × 15 mL). The organic layer was dried over $MgSO_4$, and evaporated to

afford **13** as a white solid (0.37 g, 55%). ^{1}H NMR (500 MHz, $CDCl_3$) δ 7.46 – 7.40 (m, 2H), 7.40 – 7.33 (m, 2H), 7.33 – 7.26 (m, 1H), 6.83 (d, *J* = 2.1 Hz, 1H), 6.82 (d, *J* = 8.2 Hz, 1H), 6.74 (dd, *J* = 8.2, 2.0 Hz, 1H), 5.14 (s, 2H), 3.89 (s, 3H), 3.69 (s, 3H), 3.55 (s, 2H). ^{13}C NMR (126 MHz, $CDCl_3$) δ 172.42, 149.70, 147.43, 137.30, 128.68, 127.95, 127.36, 127.09, 121.49, 114.06, 112.99, 71.14, 56.12, 52.21, 40.88. ESI-MS (*m/z*) 304.1 $[M + H_2O]^+$.

Synthesis of methyl 2,3,3-tris(4-(benzyloxy)-3-methoxyphenyl)propanoate (14)

LDA (0.18 mL, 0.37 mmol) and THF (5 mL) were added to a reaction flask under N_2 at –78 °C. After 10 minutes, the ester **13** (90 mg, 0.31 mmol) in THF (2 mL) was slowly added to the stirred solution. The mixture was stirred for 30 min at the same temperature. Then, the bromo compound **12** (179 mg, 0.34 mmol) in THF (1 mL) was added. The mixture was stirred at -78 °C for 2 hours. The reaction mixture was allowed to warm to 0 °C, quenched with cold water and extracted into ethyl acetate (3 × 15 mL). The organic layer was dried over $MgSO_4$ and the solvents were evaporated. The residue was purified on silica gel column (7:3 hexane/EtOAc) to afford ester **14** as a yellow solid (70 mg, 30%). ^{1}H NMR (500 MHz, $CDCl_3$) δ 7.43 – 7.30 (m, 15H), 6.86 (dd, *J* = 6.7, 2.0 Hz, 2H), 6.82 (d, *J* = 8.8 Hz, 1H), 6.77 (d, *J* = 1.7 Hz, 1H), 6.70 – 6.69 (m, 2H), 6.59 (d, *J* = 8.1 Hz, 1H), 6.47 – 6.43 (m, 2H), 5.11 (s, 2H), 5.07 (s, 1H), 5.00 (s, 2H), 4.47 (d, *J* = 12.0 Hz, 1H), 4.18 (d, *J* = 12.0 Hz, 1H), 3.86 (s, 3H), 3.77 (s, 3H), 3.64 (s, 3H), 3.49 (s, 3H). ^{13}C NMR (126 MHz, $CDCl_3$) δ 173.23, 162.49, 149.63, 149.46, 147.54, 147.00, 146.62, 137.39, 137.34, 136.15, 135.13, 130.24, 128.67, 128.65, 128.61, 127.97, 127.90, 127.45, 127.39, 127.36, 121.08, 120.46, 119.34, 114.03, 113.65, 112.55, 112.31, 112.01, 71.15, 71.03, 56.90, 56.17, 56.12, 56.02, 54.24, 52.15. ESI-MS (*m/z*) 742.3 $[M + H_2O]^+$, 747.3 $[M + Na]^+$.

Synthesis of 2,3,3-tris(4-(benzyloxy)-3-methoxyphenyl)propan-1-ol (15)

To a solution of ester **14** (70 mg, 0.09 mmol) in THF (5 mL) was added portion wise $LiAlH_4$ (8 mg, 0.21 mmol). The reaction was refluxed overnight (18 hours) under N_2. The mixture was cooled to 0 ^oC and quenched with water (added slowly) followed by saturated NH_4Cl solution (5 mL). Ethyl acetate (15 mL) was added and the solution was stirred for 30 minutes. The organic layer was collected, and the aqueous layer extracted with ethyl acetate (3 × 15 mL). The combined organic layers were dried over $MgSO_4$, filtered and evaporated under reduced pressure. The residue was purified on a silica gel column (3:2 Hexanes/EtOAc) to give the alcohol **15** as a white solid (33 mg, 49 %). ^1H NMR (500 MHz, $CDCl_3$) δ 7.44 – 7.29 (m, 15H), 6.88 – 6.85 (m, 2H), 6.82 (d, *J* = 8.0 Hz, 1H), 6.74 (d, *J* = 8.1 Hz, 1H), 6.73 – 6.69 (m, 1H), 6.69 – 6.66 (m, 2H), 6.62 – 6.59 (m, 2H), 5.12 (s, 2H), 5.07 (s, 2H), 5.00 (s, 2H), 4.09 (d, *J* = 11.5 Hz, 1H), 3.87 (s, 3H), 3.77 (s, 3H), 3.69 (s, 3H), 3.68 (d, *J* = 3.8 Hz, 1H), 3.63 (dd, *J* = 11.0, 7.5 Hz, 2H), 3.46 (ddt, *J* = 11.5, 7.5, 3.7 Hz, 1H).^{13}C NMR (126 MHz, $CDCl_3$) δ 149.80, 149.62, 149.12, 147.01, 146.42, 137.41, 137.30, 136.68, 136.46, 133.96, 128.68, 128.66, 128.60, 127.96, 127.87, 127.43, 127.38, 120.79, 120.43, 120.02, 114.24, 114.06, 113.76, 112.79, 112.63, 111.97, 71.19, 71.12, 71.07, 66.06, 60.56, 56.20, 56.14, 56.07, 53.18, 52.54. ESI-MS (*m/z*) 759.6 $[M + Cl]^-$

Synthesis of 4,4',4''-(3-hydroxypropane-1,1,2-triyl)tris(2-methoxyphenol) (Quebecol)

Pd/C (10% w/w, 2.8 mg) was added to a reaction flask under N_2. The flask was sealed, and dry THF (5 mL) was added. The alcohol **15** (28 mg) in dry THF (2 mL) was added to the reaction dropwise. The flask was evacuated, then flushed with H_2 gas. The reaction was left to stir under H_2 overnight. The reaction mixture was filtered through a Celite pad and washed with MeOH. The solvent was removed under reduced pressure to give racemic quebecol as a dark solid (16 mg, 94%). ^1H NMR (500 MHz,

$CDCl_3$) δ 6.90 (dd, *J* = 8.3, 1.9 Hz, 1H), 6.87 (d, *J* = 8.1 Hz, 1H), 6.82 (d, *J* = 1.9 Hz, 1H), 6.80 (d, *J* = 8.1 Hz, 1H), 6.76 (dd, *J* = 8.1, 1.9 Hz, 1H), 6.66 (d, *J* = 0.8 Hz, 2H), 6.61 (d, *J* = 1.9 Hz, 1H), 6.52 (s, 1H), 5.50 (s, 1H), 5.44 (s, 1H), 5.32 (s, 1H), 4.35 (q, *J* = 6.6, 6.1 Hz, 1H), 4.07 (d, *J* = 11.7 Hz, 1H), 3.88 (s, 3H), 3.78 (s, 3H), 3.71 (s, 3H), 3.67 – 3.62 (m, 2H), 3.46 (ddd, *J* = 11.6, 7.6, 4.2 Hz, 1H). ^{13}C NMR (126 MHz, $CDCl_3$) δ 146.58, 146.22, 146.12, 144.37, 143.66, 135.64, 135.47, 132.82, 121.23, 120.83, 120.58, 114.63, 114.53, 114.14, 111.72, 111.33, 110.57, 66.14, 56.03, 55.91, 53.43, 52.61. HRMS (TOF ESI-MS) calcd for $C_{24}H_{26}O_7$ $(M-H)^-$ 425.1606, found 425.1597.

4.3.3.2 Validation of HPLC-UV Method

The analytical method using HPLC-UV was validated following the U.S. Food and Drug Administration (FDA) and European Medicines Agency (EMA) guidelines [105,106]. In the method validation selectivity, linearity, accuracy, and precision were assessed.

Working standards were prepared in methanol by serial dilution, with concentrations ranging from 0.5 mM to 6 mM. Quality controls were prepared likewise, with concentrations of: 1.5 mM for low-quality control (LQC), 3 mM for medium-quality control (MQC), and 4 mM for high-quality control (HQC). All working standards were prepared on the day of analysis.

The matrix consisted of inactivated HLM (0.5 mg/mL), 5 mM $MgCl_2$, 5 mM D-saccharic acid 1,4-lactone monohydrate, 5 mM uridine 5'-diphosphoglucuronic acid trisodium salt and 100 mM potassium phosphate buffer (pH 7.4). The standard curves were prepared with final concentrations ranging from 2.5 to 30 µM. Quality controls followed the same procedure, with final concentrations of 7.5 µM LQC, 15 µM MQC, and 20 µM HQC.

For sample processing, acetonitrile spiked with internal standard MMPPD was added for protein

precipitation. Samples were vortex-mixed for one minute and centrifuged at 14,000 x g for 10 minutes at room temperature. Supernatant was collected and transferred to a LC vial and injected into the HPLC for analysis.

The lower limit of detection (LOD) and the lowest limit of quantification (LLOQ) were used to determine the sensitivity of the analytical method developed. For LOD, it was considered the lowest detectable concentration based on a signal-to-noise ratio of 3. LLOQ was defined as the lowest concentration that could be reliably quantified at least 5 times the signal of a blank sample.

Accuracy was expressed as percentage with mean concentrations within acceptable limits of 15%, except for LLOQ that should be within 20% of nominal value. Similarly, precision was expressed as percentage with acceptable level within 15% of the coefficient of variation (CV), except for LLOQ, where the limit should be within 20% of CV.

Additionally, intra-day accuracy and precision were also determined by analyzing six replicates of each quality control (LQC, MQC, HQC) on a single day. At least five samples should be within the CV of 15%, and CV of 20% for LLOQ. Between-run (or inter-day) accuracy and precision were determined using the same quality control samples in three runs on at least two different days as per EMA guidelines. Similarly to the intra-day analysis, at least five samples should be within the CV of 15%, and CV of 20% for LLOQ.

Linearity was assessed by processing 8-point standard curve ranging from 2.5 to 30 µM on different days. The peak area ratio (quebecol/internal standard) was plotted against the nominal concentrations of quebecol. A linear regression analysis was performed to determine slope (k), intercept, and coefficient of determination (r^2) to check the linearity of standard curves.

4.3.3.3 Microsomal incubations

4.3.3.3.1 P450-mediated microsomal incubation

A previous method was developed and optimized to investigate P450-mediated microsomal metabolism using liver microsomes [79]. Positive control (chlorzoxazone) was used to determine the human liver microsomes viability, and to evaluate if the method is working as expected.

The incubation mixture consisted of 5 mM $MgCl_2$, 10 mM SPP, 0.5 mg/mL human or rat liver microsomes, 30 µM of quebecol, and 100 mM potassium phosphate buffer at pH 7.4. This mixture was pre-incubated for 5 minutes at 37 °C in a shaking water bath, and 10 µL of 20 mM NADPH was added to initiate the reaction. Metabolism reactions were prepared in duplicate along with two negative controls: without the NADPH mixture and heated inactivated human or rat liver microsomes.

The reaction was stopped after 1 hour by adding 200 µL of ice-cold acetonitrile containing internal standard MMPPD (100 µM) for protein precipitation. Samples were vortex mixed for 1 minute, and centrifuged at 14,000 × g for 10 minutes at room temperature. Supernatant (200 µL) was collected and transferred to a LC vial and injected into HPLC for analysis.

4.3.3.3.2 UGT-mediated microsomal metabolism

A previous method developed to assess glucuronidation using hepatic microsomal fractions from humans was optimized [56]. Positive control (enterolactone) was used to determine the human or rat liver microsomes viability, and to evaluate if the method is working as expected.

The incubation mixture consisted of 5 mM $MgCl_2$, 5 mM D-saccharic acid 1,4-lactone monohydrate, 0.5 mg/mL human or rat liver microsomes, 30 µM of quebecol, and 100 mM potassium phosphate buffer at pH 7.4. This mixture was pre-incubated for 5 minutes at 37 °C in a shaking water

bath, and 10 µL of 5 mM uridine 5'-diphosphoglucuronic acid trisodium salt was added to initiate the reaction. Metabolism reactions were prepared in duplicate along with two negative controls: without the UDP mixture and heated inactivated human or rat liver microsomes.

The reaction was stopped after 1 hour by adding 200 µL of ice-cold acetonitrile containing internal standard MMPPD (100 µM) for protein precipitation. Samples were vortex mixed for 1 minute, and centrifuged at 14,000 × g for 10 minutes at room temperature. Supernatant (200 µL) was collected and transferred to a LC vial and injected into HPLC for analysis.

4.3.3.4 UGT-mediated Microsomal Metabolism Kinetics

The incubation mixture for the metabolism kinetics had the same components as listed in the previous section. A range of final concentration of quebecol (5-30 µM) was incubated in HLM. A total of 7 timepoints were chosen for the kinetics: 0, 4, 8, 12, 16, 20, and 25 minutes.

Incubation mixtures (200 µL) were prepared for each timepoint in different Eppendorf tubes and placed in a shaking water bath at 37 °C. Reaction was initiated by the addition of UDP (pre-incubated at 37 °C). Samples were removed from the shaking water bath at their respective timepoints and 200 µL of ice-cold acetonitrile containing internal standard MMPPD (100 µM) was added for protein precipitation. Samples were vortex mixed for 1 minute and centrifuged at 14,000 × g for 10 minutes at room temperature. Supernatant (200 µL) was collected and transferred to a LC vial and injected into HPLC for analysis.

4.3.3.5 Data Analysis

To calculate the kinetic parameters, the substrate depletion approach was used [107–110]. The peak area ratio (quebecol/internal standard) was normalized to the ratio obtained at t = 0 as 100%. Then, the natural log of quebecol percentage was determined and plotted against time. A linear regression was performed to calculate the substrate depletion rate (k_{dep}) for each quebecol concentration. For each concentration, k_{dep} was expressed as the mean ± standard deviation (SD) of replicate determinations.

Next, the k_{dep} obtained were plotted against the different quebecol concentrations using a nonlinear least squares regression analysis with GraphPad Prism 8.0. To calculate K_M and $k_{dep([S]\rightarrow 0)}$, the following equation was used:

$$\boldsymbol{k_{dep} = k_{dep([S]\rightarrow 0)}\ \mathbf{x}\ \left(1 - \frac{[S]}{[S]+K_m}\right)} \qquad (4.1)$$

In the equation 4.2, [S] represents the substrate concentration, $k_{dep([S]\rightarrow 0)}$ is defined as the depletion rate constant at infinitesimal substrate concentrations, and K_M the Michaelis-Menten constant. Other kinetics parameters, such as intrinsic clearance at an infinitesimally low substrate concentration ($Cl_{int, dep([S]\rightarrow 0)}$) was calculated by dividing the acquired $k_{dep([S]\rightarrow 0)}$ in the last step by the human microsomal protein concentration (0.5 mg/mL). Lastly, the maximum velocity (V_{max}) was obtained from K_M and $Cl_{int, dep([S]\rightarrow 0)}$ [111].

4.4 Results

4.4.1 Synthesis and characterization of Quebecol

We accomplished the synthesis of quebecol by modifying existing literature procedures as shown in Scheme **4.1** [101]. First, we carried out a benzylation on the commercially available 4-bromo-2-methoxyphenol and 4-hydroxy-3-methoxybenzaldehyde (vanillin) using benzyl bromide and potassium carbonate in methanol achieving good yields (91 and 70%, respectively). We used the benzylated products for the next step in which we performed a lithiation of 1-(benzyloxy)-4-bromo-2-methoxybenzene (**9**) using n-BuLi and subsequent reaction with the 4-(benzyloxy)-3-methoxybenzaldehyde (**10**) to yield the biphenyl alcohol (**11**).

Bromination of the biphenyl alcohol (**11**) was performed using acetyl bromide in THF. Due to the instability of the brominated product, we were unable to purify the brominated biphenyl compound (**12**). Therefore, we dried the resultant crude under high vacuum and carried over to the next step without further purification.

LDA was used to treat the ester (**13**) followed by the addition of the bromo intermediate (**12**) at -78 °C. We achieved the coupled product (**14**) with reasonable yield (30%) and we confirmed its structure by NMR and MS. In our ^{1}H NMR we observed the presence of two doublets at δ 4.47 (d, J = 12.0 Hz, 1H) and δ 4.18 (d, J = 12.0 Hz, 1H) in addition to ESI-MS (*m/z*) of 742.3 $[M + H_2O]^+$ and 747.3 $[M + Na]^+$ which allowed us to confirm formation of the coupled product.

Reduction of the coupled product was achieved using lithium aluminum hydride in THF. We observed reasonable yields (49%) for this step when the reaction was allowed to proceed longer than 16 hours. We recovered the unreacted ester after silica gel column purification, and we repeated the reduction reaction. For the last step, we performed a hydrogenolysis of **15** to remove the benzyl protecting

groups by using Pd/C under H_2 atmosphere to yield quebecol with excellent yield (94%).

We obtained quebecol with an overall yield of 4.4%. We have confirmed quebecol through ESI-MS (negative mode) which yielded an *m/z* of 425.0. Additionally, we used ^{1}H and ^{13}C NMR for the characterization and comparison with literature (Supporting Information).

4.4.2 HPLC-UV Method Validation

We have successfully validated an HPLC-UV method using FDA and EMA guidelines to measure the concentration of quebecol accurately and precisely in human liver microsomes. We did not find any endogenous substance in the matrix that could interfere with quebecol or MMPPD (internal standard) retention times (Figure 4.2). Under the chromatographic conditions we used, the retention time for quebecol and MMPPD was 13.8 minutes and 17.5 minutes, respectively.

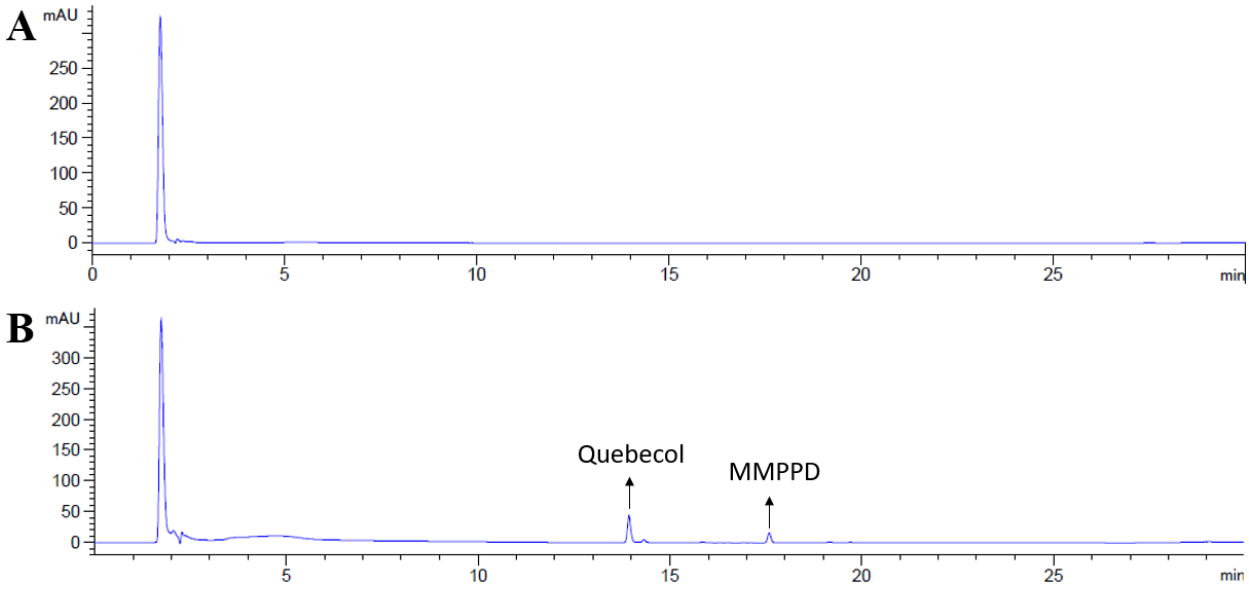

Figure 4.2. Specificity of the method. HPLC-UV chromatograms of HLM without quebecol and MMPPD (A) and HLM spiked with quebecol and MMPPD (B).

The calibration curve was prepared in the same biological matrix (human liver microsomes) as the samples for this study. A total of 8 calibration points were used, including the LLOQ and the ULOQ. The chromatographic method was linear between 2.5 and 30 µM with r^2 values ≥ 0.998 (n = 3).

We determined an LLOQ of 2.5 µM with signal to noise ratio of 7. Full validation parameters are presented for intra-day (

Table 4.1) and inter-day (Table 4.2). Intra-day accuracy varied from 90.5 to 107.1%, precision from 2.92 to 13.7% for all quality controls and LLOQ, with the observed ranges compliant with both FDA and EMA guidelines. Similarly, inter-day accuracy and precision varied from 97.8 to 103.9%, and from 4.01 to 11.58% respectively. Overall, the intra- and inter-day precision and accuracy were within the acceptable limits as per the guidelines.

Table 4.1. Intra-day assay precision and accuracy for quebecol in human liver microsomes

Quality control	Replicates	Analysis day (#)	Observed concentration (mean ± SD; µM)	Precision (RSD%)	Accuracy (%)
LLOQ (2.5 µM)	5	1	2.26 ± 0.20	8.06	90.5
	6	2	2.37 ± 0.15	5.95	95.0
	6	3	2.60 ± 0.34	13.7	104.1
LQC (7 µM)	5	1	6.76 ± 0.59	8.5	96.6
	6	2	6.99 ± 0.36	5.23	100.0
	6	3	7.33 ± 0.24	3.46	104.8
MQC (15 µM)	5	1	16.06 ± 1.47	9.8	107.1
	5	2	14.43 ± 1.32	8.85	96.3
	5	3	15.18 ± 1.60	10.71	101.2
HQC (20 µM)	5	1	20.86 ± 0.83	4.17	104.3
	6	2	20.13 ± 0.58	2.92	100.7
	6	3	21.37 ± 0.62	3.11	106.9

SD = standard deviation, RSD = relative standard deviation

Table 4.2. Inter-day assay precision and accuracy for quebecol in human liver microsomes

Quality control	Replicates	Observed concentration (mean ± SD; µM)	Precision (RSD%)	Accuracy (%)
LLOQ (2.5 µM)	17	2.44 ± 0.28	11.58	97.8
LQC (7 µM)	17	7.04 ± 0.45	6.43	100.7
MQC (15 µM)	15	15.22 ± 1.52	10.02	101.5
HQC (20 µM)	17	20.78 ± 0.83	4.01	103.9

SD = standard deviation, RSD = relative standard deviation

4.4.3 *In vitro* Metabolism of Quebecol in HLM

We assessed the *in vitro* P450-mediated metabolism of quebecol in both human and rat liver

microsomes using NADPH as a cofactor. We were unable to detect any P450 metabolites in either incubation and could not measure any change in quebecol after the 1 h incubation (Figure 4.3). Due to the sensitivity of the HPLC-UV method, we confirmed no metabolite formation by analyzing our samples using LC/MS.

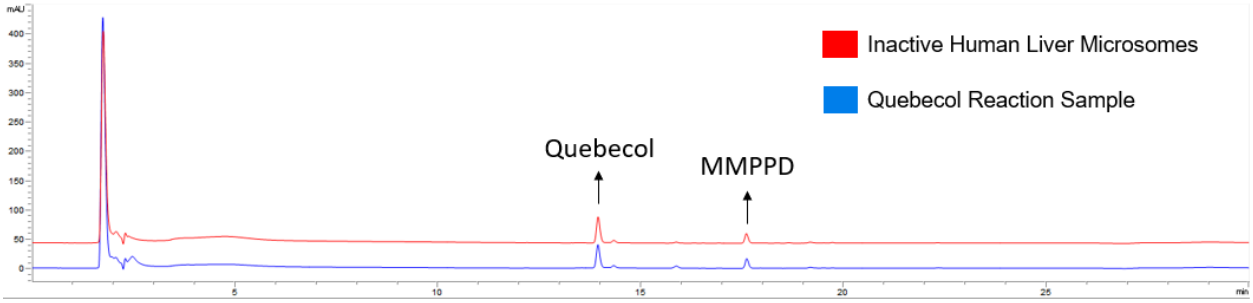

Figure 4.3. HPLC-UV chromatogram of 20 µL injection of 30 µM samples from *in vitro* metabolism in human liver microsomes of quebecol containing NADPH as a cofactor. Quebecol and MMPPD were detected at 13.8 and 17.5 minutes, respectively.

We investigated whether quebecol was a substrate for uridine diphosphate glucuronosyl transferase (UGT) (i.e. phase II metabolism) by carrying out *in vitro* incubations in the presence of the cofactor UDP-glucuronic acid in both human and rat liver microsomes. Under these incubation conditions we detected the formation of three glucuronides of quebecol (Figure 4.4) with human and rat liver microsomes both showing the same glucuronides (rat liver microsomes data not shown).

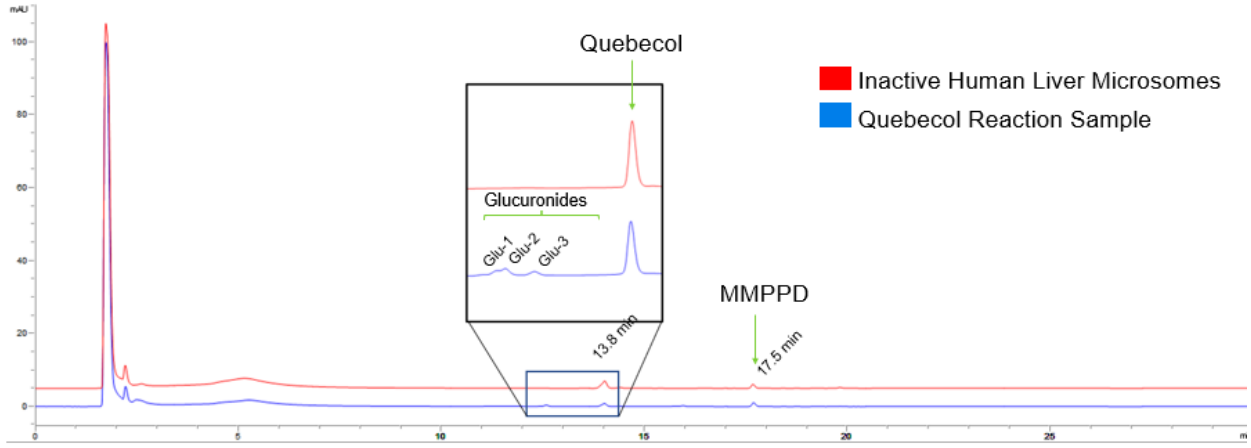

Figure 4.4. HPLC-UV chromatogram of 20 µL injection of 30 µM samples from *in vitro* glucuronidation in human liver microsomes of quebecol. Three glucuronide metabolites Glu-1, Glu-2, and Glu-3 were detected at 12.5, 12.9, and 13.1 minutes, respectively.

After the detection of the three metabolites, we performed LC-MS analysis for metabolite identification. Samples were diluted (1:100) in LC-MS mobile phase grade (acetonitrile:water) and injected (5 µL) for LC-MS analysis using ESI-MS. All three quebecol glucuronides have the same *m/z* of 601.2 in negative mode (Figure 4.5).

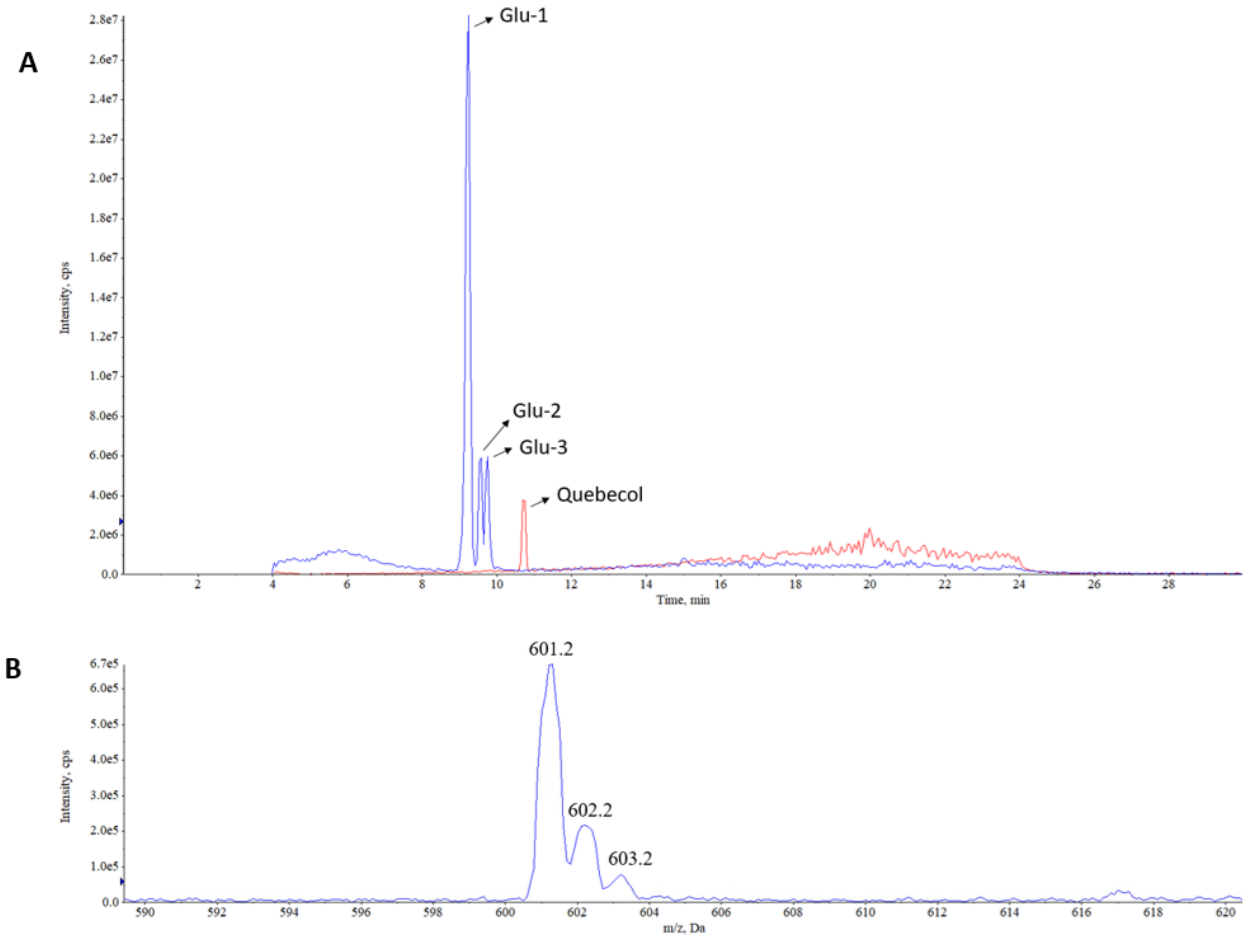

Figure 4.5. A) LC-MS extracted ion chromatogram (XIC) for glucuronides adducts at *m/z* 601.2 ± 0.5 (blue) and for quebecol at *m/z* 425.0 ± 0.5 (red). B) Corresponding mass spectrum for one of the glucuronides.

Tandem mass spectrometry (LC-MS/MS) was used to further identify and confirm the formation of the glucuronides, with substitution most likely occurring at the three phenolic groups. Cleavage of the anomeric C-O bond of the glucuronide conjugate has been previously reported leading to fragmentation as shown in Figure 4.6D producing the diagnostic ion at *m/z* 425. [112]. Additionally, the ions at *m/z* 113 and 85 are coming from the glucuronide conjugate by losing water and carbon dioxide, and water, carbon dioxide, and carbon monoxide respectively [112,113].

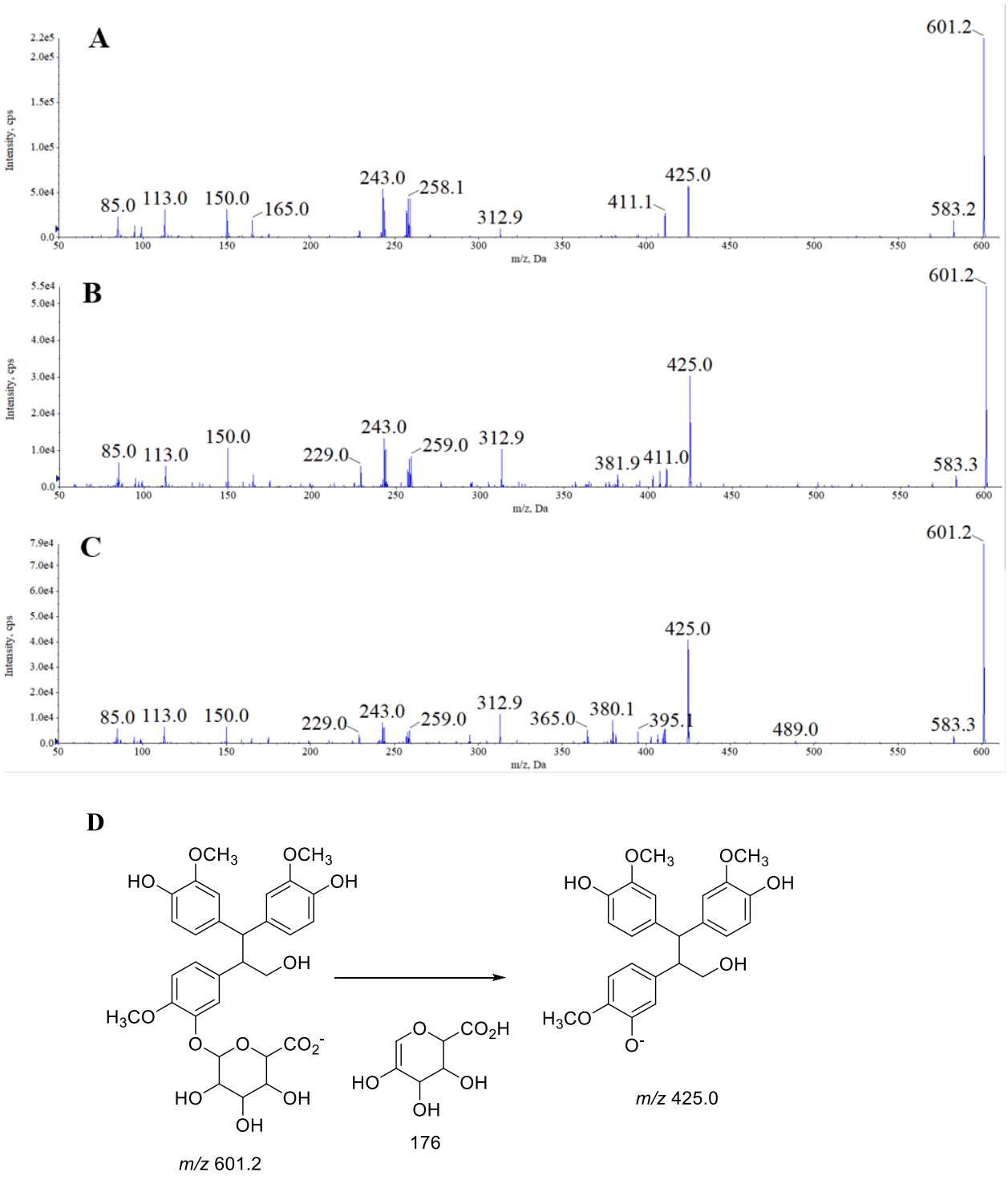

Figure 4.6. ESI-MS/MS enhanced product ion (EPI) spectrum for Glu-1 (A), Glu-2 (B), and Glu-3 (C) performed in negative mode. Fragmentation of one of the proposed quebecol glucuronides (D).

4.4.4 UGT-mediated Microsomal Metabolism Kinetics

We calculated the kinetics parameters to assess the extent of glucuronidation of quebecol in human liver microsomes using the substrate depletion approach to determine the *in vitro* parameter values [111]. Negative controls consisted of incubation mixtures containing heat inactivated microsomes and no UDP, which showed no loss of starting material over time.

The substrate depletion rate (k_{dep}) was extracted from the linear regression plot of the natural log of percentage quebecol against time (Figures S13, S14). For nonlinearity samples ($r^2<0.98$), we only used the initial points with linearity to determine k_{dep}. For each concentration, we reported the k_{dep} as the mean ± standard deviation (SD) of replicate determinations (Table S3).

We performed nonlinear least squares regression analysis in a plot containing the k_{dep} values and the quebecol concentrations as shown in Figure 4.7. The *in vitro* Cl_{int} values of quebecol glucuronidation and other kinetics parameters were determined, and we reported them in Table 4.3.

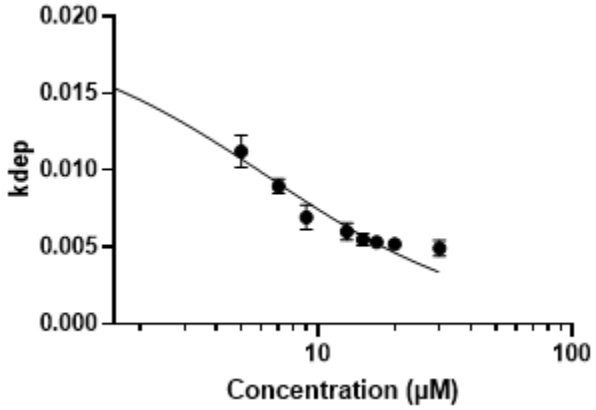

Figure 4.7. Plot of in vitro depletion rate (k_{dep}) (min^{-1}) versus quebecol concentrations (µM) for quebecol glucuronidation in human liver microsomes

Table 4.3. Cl_{int} and Michaelis-Menten constants of quebecol glucuronidation by human liver microsomes

Cl_{int} (mL/min/mg)	95% CI for Cl_{int}	K_M (µM)	95% CI for K_M	V_{max} (µmol/min/mg)
0.04	0.03 to 0.06	5.1	2.9 to 8.3	0.22

4.5 Discussion

We hypothesized that due to the presence of multiple OH groups on quebecol, phase 2 metabolic processes such as glucuronidation and sulfonation would predominate *in vitro*. In order to test this hypothesis we synthesized quebecol adapting literature methods for our studies [61]. As quebecol is not found naturally in maple sap, rather it is produced during heating and concentration of maple sap to maple syrup, quebecol is present as a racemic mixture and we did not attempt an enantiomeric separation on our synthetic product (Figure 4.8).

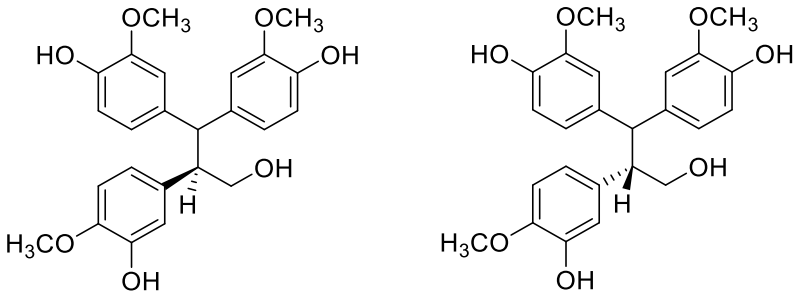

Figure 4.8. Possible enantiomers of quebecol.

Our microsomal Phase 1 experiments demonstrated that no cytochrome P450 metabolites of quebecol were formed at detectable levels. Minimal P450-mediated metabolism has been previously

observed for polyphenolics such as the lignan nordihydroguaiaretic acid which also predominantly undergoes phase 2 glucuronidation which concurs with our results [19]. We were able to detect three phase 2 glucuronide metabolites in our microsomal incubations. The glucuronide metabolites appear to be the result of reaction at the phenolic OH groups and the HPLC UV peaks suggest that the three glucuronides are formed in similar amounts. Although the 3-position of the propanol substituted with the 3-methoxy, 4-hydroxy phenyl groups is not chiral, glucuronide substitution of either phenol would create a chiral center and therefore a novel stereoisomer. This results in the potential formation of six glucuronides consisting of three enantiomeric pairs (Figure 4.9. R and S, R,R and S,S, R,S and S,R) producing three distinct glucuronide signals in the HPLC (Figure 4.4) although we note that enzymatic selectivity for the formation of specific glucuronide isomers remains a possibility. However, the ESI-MS/MS fragmentation did not allow us to distinguish between the stereoisomers as loss of the glucuronide (176.2) occurred for all three metabolites.

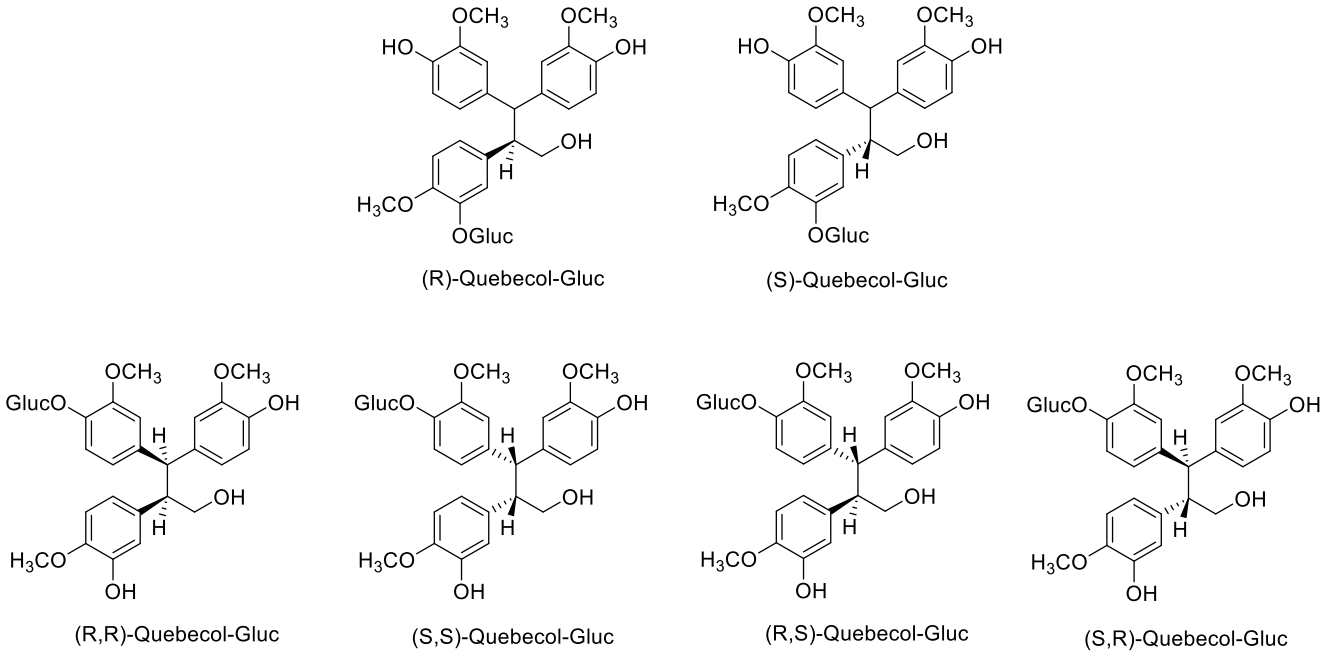

Figure 4.9. Proposed phenol-substituted glucuronides. Enantiomeric pairs are: R and S; R,R and S,S;

R,S and S,R.

The identification of the metabolites and the elucidation of the disposition pathways provide an understanding into the extent of metabolism. Another important concept for drug metabolism consists of the rate of metabolism which can be measured by the kinetics of depletion of substrates and/or formation of metabolites [114]. Monitoring kinetics by metabolite formation requires authentic metabolite standards to prepare calibration curves in the analytical method, whereas the substrate depletion approach is a reliable alternative to calculate the kinetic parameters by monitoring the depletion of the substrate as a function of time [107–110]. We have previously used the substrate depletion approach to follow UGT metabolism [56] and for this study, we have validated an HPLC-UV method to measure the phase 2 glucuronidation using the substrate depletion approach.

Normally, the use of this approach can lead to an overestimation of the intrinsic clearance (Cl_{int}) and K_M values since the formation of individual metabolites are potentially missed. In this case, the calculated values would represent an accumulation of kinetic parameters for different metabolic pathways [107]. However, this is of least concern for quebecol since no cytochrome P450 metabolites were formed at detectable levels, and only glucuronides were formed.

Glucuronidation is a well-known metabolism and detoxification pathway of drugs in humans which takes place predominantly in the liver [115]. We determined the *in vitro* hepatic glucuronidation kinetic parameters of quebecol in pooled HLM (Table 4.3) to generate accurate data to predict *in vivo* human clearance. The Michaelis-Menten constant (K_M) is one of the pharmacokinetic parameters that allows understanding the role of the metabolizing enzymes. Lower K_M values indicate a greater affinity of the substrate to the enzyme, which can lead to the saturation of the clearance pathway. We calculated a K_M value for quebecol of 5.1 µM. Similarly, the major elimination mechanism of tamoxifen is via

glucuronidation of its major active metabolites, 4-hydroxytamoxifen (4-OH-TAM) and endoxifen [116]. *In vitro* kinetics showed that UGT1A7 (K_M = 7.4 µM) and UGT2B7 (K_M = 3.7 µM) are the main hepatic enzymes responsible for the *O*-glucuronidation of the *cis*- and *trans*-4-OH-TAM respectively [117] which is comparable to K_M values we determined for quebecol and for glucuronidation of the lignan enterolactone (K_M 8.91 µM) [56]. We also determined that quebecol had a Cl_{int} = 0.04 mL/mg/min which is *ca.* 29 times less than observed for enterolactone (Cl_{int} = 1.18 mL/mg/min), suggesting slower clearance of quebecol [56]. The analogs reported by Pericherla *et. al.* with greater antiproliferative activity than quebecol (Figure **4.10**) all have two *para*-phenols and would be anticipated to undergo glucuronidation at a similar rate to quebecol [61].

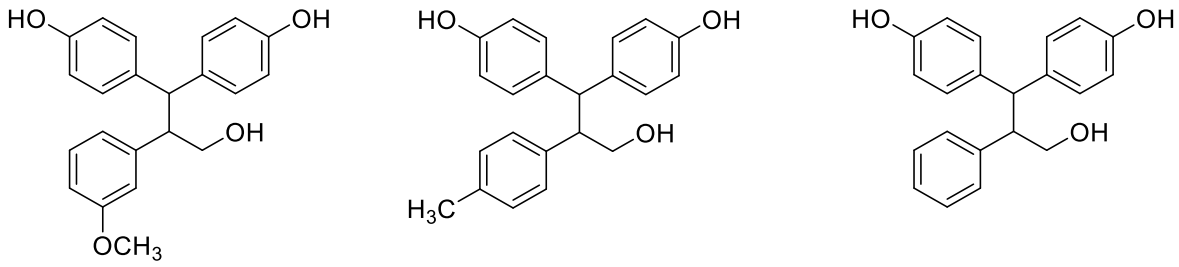

Figure 4.10. Structures of antiproliferative quebecol analogs from Pericherla *et. al.* [101]

In summary, we have investigated the metabolic fate of the natural product quebecol in both human and rat liver microsomes. We were unable to detect any P450 metabolites, but did observe formation of glucuronide conjugates, although the Cl_{int} we determined suggests quebecol glucuronidation occurs at only a moderate rate. We did not assess sulfonate conjugation but anticipate that it may also contribute to phase 2 metabolic clearance of quebecol. Our work also highlighted the method development and validation of an HPLC-UV method to measure UGT-mediated microsomal metabolism

kinetics parameters in human liver microsomes.

Chapter 5: The Natural Product Quebecol is Resistant to Bioactivation in Hepatic Microsomes

Gabriel Bernardes & Ed S. Krol

Drug Discovery and Development Research Group, College of Pharmacy and Nutrition, University of Saskatchewan, Saskatoon, SK

Transitioning rationale: In the last chapter, we did not detect any P450 metabolites for quebecol rather, we found extensive glucuronide formation. There are many phenol-containing drugs that are similar to quebecol known to form quinone metabolites. Even though phase 2 metabolism of quebecol is likely the main clearance pathway, it is important to investigate metabolic formation of *p*-QM. In this chapter, we assess quinone formation using GSH trapping in RLM and HLM and using chemical oxidants.

Contribution statement: Gabriel Bernardes contributed to the experimental design, conducted the experimental work and data analysis, and drafted the manuscript. Dr Ed Krol supervised the work and revised the manuscript.

5.1 Abstract

Quebecol (2,3,3-tri-(3-methoxy-4-hydroxyphenyl)-1-propanol) is a polyphenolic compound, which is formed during maple syrup production from *Acer saccharum* spp. Quebecol is similar in structure to the chemotherapy drug tamoxifen, which has led to synthesis of structural analogs and investigations into their pharmacological properties. Previously, we were unable to detect any P450 metabolites in either RLM or HLM. In this study, we found no evidence of reactive intermediate formation by performing glutathione (GSH) trapping experiments. We prepared standards of the quebecol *para*-quinone methide (*p*-QM) using manganese dioxide, trapped as GSH adducts. In an effort to confirm whether or not quebecol could form a p-QM we synthesized a series of diphenylethane analogs to probe p-QM reactivity. We determined that quebecol was resistant to *p*-QM formation, even when oxidized by MnO_2 and instead formed *ortho*-quinones. A combination of steric and electronic factors likely contribute to resistance to *p*-QM formation.

5.2 Introduction

The polyphenol quebecol is a product of maple syrup production and has reported pharmacological properties [59,101,102,118] and analogs of quebecol are currently under investigation for their pharmacological properties [101–103,119]. The presence of three phenol groups and a primary alcohol make quebecol susceptible to hepatic phase 2 processes and we have reported that quebecol predominantly forms three glucuronide metabolites in human liver microsomes (HLM) (manuscript in preparation). Surprisingly, we were unable to detect any metabolites associated with P450-mediated processes such as de-methylation, aromatic hydroxylation or *para*-quinone methide (*p*-QM) formation. We were especially concerned with the potential for formation of *p*-QMs (Figure 5.1) which are electrophilic reactive intermediates capable of toxicity as a result of covalent modification of biological nucleophiles [120,121]. Quebecol is racemic so the possible *p*-QMs include three distinct mono-*p*-QMs and two possible di-*p*-QMs (Figure 5.1).

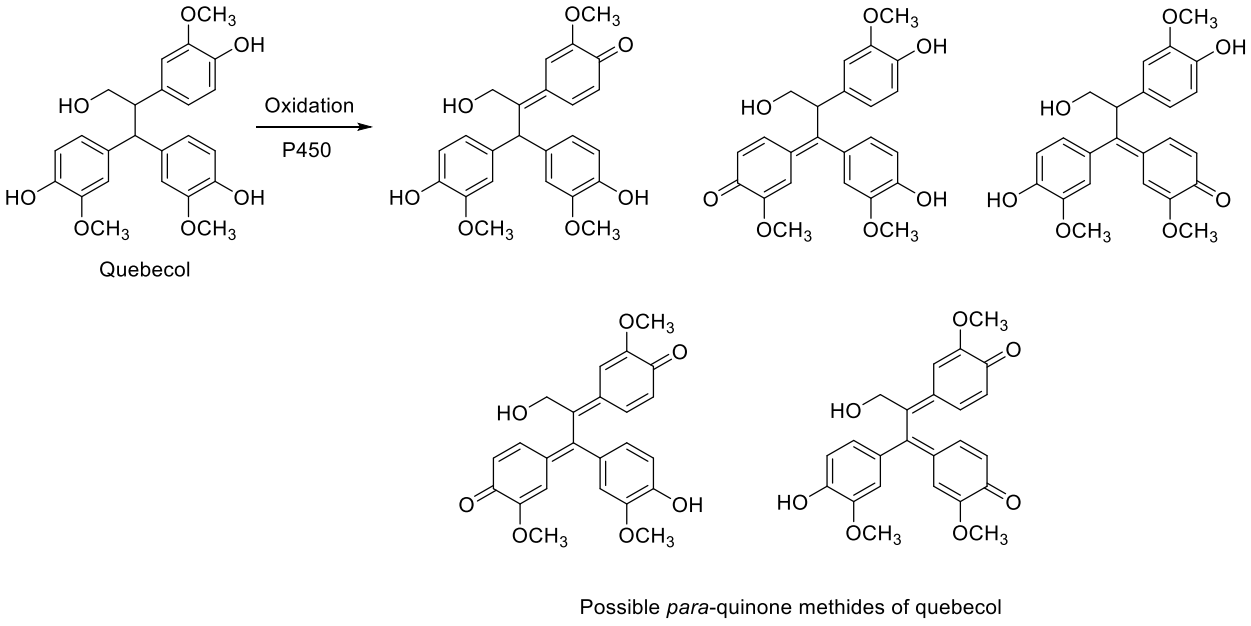

Figure 5.1. Quebecol and potential *para*-quinone methides (*p*-QMs).

Numerous phenol-containing compounds such as raloxifene [122] and 4-hydroxylated metabolites of tamoxifen and toremifene [123] are known to form quinone metabolites, including *p*-QMs, and numerous drugs have associated warnings due to the formation of reactive metabolites [124,125]. The low levels of quebecol present in maple syrup (~0.04 ppm) [59] and its clearance mainly via phase 2 metabolism as reported by our group suggest *p*-QM formation is unlikely to be a concern. However due to interest in the biological properties of quebecol analogs [101–103,119], metabolic formation of *p*-QMs requires further examination. We hypothesize that quebecol can form electrophilic *p*-QMs and in order to study this we will assess quinone formation in HLM *in vitro* and using chemical oxidants and trap the resulting *p*-QMs as glutathione (GSH) adducts.

5.3 Materials and Methods

5.3.1 Materials

Sigma-Aldrich (St. Louis, MO): dipotassium orthophosphate (K_2HPO_4), potassium dihydrogen orthophosphate (KH_2PO_4), magnesium sulfate ($MgSO_4$), silver nitrate ($AgNO_3$), potassium permanganate ($KMnO_4$), Reduced glutathione (GSH), acetonitrile (LC-MS grade), methanol (HPLC grade), formic acid (LC-MS grade). Fisher Scientific (Fairlawn, NJ): magnesium chloride ($MgCl_2$), potassium hydroxide (KOH), sodium pyrophosphate decahydrate (SPP). Anachemia (Quebec, CA): manganese sulfate ($MnSO_4$). Roche Diagnostics (Indianapolis, IN): reduced nicotinamide adenine dinucleotide (NADPH). Water was purified via a Millipore (Mississauga, ON) Milli-Q system with a Quantum EX Cartridge. Gibco (Waltham, MA): pooled human liver microsomes were purchased from Fisher Scientific (Ottawa, ON). Quebecol, 2,2-di-(3-methoxymethylphenyl)-1,3-propanediol (MMPPD), silver oxide and manganese dioxide were prepared following literature procedures [101,104,122,126].

5.3.2 Instrumentation

5.3.2.1 HPLC-UV Diode Array Analysis

Analysis of the autoxidation studies and reaction kinetics were performed on an Agilent 1200 high-performance liquid chromatography (HPLC) (Agilent Technologies; Mississauga, ON) equipped with a degasser (G1379A), quaternary pump (G1311A), autosampler (G1329A), and diode array detector (G1315D). The HPLC column was a Restek Ultra Biphenyl (2.1 x 100 mm, 5 μm) and the solvent system consisted of 0.1% LC-MS grade formic acid in water (solvent A) and 0.1% LC-MS grade formic acid in acetonitrile (solvent B) operating at a flow rate of 0.2 mL/min. The gradient method consisted of an initial isocratic phase at 90% solvent A for 2.5 minutes, decreased gradually to 10% solvent A over 12.5 minutes, and holding for 5 minutes before returning to the initial conditions, equilibrating for 10 minutes.

5.3.2.2 ESI-MS Analysis

Mass spectrometric analysis of quebecol and its intermediates was conducted using an AB SCIEX 4000 QTRAP (AB SCIEX, Redwood City, CA, USA) quadrupole linear ion trap mass spectrometer. Samples were infused directly using a flow of 10 μL/min. Phase I metabolite formation of reactive intermediates was conducted using LC-MS which consisted of an Agilent 1100 high-performance liquid chromatography (HPLC) (Agilent technologies, Mississauga, ON) coupled to an AB SCIEX 4000 QTRAP (AB SCIEX, Redwood City, CA, USA) quadrupole linear ion trap mass spectrometer. The reverse phase column and gradient method was the same as the HPLC-UV analysis. The mass spectrometric analysis was performed in negative ion mode, and fragmentation patterns were studied by tandem ESI-MS/MS operated in the negative ion mode. Data acquisition and analyses were performed using Analyst 1.7 software from AB SCIEX.

5.3.2.3 NMR Analysis

All NMR experiments were performed on a Bruker AVANCE DPX-500 spectrometer (Karlsruhe, Germany) and data processed by MestreNova 14.1. All compounds were drawn and named using ChemDraw 20.0.

5.3.3 Methods

5.3.3.1 *Synthesis and Characterization of* 4,4'-(ethane-1,2-diyl)bis(2-methoxyphenol) ($(MeO)_2$-DPE)

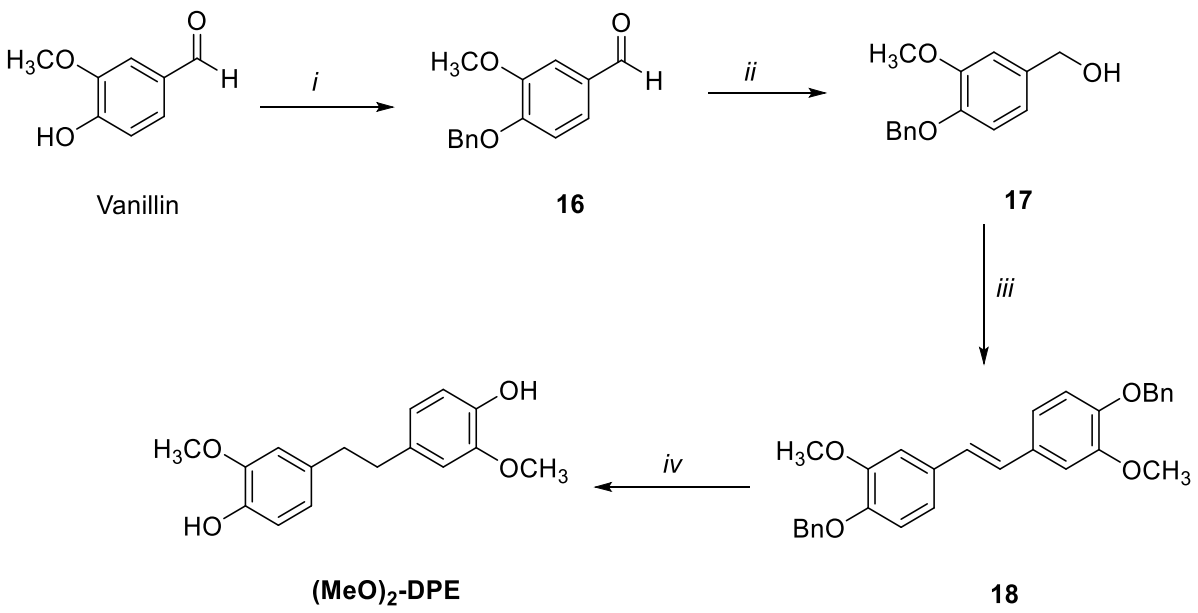

Scheme 5.1. Synthesis of $(MeO)_2$-DPE. Reagents and Conditions: i) BnBr, K_2CO_3, MeOH, reflux, 4h, 70%; ii) $NaBH_4$, THF, r.t, 18h, 97%; iii) NBS, PPh_3, K_2CO_3, toluene, reflux, 18h, 7%; iv) Pd/C, H_2, THF, r.t., 99%.

Synthesis of 4-(benzyloxy)-3-methoxybenzaldehyde (16)

K_2CO_3 (1.8 g, 13.1 mmol) and MeOH (20 mL) were added to a reaction flask, and the mixture was stirred at 0 °C under N_2. Vanillin (1 g, 6.57 mmol) was dissolved in MeOH (5 mL) and added dropwise to the reaction. After 5 minutes, benzyl bromide (2.2 g, 13.1 mmol) was added dropwise to the mixture, and reaction was refluxed at 85 °C for 4 hours. On completion, the reaction was cooled to room temperature, and solvent evaporated. The residue was dissolved in chloroform (80 mL) and washed with water. The organic layer was dried over $MgSO_4$, and evaporated to afford **16** as a yellow oil (1.1 g, 70%). ^{1}H NMR (500 MHz, $CDCl_3$) δ 9.84 (s, 1H), 7.46 – 7.42 (m, 3H), 7.41 – 7.37 (m, 3H), 7.35 – 7.31 (m, 1H), 6.99 (d, *J* = 8.2 Hz, 1H), 5.25 (s, 2H), 3.95 (s, 3H).

Synthesis of (4-(benzyloxy)-3-methoxyphenyl)methanol (17)

$NaBH_4$ (0.2 g, 6.1 mmol) was added into a flask containing THF (10 mL). Mixture was stirred at 0 °C under N_2. Compound **16** (1 g, 4.1 mmol) in THF was added dropwise to the mixture. Reaction was warmed to room temperature and stirred under N_2 overnight. Mixture was poured slowly into cold water (20 mL), extracted with chloroform (3 × 20 mL). The organic layer was dried over $MgSO_4$, and evaporated to afford **17** as a white powder (0.97 g, 97%). ^{1}H NMR (500 MHz, CDCl3) δ 7.46 – 7.40 (m, 2H), 7.38 – 7.34 (m, 2H), 7.32 – 7.28 (m, 1H), 6.95 (d, J = 1.9 Hz, 1H), 6.85 (d, J = 8.2 Hz, 1H), 6.82 (dd, J = 8.1, 1.9 Hz, 1H), 5.16 (s, 2H), 4.61 (s, 2H), 3.91 (s, 3H), 3.39 (s, 1H).

Synthesis of (*E*)-1,2-bis(4-(benzyloxy)-3-methoxyphenyl)ethene (18)

To a stirred solution of **17** (0.2 g, 0.81 mmol) and triphenylphosphine (0.53 g, 2.04 mmol) in toluene (10 mL), N-Bromosuccinimide (0.14 g, 0.81 mmol) was added. The reaction mixture was

refluxed under N_2 for 4 hours. After completion, the mixture was cooled to room temperature. At room temperature, a solution of **16** (0.19 g, 0.81 mmol) was added followed by K_2CO_3 (1.11 g, 8.1 mmol) and then refluxed overnight. After cooling to room temperature, toluene was removed under reduced pressure. The residue was dissolved in ethyl acetate, and washed with brine and dried over $MgSO_4$. After evaporation of solvents, the residue was purified on silica gel column (3:2 Hexanes/EtOAc) to give alkene (*Z*)-**18** as a white solid (27 mg, 7%).^{1}H NMR (500 MHz, $CDCl_3$) δ 7.46 – 7.43 (m, 2H), 7.40 – 7.34 (m, 2H), 7.33 – 7.28 (m, 1H), 7.06 (d, *J* = 2.0 Hz, 1H), 6.96 (dd, *J* = 8.3, 2.0 Hz, 1H), 6.90 (s, 1H), 6.85 (d, *J* = 8.3 Hz, 1H), 5.18 (s, 2H), 3.95 (s, 3H). ^{13}C NMR (126 MHz, $CDCl_3$) δ 149.89, 137.22, 131.27, 128.71, 128.00, 127.39, 126.89, 119.58, 114.11, 109.29, 71.15, 56.13. ESI-MS (*m/z*) 453.2 $[M + H]^+$, 470.0 $[M + H_2O]^+$.

Synthesis of 4,4'-(ethane-1,2-diyl)bis(2-methoxyphenol) ($(MeO)_2$-DPE)

Pd/C (10% w/w, 2.6 mg) was added to a reaction flask under N_2. The flask was sealed, and dry THF (5 mL) was added. The compound **18** (26 mg) in dry THF (2 mL) was added to the reaction dropwise. The flask was evacuated, then flushed with H_2 gas. The reaction was left to stir under H_2 overnight. The reaction mixture was filtered through a Celite pad and washed with MeOH. The solvent was removed under reduced pressure to give $(MeO)_2$-DPE as a dark solid (16.2 mg, 99%). ^{1}H NMR (500 MHz, $CDCl_3$) δ 6.83 (d, *J* = 8.0 Hz, 1H), 6.67 (dd, *J* = 8.0, 2.0 Hz, 1H), 6.61 (d, *J* = 1.9 Hz, 1H), 5.46 (s, 1H), 3.84 (s, 3H), 2.81 (s, 2H). ^{13}C NMR (126 MHz, $CDCl_3$) δ 146.34, 143.84, 133.88, 121.17, 114.27, 111.31, 55.98, 38.09. ESI-MS (*m/z*) 275.1 $[M + H]^+$.

5.3.3.2 Preparation of Silver Oxide

A solution of potassium hydroxide (0.36g in 10 mL of water) was added to a silver nitrate solution (1g in 10 mL of water) [122]. The mixture was stirred at room temperature for 15 minutes. The precipitate was filtered, washed with water, and dried to yield a fine black powder (0.5g).

5.3.3.3 Preparation of Manganese Dioxide

To a solution of potassium permanganate (0.43g in 8 mL of water) stirring at 60 °C, a solution of manganese sulfate (0.62 g in 12 mL of water) was added [126]. The suspension was stirred at 60 °C for 1 h, the suspension was filtered, and the precipitate washed several times with water. The precipitated was dried under high vacuum to yield a dark-brown powder (0.4 g).

5.3.3.4 Cytochrome P450 Oxidation Studies

A previous method was developed and optimized to investigate P450-mediated oxidation of quebecol [79]. Reduced glutathione (GSH) was added either at the beginning of the incubation (method A) or after the incubation (method B). All experiments were performed in triplicate. Negative controls were incubated with no NADPH and using heat inactivated liver microsomes. Positive control (chlorzoxazone) was used to determine the human liver microsomes viability.

The incubation mixture of method A consisted of 5 mM $MgCl_2$, 10 mM SPP, 0.5 mg/mL human or rat liver microsomes, 30 µM of quebecol and 100 mM potassium phosphate buffer at pH 7.4 containing GSH (0.3 mM). This mixture was pre-incubated for 5 minutes at 37 °C in a shaking water bath, and 10 µL of 20 mM NADPH was added to start the reaction. The reaction was stopped after 1 hour by addition of ice-cold acetonitrile containing internal standard MMPPD (100 µM) for protein precipitation. Samples were vortex mixed for 1 minute, and centrifuged at 14,000 × g for 10 minutes at room temperature. Supernatant (200 µL) was collected and transferred to a LC vial and injected into HPLC for analysis.

The incubation mixture of method B consisted of 5 mM $MgCl_2$, 10 mM SPP, 0.5 mg/mL human or rat liver microsomes, 30 µM of quebecol and 100 mM potassium phosphate buffer at pH 7.4. This mixture was pre-incubated for 5 minutes at 37 °C in a shaking water bath, and 10 µL of 20 mM NADPH was added to start the reaction. The reaction was stopped after placing it on an ice bath, and a 20-fold excess of GSH was added, as well as addition of ice-cold acetonitrile containing internal standard MMPPD (100 µM) for protein precipitation. Samples were vortex mixed for 1 minute, and centrifuged at 14,000 × g for 10 minutes at room temperature. Supernatant (200 µL) was collected and transferred to a LC vial and injected into HPLC for analysis.

5.3.3.5 Preparation of *p*-QM standards

Quebecol or $(MeO)_2$-DPE was added to 100 mM potassium phosphate buffer at pH 7.4 to give a final concentration of 0.5 mM and the mixture was stirred at 0 °C [6]. Freshly prepared manganese dioxide (5 mg) was carefully added to the solution [126]. The suspension was stirred for 1 h at 0 °C, and filtered using 0.2 µM PVDF 13 mm syringe filter (GE Healthcare Life Sciences, NJ, USA). The filtrate was added to potassium phosphate buffer at pH 7.4 containing GSH to a final concentration of 1:10 substrate-GSH. The samples were diluted in mobile phase (1:1 acetonitrile/water) and analyzed by LC-MS. All experiments were performed in triplicate. Control experiments contained eugenol as a test compound to validate the oxidation and the analytical method.

5.4 Results

5.4.1 Cytochrome P450 Oxidation Studies

We assessed the formation of quebecol *p*-QMs by incubating quebecol in human liver microsomes with glutathione (GSH). This experiment was designed to confirm whether quebecol could form reactive quinones via P450-mediated *in vitro* metabolism and use GSH as a nucleophilic trapping agent. HPLC was used to follow the possible loss of starting material and GSH adduct formation.

We observed no significant loss of quebecol after the microsomal metabolism incubation and no GSH adduct was detected. Due to the moderate sensitivity of HPLC-UV, we used a more sensitive method, LC/MS, to further analyze our sample for GSH adducts by scanning for neutral loss (NL) of *m/z* 129 and 307 in positive mode, or product ion (PI) *m/z* 272 in negative mode [83]. In spite of this more sensitive technique, we were unable to detect any quebecol metabolites or GSH adducts. Since we found no evidence of *p*-QM formation in the microsomal incubation, we proposed to synthetically prepare *p*-QM standards of quebecol for characterization and to confirm the absence of a *p*-QM in the microsomal incubation.

5.4.2 Preparation of *p*-QM standard

5.4.2.1 Silver Oxide (Ag_2O) as oxidant

Control experiments were employed with silver oxide using eugenol to validate the method. GSH adducts of eugenol were detected by NL *m/z* 307 in ESI (positive mode). The *m/z* of 470.2 found was consistent with GSH adduct of eugenol.

Initially, we attempted to prepare the *p*-QM of quebecol using silver oxide. We observed a

significant loss of quebecol after the incubation with silver oxide followed by an increased column backpressure in the HPLC which potentially indicated that a polymerization was occurring. No peaks corresponding to GSH adducts were observed. To further assess this observation, we prepared a diphenylethane model compound $(MeO)_2$-DPE (Scheme 5.1).

5.4.2.2 Synthesis and characterization of $(MeO)_2$-DPE

We confirmed $(MeO)_2$-DPE through ESI (negative mode) which yielded an *m/z* of 275.1. In our ^{1}H NMR we observed aromatic C-H signals at δ6.83, 6.67 and 6.61, aromatic OH signals at δ5.46 and a benzyl H signal at δ2.81. Due to the symmetry of this compound, the benzyl protons appear as a singlet corresponding to 2H.

As with quebecol however, after incubation with silver oxide, we observed a significant loss of this substrate with an increased backpressure in the HPLC and no evidence of the formation of GSH adducts.

5.4.2.3 Preparation of *p*-QM using Manganese dioxide (MnO_2)

In an attempt to find an alternative oxidation system to form a *p*-QM we tried MnO_2 as an oxidant based on the observation that 4-hydroxy-tamoxifen treated with MnO_2 can produce *p*-QMs [123]. Considering the structural similarity between tamoxifen and quebecol, we prepared fresh MnO_2 following literature procedures [126] and used it to oxidize $(MeO)_2$-DPE and quebecol. The same LC/MS method from the P450 oxidation studies was used to detect the GSH adducts by scanning for neutral loss (NL) of *m/z* 129 and 307 in positive mode, or product ion (PI) *m/z* 272 in negative mode.

Incubation of $(MeO)_2$-DPE with MnO_2 yielded GSH trapped products. Two GSH-adducts were observed in ESI (positive mode): *m/z* 580.2 and 885.3 (Figure 5.2). The adduct at *m/z* 580.5 is a mono-GSH, while the *m/z* 885.4 is consistent with two GSH added to the molecule producing a di-GSH conjugate. Both mono and di-GSH adducts were detected by NL *m/z* 129 in positive mode, but only the di-GSH detected a precursor ion (PI) *m/z* 272 in negative mode, indicating that at least one GSH formed an adduct on an aromatic ring [83].

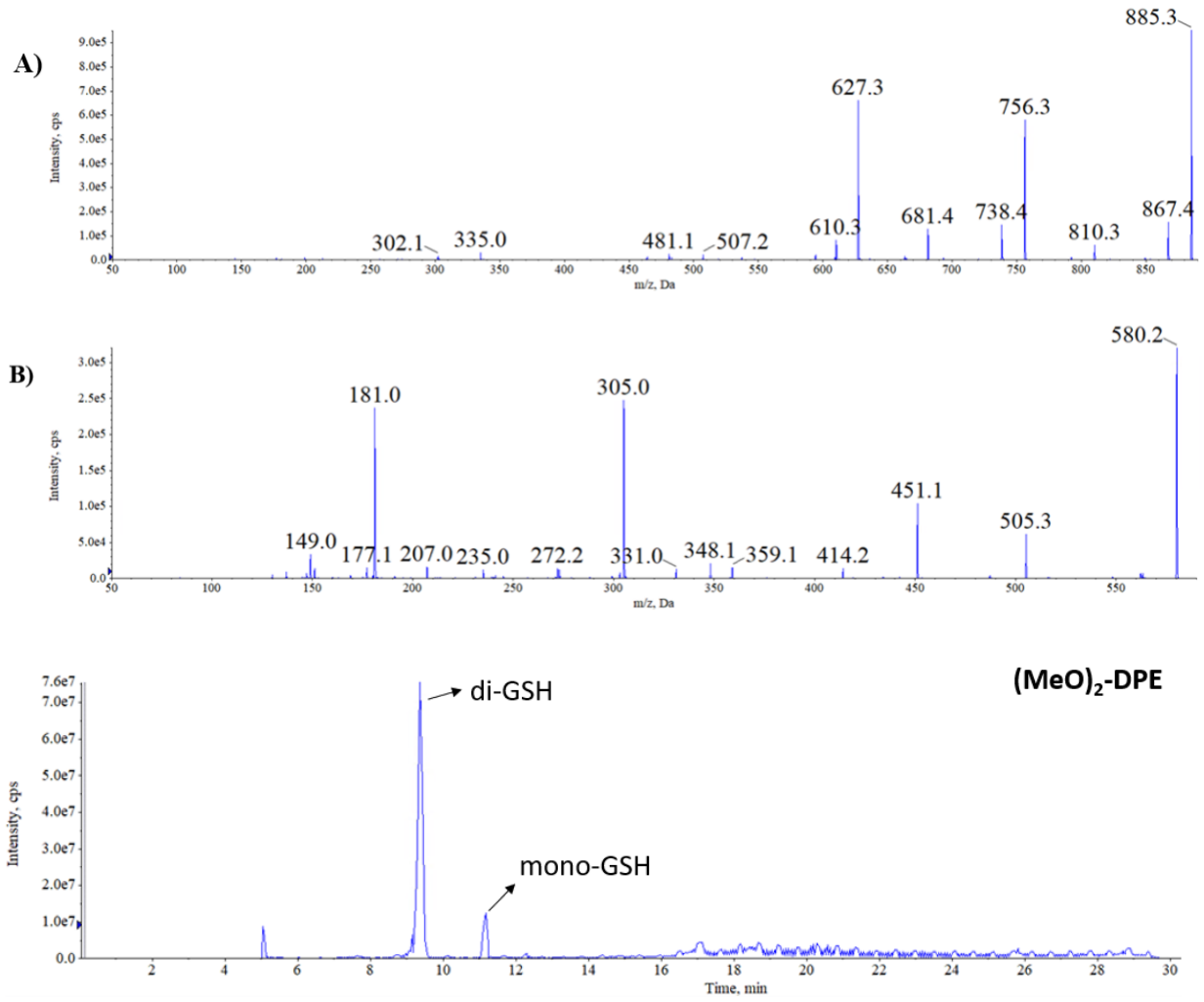

Figure 5.2. ESI-MS/MS enhanced product ion (EPI) mass spectra of $(MeO)_2$-DPE di-GSH *m/z* 885.3 (A) and mono-GSH *m/z* 580.2 (B). (C) LC-MS extracted ion chromatogram (XIC) in positive mode for mono-GSH adduct (9.3 minutes) at *m/z* 580.5 ± 0.5 and di-GSH (11.1 minutes) at *m/z* 885.4 ± 0.5 in $(MeO)_2$-DPE incubation mixture with MnO_2 followed by GSH trapping.

Considering the successful MnO_2-catalyzed oxidation of $(MeO)_2$-DPE that formed two *p*-QMs trapped by GSH, we then attempted to use MnO_2 to prepare *p*-QMs of quebecol. Incubation of quebecol with MnO_2 produced three products that were trapped with GSH. We expected that in positive mode we

would observe a quebecol mono-GSH of *m/z* 732.1 and/or a di-GSH of *m/z* 1,037.1. However, we detected GSH adducts with *m/z* 1,007.6, 1,007.7, and 716.5 in positive mode (Figure 5.3).

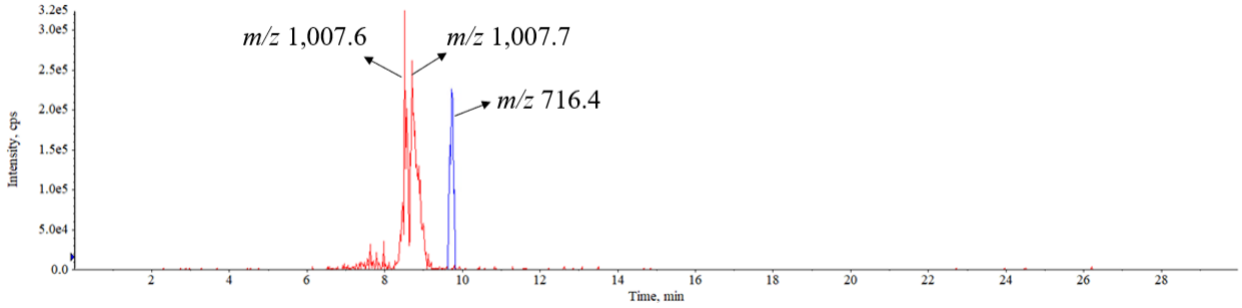

Figure 5.3. LC-MS extracted ion chromatogram (XIC) in positive mode at *m/z* 1,007.6 ± 0.5 (red) and at *m/z* 716.5 ± 0.5 (blue) of quebecol incubation mixture with MnO_2 followed by GSH trapping.

The product of *m/z* 716.5 was consistent with formation of a mono-GSH adduct of quebecol in which one demethylation reaction had occurred followed by intramolecular cyclization of the primary alcohol to form either a five or a six-membered ring (Figure 5.4).

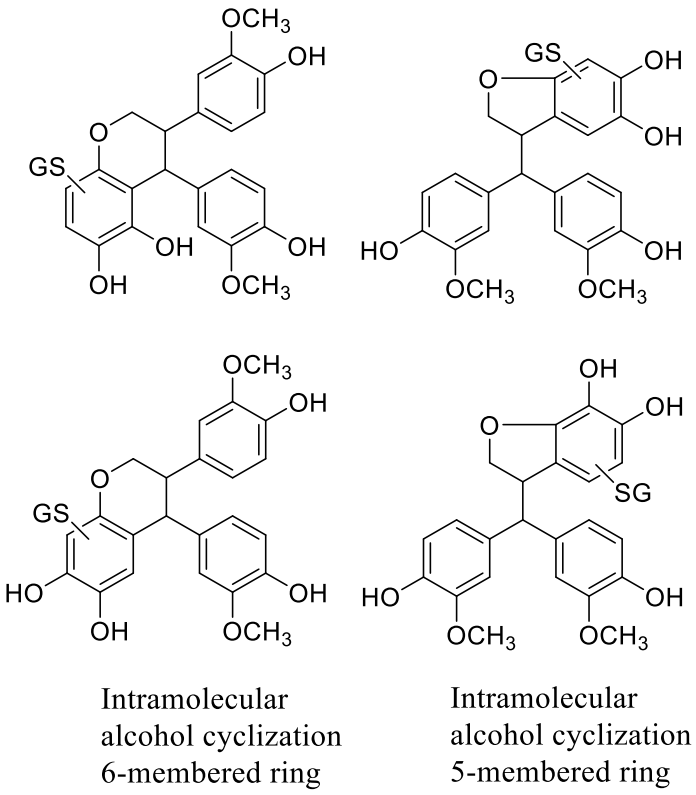

Figure 5.4. Possible *m/z* 716.5, GSH trapped MnO_2 oxidation products of quebecol.

The products of *m/z* 1,007.6 and 1,007.7 were consistent with formation of a di-GSH adduct of quebecol with two demethylation reactions followed by the intramolecular cyclization of either the primary alcohol forming either a five- or six-membered ring, or C-C bond formation resulting from intramolecular cyclization of the catechol rings to form either dibenzocyclopentadienes or dibenzocyclohexadienes (Figure 5.5).

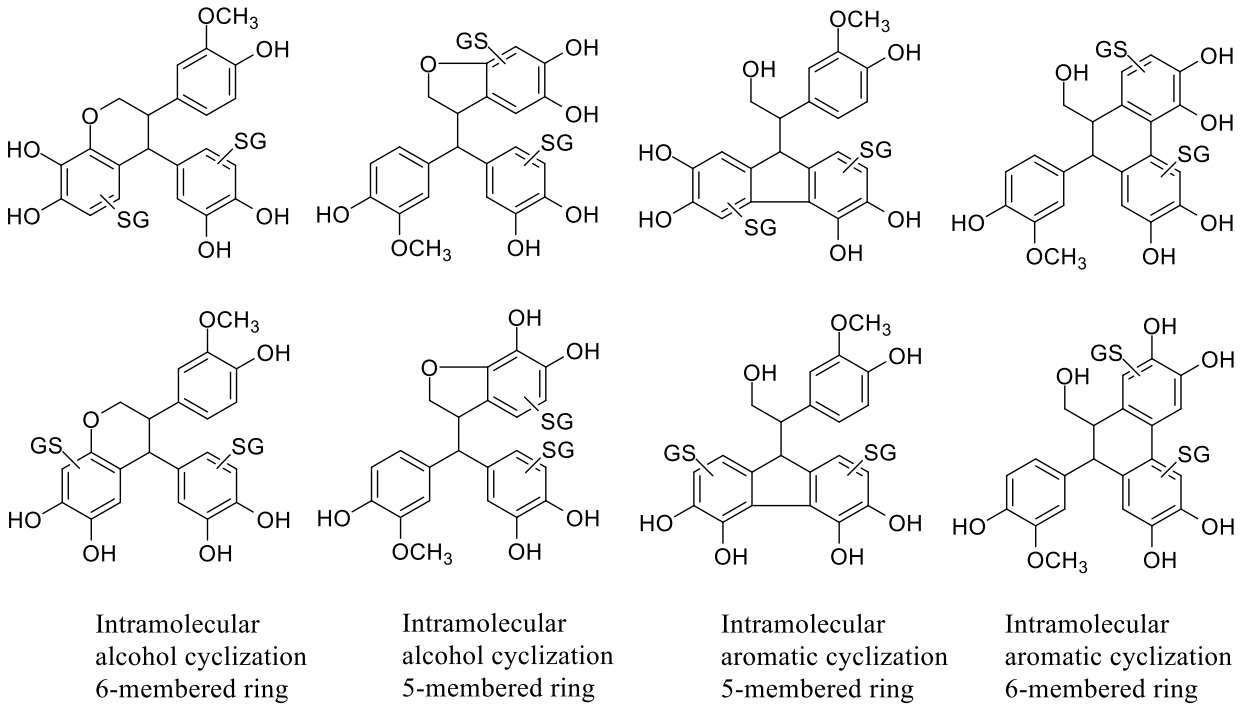

Figure 5.5 Proposed di-GSH conjugates of quebecol. Structures are depicted only and have not been fully characterized to determine which methoxy group was dealkylated or the position of the GSH adduct.

In an effort to determine whether the GSH adducts were formed on the aromatic ring or at the benzyl position, we utilized previously established mass spectrometric diagnostics for aromatic adducts (ESI(-) *m/z* 272) and benzyl adducts (ESI(+) neutral loss 307) [83]. All GSH adducts are expected to show a neutral loss of 129 in ESI(+) resulting from formation of pyroglutamic acid regardless of the site of adduction. We confirmed that all three quebecol GSH conjugates showed a NL *m/z* 129 in positive mode, but only the mono-GSH conjugate showed a *m/z* 272 in negative mode indicative of adduction directly on the aromatic ring.

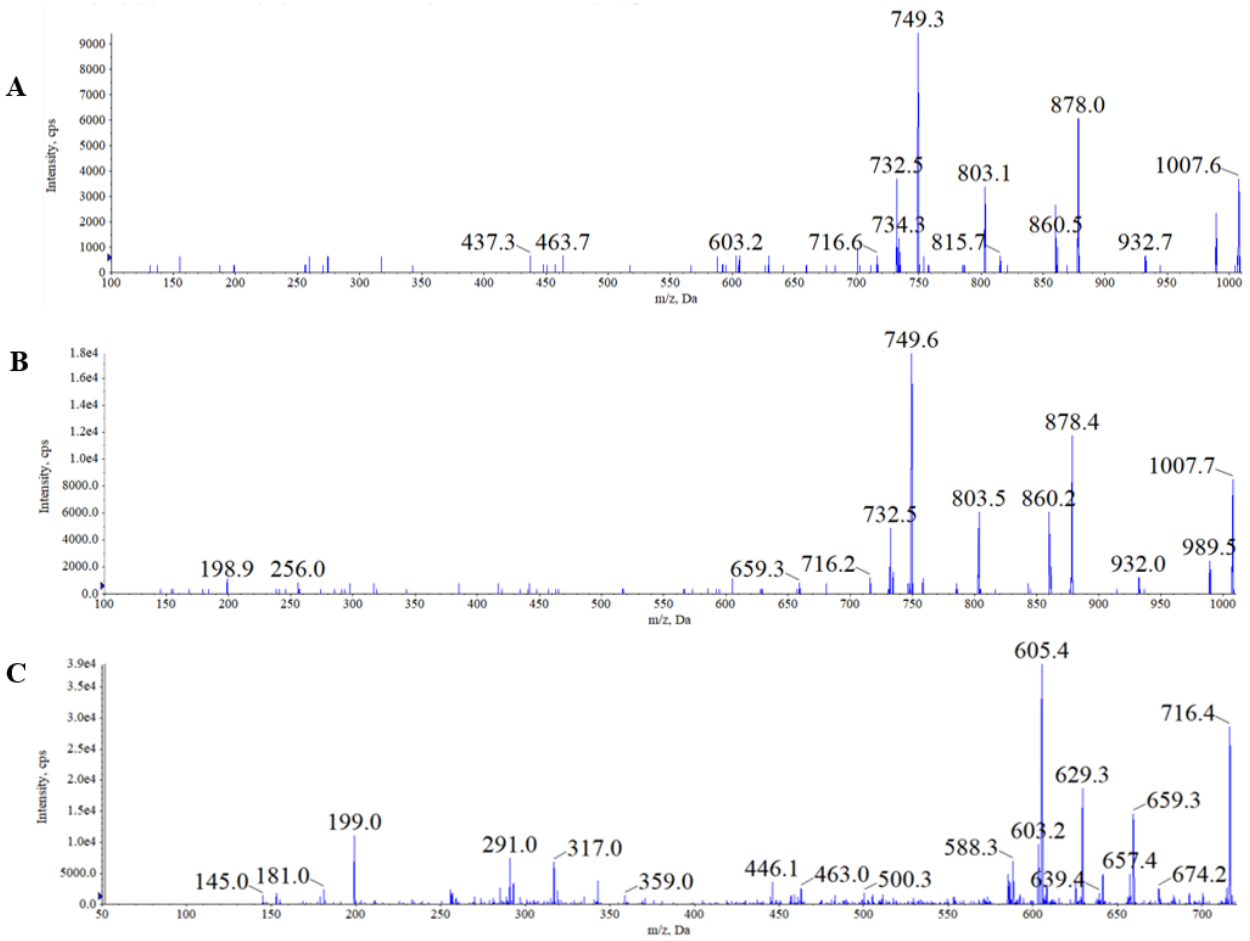

Figure 5.6. ESI-MS/MS enhanced product ion (EPI) mass spectra of quebecol di-GSH *m/z* 1,007.6 (A) and *m/z* 1,007.7 (B); quebecol mono-GSH *m/z* 716.4 (C).

5.5 Discussion

Metabolic formation of electrophilic reactive intermediates prevent the advancement of drug candidates and several pharmaceutical companies have reported on screening methods to identify potential reactive metabolites. These methods include *in vitro* hepatic metabolism and forming adducts with a variety of trapping agents [127] and also assessing the relative contribution to overall metabolism of the reactive intermediate [128]. *para*-Quinone methide formation in phenols with an alkyl group possessing at least one H-atom in the *para*-position has been previously observed although quinone

formation occurs most rapidly when the alkyl group is substituted with an alkene [129] as is the case in hydroxy tamoxifen or eugenol [130,131]. The benzyl positions of quebecol each have one H-atom and should be capable of *p*-QM formation, however we were unable to observe any *p*-QMs in hepatic microsomes or when using typical chemical oxidants such as Ag_2O or MnO_2. Ag_2O resulted in loss of quebecol and a distinct color change in the reaction solution consistent with oxidation, although given the high backpressure seen upon injection of the mixture on HPLC, suggests to us that formation of a poorly soluble polymer may have occurred. The steric bulk present at the benzyl positions of the phenols in quebecol likely contributes to the lack of *p*-QM formation. When we used MnO_2 we were able to identify GSH adducts, but demethylation of the methoxy groups also appears to have occurred, resulting in the formation of catechols which apparently underwent oxidation to *ortho*-quinones which were subsequently trapped as GSH adducts. Our results suggest that MnO_2 may catalyze dealkylation and although we could not find evidence in the literature of MnO_2-mediated O-dealkylation, there are reports of MnO_2-mediated N-methyl dealkylation [132].

The subsequent metabolites of MnO_2-catalyzed oxidation detected by LC/MS indicate that in addition to GSH adduct formation, an intramolecular cyclization has likely occurred for both the mono and di-GSH adducts as determined by the loss of two additional H-atoms. There are several possible reaction pathways which could rationalize these results. First, dealkylation would lead to catechol formation which would readily undergo oxidation to an *ortho*-quinone. Intramolecular cyclization of the alcohol could lead to either a 5 or 6-membered ring which subsequently re-oxidizes to an *ortho*-quinone and is trapped by GSH (Scheme 5.2-A, B respectively). Ito *et. al.* reported that GSH addition to rhododendrol during tyrosinase-catalyzed oxidation was more rapid than intramolecular cyclization of an alcohol [133], but our system differs in that GSH is not added until the oxidant (MnO_2) has been

removed, so would likely proceed in the manner shown in Scheme 5.2. Although only shown for the mono-dealkylated species in Scheme 5.2, these reactions could also occur for the di-dealkylated compounds.

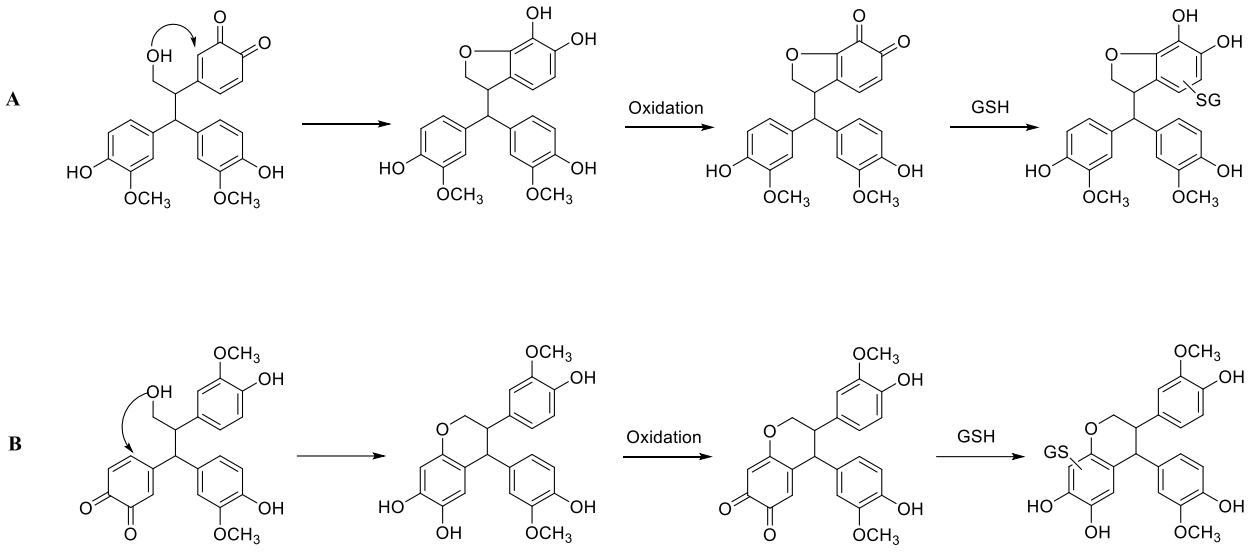

Scheme 5.2. Proposed intramolecular cyclization and GSH adduct formation reaction pathways for (A) 5-membered C-O ring formation, (B) 6-membered C-O ring formation.

A second potential intramolecular cyclization is the formation of a C-C bond between two aromatic rings as described previously by us in which catechols linked by a 2-carbon alkyl chain can each undergo one-electron oxidation and subsequent radical recombination to form a dibenzocyclohexadiene (Scheme 5.3A) (This thesis, chapter 3) or a dibenzocyclopentadiene (Scheme 5.3B) [134].

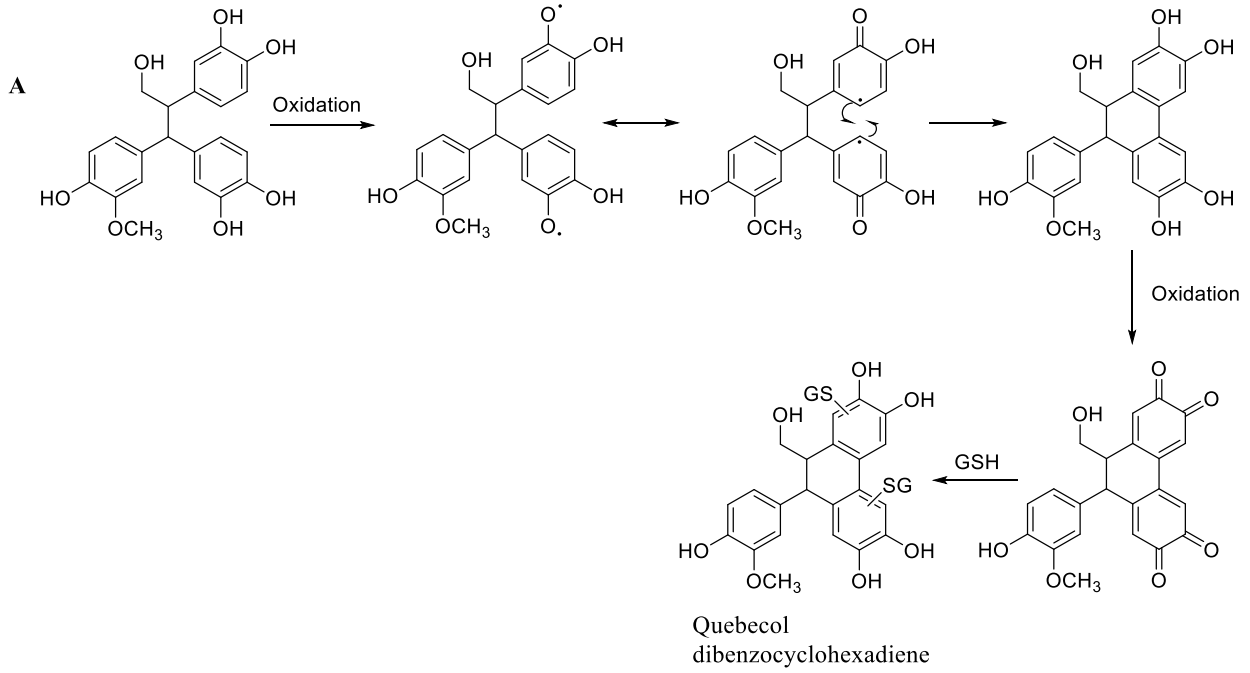

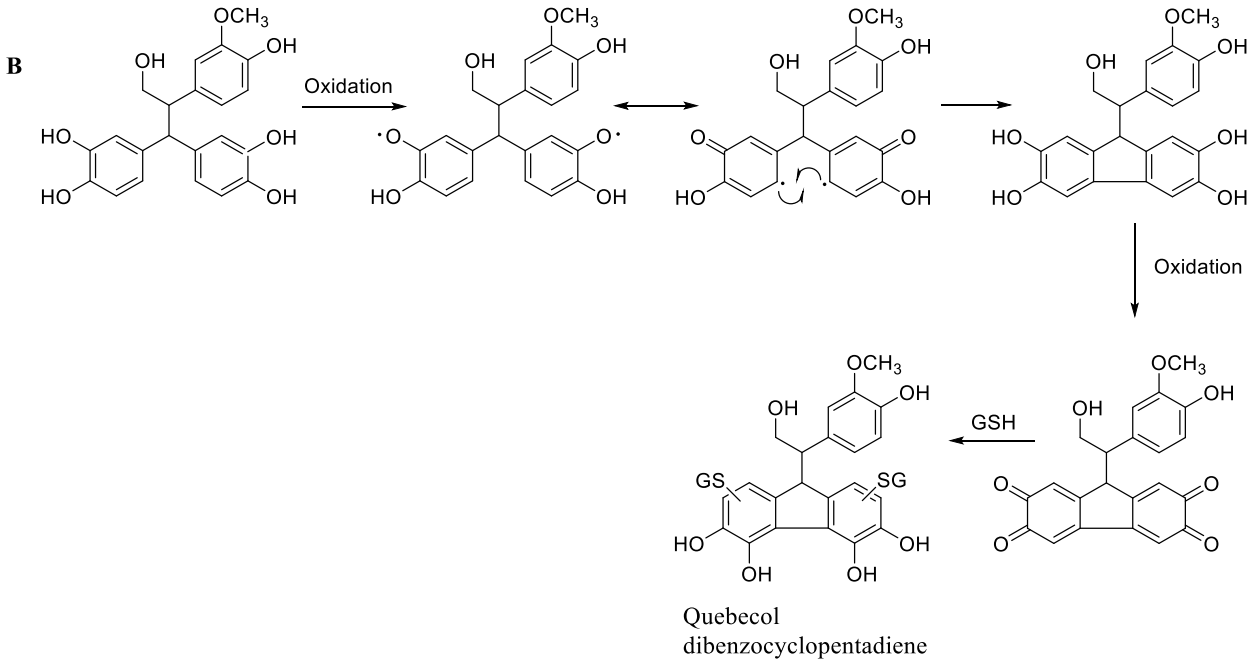

Scheme 5.3. Proposed intramolecular cyclization and GSH adduct formation reaction pathways for (A) 6-membered C-C ring formation, (B) 5-membered C-C ring formation.

We determined that cyclization to form dibenzocyclohexadienes from substituted

diphenylethanes occurs at pH 7.4 with a half-life of *ca.* 8-24 minutes depending on linker substitution (This thesis, chapter 3). Under the same conditions, however, we have identified formation of an intramolecular C-O cyclization product with a half-life of 9 hours for a catechol analog of secoisolariciresinol (Scheme 5.4) resulting in either a 5 or 6-membered ring [135]. Together these results suggest to us that the C-C intramolecular cyclizations likely predominate over the C-O intramolecular cyclizations.

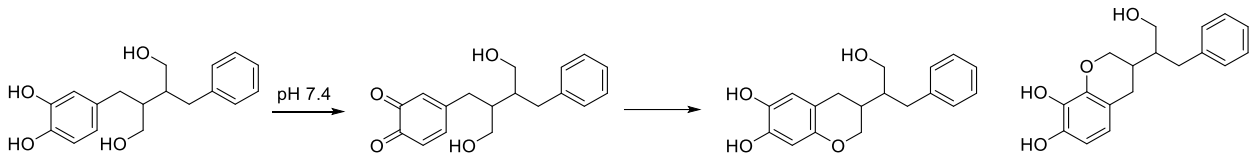

Scheme 5.4. Possible C-O intramolecular cyclization products for pH 7.4 oxidation of a secoisolariciresinol mono-catechol analog. Half-life for loss of starting material is *ca.* 9 hours [135].

5.6 Conclusion

The formation of electrophilic reactive intermediates such as *p*-QMs formed via hepatic metabolism is a concern for *para*-methyl phenols. We have observed that the natural product quebecol, with 3 *para*-methyl phenols in its structure, is resistant to P450-mediated metabolism to *p*-QMs or any other P450 metabolic products. Furthermore, we were unable to prepare *p*-QMs using standard chemical oxidative methods as the only quinones we could prepare were the result of apparent MnO_2-catalyzed demethylation and oxidation, presumably leading to *ortho*-quinones. This resistance to P450-mediated metabolism and the predominant clearance via glucuronidation suggests to us that any potential formation of electrophilic metabolites of quebecol is unlikely. We are currently attempting to identify the exact structures of the quebecol GSH adducts we prepared from MnO_2.

Chapter 6: Attempt to Prepare the Tetra-Methyl NDGA Analogue to investigate the Formation of Dibenzocyclooctadienes

Gabriel Bernardes, Taylor Koshtyshyn, Bryan M. Hill, Ed S. Krol

Drug Discovery and Development Research Group, College of Pharmacy and Nutrition, University of Saskatchewan, Saskatoon, SK

Transitioning rationale: In the previous chapters, we have investigated the stability and metabolism of polyphenols. In Chapter 3, we determined that the number of methyl groups in a diphenylethane dicatechol increases the rate of intramolecular cyclization to form dibenzocyclohexadienes. In contrast, our group reported that this rate for NDGA to form a dibenzocyclooctadiene is slower when compared to its analogue without a methyl substituents. This would imply that additional methyl groups would decrease or prevent the intramolecular cyclization. Therefore, in this chapter we aim to prepare the tetra-methyl NDGA and investigate its stability in vitro.

Contribution statement: Gabriel Bernardes contributed to the experimental design, conducted the experimental work and data analysis, and drafted the chapter. Taylor Koshtyshyn contributed to the optimization of the first steps of the chemical synthesis. Dr Bryan Hill (Brandon University) co-supervised the work. Dr Ed Krol supervised the work and revised the manuscript.

6.1 Introduction

Nordihydroguaiaretic acid (NDGA) is a lignan found in the leaves of the creosote bush [2]. The aqueous extract of creosote bush, also referred to as Chaparral tea, has been used in traditional medicine for a wide range of ailments due to its suggested medicinal properties [17]. Despite the proposed biological activity, this natural polyphenol has been also associated with kidney and liver toxicity when ingested at higher doses [3]. Previously, our group have reported that NDGA can undergo *in vitro* biotransformation to form reactive *ortho*-quinones, which are likely responsible for toxicity *in vivo*, such as severe hepatic and renal injuries [4]. In addition,we reported that NDGA can spontaneously cyclize at pH 7.4 to form a dibenzocyclooctadiene that may be responsible for the pharmacological properties *in vitro* [5]. The intramolecular cyclization process was investigated by synthesizing a series of NDGA analogs to determine the structural features required for cyclization [6]. The two major findings were the requirement of a dicatechol and the methyl groups on the alkyl linker influenced the rate of intramolecular cyclization [6]. The NDGA analogue without methyl groups (1) was determined to cyclize more rapidly (13.1×10^{-5} s^{-1}) than NDGA (4.88×10^{-5} s^{-1}). It is likely that the more rapid cyclization for **1** is a result of decreased steric interactions between the methyl groups during cyclization. This would imply that additional methyl groups on the alkyl chain would slow intramolecular cyclization. Therefore, we propose the preparation of **2** to confirm that the additional methyl groups will further slow cyclization and whether that may be sufficient to prevent cyclization

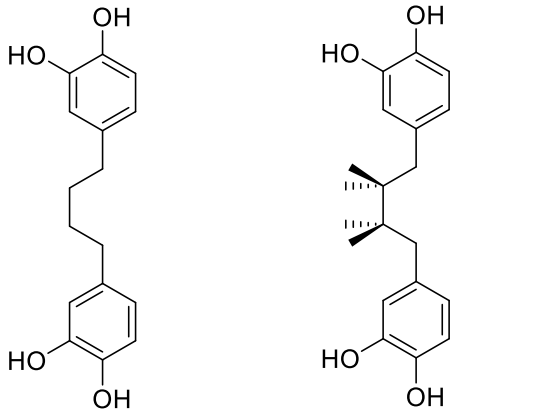

de-Me-NDGA Tetra-methyl NDGA

Figure 6.1. Structure of NDGA analogs 1 and 2

6.2 Materials and Methods

6.2.1 Materials

Sigma-Aldrich (St. Louis, MO): 3,4- Dimethoxybenzyl alcohol, phosphorus tribromide (PBr_3), sodium hydride (NaH), 1,1,2,2-ethane tetracarboxylate, lithium aluminum hydride ($LiAlH_4$), mesyl chloride (MsCl). Organic solvents were obtained from Fisher Scientific (Fairlawn, NJ).

6.2.2 Instrumentation

6.2.2.1 ESI-MS Analysis

Mass spectroscopy analysis of intermediates was conducted using an AB SCIEX 4000 QTRAP (AB SCIEX instruments, Farmingham, MA) quadrupole linear ion trap mass spectrometer. Samples were infused directly using a flow of 10 μL/min. Data acquisition and analyses were performed using Analyst 1.7 software from AB SCIEX.

6.2.2.2 NMR Analysis

All NMR experiments were performed on a Bruker AVANCE DPX-500 spectrometer (Karlsruhe, Germany) and data processed using MestRreNova 14.1. All compounds were drawn and named using ChemDraw 20.0.

6.2.3 Methods

6.2.3.1 Synthesis and Characterization of Tetra-Methyl NDGA

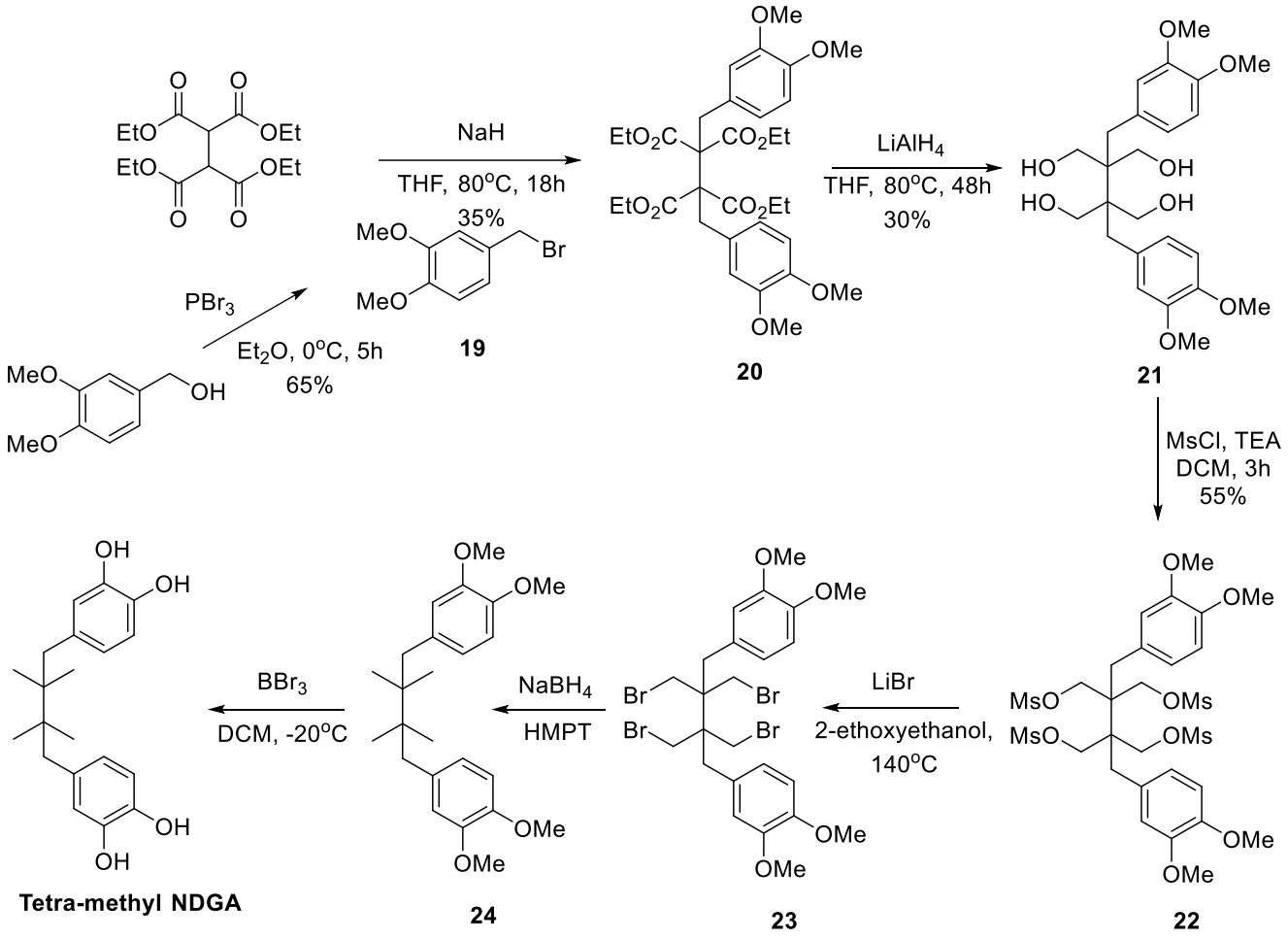

Scheme 6.1. Proposed synthesis of tetra-methyl NDGA analogue starting from tetraethyl 1,1,2,2-ethanetetracarboxylate.

Synthesis of 4-(bromomethyl)-1,2-dimethoxybenzene (19)

3,4-Dimethoxybenzyl alcohol (500 mg, 4.16 mmol) and diethyl ether (7 mL) were added into the reaction flask under N_2 gas at 0 °C. After 10 minutes, phosphorus tribromide (0.47mL, 4.99 mmol) was

added dropwise to the stirring mixture. The reaction was stirred at 0 °C for one hour, and then stirred at room temperature for four hours. The mixture was poured into ice water and extracted with ethyl acetate (4 × 15 mL). The organic layer was washed with cold water, dried over $MgSO_4$, filtered, and concentrated *in vacuo* to give **1** as a white solid (447 mg, 65%). ^{1}H NMR (500Hz, $CDCl_3$): δ (ppm) 6.96 (dd, 1H), 6.94 (d, 1H), 6.91 (d, 1H), 4.5 (s, 2H), 3.89 (s, 3H), 3.88 (s, 3H).

Synthesis of tetraethyl 1,4-bis(3,4-dimethoxyphenyl)butane-2,2,3,3-tetracarboxylate (20)

A suspension of sodium hydride (60% in mineral oil, 153 mg, 6.38 mmol) and anhydrous THF (10 mL) was stirred under N_2 and cooled to 0 °C. The 1,1,2,2-ethane tetracarboxylate (203 mg, 0.638 mmol) was slowly added. The mixture was stirred for 20 minutes at 0ºC. Bromo compound **19** (323 mg, 1.4 mmol) was dissolved in 1 mL of ether, and added dropwise to the reaction. The reaction was refluxed for 24 hours under N_2. The mixture was cooled to 0 °C and saturated ammonium chloride solution was added. The aqueous layer was extracted with ethyl acetate (4 × 15 mL), and the organic layer washed with brine, dried over $MgSO_4$, filtered and concentrated *in vacuo*. Flash chromatography over silica (3:2 Hexane/Ethyl Acetate) gave dialkylated **20** as yellowish oil (266 mg, 35%). ^{1}H NMR (500Hz, $CDCl_3$): δ (ppm) 6.95 (d, 1H), 6.86 (dd, 1H), 6.73 (d, 1H), 4.10 (m, 6H), 3.25 (s, 3H), 3.24 (s, 3H), 1.26 (t, 6H).

Synthesis of 2,3-bis(3,4-dimethoxybenzyl)-2,3-bis(hydroxymethyl)butane-1,4-diol (21)

To a solution of dialkylated **20** (115 mg, 0.185 mmol) in THF (10 mL) was added portion wise lithium aluminum hydride (70.5 mg, 1.85 mmol). The reaction was refluxed for 48 hours under N_2. The mixture was cooled to 0 °C and the mixture was diluted with ether (10 mL). Water (1 mL) was carefully

added via syringe, followed with 10% NaOH (1 mL). Water (3 mL) was added after allowing the mixture to warm up to room temperature. Ethyl acetate (20 mL) and $MgSO_4$ were added and stirred for 30 minutes. The mixture was filtered and evaporated *in vacuo*. Flash chromatography over silica (3:1:1 Ethyl Acetate/Hexane/Methanol) gave tetra-alcohol **21** as a white powder (19 mg, 30 %). ^{1}H NMR (500Hz, DMSO-d_6): δ (ppm) 6.91 (d, 1H), 6.84 (dd, 1H), 6.79 (d, 1H), 5.5 (s, 2H), 3.72 (s, 6H), 3.4 (s, 4H), 2.89 (s, 2H). ESI-MS (*m/z*) 449.3 $[M - H]^-$.

Synthesis of 1,4-bis(3,4-dimethoxyphenyl)butane-2,2,3,3-tetrayl tetramethanesulfonate (22)

The 2,3-bis(3,4-dimethoxybenzyl)-2,3-bis(hydroxymethyl)butane-1,4-diol (90 mg, 0.2 mmol) was added in DCM (5 mL) under N_2. DMAP (7.3 mg, 0.06 mmol) was added. The reaction was placed on an ice bath, and TEA (0.08 mL, 0.6 mmol) was added dropwise. After 10 minutes, mesyl chloride (0.09 mL, 1.2 mmol) was added dropwise at 0 °C. The reaction was stirred for 3 hours under N_2 at 0 °C. Methanol (5 mL) and water (10 mL) were added to quench the reaction and the aqueous layer was extracted with ethyl acetate (3 × 15 mL). The organic layer was washed with 1M HCl solution, brine, saturated ammonium chloride solution and saturated sodium bicarbonate solution, and dried over $MgSO_4$ to give a brown oil. The product was used in the next step without purification.

6.3 Results and Discussion

The synthesis of tetra-methyl NDGA is a challenge essentially because of the presence of two adjacent quaternary carbons in the alkyl chain. Unsuccessful prior attempts to prepare this compound using different routes by our group suffered from low yields, cost of starting materials and poor reactivity.

We have adapted a synthetic pathway (Scheme 6.2) using tetraethyl 1,1,2,2-ethanetetracarboxylate as starting material that has better reported yields and low cost of starting materials [136].

The first step involves the conversion of the benzyl alcohol to benzyl bromide **19** using phosphorus tribromide (PBr_3). The reaction with PBr_3 proceeded smoothly, but the purification was found challenging due to the labile nature of the bromo compound towards moisture. Therefore, compound **19** was isolated and used as is in the second step to react with the di-malonate using sodium hydride to yield the dialkylated product **20**. Using the reducing agent lithium aluminum hydride, the four esters are reduced to give tetra-ol **21**. Treatment of **21** with methanesulfonyl chloride in DCM yielded the tetra-mesyl compound **22**. Purification of compound **22** was found to be tricky, and several attempts were made to use this compound without purification in the next step. Bromination of compound **22** using lithium bromide to yield **23**, or a direct reduction of **22** using sodium borohydride to give **24** were also carried out without success. Additionally, tosylation of compound **21** was also attempted without success.

An alternative attempt to make the tetra-methyl NDGA was made using a similar synthetic route previously reported for the preparation of a diphenylethane M4-DPE (Chapter 3) by preparing a tertiary alcohol which underwent $TiCl_4$-mediated coupling [81]. Treatment of compound 3,4-dimethoxyphenyl acetophenone with the Grignard reagent which was generated *in situ* did not yield the proposed tertiary alcohol (Scheme 6.2). However, we could not find an example in the literature to prepare this alcohol via a Grignard. It is likely that this reaction is not favorable for benzyl alcohols, and the α-proton abstraction competed with nucleophilic addition.

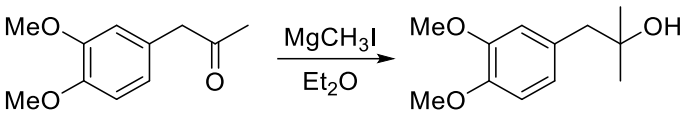

Scheme 6.2 Attempt to make a tertiary alcohol from 3,4-Dimethoxyphenyl acetophenone

Remarkably, the preparation of the tetramethyl NDGA has been extremely challenging. It is likely that steric hindrance contributes significantly to the difficulty in incorporation of the methyl groups. The approach used in this synthetic route consisted of forming a basic lignan skeleton. Once the skeleton was formed, the side chains of the intermediates were bulky and could be responsible for the poor reactivity.

A new procedure has been identified as a potential synthetic approach to prepare tetra-methyl NDGA (Scheme 6.3), with precedent in the literature [137]. The original procedure was designed to synthesize 1,2-diphenyl-3,3,4,4-tetramethylcyclobutene which has a similar chemical structure to the proposed tetra-methyl NDGA, except for the absence of phenol groups. One of the reasons that makes this synthetic scheme more appealing is the fact that the starting material is an intermediate for the synthesis of the diphenylethane DPE reported in chapter 3. Key steps in this proposed synthesis are alkyne formation from the dibromide, photochemical formation of the tetra-methyl substituted cyclobutene and ozonolysis of the cyclobutene. We have not performed these three reactions although we have experience with all of the other transformations shown.

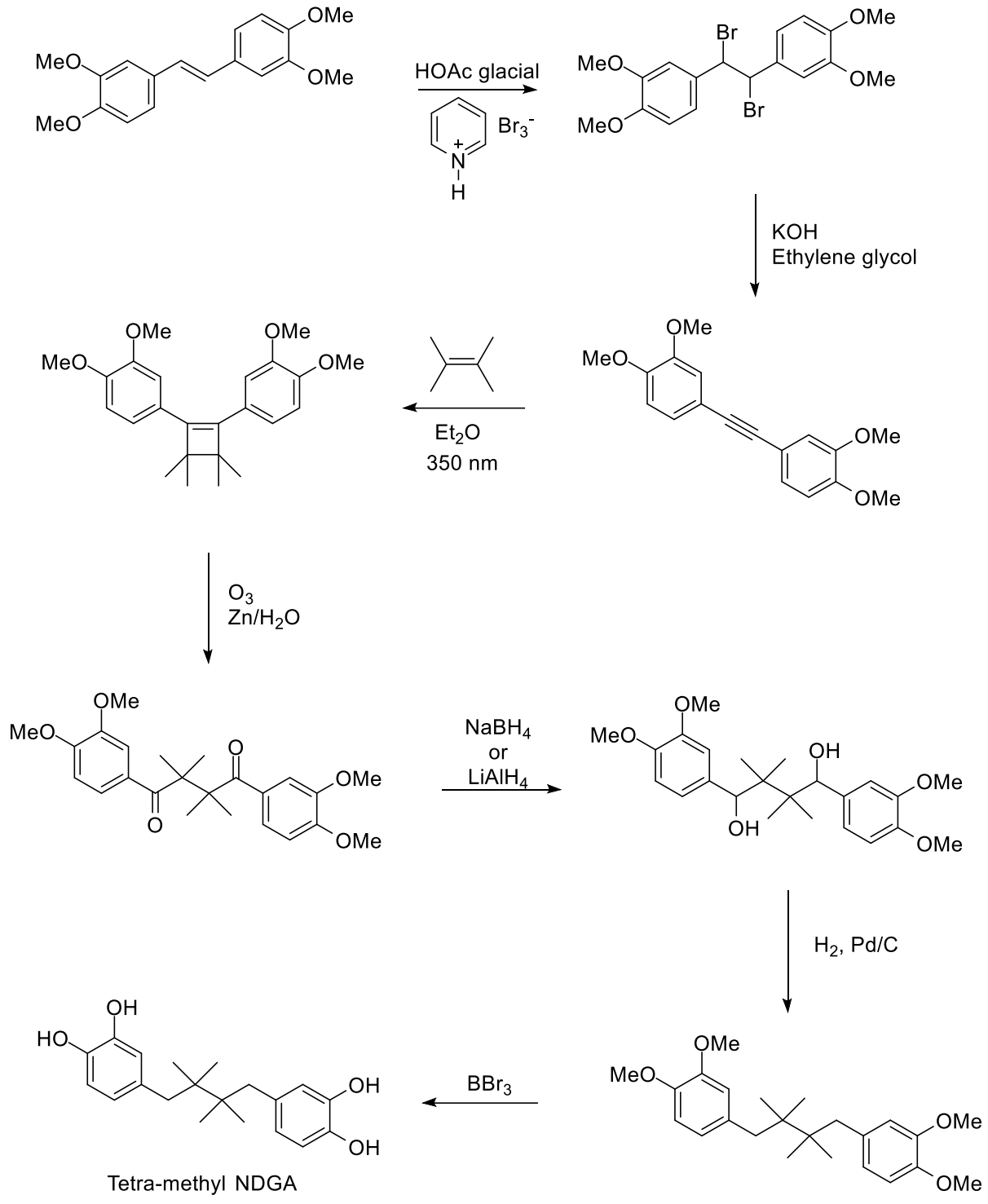

Scheme 6.3. Potential synthetic approach for the synthesis of tetra-methyl NDGA

The successful preparation of the tetra-methyl NDGA will be required to provide an understanding of how additional methyl groups influence the rate of oxidative cyclization.

Chapter 7: General Discussion

Historically, natural products have been used to treat many diseases and illnesses [138]. Natural products possess a range of pharmacological properties *in vivo*, yet their metabolic fate can differ from their metabolism *in vitro* due to their instability when exposed to aqueous buffers used in *in vitro* incubation systems [72–75]. Some well-understood examples include curcumin [72,73] and numerous flavonols and catechins [74,75]. Previously we have reported that the natural polyphenol NDGA is not stable in aqueous solution at pH 7.4 and cyclizes to form a dibenzocyclooctadiene (cNDGA) [5]. Similar cyclized lignans, the schisandrins (Figure 7.1) are naturally-occurring metabolites in plants, and have been extensively studied for various pharmacological properties [84]

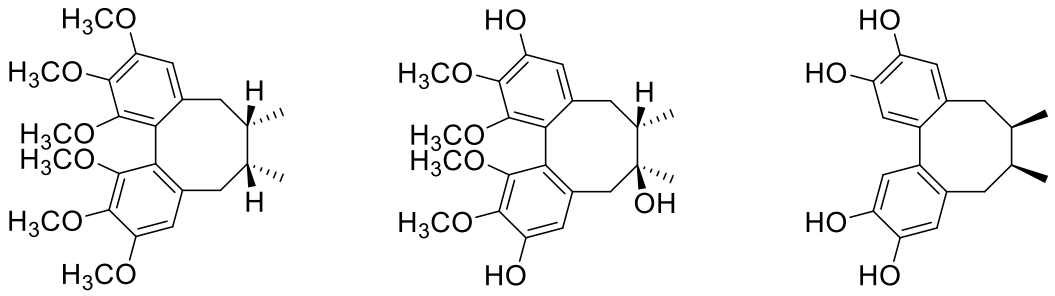

Figure 7.1 Chemical structures of dibenzocyclooctadienes. Schisandrins (schisandrin A and gomisin J) isolated from *Schisandra chinensis* and cNDGA formed from the autoxidation of NDGA.

NDGA has been used in traditional medicine, and many *in vitro* experiments have been done under these conditions to investigate its biological properties [139]. It is important to determine whether the oxidation product cNDGA is responsible for the biological activity reported *in vitro*. Both NDGA and cNDGA were found to inhibit α-synuclein aggregation *in vitro* and the activity was abolished when

reducing agents were present preventing oxidation of either NDGA or cNDGA [11]. Whether the oxidation process alone or oxidation and NDGA/cNDGA are required to prevent α-synuclein aggregation is unknown.

Similarly to dibenzocyclooctadienes, six-membered rings are also naturally-occurring metabolites found in plants with biological properties reported (Figure 7.2), such as lusianthridin [140], confusarin [141], and flavanthrinin [142]. Additionally, we found a series of substituted diphenylethane dicatechols in the patent literature reported to inhibit α-synuclein aggregation *in vitro* [9]. This led us to speculate whether the observed autoxidation-intramolecular cyclization process for NDGA also occurs to dicatechols containing shorter alkyl linkers, and whether the autoxidation product is responsible for the biological activity seen *in vitro*. Therefore, we designed and synthesized a series of diphenylethanes (DPE, M2-DPE, and M4-DPE) to evaluate their autoxidative potential in buffer at pH 7.4.

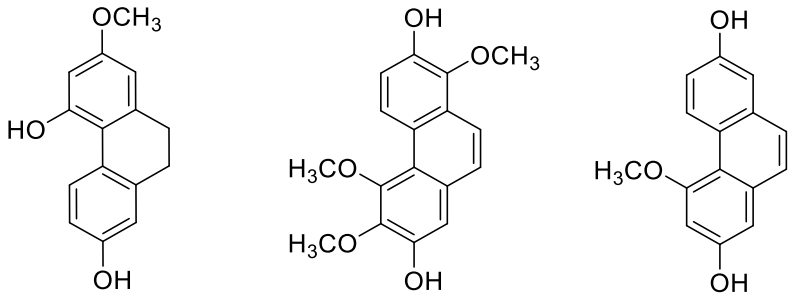

Figure 7.2. Naturally-occurring dibenzocyclohexadienes. Lusianthridin, metabolite from *Dendrobium venustum*. Confusarin and flavanthrinin are found in the orchids *Eria confusa* and *Bulbophyllum reptans*.

The DPEs underwent autoxidation to form dibenzocyclohexadienes, although 10-30 times more rapidly than NDGA formed dibenzocyclooctadienes. We have also verified that the presence of oxygen

increases the oxidation rate, whereas nitrogen and ambient conditions are comparable at a slower rate. Interestingly, the intramolecular cyclization rate increased with the number of methyl substituents on the alkyl linker in the DPEs, in agreement with the vicinal dimethyl effect reported for lactone cyclization [85]. It would be interesting to see if the opposite trend observed for NDGA holds with tetra-methyl NDGA. As opposed to NDGA, we observed the formation of a mixture of regioisomers for all of our diphenylethane analogs (Figure 7.3).

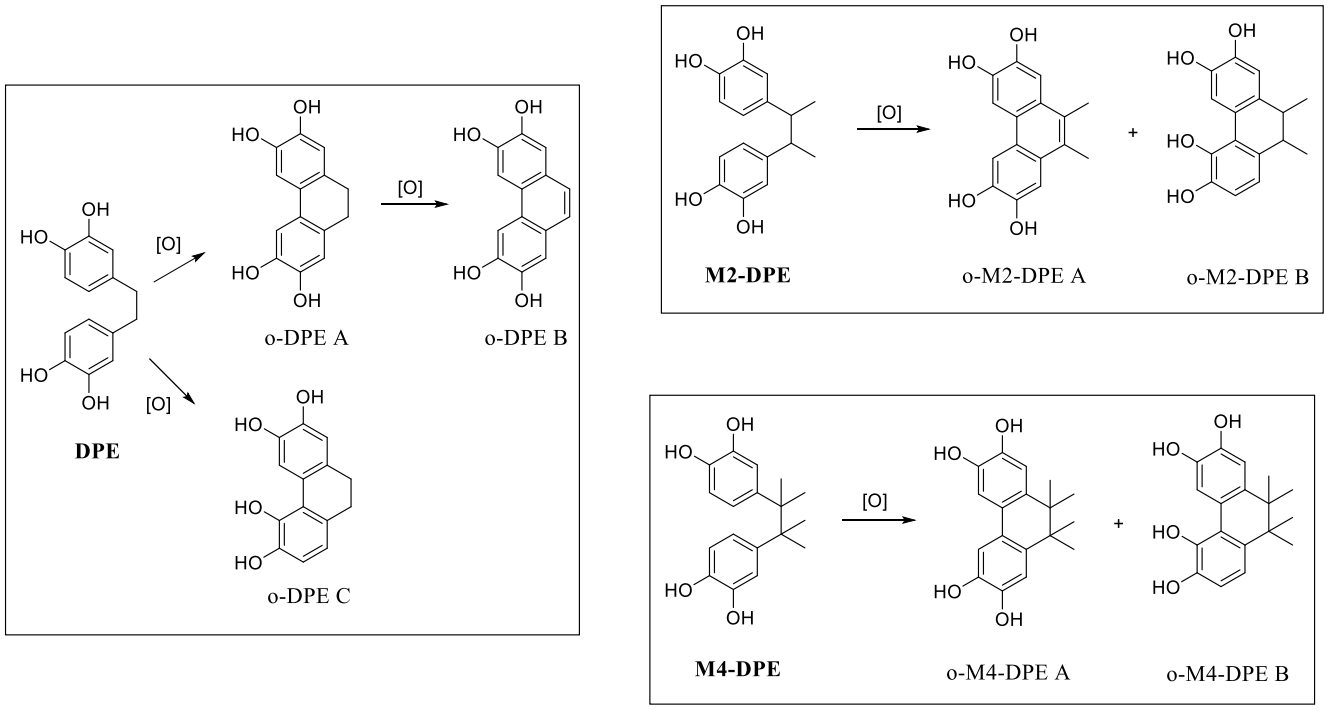

Figure 7.3. Autoxidative products of DPE (o-DPE A, o-DPE-B, o-DPE C), M2-DPE (o-M2-DPE A, o-M2-DPE B), and M4-DPE (o-M4-DPE A, o-M4-DPE B).

The DPEs and their cyclized products from autoxidation were found to significantly inhibit α-synuclein aggregation at two concentrations of 100 and 500 μM. In fact, M2-DPE cyclized products and o-M4-DPE A significantly reduced ($p < 0.05$) the aggregation as compared to cNDGA at the same concentration. Even though for the other compounds this difference was not statistically significant, we

were able to observe a concentration-dependent inhibition of α-synuclein aggregation.

As discussed previously, besides the known pharmacological properties of NDGA there are toxicological effects reported possibly mediated by reactive metabolite formation [143]. Our group have reported that cNDGA and other dibenzocyclooctadiene derivatives are not stable in aqueous solution over time, and the resulting product was trapped with GSH indicating reactive quinone formation [6]. We anticipated that the autoxidation products for DPE, M2-DPE and M4-DPE would also decompose to reactive quinone species. Indeed, we were able to trap quinones using GSH for o-DPE-A, o-DPE-C, o-M2-DPE-B, o-M4-DPE-A and o-M4-DPE-B, but not with the fully aromatized compounds o-DPE B and o-M2-DPE-A (stable up to 24 hours).

Considering our interest in studying the stability of natural products, we were interested in the polyphenol quebecol which has been isolated from maple syrup and has reported chemopreventive and chemotherapeutic properties [61]. Quebecol analogs have been prepared as potential drug leads, and yet no hepatic metabolism data is available. Phase I metabolism could lead to dealkylation of the methoxy groups, and formation of dicatechols. Since we have determined that substituted diphenylethane dicatechols can undergo intramolecular cyclization to dibenzocyclohexadienes, we speculated that a quebecol dicatechol produced by dealkylation could undergo intramolecular cyclization to form 5 or 6-membered rings. At the same time, quebecol could extensively undergo phase 2 metabolism given the number of phenols in its structure. We were also concerned with the possibility that quebecol could undergo oxidation to a *p*-QM which could have toxicological implications.

The results from our *in vitro* metabolism studies have demonstrated that no cytochrome P450 metabolites were detected using rat, mouse, and human liver microsomes. In contrast, extensive phase 2 glucuronidation was observed with the formation of three glucuronide conjugates in similar amounts.

This is not the first study to demonstrate a minimal phase 1 metabolism for polyphenol natural products. In agreement with our results, the polyphenols NDGA and enterolactone predominantly undergo phase 2 glucuronidation and minor P450-mediated metabolism [19,56]. It is important to note that we would also expect contributions to phase 2 metabolism by sulfotransferases, however we did not determine quebecol sulfonation in this study.

Since phase 2 glucuronidation was detected as the major *in vitro* metabolic route, we carried out *in vitro* enzyme kinetic studies to estimate the relative contribution of the liver to presystemic glucuronidation of quebecol by determining Cl_{int} and K_M. Monitoring kinetics using the substrate depletion approach is an alternative to the traditional method by monitoring product formation [111]. By using this approach, the calibration curves in the analytical method are prepared based on the parent compound instead of the metabolite standards [107–110]. It has been determined that kinetics parameters obtained using the substrate depletion approach are comparable with those studies obtained by measuring product formation [111]. Previously, we used the substrate depletion approach to follow UGT metabolism [56] and herein, we have validated an HPLC-UV method to measure the phase 2 glucuronidation using the substrate depletion approach.

We have determined that the Michaelis constant (K_M) value for quebecol is 5.1 µM. This is an important pharmacokinetic parameter to understand the role of the metabolizing enzyme, and the potential of a substrate's ability to saturate a specific enzyme in the metabolism. As a comparison, 4-hydroxy tamoxifen is a tamoxifen phase 1 metabolite and its major elimination route is via glucuronidation. The K_M values of this metabolite in UGT1A7 (K_M = 7.4 µM) and UGT2B7 (K_M = 3.7 µM) are comparable to the value we determined for quebecol glucuronidation [117].

The metabolite 4-hydroxy tamoxifen is formed via cytochrome P450-mediated hydroxylation,

which can further oxidize to generate a *p*-QM leading to potential toxicological effects due to the formation of DNA adducts [120,121]. Due to the structural similarity between tamoxifen and quebecol, in this study we also investigated whether quebecol could form P450 reactive intermediates in liver microsomes. However, we were unable to detect any *p*-QMs in hepatic microsomes.

We then attempted to prepare quebecol *para*-quinone methide (*p*-QM) standards by chemical oxidation using Ag_2O. Incubation of quebecol with Ag_2O led to a color change compatible with oxidation, however resulted in loss of quebecol and an increase in the backpressure on HPLC. This suggested to us the formation of an insoluble polymer. Another chemical oxidant, MnO_2, was used to prepare tamoxifen quinone methides. We used MnO_2, and we were able to trap quinones as GSH adducts. However, we observed demethylation of the methoxy groups in quebecol, leading to further oxidation and *o*-quinone formation. *O*-Demethylation by MnO_2 was not found in literature, but we were able to locate reports of MnO_2-mediated *N*-methyl dealkylation [132]. Our results suggest formation of a *p*-QM from quebecol is unlikely to occur as a result of steric crowding *para* to the phenolic OH and rapid phase 2 metabolism.

Our initial hypothesis was that P450-mediated dealkylation products of quebecol could undergo intramolecular cyclization to form 6-membered rings. We were able to demonstrate intramolecular cyclization in our DPE model compounds but were unable to confirm if this was the result of C-C bond formation or C-O bond formation. For quebecol P450-mediated metabolism did not occur, although we reported that an intramolecular cyclization has likely occurred after MnO_2 incubation. Based on our data, intramolecular cyclization of the alcohol could have occurred, and it is unknown whether it results preferentially in a 5 or 6-membered ring.

Chapter 8: Future Directions

We have attempted to make the tetra-methyl NDGA without success. The successful synthesis of the tetra-methyl NDGA and its autoxidation potential at pH 7.4 will provide an understanding of how additional methyl groups influence the rate of oxidative cyclization. A new synthetic scheme has been proposed in Chapter 6.

Similar to cNDGA, we have reported that cyclized DPEs can inhibit α-synuclein. It is unclear how this interaction occurs. Photoaffinity labeling is one of the techniques that may be useful to determine how the cyclized DPEs interact with α-synuclein. Currently, there is a student in our group who will be exploring this pathway by preparing cyclized DPEs labeled with diazirines.

One of our hypotheses was that quebecol could form a *p*-QM, however we were unable to find evidence of its formation in microsomes and using chemical oxidation procedures. To better understand this process, three compounds (Figure 8.1) could serve as models to study *p*-QM formation. Compound **26** is a $(MeO)_2$-DPE analogue (Chapter 3) with only one ring substituted, and **27** is a diphenylmethane. Compound **28** is a quebecol analogue with only one ring substituted and without the presence of the alcohol.

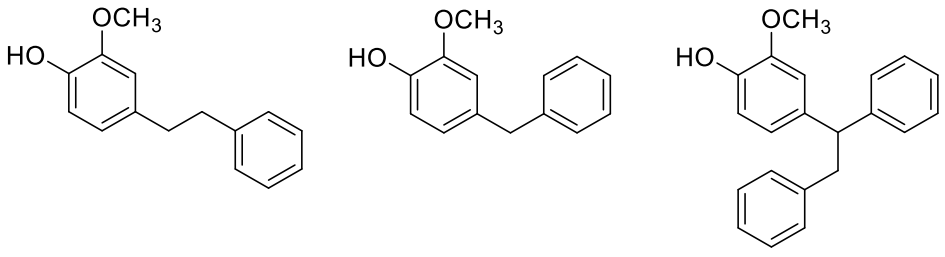

26 27 28

Figure 8.1. Proposed model compounds to study *p*-QM reactivity

Another important experiment that could be done is to prepare a series of compounds (Figure 8.2) to understand whether the oxidized quebecol cyclizes through a C-C or C-O bond (Chapter 5). Using the same approach as the DPEs, measuring the stability of **30** and **31** at pH 7.4 would provide important information whether the alcohol prefers to attack one position or the other by determining the products of autoxidation at pH 7.4 and determining the *in vitro* kinetics. Preparation of standards by oxidizing the catechols into quinones is necessary for NMR characterization and to confirm the 5- or 6-membered ring formed at pH 7.4. In addition, if no cyclized product is formed it would suggest that C-C formation in quebecol likely predominates.

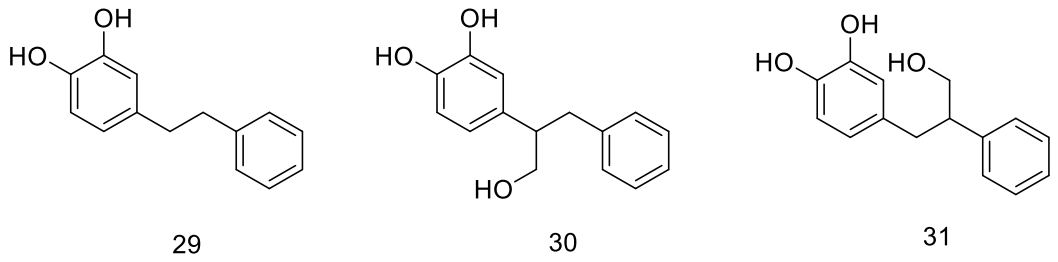

29 30 31

Figure 8.3. Proposed model compounds to probe ring closure

Preparing quebecol analogs with only one ring substituted to direct the 5- or 6-membered ether ring formation can serve as another strategy (Figure 8.4).

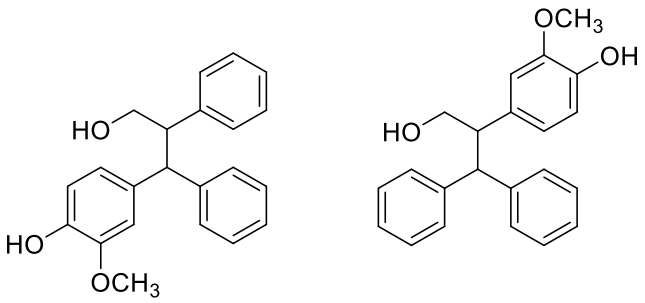

32 33

Figure 8.5. Proposed quebecol analogs to study 5- or 6-membered ring formation.

References

1. Abbas M, Saeed F, Anjum FM, Afzaal M, Tufail T, Bashir MS, et al. Natural polyphenols: An overview. Int J Food Prop. 2017;20:1689–99.
2. Chan JKW, Bittner S, Bittner A, Atwal S, Shen W-J, Inayathullah M, et al. Nordihydroguaiaretic Acid, a Lignan from *Larrea tridentata* (Creosote Bush), Protects Against American Lifestyle-Induced Obesity Syndrome Diet-Induced Metabolic Dysfunction in Mice. J Pharmacol Exp Ther. 2018;365:281–90.
3. Lambert JD, Zhao D, Meyers RO, Kuester RK, Timmermann BN, Dorr RT. Nordihydroguaiaretic acid: hepatotoxicity and detoxification in the mouse. Toxicon. 2002;40:1701–8.
4. Billinsky JL, Marcoux MR, Krol ES. Oxidation of the Lignan Nordihydroguaiaretic Acid. Chem Res Toxicol. 2007;20:1352–8.
5. Billinsky JL, Krol ES. Nordihydroguaiaretic Acid Autoxidation Produces a Schisandrin-like Dibenzocyclooctadiene Lignan. J Nat Prod. 2008;71:1612–5.
6. Asiamah I, Hodgson HL, Maloney K, Allen KJH, Krol ES. Ring substitution influences oxidative cyclisation and reactive metabolite formation of nordihydroguaiaretic acid analogues. Bioorg Med Chem. 2015;23:7007–14.
7. Niemeyer HB, Honig DM, Kulling SE, Metzler M. Studies on the metabolism of the plant lignans secoisolariciresinol and matairesinol. J Agric Food Chem. 2003;51:6317–25.
8. Toure A, Xueming X. Flaxseed Lignans: Source, Biosynthesis, Metabolism, Antioxidant Activity, Bio-Active Components and Health Benefits. Compr Rev Food Sci Food Saf. 2010;9:261–9.
9. Snow A, Nguyen B, Castillo G, Sanders V, Lake T, Larsen L, et al. Compounds, Compositions and Methods for the Treatment of Amyloid Diseases and Synucleinopathies such as Alzheimer's Disease, Type 2 Diabetes, and Parkinson's Disease. WIPO WO2003101927A1. 2004.
10. Cardinal S, Voyer N. Total synthesis of quebecol. Tetrahedron Lett. 2013;54:5178–80.
11. Daniels MJ, Nourse JB, Kim H, Sainati V, Schiavina M, Murrali MG, et al. Cyclized NDGA modifies dynamic α-synuclein monomers preventing aggregation and toxicity. Sci Rep. 2019;9:2937.
12. Albertson AKF, Lumb J-P. A Bio-Inspired Total Synthesis of Tetrahydrofuran Lignans. Angew Chemie Int Ed. 2015;54:2204–8.
13. Teponno RB, Kusari S, Spiteller M. Recent advances in research on lignans and neolignans. Nat Prod Rep. 2016;33:1044–92.
14. Alfaifi MY. Bioactive Lignans: A Survey Report on their Chemical Structures? Nat Prod Chem Res. 2016. p. 1–15.
15. Xu W, Zhao P, Wang M, Liang Q. Naturally occurring furofuran lignans: structural diversity and biological activities. Nat Prod Res. 2019;33:1357–73.
16. Zhang H, Li Y, Hu J, Shen W-J, Singh M, Hou X, et al. Effect of Creosote Bush-Derived NDGA on Expression of Genes Involved in Lipid Metabolism in Liver of High-Fructose Fed Rats: Relevance to NDGA Amelioration of Hypertriglyceridemia and Hepatic Steatosis. PLoS One. 2015;10:1–21.
17. Holmgren CA, Hunter KL, Betancourt JL. Creosote bush (*Larrea tridentata*) ploidy history along its diploid-tetraploid boundary in southeastern Arizona-southwestern New Mexico, USA. J Arid

Env. 2019;164:7–11.
18. Arteaga S, Andrade-Cetto A, Cárdenas R. *Larrea tridentata* (Creosote bush), an abundant plant of Mexican and US-American deserts and its metabolite nordihydroguaiaretic acid. J Ethnopharmacol. 2005;98:231–9.
19. Jeong H, Kim S, Lee J, Park JY, Zhou W, Liu X, et al. Characterization of Phase I and Phase II Hepatic Metabolism and Reactive Intermediates of *Larrea nitida* Cav. and Its Lignan Compounds. Phyther Res. 2017;31:140–51.
20. Szopa A, Dziurka M, Warzecha A, Kubica P, Klimek-Szczykutowicz M, Ekiert H. Targeted Lignan Profiling and Anti-Inflammatory Properties of *Schisandra rubriflora* and *Schisandra chinensis* Extracts. Mol. 2018.
21. Sowndhararajan K, Deepa P, Kim M, Park SJ, Kim S. An overview of neuroprotective and cognitive enhancement properties of lignans from *Schisandra chinensis*. Biomed Pharmacother. 2018;97:958–68.
22. Jung ME, Piizzi G. gem-Disubstituent Effect: Theoretical Basis and Synthetic Applications. Chem Rev. 2005;105:1735–66.
23. Gnabre J, Bates R, Huang RC. Creosote bush lignans for human disease treatment and prevention: Perspectives on combination therapy. J Tradit Complement Med. 2015;5:119–26.
24. Stickel F, Egerer G, Seitz HK. Hepatotoxicity of botanicals. Public Heal Nutr. 2000;3:113–24.
25. Sahu SC, Ruggles DI, O'Donnell MW. Prooxidant activity and toxicity of nordihydroguaiaretic acid in clone-9 rat hepatocyte cultures. Food Chem Toxicol. 2006;44:1751–7.
26. Chen D-F, Zhang S-X, Kozuka M, Sun Q-Z, Feng J, Wang Q, et al. Interiotherins C and D, Two New Lignans from Kadsura interior and Antitumor-Promoting Effects of Related Neolignans on Epstein−Barr Virus Activation. J Nat Prod. 2002;65:1242–5.
27. Nomura M, Nakachiyama M, Hida T, Ohtaki Y, Sudo K, Aizawa T, et al. Gomisin A, a lignan component of Schizandora fruits, inhibits development of preneoplastic lesions in rat liver by 3′-methyl-4-dimethylamino-azobenzene. Cancer Lett. 1994;76:11–8.
28. Wu M-D, Huang R-L, Kuo L-MY, Hung C-C, Ong C-W, Kuo Y-H. The Anti-HBsAg (Human Type B Hepatitis, Surface Antigen) and Anti-HBeAg (Human Type B Hepatitis, e Antigen) C18 Dibenzocyclooctadiene Lignans from Kadsura matsudai and Schizandra arisanensis. Chem Pharm Bull. 2003;51:1233–6.
29. Han Y-S, Xiao W-L, Xu H, Kramer VG, Quan Y, Mesplède T, et al. Identification of a dibenzocyclooctadiene lignan as a HIV-1 non-nucleoside reverse transcriptase inhibitor. Antivir Chem Chemother. 2015;24:28–38.
30. Choi Y-W, Takamatsu S, Khan SI, Srinivas P V, Ferreira D, Zhao J, et al. Schisandrene, a Dibenzocyclooctadiene Lignan from *Schisandra chinensis*: Structure−Antioxidant Activity Relationships of Dibenzocyclooctadiene Lignans. J Nat Prod. 2006;69:356–9.
31. Park SY, Bae Y-S, Ko MJ, Lee S-J, Choi Y-W. Comparison of anti-inflammatory potential of four different dibenzocyclooctadiene lignans in microglia; action via activation of PKA and Nrf-2 signaling and inhibition of MAPK/STAT/NF-κB pathways. Mol Nutr Food Res. 2014;58:738–48.
32. Beitz J. Parkinson's disease: a review. Front Biosci. 2014;S6:65–74.
33. Barbosa AF, Chen J, Freitag F, Valente D, Souza CDO, Voos MC, et al. Gait, posture and cognition in Parkinson's disease. Dement Neuropsychol. 2016;10:280–6.
34. Alvarez M V, Evidente VGH, Driver-dunckley ED. Differentiating Parkinson's Disease from Other Parkinsonian Disorders. Semin Neurol. 2007;27:356–62.

35. Hardy J, Cai H, Cookson MR, Gwinn-hardy K, Singleton A. Genetics of Parkinson's Disease and Parkinsonism. Ann Neurol. 2006;60:389–98.
36. Kalia L V, Lang AE, Shulman G. Parkinson's disease. Lancet. 2015;386:896–912.
37. Coelho M, Ferreira JJ. Late-stage Parkinson disease. Nat Rev Neurol. 2012;8:435–42.
38. Duyckaerts C, Lebouvier T, Chaumette T, Bruley S, Neunlist M, Derkinderen P. The second brain and Parkinson's disease. Eur J Neurosci. 2009;30:735–41.
39. Twelves D, Perkins KSM, Uk M, Counsell C. Systematic Review of Incidence Studies of Parkinson's Disease. Mov Disord. 2003;18:19–31.
40. Canada. Mapping connections: An understanding of neurological conditions in Canada [Internet]. Public Heal. Agency Canada. 2014 [cited 2018 Oct 25]. Available from: www.canada.ca/en/public-health/services/%0Areports-publications/mapping-connections-understandingneurological-conditions.html.
41. Diem-Zangerl A, Seppi K, Wenning GK, Trinka E, Ransmayr G, Oberaigner W, et al. Mortality in Parkinson's Disease : A 20-Year Follow-Up Study. Mov Disord. 2009;24:819–25.
42. Pinter B, Diem-Zangerl A, Wenning GK, Scherfler C, Oberaigner W, Seppi K. Mortality in Parkinson's Disease: A 38-Year Follow-up Study. Mov Disord. 2015;30:1–3.
43. Van Den Eeden S, Tanner C, Bernstein A, Fross R, Leimpeter A, Bloch D, et al. Incidence of Parkinson's disease: variation by age, gender, and race/ethnicity. Am J Epidemiol. 2003;157:1015–22.
44. Mehanna R, Moore S, Hou JG, Sarwar AI, Lai EC. Comparing Clinical Features of Young Onset, Middle Onset and Late Onset Parkinson's Disease. Park Relat Disord. Elsevier Ltd; 2014;1:1–21.
45. Miller IN, Cronin-Golomb A. Gender Differences in Parkinson's Disease: Clinical Characteristics and Cognition. Mov Disord. 2010;25:2695–703.
46. Fernandez H, Lapane K, Friedman J. Gender differences in the frequency and treatment of behavior problems in Parkinson's disease. Mov Disord. 2000;15:490–496.
47. Ozekmekc S, Kilic E. Clinical features of 35 patients with Parkinson's disease displaying REM behavior disorder. 2005;107:306–9.
48. Marras C, Saunders-Pullman R. The Complexities of Hormonal Influences and Risk of Parkinson's Disease. Mov Disord. 2014;29:845–8.
49. Chaudhuri KR, Schapira AH V. Non-motor symptoms of Parkinson's disease: dopaminergic pathophysiology and treatment. Lancet Neurol. 2009;8:464–74.
50. Kim WS, Kågedal K, Halliday GM. Alpha-synuclein biology in Lewy body diseases. Alzheimers Res Ther. 2014;6:73.
51. Angot E, Steiner JA, Lema Tomé CM, Ekström P, Mattsson B, Björklund A, et al. Alpha-synuclein cell-to-cell transfer and seeding in grafted dopaminergic neurons in vivo. PLoS One. 2012;7:1–11.
52. Recasens A, Dehay B. Alpha-synuclein spreading in Parkinson's disease. Front Neuroanat. 2014;8:159.
53. Tran HT, Chung CH-Y, Iba M, Zhang B, Trojanowski JQ, Luk KC, et al. α-synuclein immunotherapy blocks uptake and templated propagation of misfolded α-synuclein and neurodegeneration. Cell Rep. 2014;7:2054–65.
54. Landete JM. Plant and mammalian lignans: A review of source, intake, metabolism, intestinal bacteria and health. Food Res Int. 2012;46:410–24.
55. Gaya P, Medina M, Sánchez-Jiménez A, Landete JM. Phytoestrogen Metabolism by Adult Human Gut Microbiota. Molecules. 2016;21:1034.

56. Lin C, Krol ES, Alcorn. J. The Comparison of Rat and Human Intestinal and Hepatic Glucuronidation of Enterolactone Derived from Flaxseed Lignans. Nat Prod J. 2013;3:159–71.
57. Jansen GHE, Arts ICW, Nielen MWF, Müller M, Hollman PCH, Keijer J. Uptake and metabolism of enterolactone and enterodiol by human colon epithelial cells. Arch Biochem Biophys. 2005;435:74–82.
58. Adolphe JL, Whiting SJ, Juurlink BHJ, Thorpe LU, Alcorn J. Health effects with consumption of the flax lignan secoisolariciresinol diglucoside. Br J Nutr. 2010;103:929–38.
59. Li L, Seeram NP. Quebecol, a novel phenolic compound isolated from Canadian maple syrup. J Funct Foods. 2011;3:125–8.
60. Jordan VC. Tamoxifen: a most unlikely pioneering medicine. Nat Rev Drug Discov. 2003;2:205–13.
61. Pericherla K, Shirazi AN, Rao VK, Tiwari RK, DaSilva N, McCaffrey KT, et al. Synthesis and antiproliferative activities of quebecol and its analogs. Bioorg Med Chem Lett. 2013;23:5329–31.
62. Cardinal S, Azelmat J, Grenier D, Voyer N. Anti-inflammatory properties of quebecol and its derivatives. Bioorg Med Chem Lett. 2016;26:440–4.
63. Brito AF, Zang Y. A Review of Lignan Metabolism, Milk Enterolactone Concentration, and Antioxidant Status of Dairy Cows Fed Flaxseed. Molecules. 2018;24:41.
64. Parvathy KS, Negi PS, Srinivas P. Antioxidant, antimutagenic and antibacterial activities of curcumin-β-diglucoside. Food Chem. 2009;115:265–71.
65. Apisariyakul A, Vanittanakom N, Buddhasukh D. Antifungal activity of turmeric oil extracted from *Curcuma longa* (Zingiberaceae). J Ethnopharmacol. 1995;49:163–9.
66. Narlawar R, Pickhardt M, Leuchtenberger S, Baumann K, Krause S, Dyrks T, et al. Curcumin-Derived Pyrazoles and Isoxazoles: Swiss Army Knives or Blunt Tools for Alzheimer's Disease? ChemMedChem. 2008;3:165–72.
67. Wang MS, Boddapati S, Emadi S, Sierks MR. Curcumin reduces alpha-synuclein induced cytotoxicity in Parkinson's disease cell model. BMC Neurosci. 2010;11:57.
68. Funk JL, Oyarzo JN, Frye JB, Chen G, Lantz RC, Jolad SD, et al. Turmeric extracts containing curcuminoids prevent experimental rheumatoid arthritis. J Nat Prod. 2006;69:351–5.
69. Shen L, Ji H-F. The pharmacology of curcumin: is it the degradation products? Trends Mol Med. 2012;18:138–44.
70. Pan M-H, Huang T-M, Lin J-K. Biotransformation of Curcumin Through Reduction and Glucuronidation in Mice. Drug Metab Dispos. 1999;27:486–94.
71. Metzler M, Pfeiffer E, Schulz SI, Dempe JS. Curcumin uptake and metabolism. BioFactors. 2013;39:14–20.
72. Luis PB, Boeglin WE, Schneider C. Thiol Reactivity of Curcumin and Its Oxidation Products. Chem Res Toxicol. 2018;31:269–76.
73. Jitoe-Masuda A, Fujimoto A, Masuda T. Curcumin: From Chemistry to Chemistry-Based Functions. Curr Pharm Des. 2013;19:2084–92.
74. Krafczyk N, Heinrich T, Porzel A, Glomb MA. Oxidation of the Dihydrochalcone Aspalathin Leads to Dimerization. J Agric Food Chem. 2009;57:6838–43.
75. Roginsky V, Alegria AE. Oxidation of tea extracts and tea catechins by molecular oxygen. J Agric Food Chem. 2005;53:4529–35.
76. Boston-Howes W, Williams EO, Bogush A, Scolere M, Pasinelli P, Trotti D. Nordihydroguaiaretic acid increases glutamate uptake in vitro and in vivo: Therapeutic implications for amyotrophic

lateral sclerosis. Exp Neurol. 2008;213:229–37.
77. Ono K, Hasegawa K, Yoshiike Y, Takashima A, Yamada M, Naiki H. Nordihydroguaiaretic acid potently breaks down pre-formed Alzheimer's β-amyloid fibrils *in vitro*. J Neurochem. 2002;81:434–40.
78. Barrett TN, Braddock DC, Monta A, Webb MR, White AJP. Total Synthesis of the Marine Metabolite (±)-Polysiphenol via Highly Regioselective Intramolecular Oxidative Coupling. J Nat Prod. 2011;74:1980–4.
79. Nwabufo CK, Aigbogun OP, Allen KJH, Owens MN, Lee JS, Phenix CP, et al. Employing in vitro metabolism to guide design of F-labelled PET probes of novel α-synuclein binding bifunctional compounds. Xenobiotica. 2021;51:885–900.
80. Tamaki K, Ishigami A, Tanaka Y, Yamanaka M, Kobayashi K. Self-Assembled Boronic Ester Cavitand Capsules with Various Bis(catechol) Linkers: Cavity-Expanded and Chiral Capsules. Chem Eur J. 2015;21:13714–22.
81. Hartmann RW, Kranzfelder G, Von Angerer E, Schoenenberger H. Antiestrogens. Synthesis and evaluation of mammary tumor inhibiting activity of 1,1,2,2-tetraalkyl-1,2-diphenylethanes. J Med Chem. 1980;23:841–8.
82. Zeng W, Chemler SR. Total synthesis of (S)-(+)-tylophorine via enantioselective intramolecular alkene carboamination. J Org Chem. 2008;73:6045–7.
83. Asiamah I, Krol ES. Quadrupole linear ion-trap mass spectrometry studies on glutathione conjugates of nordihydroguaiaretic acid (NDGA) analogues reveals phenol-type analogues are without reactive metabolite-mediated toxic liability. Cogent Chem. 2018;4:1562858.
84. Szopa A, Ekiert R, Ekiert H. Current knowledge of *Schisandra chinensis* (Turcz.) Baill. (Chinese magnolia vine) as a medicinal plant species: a review on the bioactive components, pharmacological properties, analytical and biotechnological studies. Phytochem Rev. 2017;16:195–218.
85. Brenna E, Dalla Santa F, Gatti FG, Gatti G, Tessaro D. Exploiting the vicinal disubstituent effect on the diastereoselective synthesis of γ and δ lactones. Org Biomol Chem. 2019;17:813–21.
86. Galano A, Macías-Ruvalcaba NA, Medina Campos ON, Pedraza-Chaverri J. Mechanism of the OH Radical Scavenging Activity of Nordihydroguaiaretic Acid: A Combined Theoretical and Experimental Study. J Phys Chem B. 2010;114:6625–35.
87. Alsoufi A, Altarawneh M, Dlugogorski BZ, Kennedy EM, Mackie JC. A DFT study on the self-coupling reactions of the three isomeric semiquinone radicals. J Mol Struct THEOCHEM. 2010;958:106–15.
88. Perkins TD, van den Berg AKBT. Maple Syrup—Production, Composition, Chemistry, and Sensory Characteristics. Adv Food Nutr Res. 2009;56:101–43.
89. Ball DW. The chemical composition of maple syrup. J Chem Educ. 2007;84:1647–50.
90. González-Sarrías A, Li L, Seeram NP. Anticancer effects of maple syrup phenolics and extracts on proliferation, apoptosis, and cell cycle arrest of human colon cells. J Funct Foods. 2012;4:185–96.
91. Yamamoto T, Uemura K, Moriyama K, Mitamura K, Taga A. Inhibitory effect of maple syrup on the cell growth and invasion of human colorectal cancer cells. Oncol Rep. 2015;33:1579–84.
92. González-Sarrías A, Ma H, Edmonds ME, Seeram NP. Maple polyphenols, ginnalins A–C, induce S- and G2/M-cell cycle arrest in colon and breast cancer cells mediated by decreasing cyclins A and D1 levels. Food Chem. 2013;136:636–42.
93. Nahar PP, Driscoll M V, Li L, Slitt AL, Seeram NP. Phenolic mediated anti-inflammatory

properties of a maple syrup extract in RAW 264.7 murine macrophages. J Funct Foods. 2014;6:126–36.
94. González-Sarrías A, Li L, Seeram NP. Effects of maple (Acer) plant part extracts on proliferation, apoptosis and cell cycle arrest of human tumorigenic and non-tumorigenic colon cells. Phytother Res. 2012;26:995–1002.
95. Rose KN, Barlock BJ, DaSilva NA, Johnson SL, Liu C, Ma H, et al. Anti-neuroinflammatory effects of a food-grade phenolic-enriched maple syrup extract in a mouse model of Alzheimer's disease. Nutr Neurosci. 2021;24:710–9.
96. Legault J, Girard-Lalancette K, Grenon C, Dussault C, Pichette A. Antioxidant activity, inhibition of nitric oxide overproduction, and in vitro antiproliferative effect of maple sap and syrup from Acer saccharum. J Med Food. 2010;13:460–8.
97. Liu W, Wei Z, Ma H, Cai A, Liu Y, Sun J, et al. Anti-glycation and anti-oxidative effects of a phenolic-enriched maple syrup extract and its protective effects on normal human colon cells. Food Funct. 2017;8:757–66.
98. Li L, Seeram NP. Maple Syrup Phytochemicals Include Lignans, Coumarins, a Stilbene, and Other Previously Unreported Antioxidant Phenolic Compounds. J Agric Food Chem. 2010;58:11673–9.
99. Liu Y, Rose KN, DaSilva NA, Johnson SL, Seeram NP. Isolation, Identification, and Biological Evaluation of Phenolic Compounds from a Traditional North American Confectionery, Maple Sugar. J Agric Food Chem. 2017;65:4289–95.
100. Ball DW. The Chemical Composition of Maple Syrup. J Chem Educ. 2007;84:1647–50.
101. Pericherla K, Shirazi AN, Rao VK, Tiwari RK, Dasilva N, McCaffrey KT, et al. Synthesis and antiproliferative activities of quebecol and its analogs. Bioorg Med Chem Lett. 2013;23:5329–31.
102. Cardinal S, Azelmat J, Grenier D, Voyer N. Anti-inflammatory properties of quebecol and its derivatives. Bioorg Med Chem Lett. 2016;26:440–4.
103. Cardinal S, Paquet-Côté P-A, Azelmat J, Bouchard C, Grenier D, Voyer N. Synthesis and anti-inflammatory activity of isoquebecol. Bioorg Med Chem. 2017;25:2043–56.
104. Chênevert R, Mohammadi-Ziarani G, Caron D, Dasser M. Chemoenzymatic enantioselective synthesis of (-)-enterolactone. Can J Chem. 1999;77:223–6.
105. U.S Food and Drug Administration. Bioanalytical Method Validation: Guidance for Industry. U.S. Dep. Heal. Hum. Serv. Food Drug Adm. Cent. Drug Eval. Res. Cent. Vet. Med. 2018.
106. European Medicines Agency. Guideline on bioanalytical method validation. Comm Med Prod Hum Use. 2011;1–23.
107. Obach RS, Reed-Hagen AE. Measurement of Michaelis constants for cytochrome P450-mediated biotransformation reactions using a substrate depletion approach. Drug Metab Dispos. 2002;30:831–7.
108. Youdim K, Dodia R. Comparison between recombinant P450s and human liver microsomes in the determination of cytochrome P450 Michaelis-Menten constants. Xenobiotica. 2010;40:235–44.
109. Schwaninger AE, Meyer MR, Barnes AJ, Gorelick DA, Goodwin RS, Huestis MA, et al. Investigation on the Enantioselectivity of the Sulfation of the Dihydroxymethamphetamine and 4-Hydroxy-3- Methoxymethamphetamine using the Substrate-Depletion Approach. Drug Metab Dispos. 2011;39:1998–2002.
110. Caspar AT, Meyer MR, Maurer HH. Human cytochrome P450 kinetic studies on six N-2-methoxybenzyl (NBOMe)-derived new psychoactive substances using the substrate depletion approach. Toxicol Lett. 2018;285:1–8.

111. Nath A, Atkins WM. A theoretical validation of the substrate depletion approach to determining kinetic parameters. Drug Metab Dispos. 2006;34:1433–5.
112. Wang R, Hartmann MF, Wudy SA. Targeted LC–MS/MS analysis of steroid glucuronides in human urine. J Steroid Biochem Mol Biol. 2021;205:105774.
113. Fabregat A, Pozo OJ, Marcos J, Segura J, Ventura R. Use of LC-MS/MS for the Open Detection of Steroid Metabolites Conjugated with Glucuronic Acid. Anal Chem. 2013;85:5005–14.
114. Nagar S, Argikar UA, Tweedie DJ. Enzyme kinetics in drug metabolism: fundamentals and applications. Methods Mol Biol. 2014. p. 1–6.
115. Yang G, Ge S, Singh R, Basu S, Shatzer K, Zen M, et al. Glucuronidation: driving factors and their impact on glucuronide disposition. Drug Metab Rev. 2017;49:105–38.
116. Lien EA, Solheim E, Lea OA, Lundgren S, Kvinnsland S, Ueland PM. Distribution of 4-Hydroxy-N-desmethyltamoxifen and Other Tamoxifen Metabolites in Human Biological Fluids during Tamoxifen Treatment1. Cancer Res. 1989;49:2175–83.
117. Sun D, Sharma AK, Dellinger RW, Blevins-Primeau AS, Balliet RM, Chen G, et al. Glucuronidation of Active Tamoxifen Metabolites by the Human UDP Glucuronosyltransferases. Drug Metab Dispos. 2007;35:2006–14.
118. Bouchard C, Grenier A, Cardinal S, Bélanger S, Voyer N, Pouliot R. Antipsoriatic Potential of Quebecol and Its Derivatives. Pharmaceutics. 2022;14:1–15.
119. Cardinal S, Ben Lagha A, Azelmat J, Grenier D. Quebecol Shows Potential to Alleviate Periodontal Tissue Damage and Promote Bone Formation in In Vitro Models. ACS Omega. 2021;6:27791–7.
120. Shibutani S, Ravindernath A, Suzuki N, Terashima I, Sugarman SM, Grollman AP, et al. Identification of tamoxifen–DNA adducts in the endometrium of women treated with tamoxifen. Carcinogenesis. 2000;21:1461–7.
121. Fan PW, Bolton JL. Bioactivation of Tamoxifen to Metabolite E Quinone Methide: Reaction with Glutathione and DNA. Drug Metab Dispos. 2001;29:891–6.
122. Yu L, Liu H, Li W, Zhang F, Luckie C, van Breemen RB, et al. Oxidation of raloxifene to quinoids: potential toxic pathways via a diquinone methide and o-quinones. Chem Res Toxicol. 2004;17:879–88.
123. Fan PW, Zhang F, Bolton JL. 4-Hydroxylated metabolites of the antiestrogens tamoxifen and toremifene are metabolized to unusually stable quinone methides. Chem Res Toxicol. 2000;13:45–52.
124. Stepan AF, Walker DP, Bauman J, Price DA, Baillie TA, Kalgutkar AS, et al. Structural Alert/Reactive Metabolite Concept as Applied in Medicinal Chemistry to Mitigate the Risk of Idiosyncratic Drug Toxicity: A Perspective Based on the Critical Examination of Trends in the Top 200 Drugs Marketed in the United States. Chem Res Toxicol. 2011;24:1345–410.
125. Claesson A, Minidis A. Systematic Approach to Organizing Structural Alerts for Reactive Metabolite Formation from Potential Drugs. Chem Res Toxicol. 2018;31:389–411.
126. Fatiadi AJ. Active Manganese Dioxide Oxidation in Organic Chemistry - Part I. Synthesis (Stuttg). 1976;1976:65–104.
127. Evans DC, Watt AP, Nicoll-Griffith DA, Baillie TA. Drug−Protein Adducts: An Industry Perspective on Minimizing the Potential for Drug Bioactivation in Drug Discovery and Development. Chem Res Toxicol. 2004;17:3–16.
128. Obach RS, Kalgutkar AS, Soglia JR, Zhao SX. Can *In Vitro* Metabolism-Dependent Covalent

Binding Data in Liver Microsomes Distinguish Hepatotoxic from Nonhepatotoxic Drugs? An Analysis of 18 Drugs with Consideration of Intrinsic Clearance and Daily Dose. Chem Res Toxicol. 2008;21:1814–22.
129. Thompson DC, Perera K, Krol ES, Bolton JL. o-Methoxy-4-alkylphenols That Form Quinone Methides of Intermediate Reactivity Are the Most Toxic in Rat Liver Slices. Chem Res Toxicol. 1995;8:323–7.
130. Bolton JL, Trush MA, Penning TM, Dryhurst G, Monks TJ. Role of Quinones in Toxicology. Chem Res Toxicol. 2000;13:135–60.
131. Bolton JL, Comeau E, Vukomanovic V. The influence of 4-alkyl substituents on the formation and reactivity of 2-methoxy-quinone methides: evidence that extended π-conjugation dramatically stabilizes the quinone methide formed from eugenol. Chem Biol Interact. 1995;95:279–90.
132. Cheney MA, Shin JY, Crowley DE, Alvey S, Malengreau N, Sposito G. Atrazine dealkylation on a manganese oxide surface. Colloids Surfaces A Physicochem Eng Asp. 1998;137:267–73.
133. Ito S, Wakamatsu K. Biochemical Mechanism of Rhododendrol-Induced Leukoderma. Int J Mol Sci. 2018;19.
134. Horner L, Weber K-H. Zur Kenntnis der o-Chinone, XXVIII. Darstellungen und Eigenschaften weiterer Chinone des Biphenyls. Chem Ber. 1967;100:2842–53.
135. McGurn L. Secoisolariciresinol (SECO) Analogues: Oxidative Metabolism, Cytochrome P450 Inhibition and Implications for Toxicity. University of Saskatchewan; 2016.
136. Endo Y, Yoshimi T, Ohta K, Suzuki T, Ohta S. Potent Estrogen Receptor Ligands Based on Bisphenols with a Globular Hydrophobic Core. J Med Chem. 2005;48:3941–4.
137. Kawamur Y, Thurnauer M, Schuster GB. Putative electrocyclic reaction of cyclobutene radical cation: 1,2-Diphenyl-3,3,4,4-tetramethylcyclobutene. Tetrahedron. 1986;42:6195–200.
138. Atanasov AG, Zotchev SB, Dirsch VM, Orhan IE, Banach M, Rollinger JM, et al. Natural products in drug discovery: advances and opportunities. Nat Rev Drug Discov. 2021;20:200–16.
139. Lambert J, Dorr R, Timmermann B. Nordihydroguaiaretic Acid: A Review of Its Numerous and Varied Biological Activities. Pharm Biol. 2004;42:149–58.
140. Sukphan P, Sritularak B, Mekboonsonglarp W, Lipipun V, Likhitwitayawuid K. Chemical Constituents of Dendrobium venustum and their Antimalarial and Anti-herpetic Properties. Nat Prod Commun. 2014;9.
141. Majumder PL, Kar A. Confusarin and confusaridin two phenanthrene derivatives of the orchid *Eria confusa*. Phytochemistry. 1987;26:1127–9.
142. Majumder PL, Banerjee S. Two stilbenoids from the orchid *Eria flava*. Phytochemistry. 1990;29:3052–5.
143. Grice HC, Becking G, Goodman T. Toxic properties of nordihydroguaiaretic acid. Food Cosmet Toxicol. 1968;6:155–61.

APPENDIX

Supporting Information

Autoxidation of diphenylethane analogs

Table S1. Different timepoints for autoxidation kinetics

Timepoints (minutes)		
DPE	**M2-DPE**	**M4-DPE**
0	0	0
5	2.5	2.5
10	5	5
15	7.5	7.5
20	10	10
25	12.5	12.5
30	15	15
35	17.5	17.5
40	20	20

Table S2. Reverse phase column gradient elution conditions

Method I			Method II			Method III		
Time (min)	**A (%)**	**B (%)**	**Time (min)**	**A (%)**	**B (%)**	**Time (min)**	**A (%)**	**B (%)**
0	90	10	0	90	10	0	90	10
5	90	10	5	90	10	2.5	90	10
10	60	40	30	50	50	25	10	90
25	10	90	34	10	90	26	90	10
26	90	10	35	90	10	36	90	10
36	90	10	42	90	10			

Autoxidation products of DPE

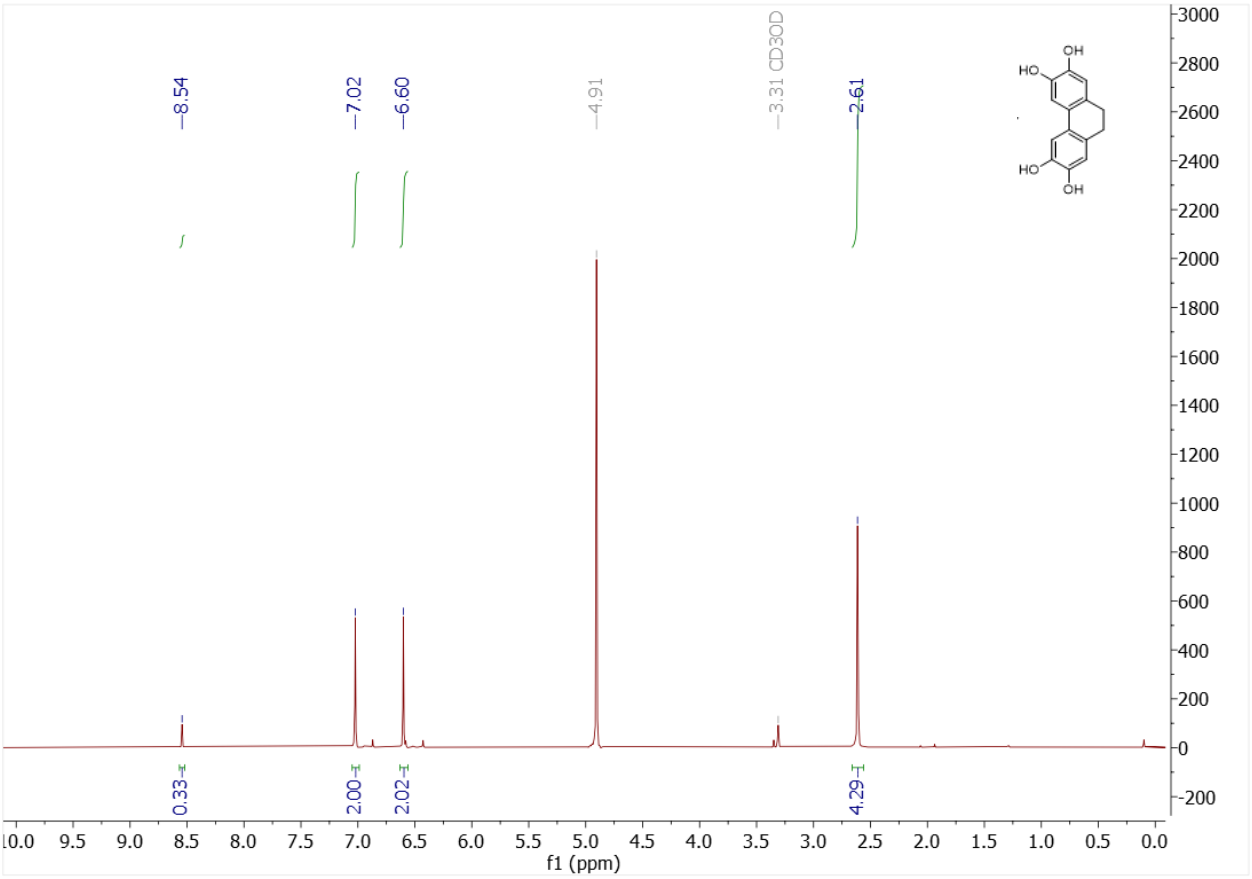

Figure S1. ^{1}H NMR for o-DPE A

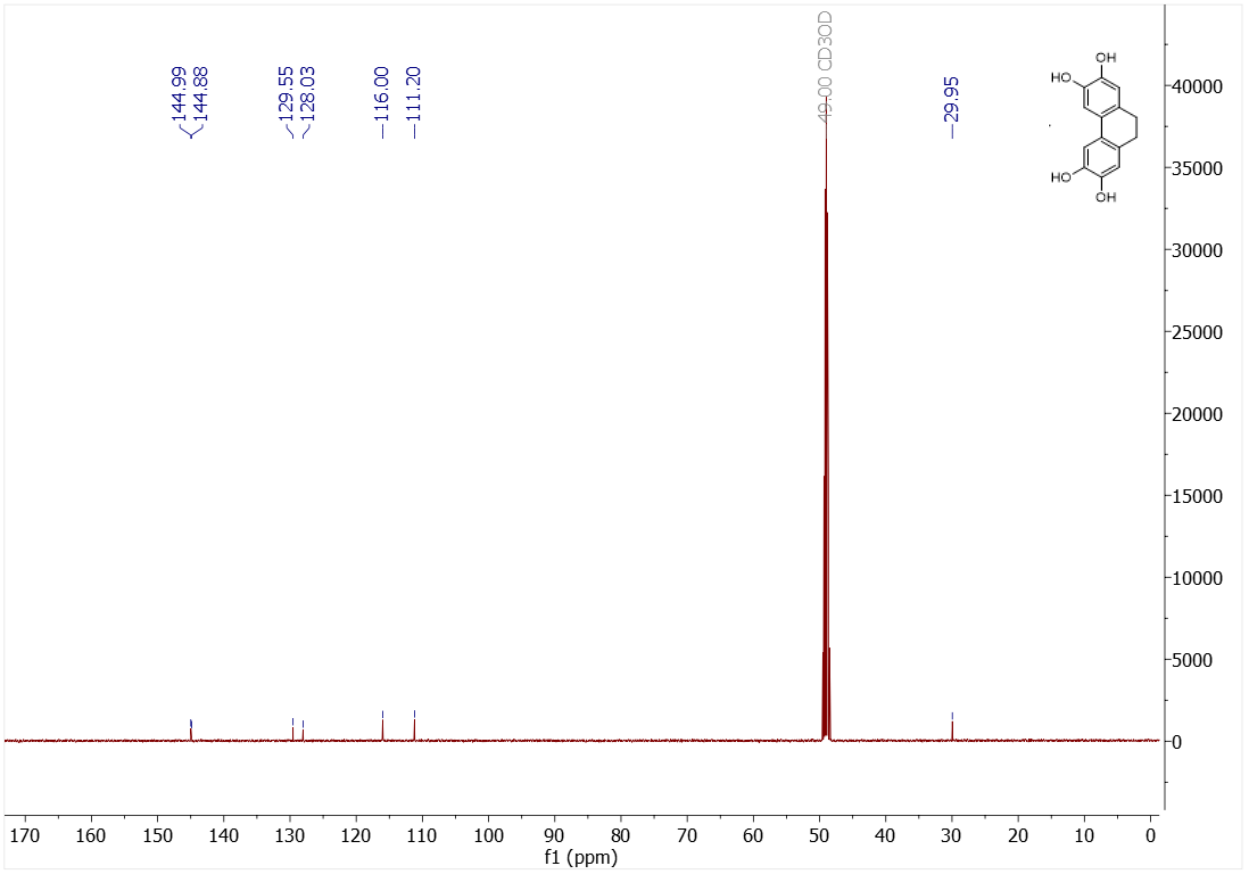

Figure S2. ^{13}C NMR for o-DPE A

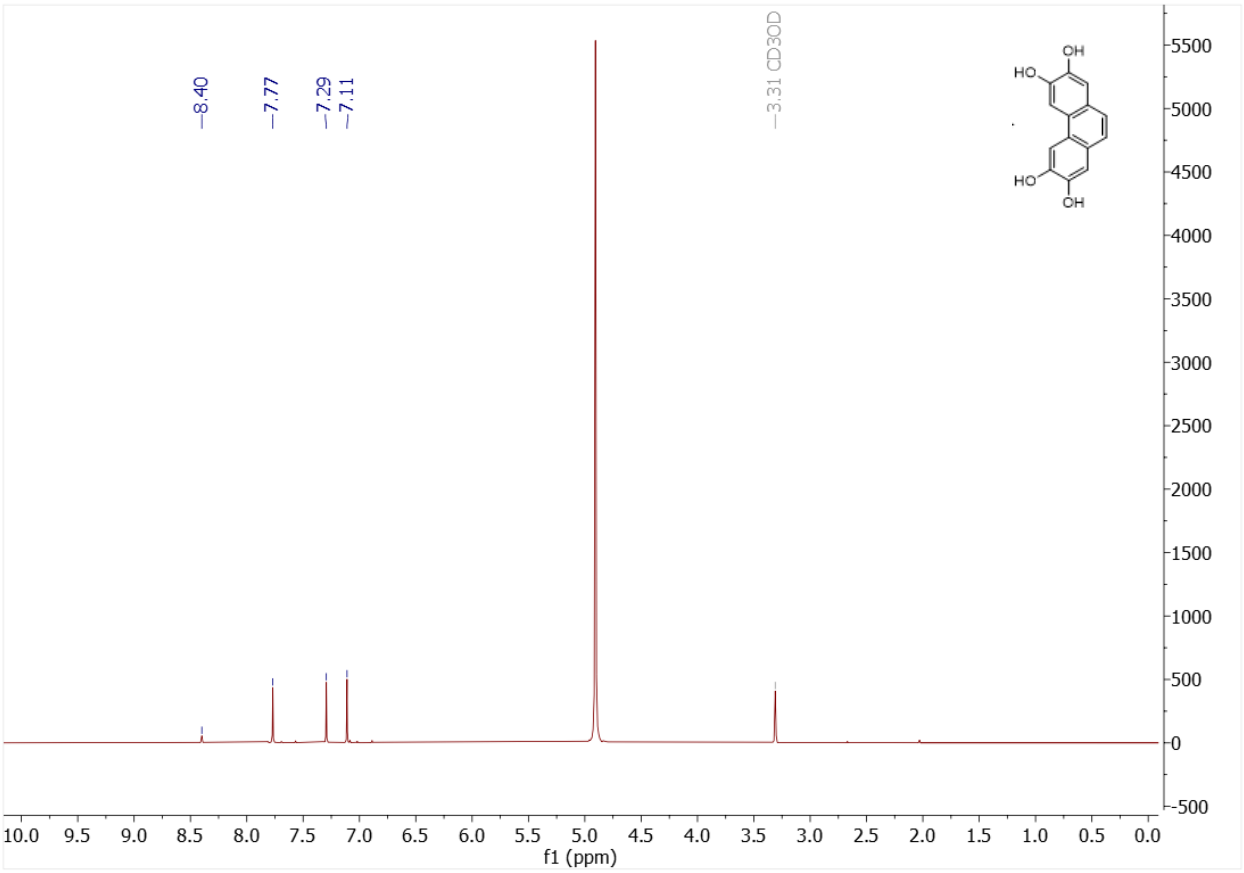

Figure S3. ^{1}H NMR for o-DPE B

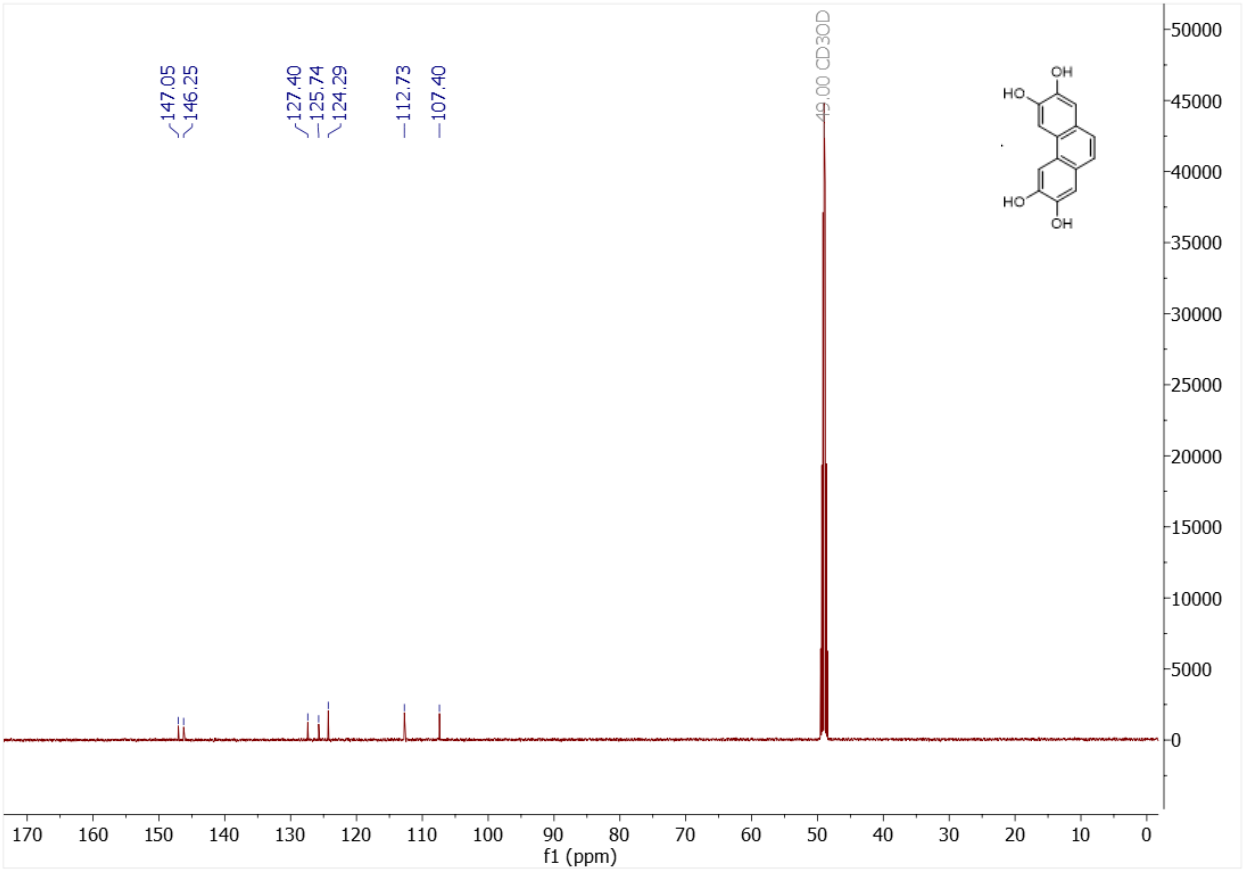

Figure S4. ^{13}C NMR for o-DPE B

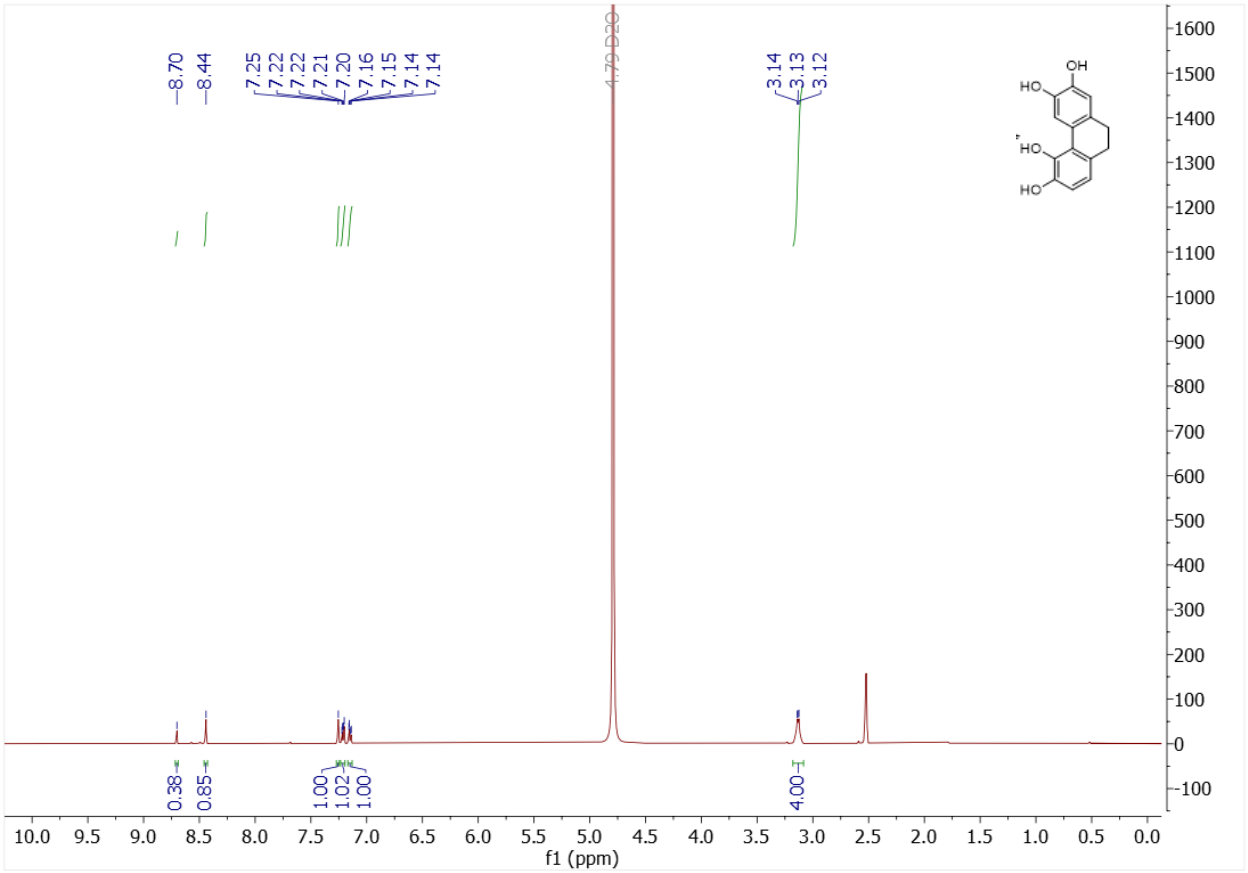

Figure S5. ^{1}H NMR for o-DPE C

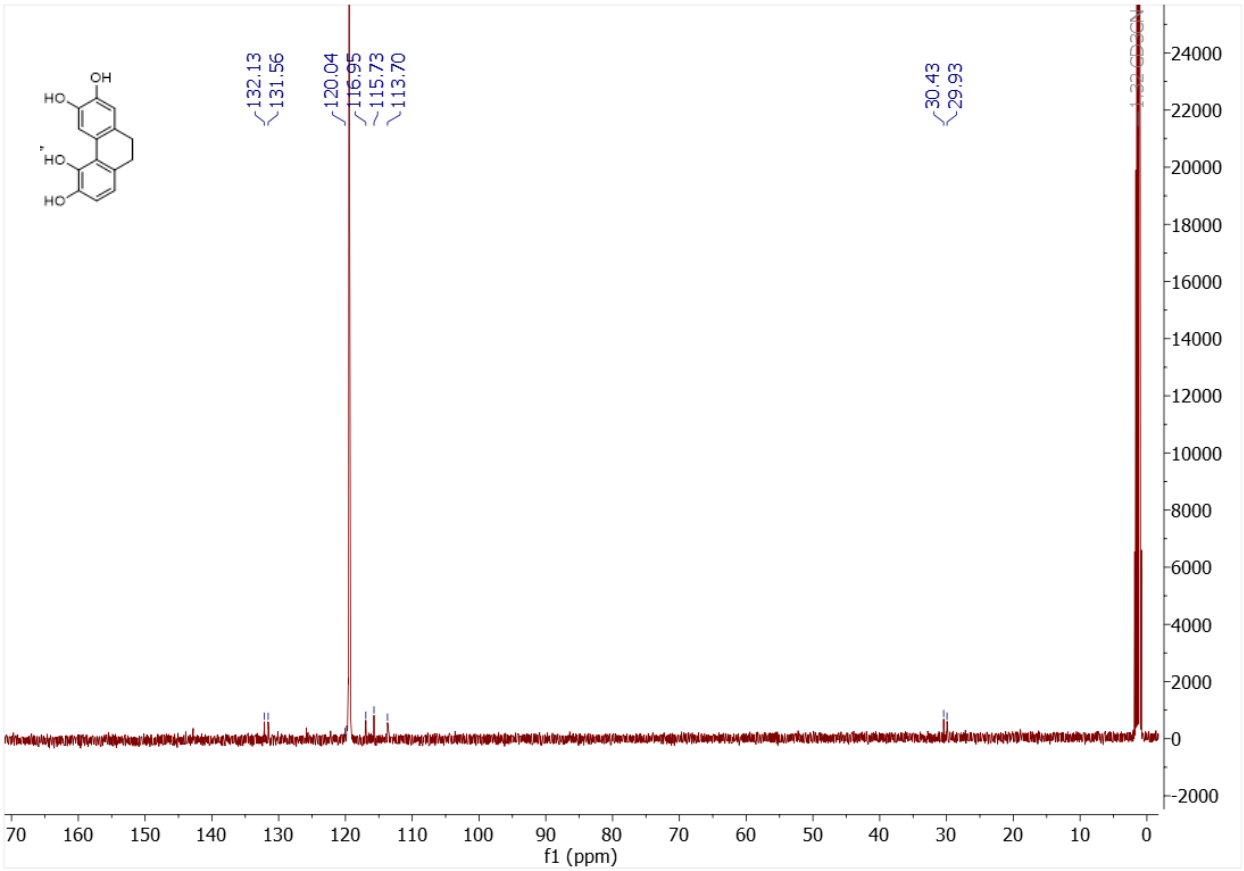

Figure S6. ^{13}C NMR for o-DPE C

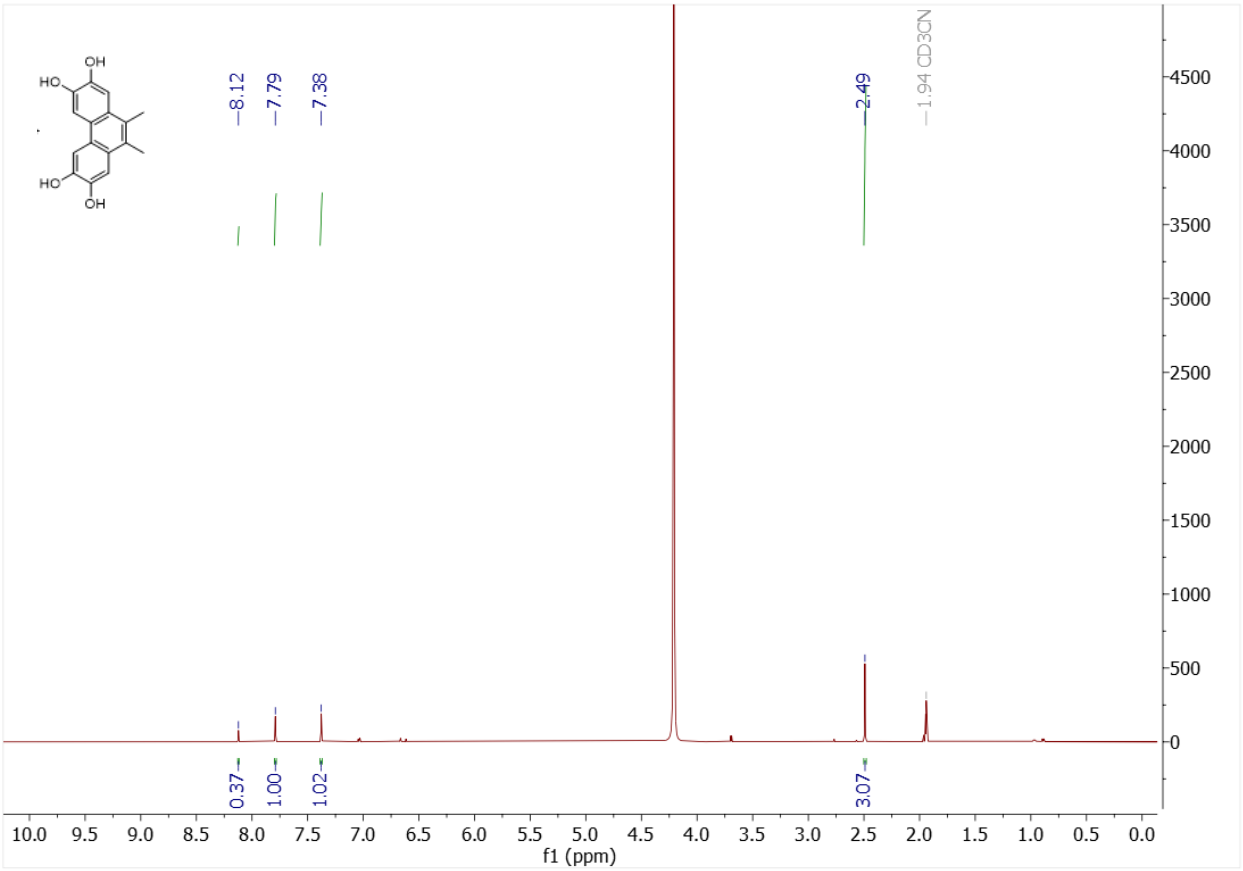

Figure S7. ^{1}H NMR for o-M2-DPE A

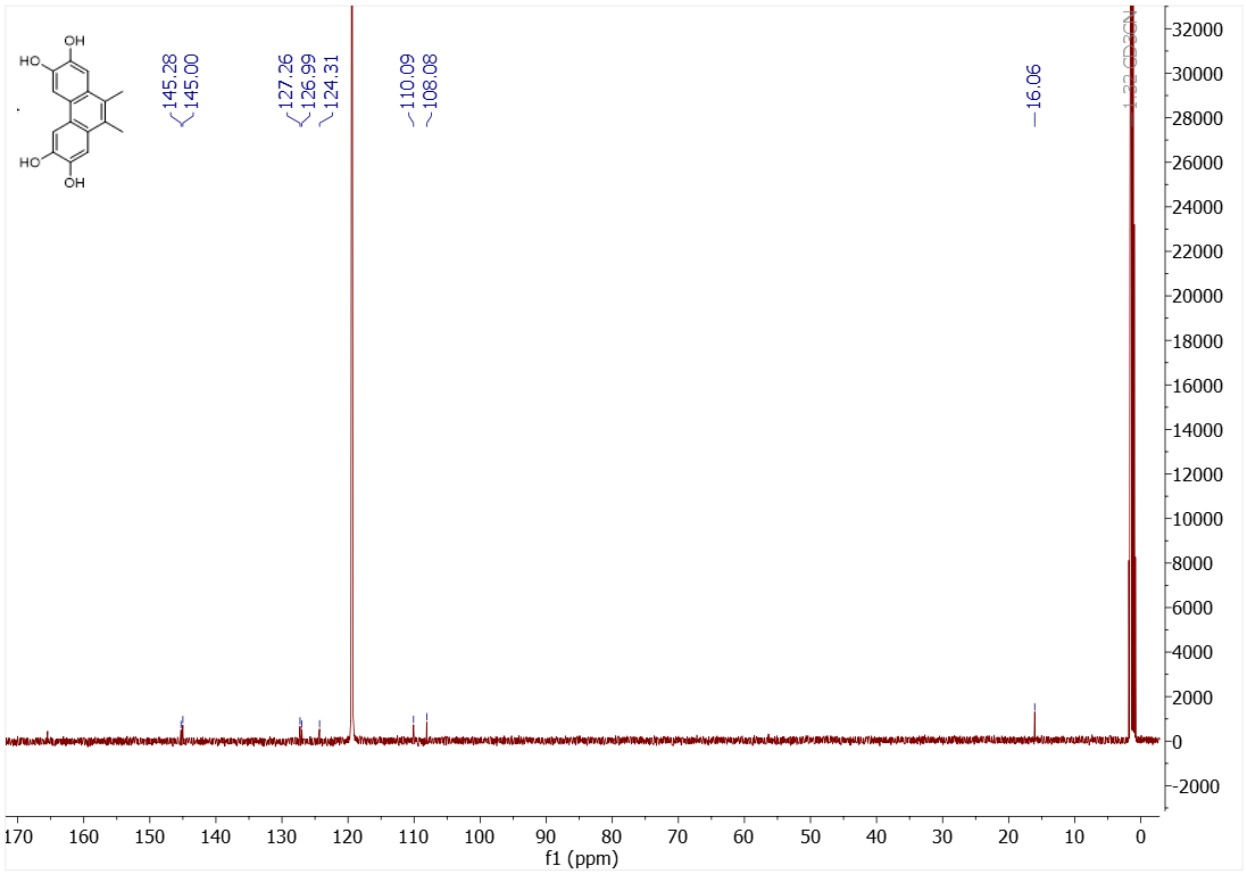

Figure S8. ^{13}C NMR for o-M2-DPE A

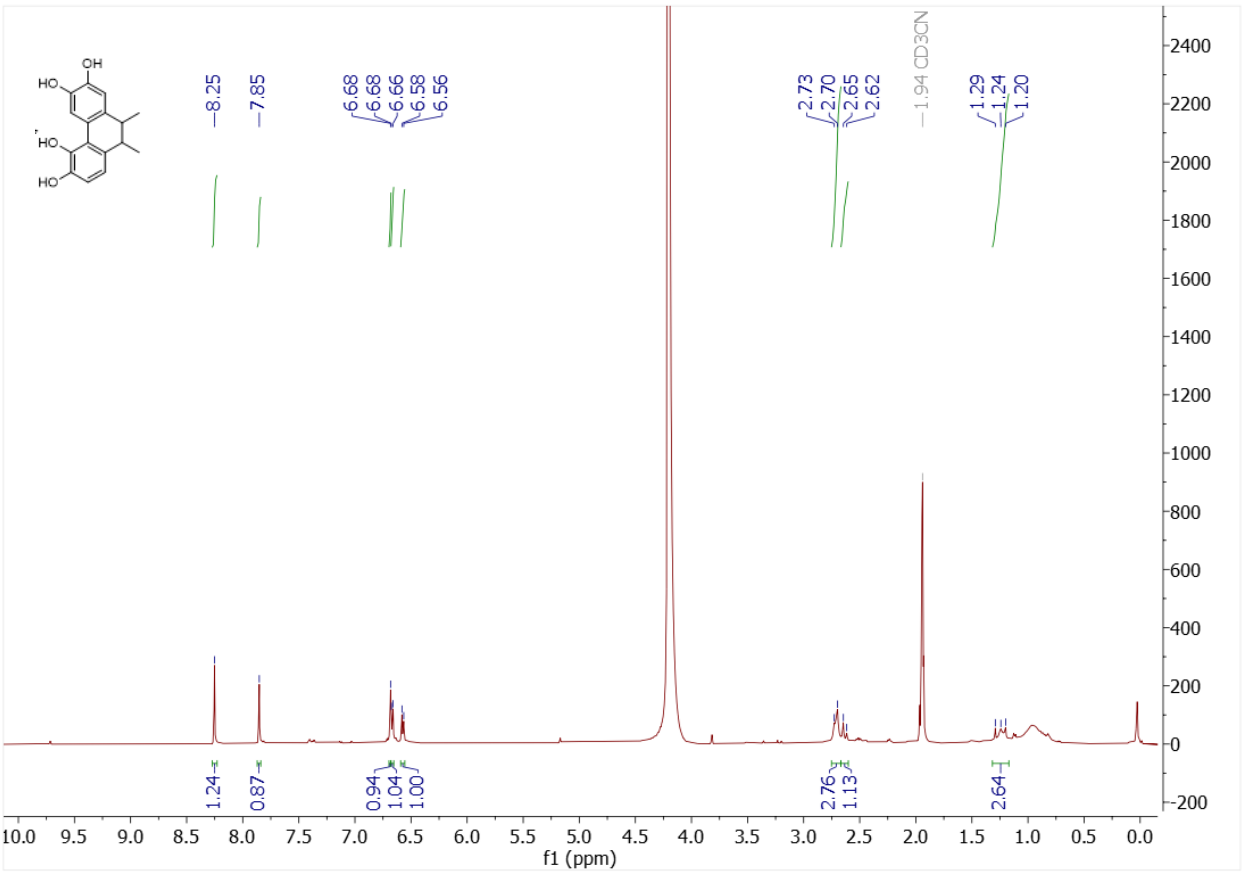

Figure S9. ^{1}H NMR for o-M2-DPE B

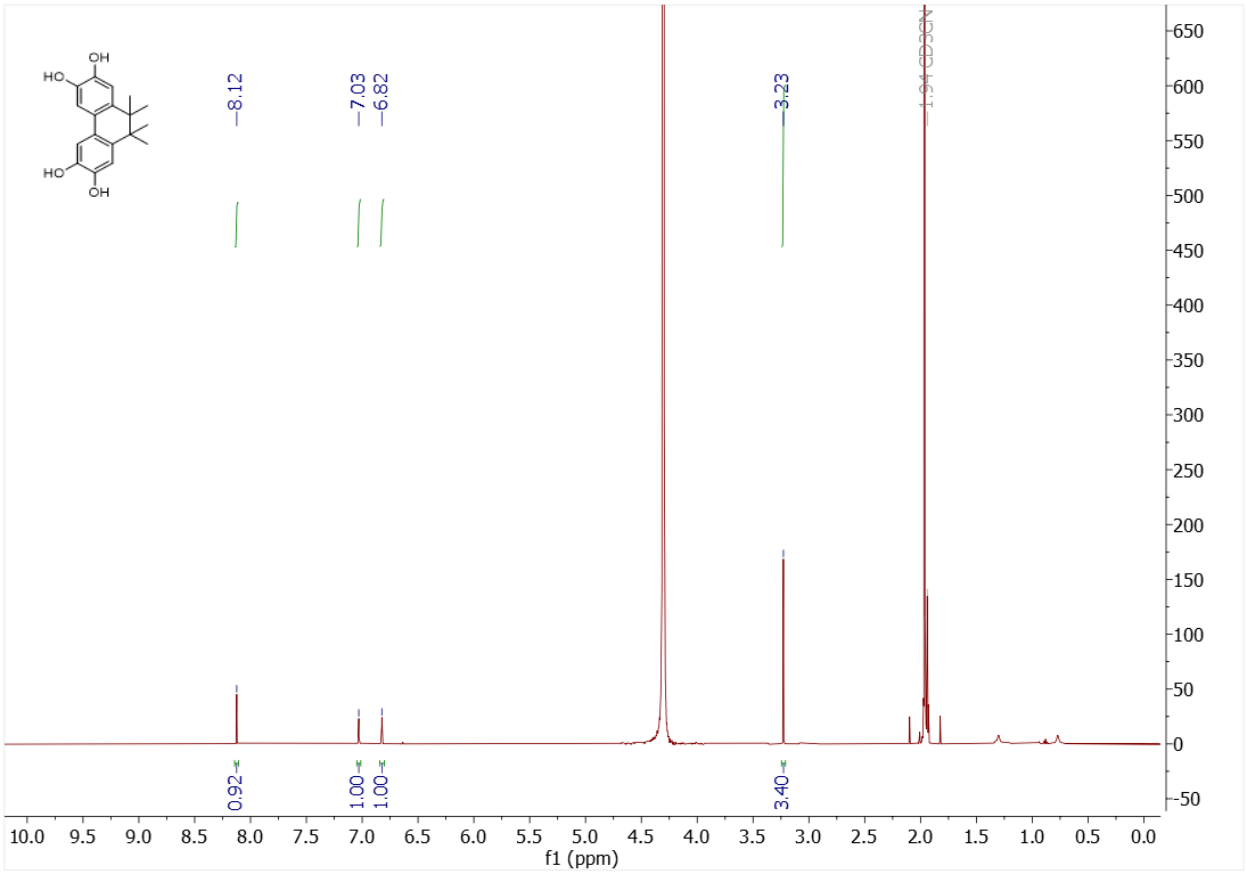

Figure S10. ^{1}H NMR for o-M4-DPE A

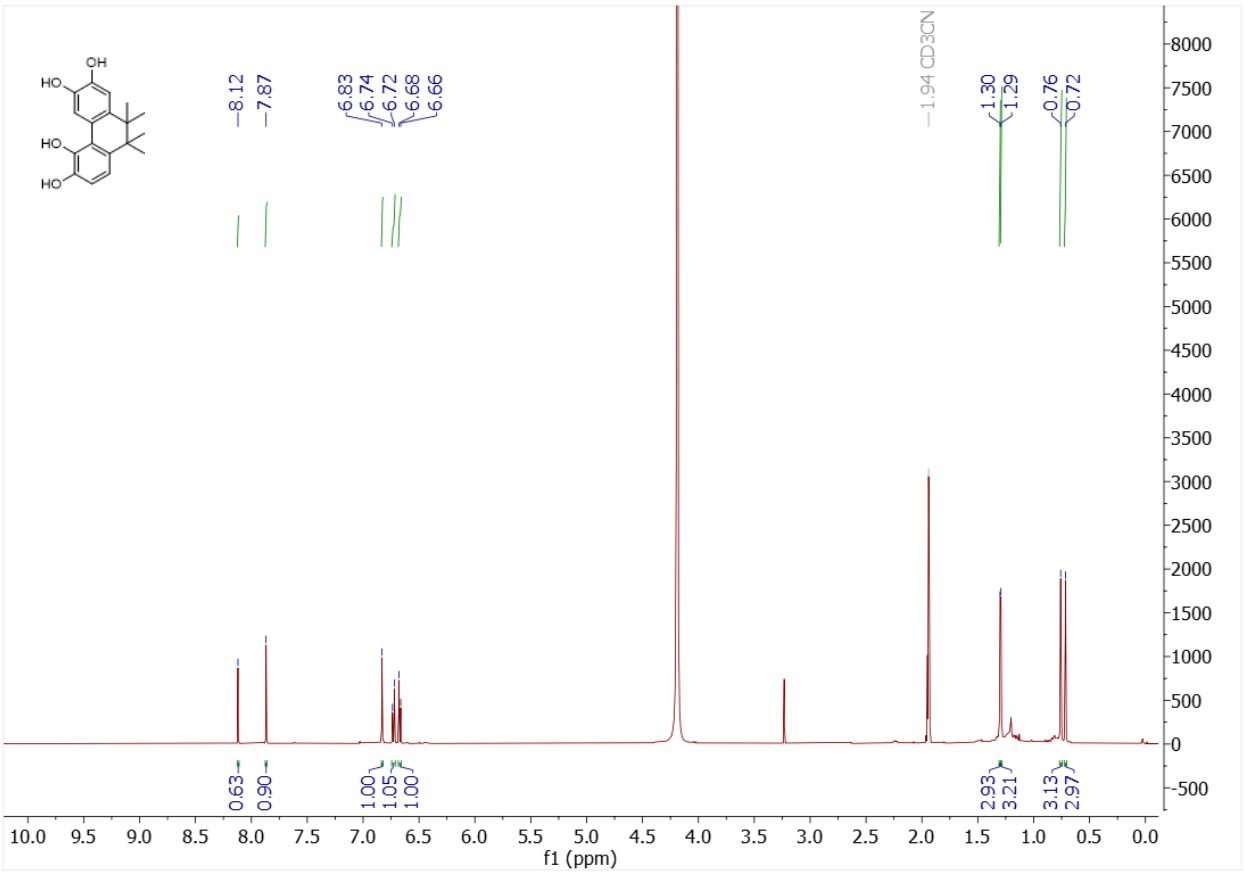

Figure S11. ^{1}H NMR for o-M4-DPE B

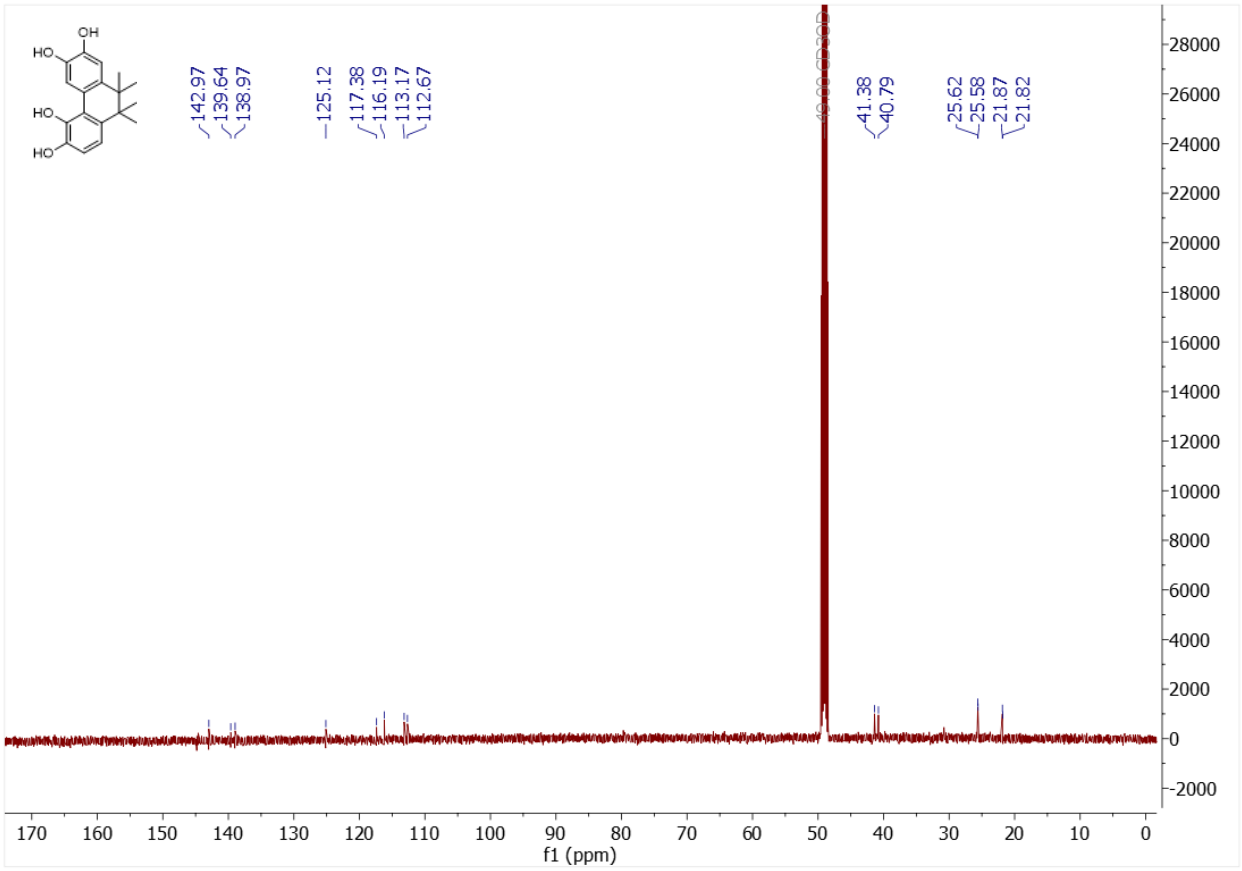

Figure S12. ^{13}C NMR for o-M4-DPE B

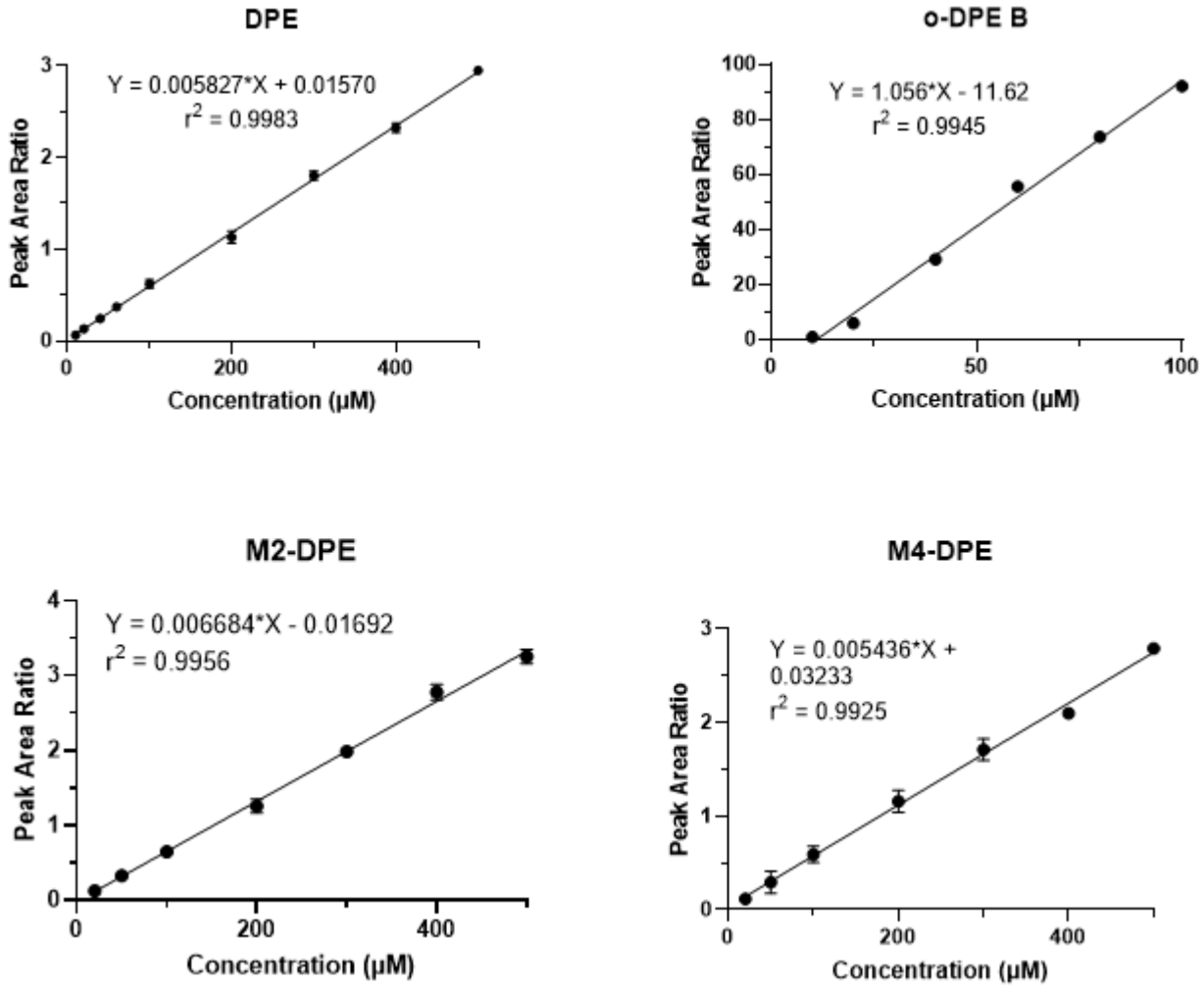

Figure S13. Standard curves of DPE, o-DPE B, M2-DPE, and M4-DPE

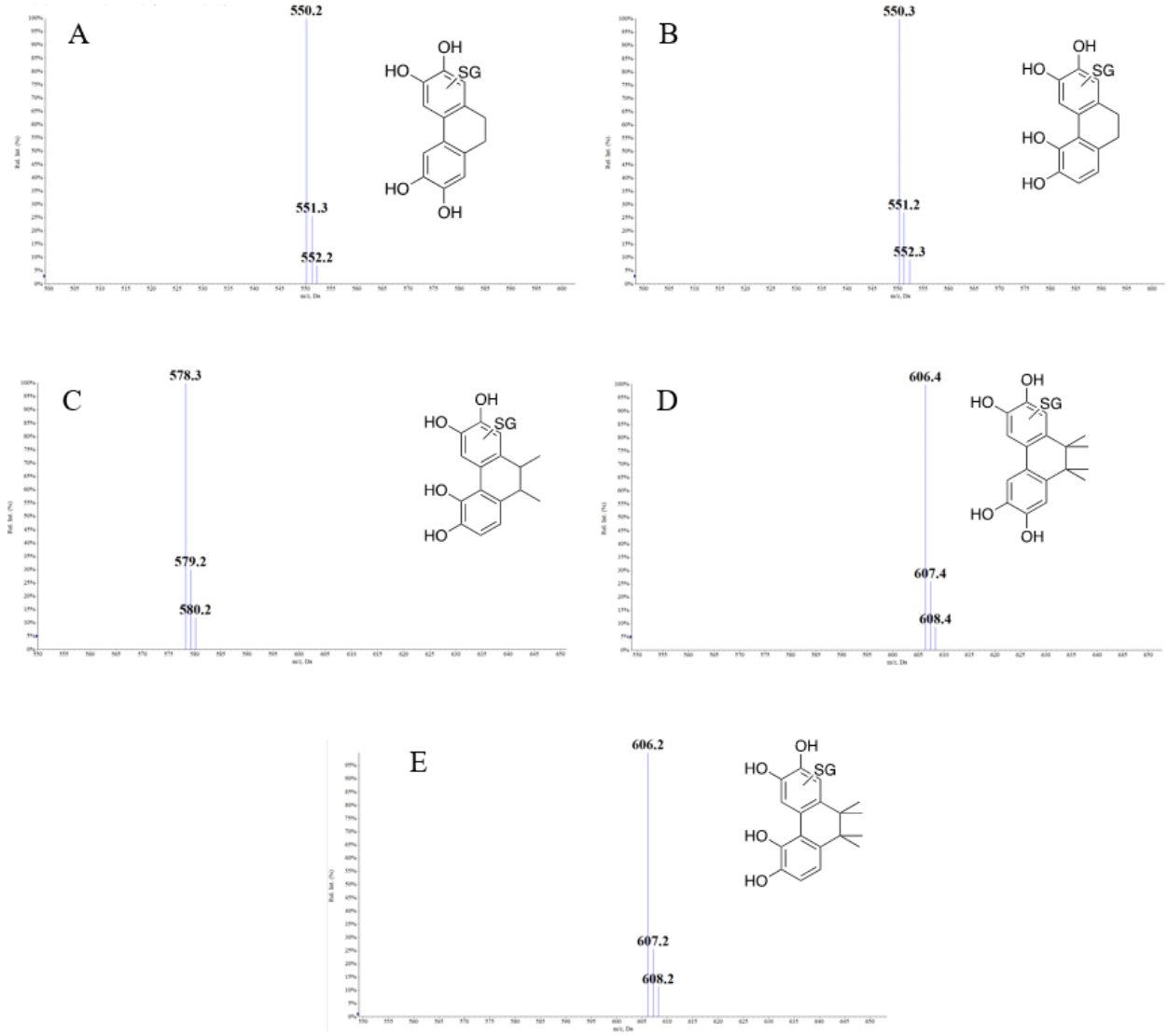

Figure S14. ESI-MS in positive mode scan for neutral loss (NL) of *m/z* 129 for the detection of GSH conjugates for o-DPE-A (A), o-DPE-C (B), o-M2-DPE-B (C), o-M4-DPE-A (D) and o-M4-DPE-B (E).

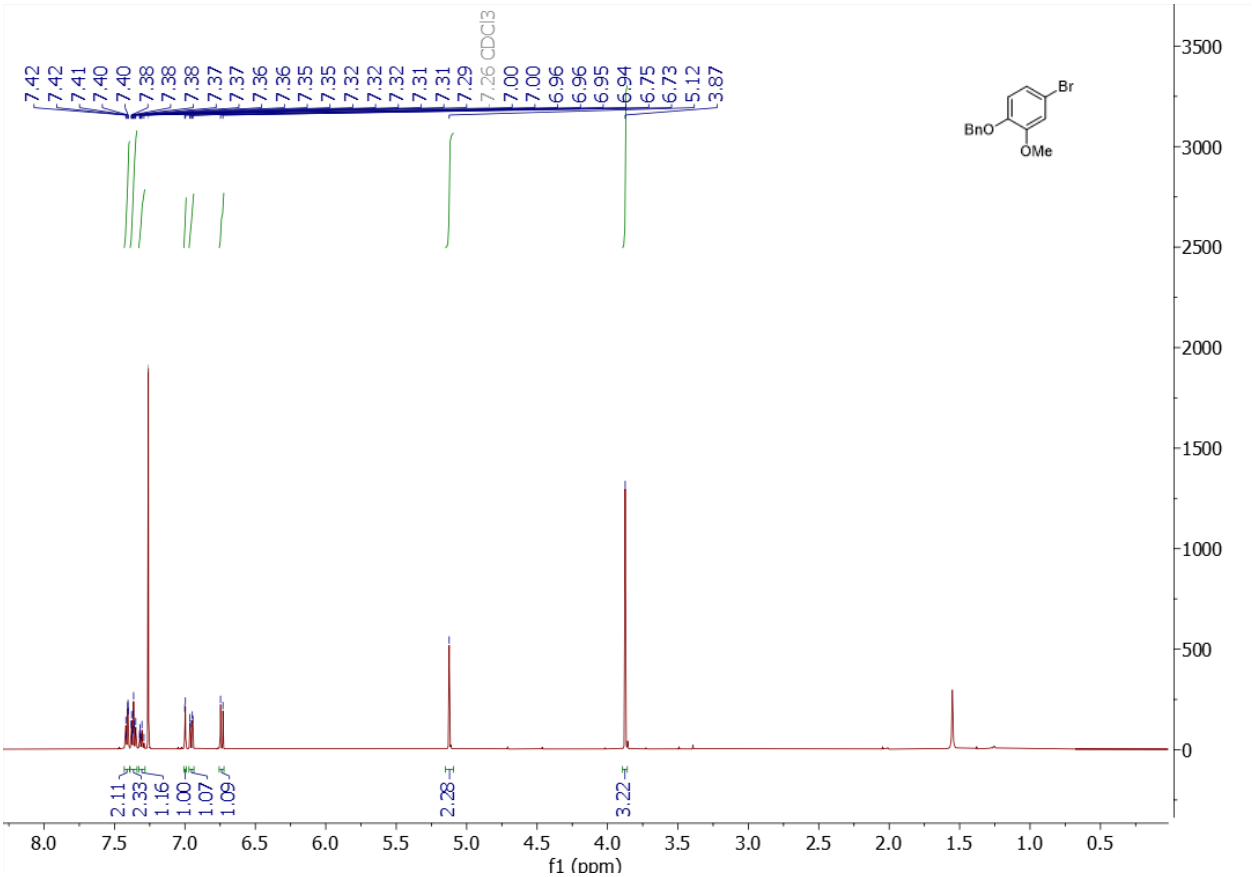

Figure S15. ^{1}H NMR for compound 1-(benzyloxy)-4-bromo-2-methoxybenzene (9)

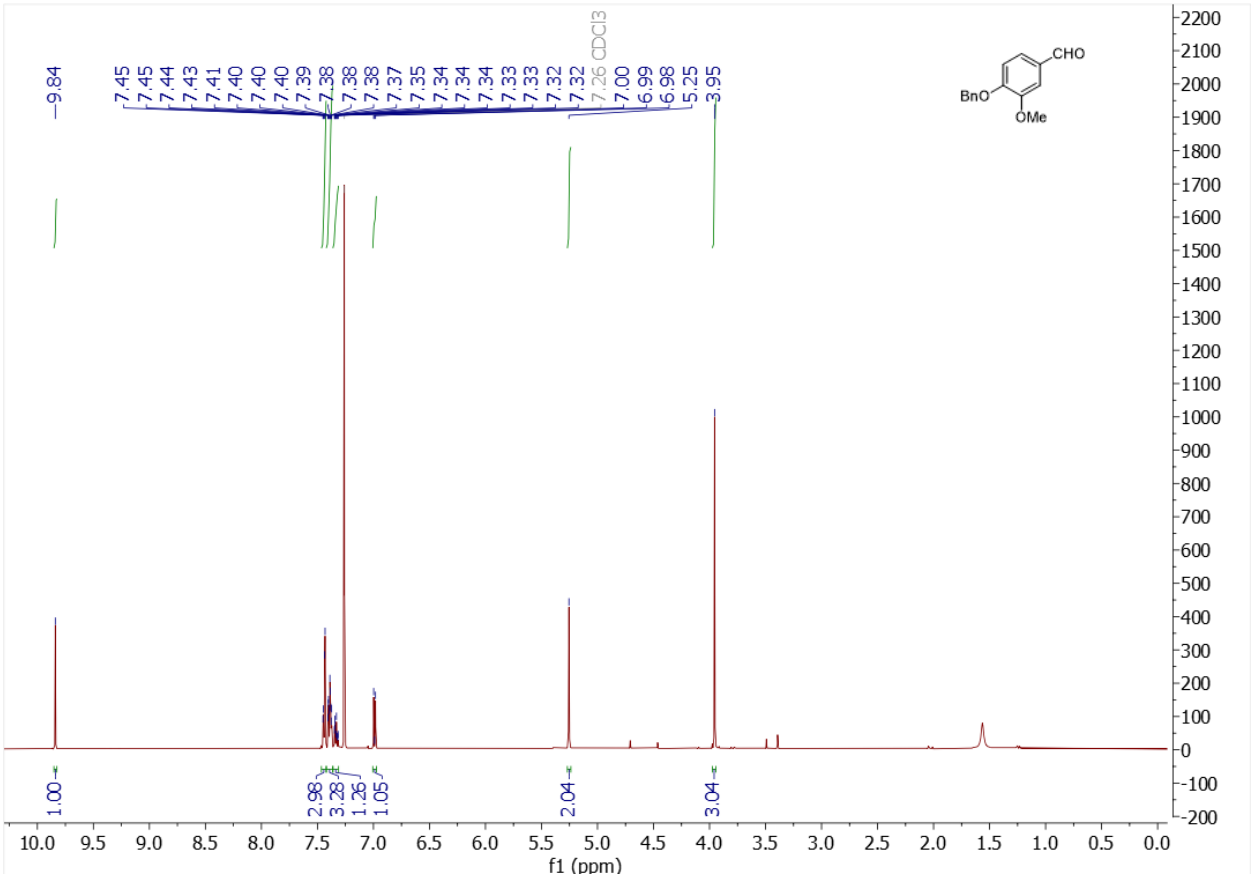

Figure S16. ^{1}H NMR for compound 4-(benzyloxy)-3-methoxybenzaldehyde (10)

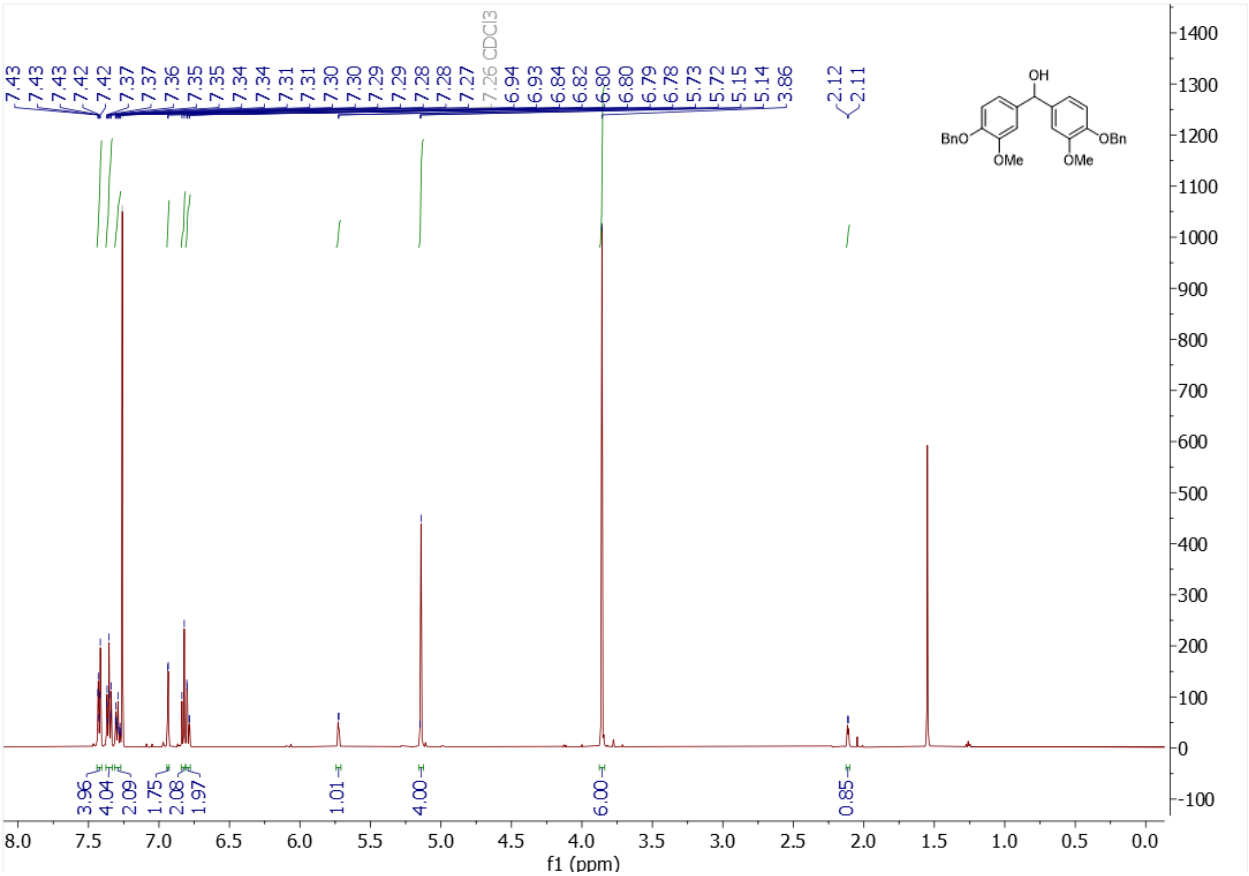

Figure S17. [1]H NMR for compound bis(4-(benzyloxy)-3-methoxyphenyl)methanol (11).

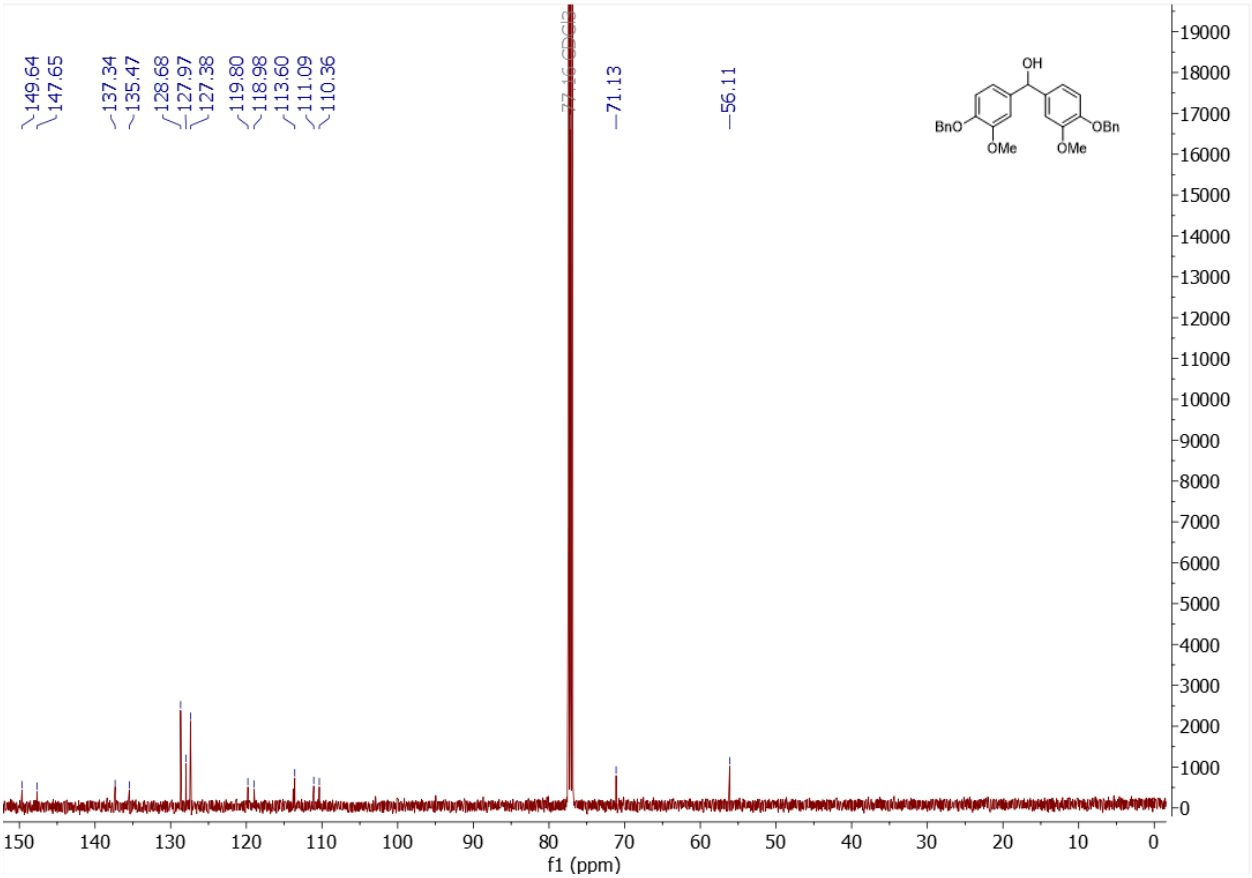

Figure S18. ^{13}C NMR for compound bis(4-(benzyloxy)-3-methoxyphenyl)methanol (11)

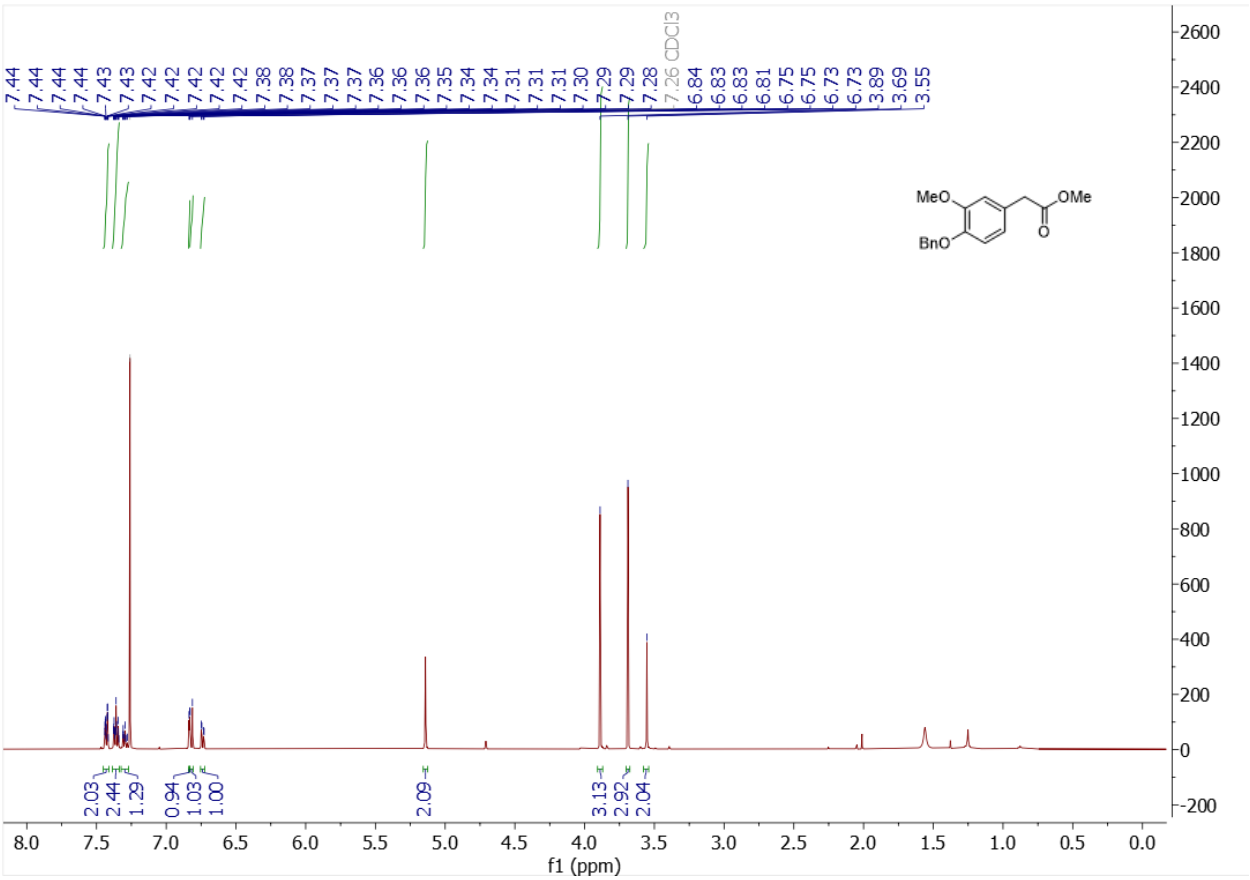

Figure S19. ^{1}H NMR for compound methyl 2-(4-(benzyloxy)-3-methoxyphenyl)acetate (13)

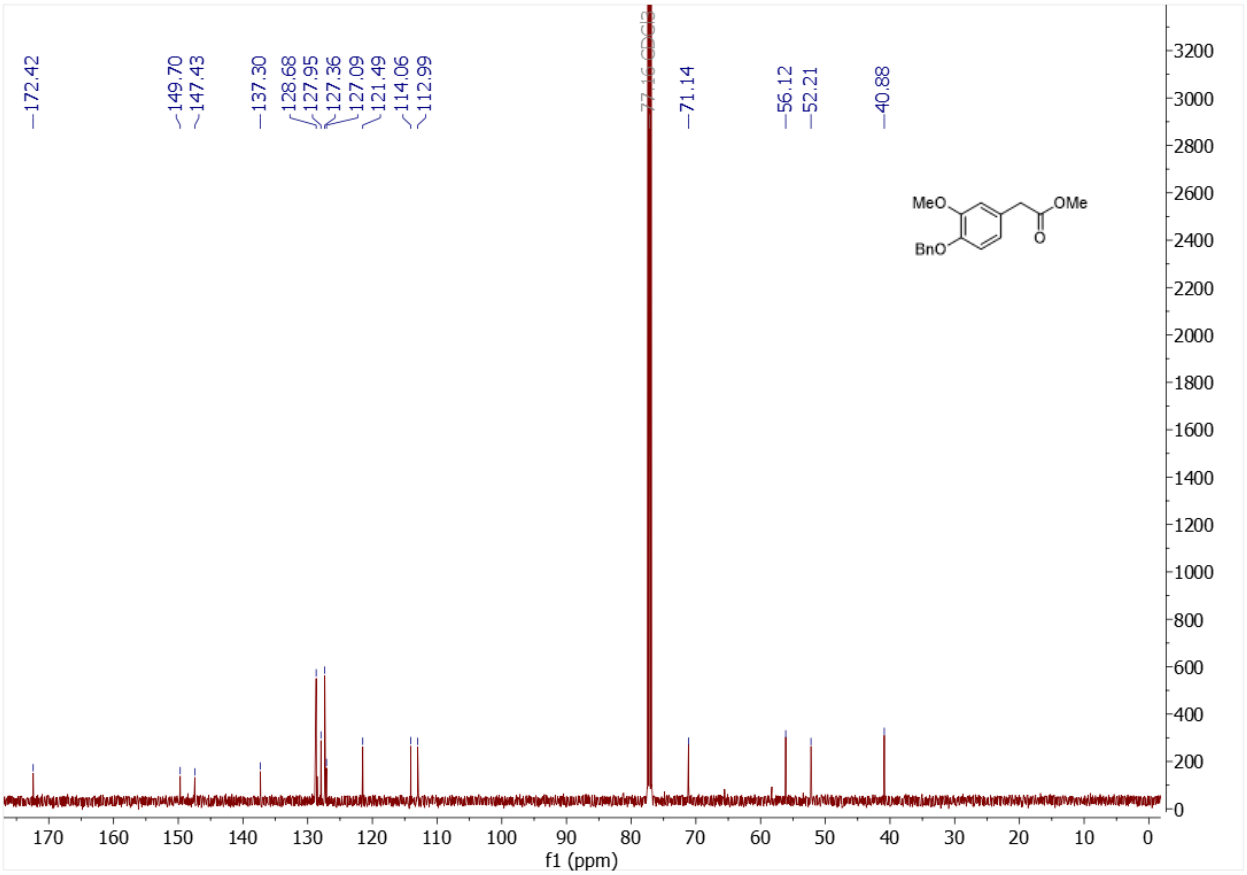

Figure S20. ^{13}C NMR for compound methyl 2-(4-(benzyloxy)-3-methoxyphenyl)acetate (13)

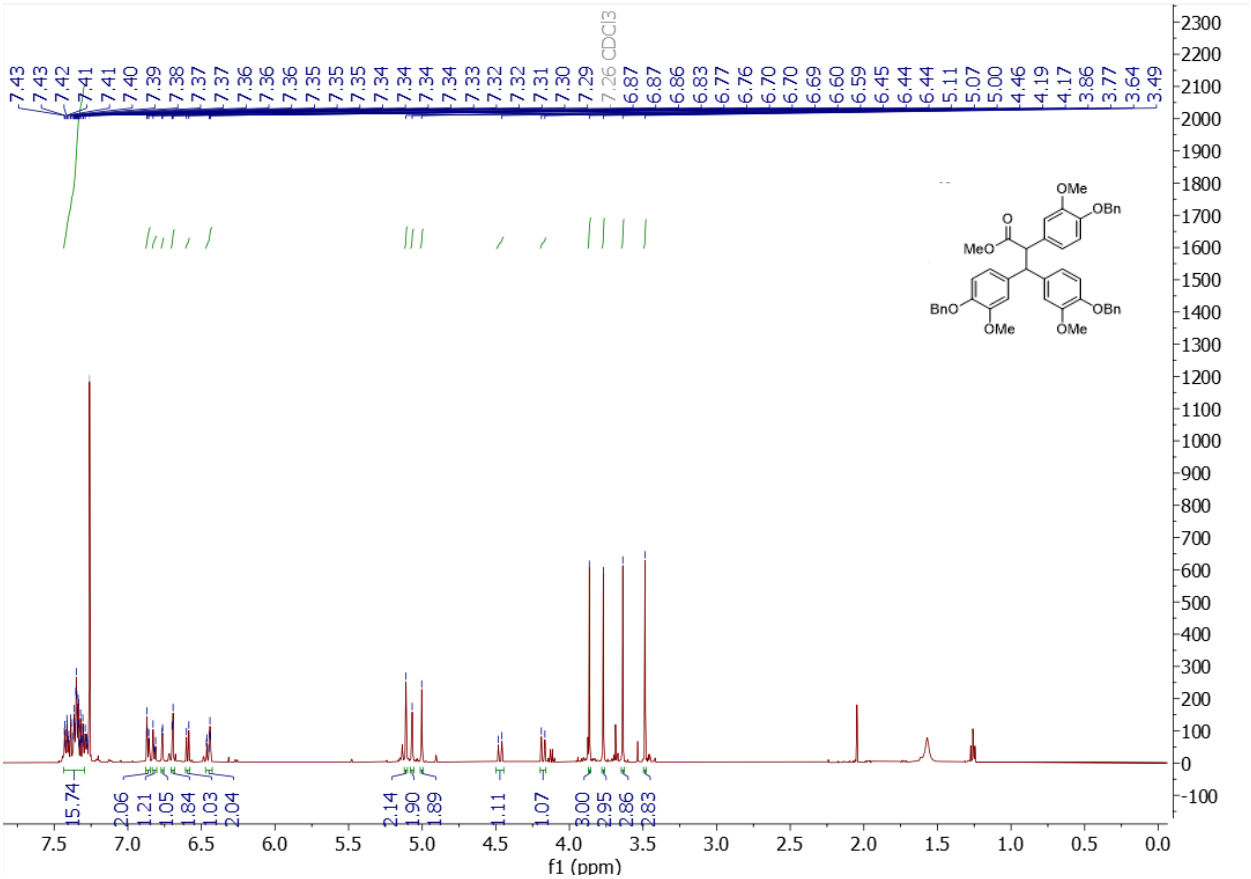

Figure S21. ^{1}H NMR for compound methyl 2,3,3-tris(4-(benzyloxy)-3-methoxyphenyl)propanoate (14)

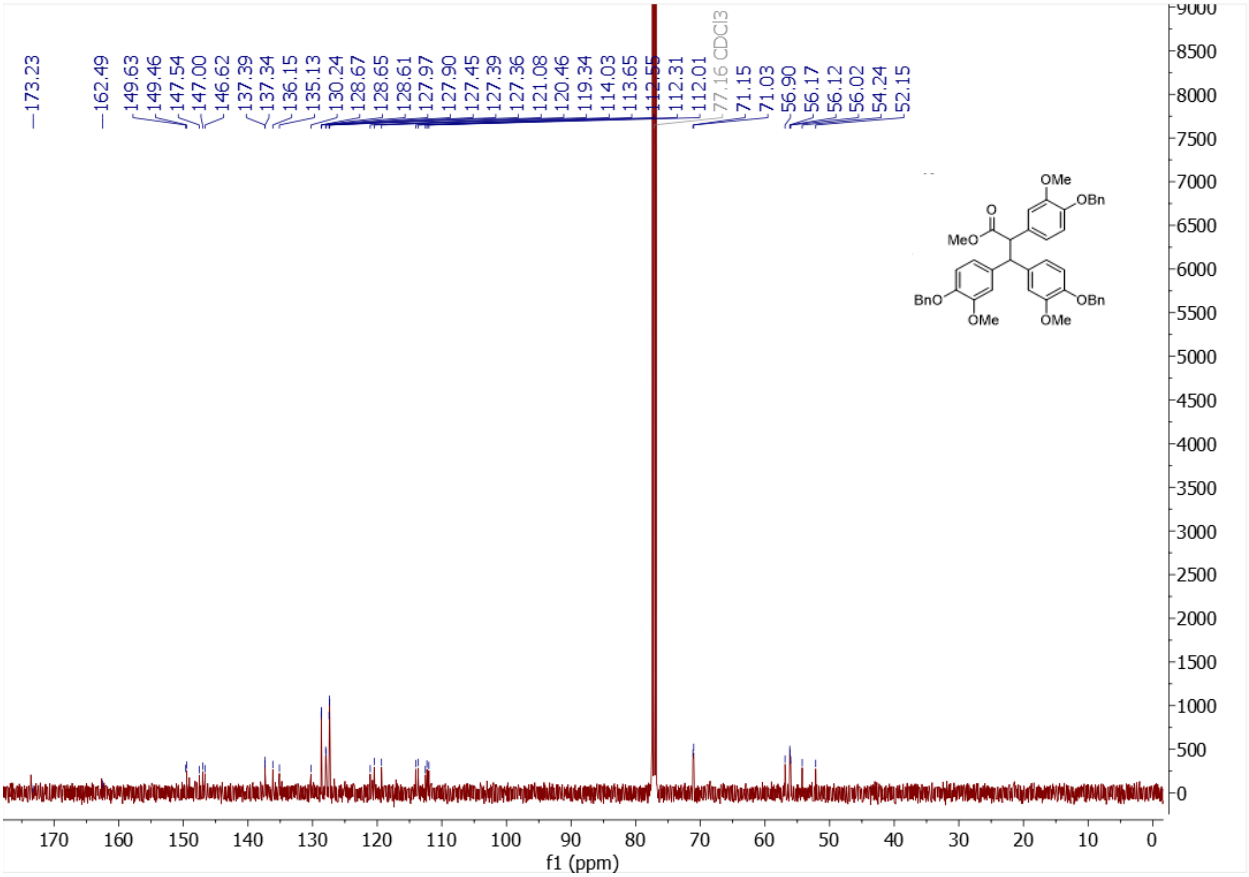

Figure S22. ^{13}C NMR for compound methyl 2,3,3-tris(4-(benzyloxy)-3-methoxyphenyl)propanoate (14)

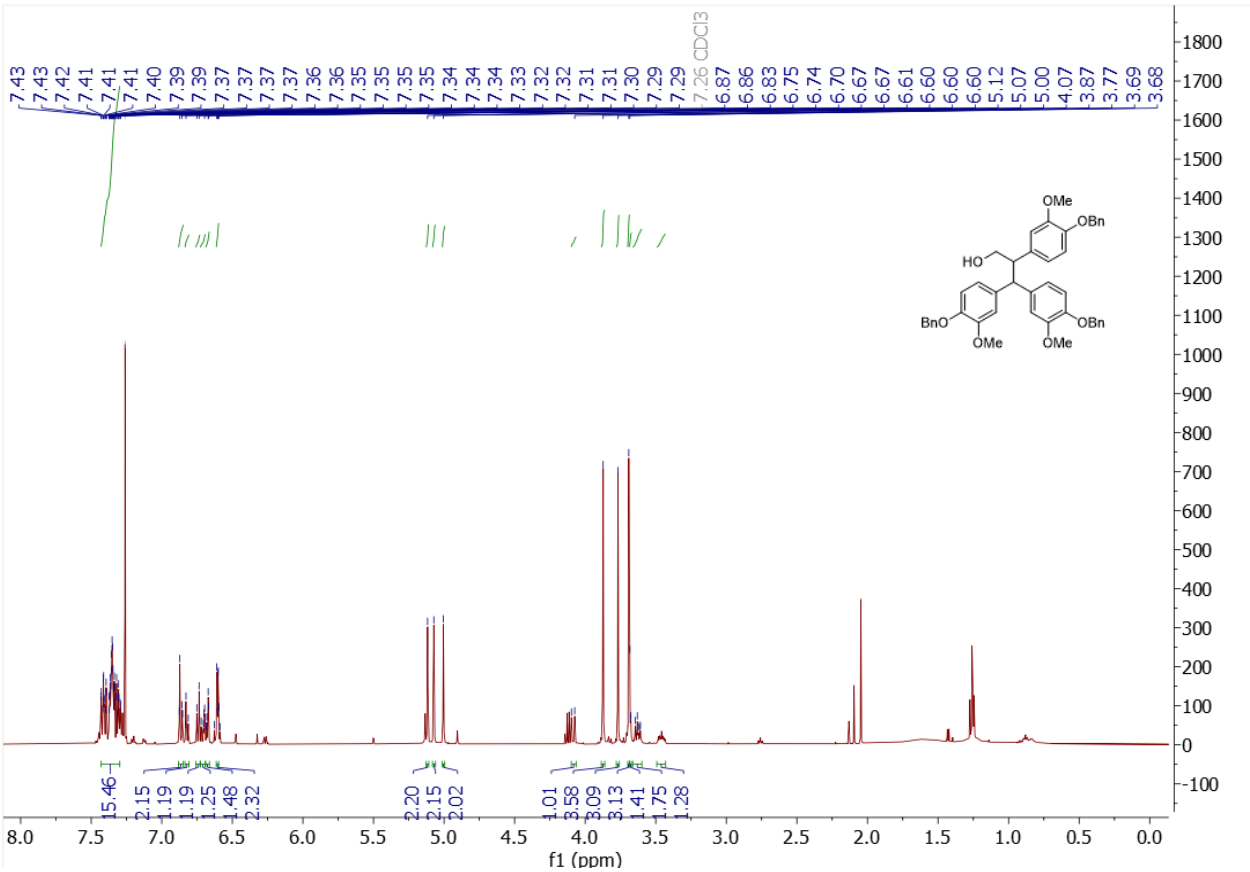

Figure S23.. ^{1}H NMR for compound 2,3,3-tris(4-(benzyloxy)-3-methoxyphenyl)propan-1-ol (15)

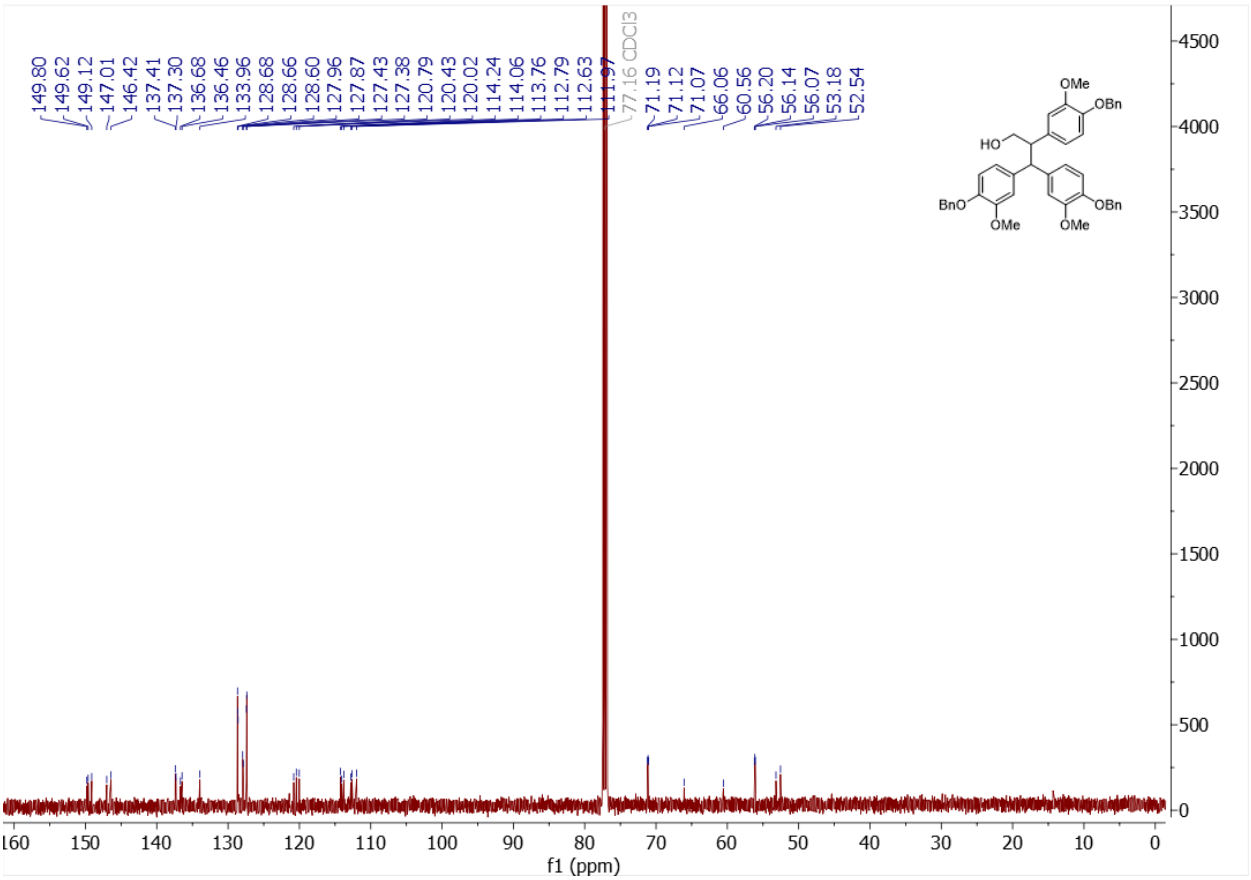

Figure S24. ^{13}C NMR for compound 2,3,3-tris(4-(benzyloxy)-3-methoxyphenyl)propan-1-ol (15)

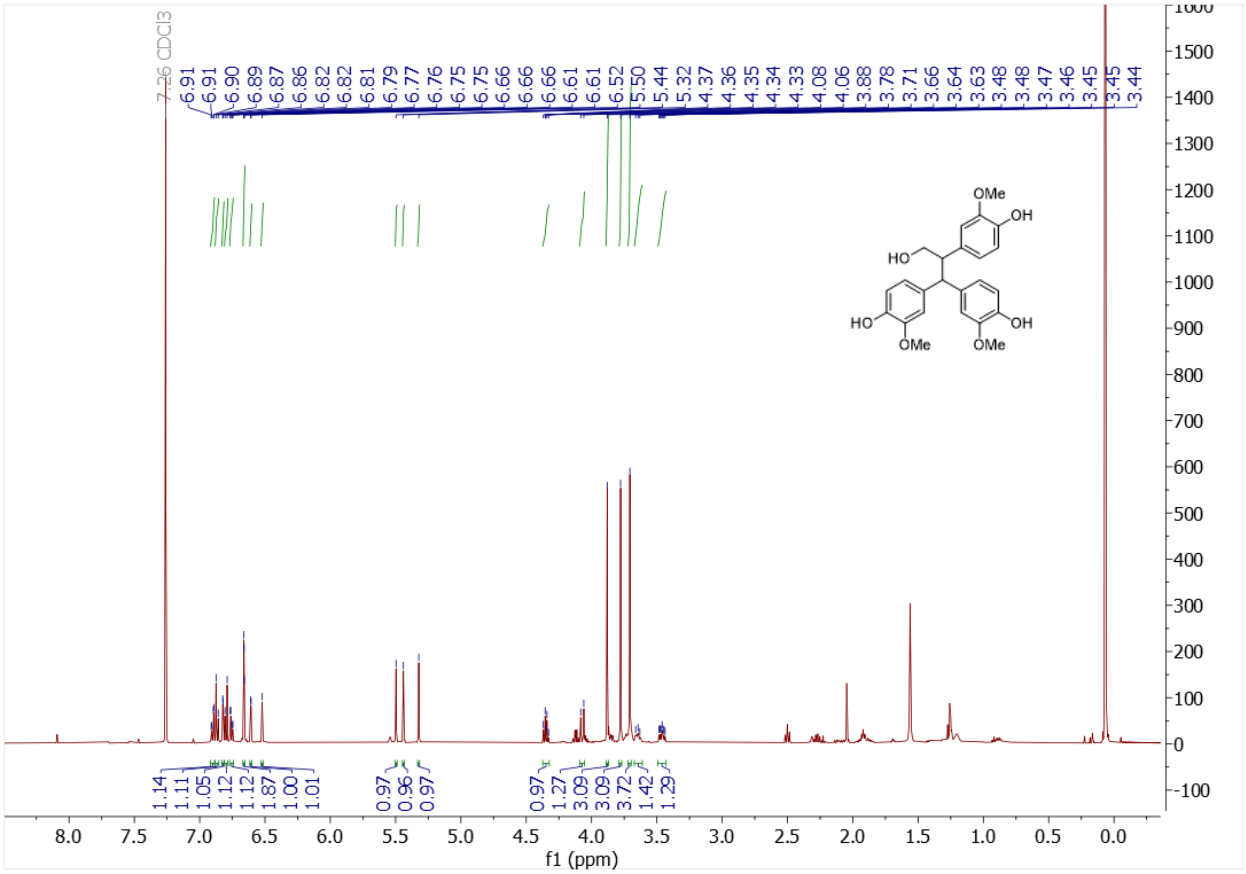

Figure S25. ^{1}H NMR for 4,4',4''-(3-hydroxypropane-1,1,2-triyl)tris(2-methoxyphenol) (Quebecol)

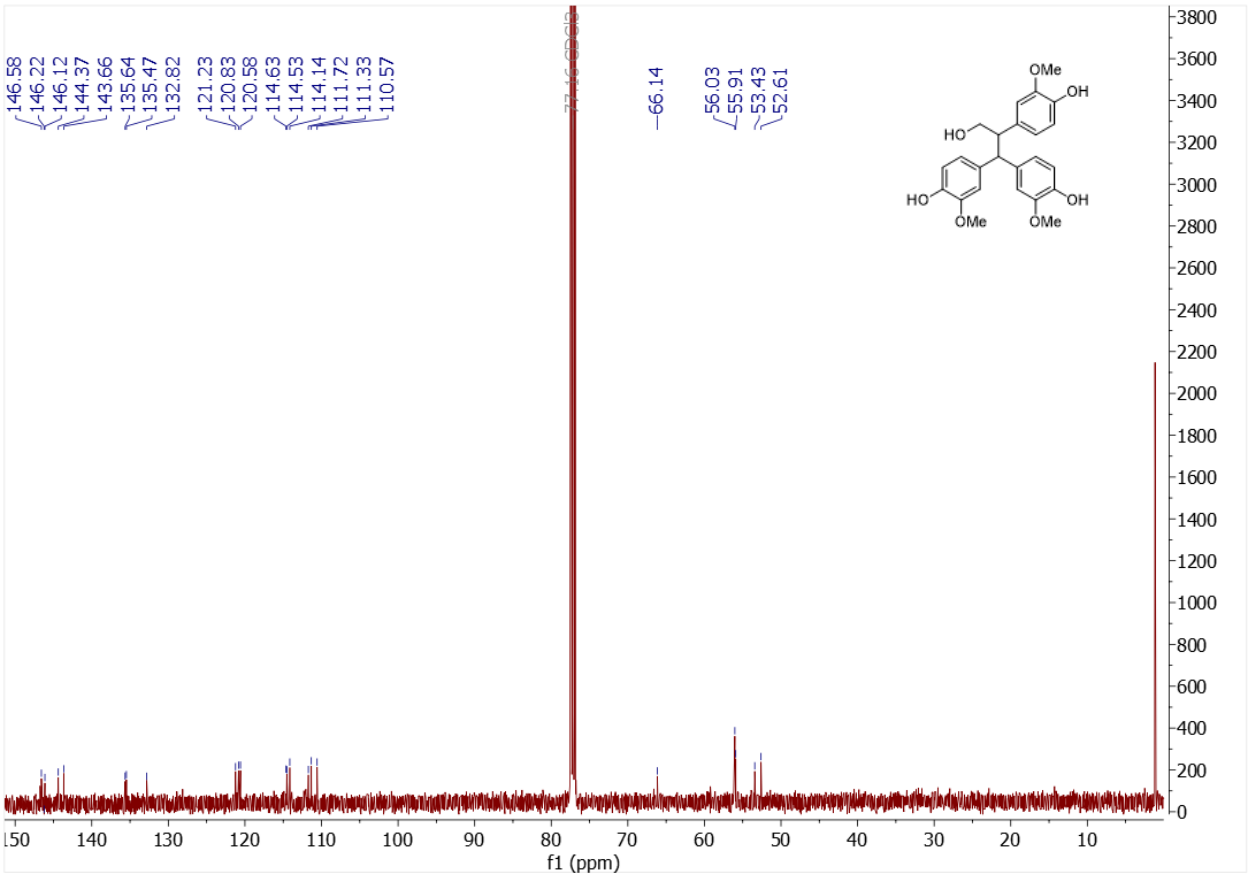

Figure S26. ^{13}C NMR for 4,4',4''-(3-hydroxypropane-1,1,2-triyl)tris(2-methoxyphenol) (Quebecol)

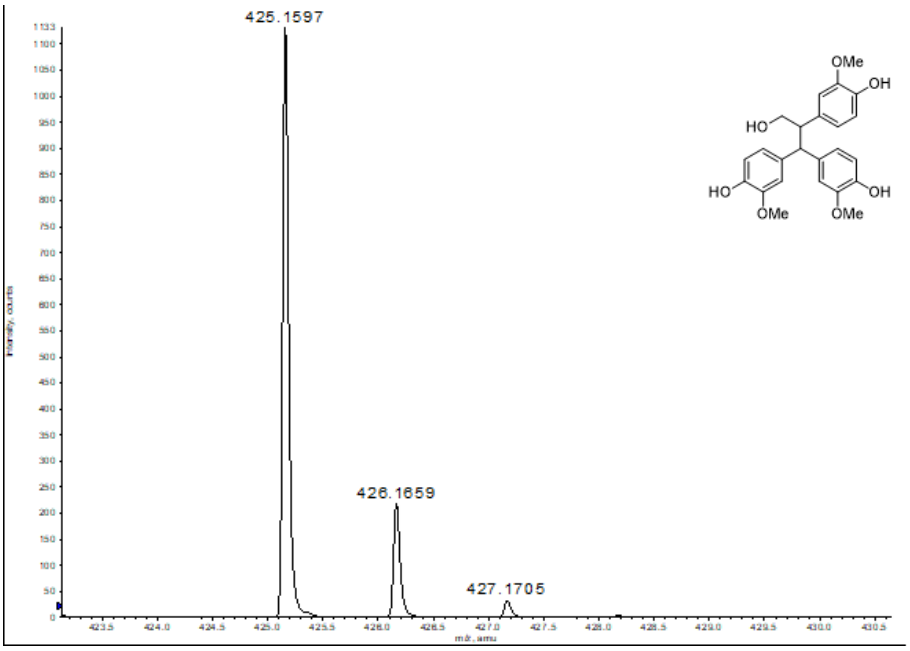

Figure S27. HRMS (TOF ESI-MS) of Quebecol in negative ion mode. Calcd for $C_{24}H_{26}O_7$ $(M-H)^-$ 425.1606, found 425.1597.

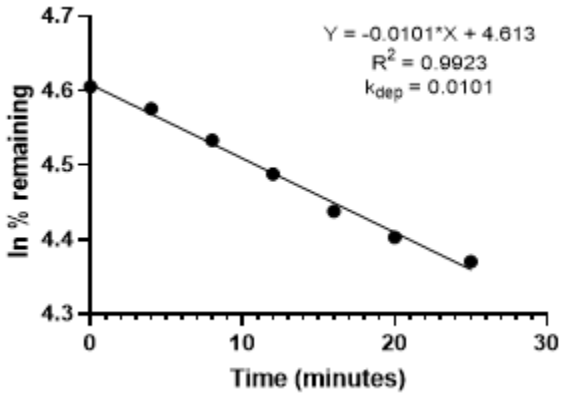

Figure S28. A plot of natural log percent remaining versus time at a low concentration (5µM)

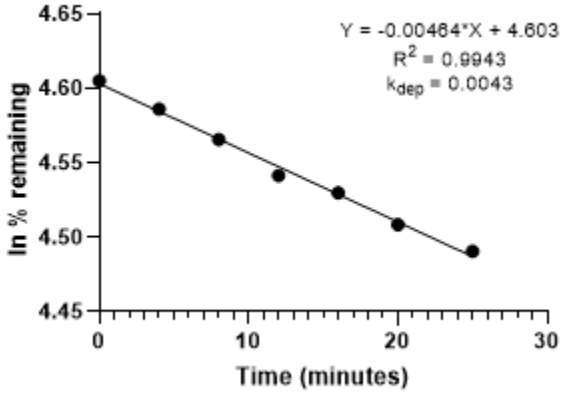

Figure S29. A plot of natural log percent remaining versus time at a higher concentration (30 µM)

Table S3. Various quebecol concentrations (5-30 µM) versus percent remaining for human liver microsomal kinetic study

Quebecol Concentration (µM)	Final percent remaining (%)	k_{dep} (min^{-1})
5	76.6	0.0112
7	78.9	0.0089
9	84.3	0.0069
13	85.2	0.0060
15	87.5	0.0055
17	92.3	0.0053
20	93.8	0.0052
30	92.1	0.0049

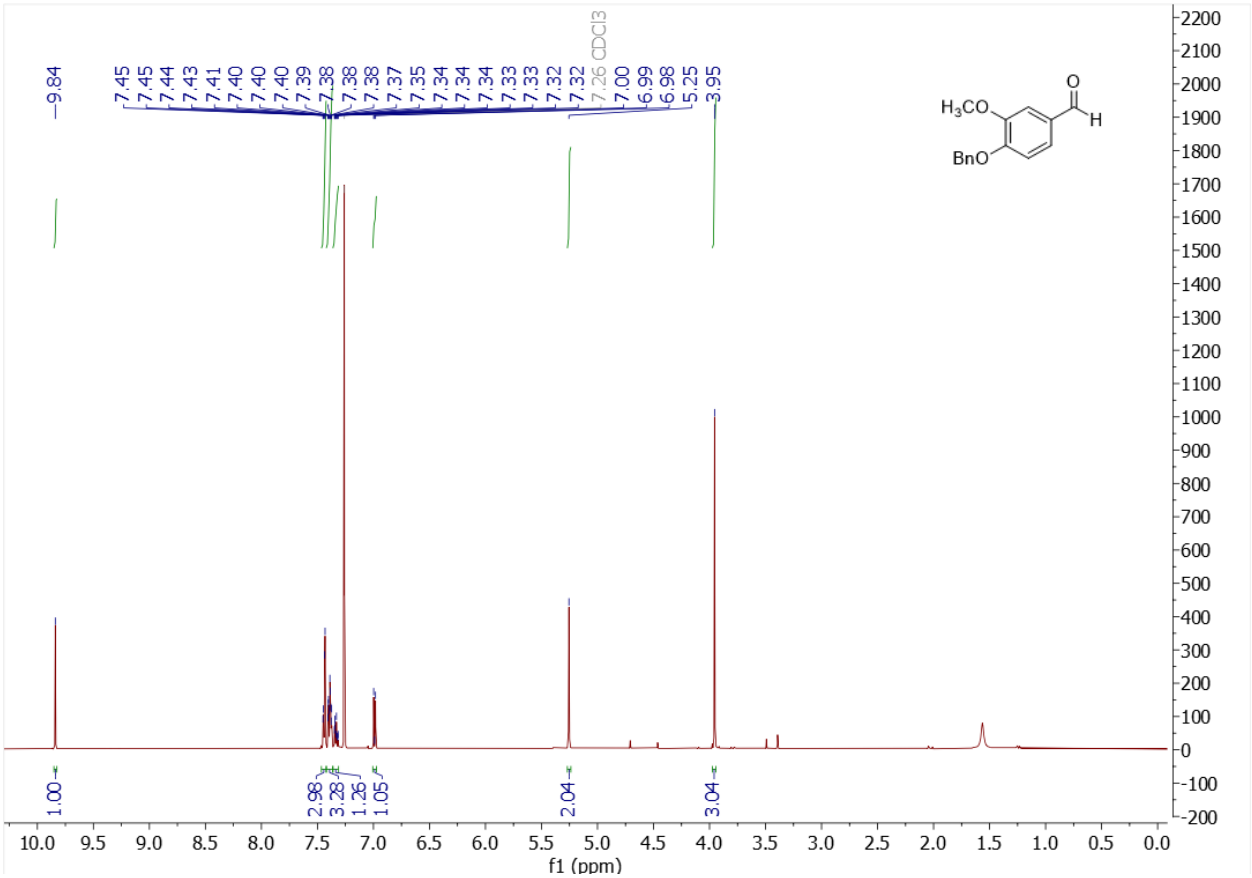

Figure S30. ^{1}H NMR for compound 16

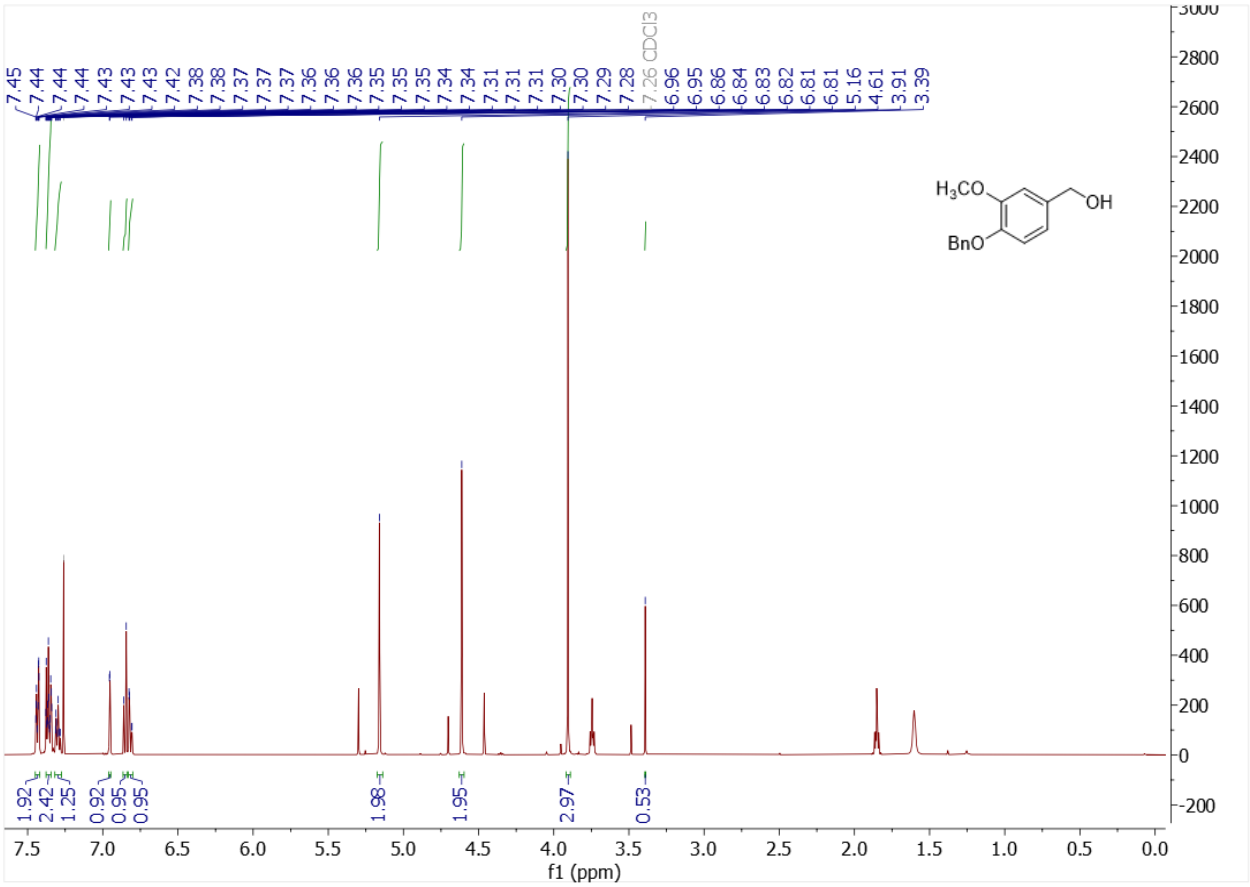

Figure S31. ^{1}H NMR for compound 17

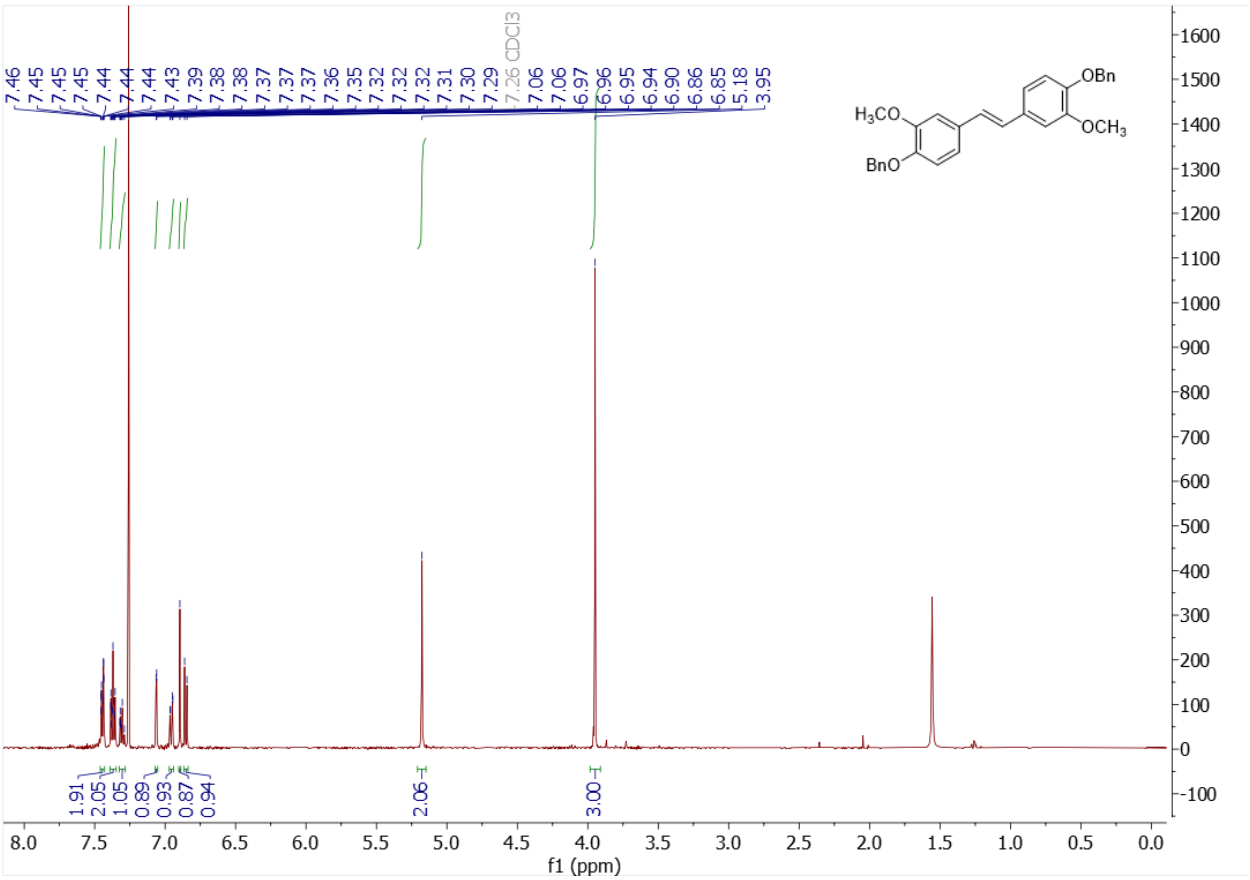

Figure S32. ^{1}H NMR for compound 18

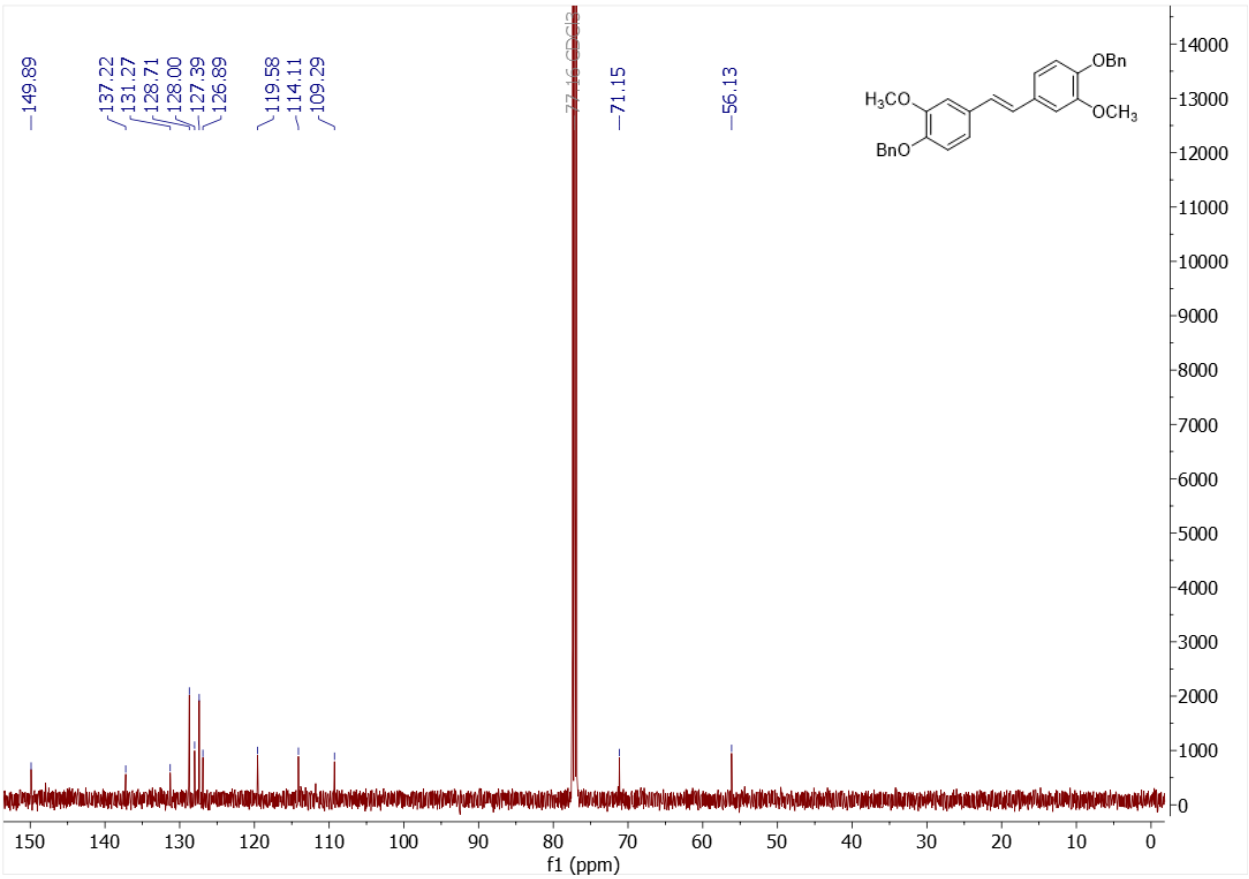

Figure S33. ^{13}C NMR for compound 18

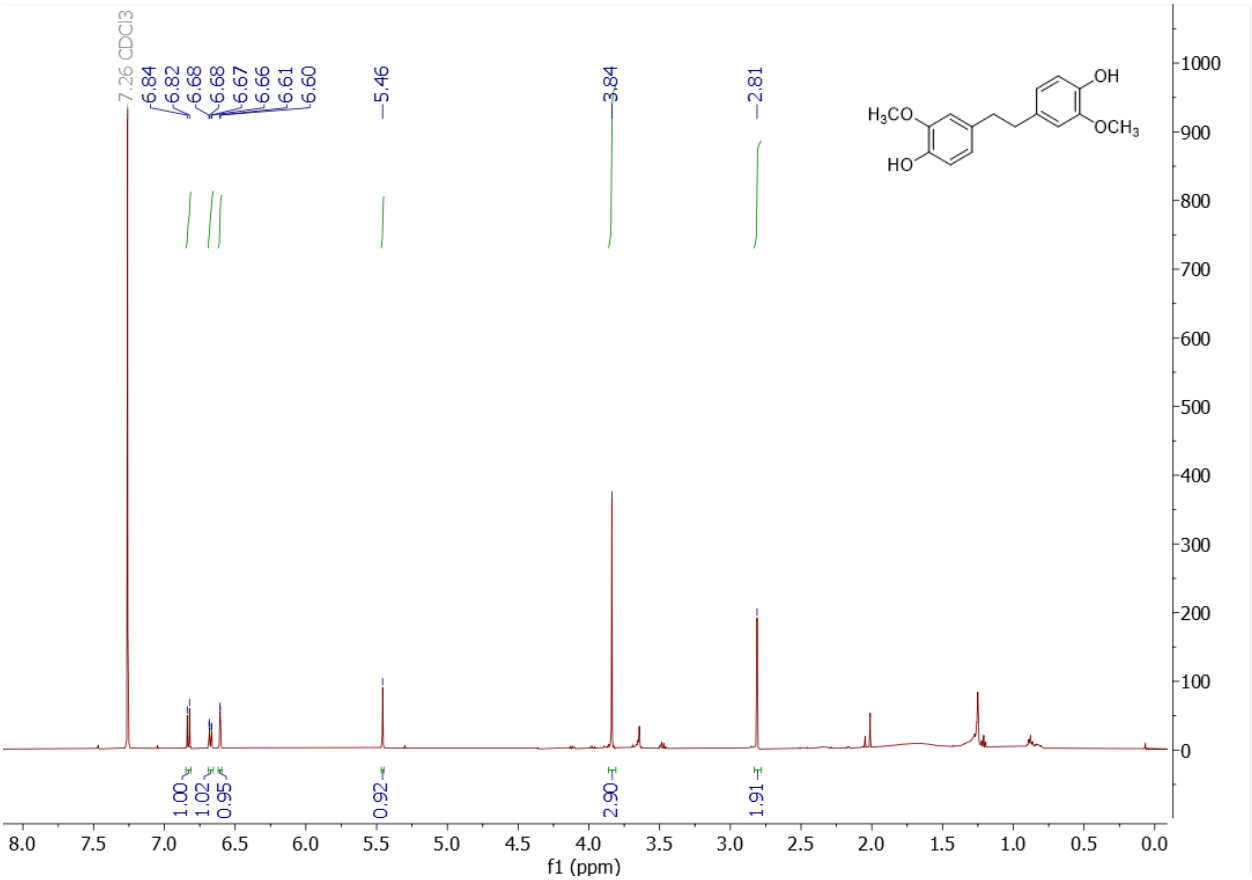

Figure S34. ^{1}H NMR for $(MeO)_2$-DPE

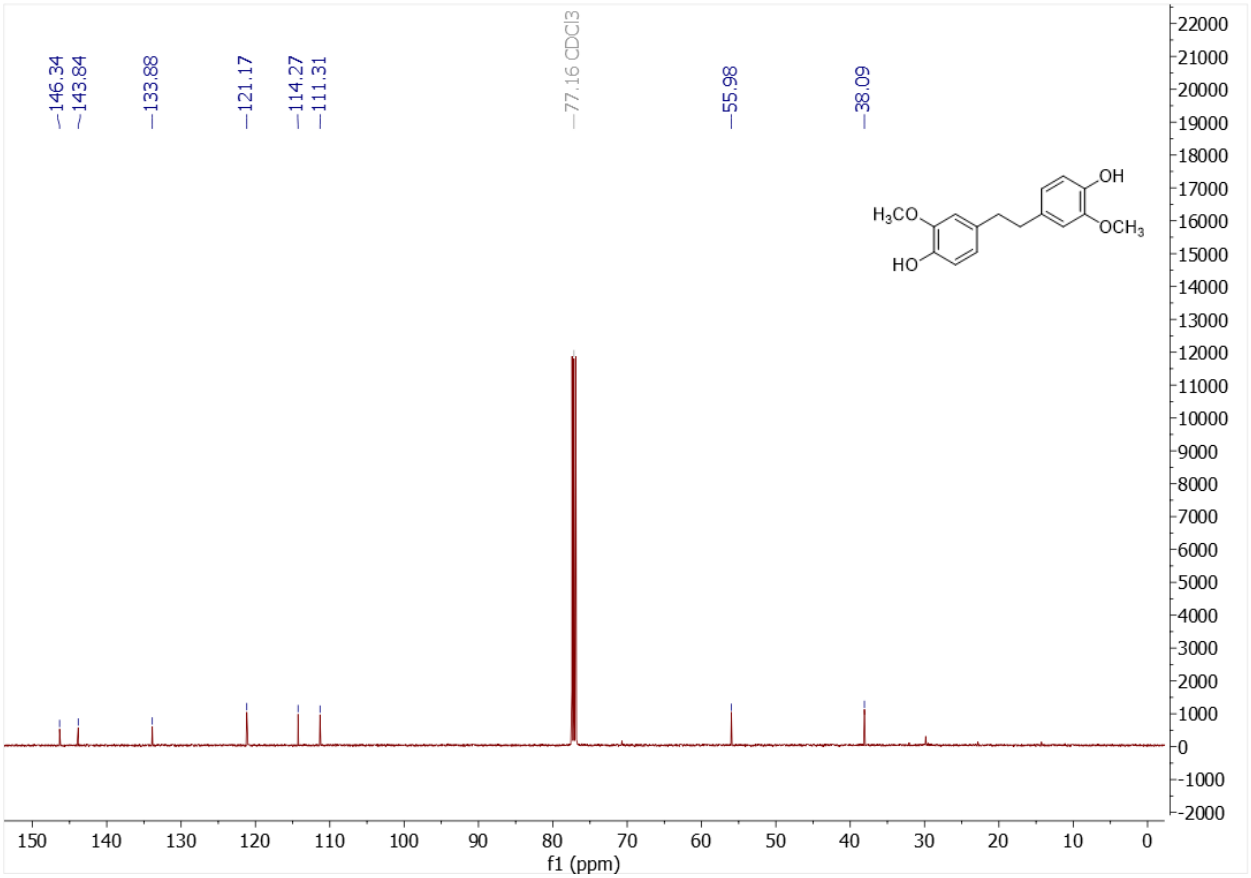

Figure S35. ^{13}C NMR for $(MeO)_2$-DPE